NOTICE

The quality of this microfiche is heavily dependent upon the quality of the original thesis submitted for microfilming. Every effort has been made to ensure the highest quality of reproduction possible.

If pages are missing, contact the university which granted the degree.

Some pages may have indistinct print especially if the original pages were typed with a poor typewriter ribbon or if the university sent us a poor photocopy.

Previously copyrighted materials (journal articles, published tests, etc.) are not filmed.

Reproduction in full or in part of this film is governed by the Canadian Copyright Act, R.S.C. 1970, c. C-30. Please read the authorization forms which accompany this thesis.

THIS DISSERTATION
HAS BEEN MICROFILMED
EXACTLY AS RECEIVED

AVIS

La qualité de cette microfiche dépend grandement de la qualité de la thèse soumise au microfilmage. Nous avons tout fait pour assurer une qualité supérieure de reproduction.

S'il manque des pages, veuillez communiquer avec l'université qui a conféré le grade.

La qualité d'impression de certaines pages peut laisser à désirer, surtout si les pages originales ont été dactylographiées à l'aide d'un ruban usé ou si l'université nous a fait parvenir une photocopie de mauvaise qualité.

Les documents qui font déjà l'objet d'un droit d'auteur (articles de revue, examens publiés, etc.) ne sont pas microfilmés.

La reproduction, même partielle, de ce microfilm est soumise à la Loi canadienne sur le droit d'auteur, SRC 1970, c. C-30. Veuillez prendre connaissance des formules d'autorisation qui accompagnent cette thèse.

LA THÈSE A ÉTÉ
MICROFILMÉE TELLE QUE
NOUS L'AVONS REÇUE

UNIVERSITÉ D'OTTAWA
UNIVERSITY OF OTTAWA

A COMPARISON OF THE IMPACT RESPONSE OF CADAVER HEADS AND ANTHROPOMORPHIC HEADFORMS

by

Gary D. Webster

Thesis presented to the School of Graduate Studies
as partial fulfillment of the requirements
for the degree of M.A.Sc. in
Mechanical Engineering

UNIVERSITY OF OTTAWA
OTTAWA, CANADA, 1976

ABSTRACT

Studies of the related biomechanical literature in the field of head injury influenced this study by attempting to find force, energy or time durational inputs to the human head that cause head injury. It was thought that a comprehensive investigation of motorcycle accidents in conjunction with laboratory impacts to helmets similar to the accident helmet would lead to the pertinent conclusions. However, studies of the literature on available headforms used for laboratory helmet tests indicated there was insufficient performance impact data comparing these headforms with the human head. Hence this study has dealt with the development and analysis of tests and equipment for the comparison of headforms to human heads during impact. From the analysis of test data for the seven types of headforms impacted, the Sierra headform results compared most closely with the results of cadaver impact tests with and without helmets. In relation to the cadaver head tests, the method for mounting cadaver heads developed for this study should prove extremely useful in future studies. The equipment developed permitted testing to all regions of the head, however, this study performed impact tests mainly to the crown, frontal and occipital regions.

This report has subsequently recommended the Sierra headform along with the other recommendations to the Canadian Standards Association Motorcycle Helmet Standard Revision Committee in compliance to their request.

This thesis has also provided the groundwork for further study in the field of biomechanical head injury and makes recommendations for topics that should receive further future consideration.

The thesis has been divided into two volumes to assist the reader. Volume II contains the raw data along with graphic and tabular interpretations of this data. Volume I contains the main body of the thesis.

ACKNOWLEDGEMENTS

The author wishes to acknowledge the excellent cooperation and help given by members of the Mechanical Engineering Department, the Department of Anatomy, the Department of Kinanthropology, the Civil Engineering Department, the Electrical Engineering Department, the Physics Department and Communications and Instructional Media Centre, all of the University of Ottawa.

The author wishes to pay particular thanks to:

Dr. J.A. Newman, who was the advisor for this thesis and who provided countless thoughtful suggestions and ideas throughout this work that enabled the end product to be reached. The author values highly the interest, encouragement, patience and dedication offered by Dr. Newman.

Dr. D.J. Gorman, who was the co-advisor for this thesis during the final twelve months, and who provided numerous recommendations and guidance throughout the duration of the study. The author is very grateful for the interest and helpful advice given by Dr. Gorman.

Dr. V.J. Sistek, who made possible the cadaver head testing for this study. The author is extremely thankful for the excellent cooperation of Dr. Sistek and his department.

Professor C. Cotton, who helped initiate the cadaver head testing programme, the author is appreciative of the advice and assistance provided by Professor Cotton.

Mrs. D. Champion-Demers, who performed the excellent thesis typing, through the difficult pre-Christmas period.

Mr. J.C. Barford, who donated through his company, JCB Plastics, the helmets and helmet liners used in this study. The author is also appreciative of the interest in this work shown by Mr. Barford.

Mr. M. Simmons and Mr. R. Grenier, who assisted in the design and development of the cadaver head steel neck mounts.

Mr. R. Moles who assisted with the cadaver head tests.

Mr. R. Morrison, who helped with the early developmental work during the first year of the project.

Mr. B. Gallup, who assisted in Phase I and II of the testing programme.

Mr. V.J. Jehu, of Transport Road and Research Laboratory, U.K., who provided warm hospitality upon the author's visit to his research centre and home.

Mr. G. Toth, who administered the large portion of technician time needed for this project. The author is very thankful for the high level of cooperation received from Mr. Toth and his staff.

Mr. G. Spak, who performed all of the welding and who on numerous occasions made repair welding on short notice during his rest periods and lunch hours.

Mr. O. Dalnoki, Mr. M. Makasare, and Mr. J. Zika, all of whom provided some portion of the precision machining and related technical work needed to fabricate the test apparatus.

Mr. G.A. Webster, who enquired about, ordered and delivered all of the low resonance cast aluminum from Alcan Products in Kingston which were used in this study.

Mr. D. Seaman, who administered the numerous equipment purchases and enquiries that were needed before the experimental work was completed.

Mr. B. Carraro, who built the velocity measurement device and who always readily provided advice and help with the electronic problems encountered throughout this research.

Dr. J. Gardner and Mr. C. Lavigne who together provided information, facilities and help during the cement pouring for the floor mounting studs.

Mr. F. Meunier, who helped with the debugging of the velocity measurement device and who occasionally provided the necessary constructive criticism that helped formulate some of the ideas and thoughts behind the manuscript.

Mr. W. Ng, who along with Mr. Meunier had to persevere many of the estimated 1000 noisy impacts of the study. The author wishes to thank both of you for your understanding and comradeship shown during the time we shared the energy conversion laboratory.

Ms. L. Brown, who provided many of the last minute modifications and additions to the thesis typing.

Special thanks are also due to my wife, Heather, who listened with interest to the project problems, who offered encouragement during times of difficulty and laboriously proof read the original hand printed draught of this manuscript.

TABLE OF CONTENTS

Volume I contains Chapters I, II, III, IV, V, VI, VII, VIII and IX

CHAPTER VIII

APPENDICES

CHAPTER I

INTRODUCTION PART (i)

I - 1 HEAD INJURY AND HEADFORMS

The earliest historical records from the Babylonians and Assyrians(1)* indicate that man has been well aware of head injury. These records show man used different forms of head protection to prevent head injury, in battle and game.

The author's interpretation of the field of head injury is shown in Figure 1. This figure flow charts the field of head injury as it relates to head forms.

Part (i) of this introduction will introduce and explain each of the areas shown in Fig. 1.

Part (ii) of the introduction will deal specifically with some of the fundamental questions in the field of head injury and their relation to this study.

As the title of this thesis indicates, the area of headforms in the overall field of head injury is of specific interest. To understand each of the general areas in relation to headforms it is desirable to discuss what is meant by the term headform.

The term headform is used to describe a material that has been contoured to approximate the shape of a human head. In practice, the material may vary from polystyrene foams to wood depending on the purpose of the headform. Headforms are used for such purposes as modelling, helmet testing, crash simulation, the study of anatomy and anthropometry.[1]

---

* Numbers in parentheses designate references at the end of the thesis.

1 Anthropometry is the area of science that deals with study of body measurement.

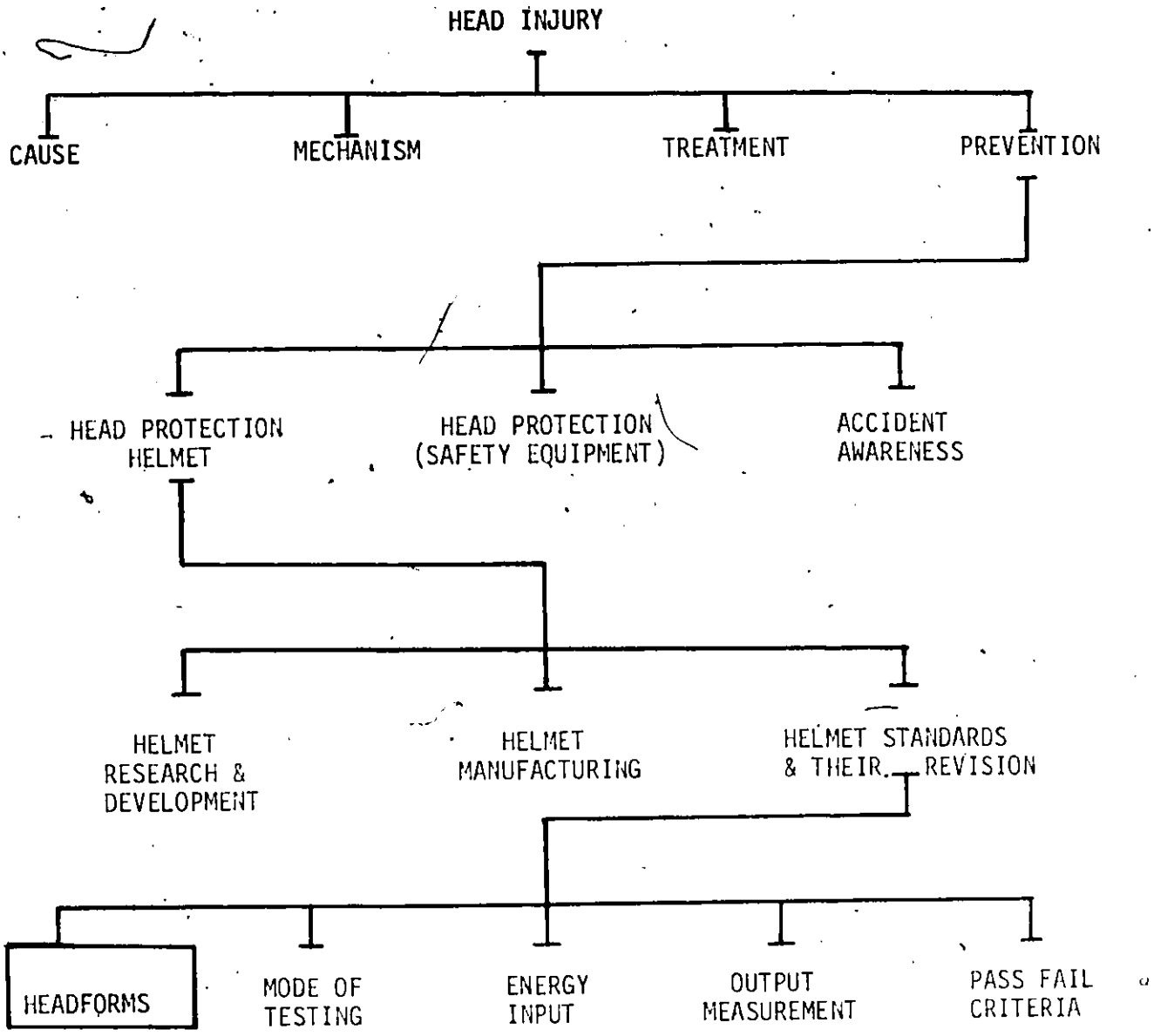

Figure 1

FLOW CHART FOR THE FIELD OF HEAD INJURY

This study has used headforms for all of the above purposes. A description of the purposes and different uses will be found in the chapters to follow.

I - 1 HEAD INJURY

In early periods, head injuries were the result of falls, hunting accidents, games and military operations. In recent times the advent of man's ability to propel himself faster than his own running speed has increased the seriousness and likelihood of head injury. Walker (2) states, "The usual immediate consequences of head injury are an impairment of consciousness and an amnesia for the events preceding and following the blow to the head".

Also according to the glossary of reference (2), two types of head injury occur.

(1) The closed type: Head injury in which continuity of the soft tissue is maintained.

(2) The open type: A head injury in which there is loss of continuity of the soft tissue.

Hodgson, et al. (3), has described in Table 1, head injuries as they relate to linear and angular acceleration.

Table 1—Types of Head Injury

Linear Acceleration	Cerebral Concussion —	Deformation of brain stem through incisura and foramen magnum.
	Brain Stem Injury of Greater Severity Than Concussion —	Includes grossly visible area of injury including hemorrhages.
Angular Acceleration	Cortical Contusion — (Bruise)	(1) Impinging against irregular areas of bone. (2) Cavitation. (3) Slapping effect of bone against underlying brain. (4) Relative movements between bone and brain.
	Laceration — (Tear)	Similar to cortical contusion but more severe.
	Intra Cerebral Hematoma — (Blood Mass)	Mechanisms similar to those causing contusion plus relative movements of brain with tearing of small intracerebral vessels.
	Subdural Hematoma —	(1) Relative movements between bone and brain cause tearing of connecting vessels. (2) Rupturing of cortical vessels from mechanisms similar to contusion.
	Epidural Hematoma —	Usually associated with linear fracture and tear of middle meningeal vessels.

(V.R. Hodgson, et al., "Severity Index", 14th Stapp Car Crash Conference, Pg. 172, Ref. 3)

I - 2 CAUSE OF HEAD INJURY

Head injuries are caused by the head striking an object, or an object striking the head. Either of these cases is usually referred to as a direct impact.

Conversely an indirect impact is a blow to another region of the body that results in a head injury. An example of this is the phenomenon of whiplash.

Head injuries are also caused by crushing type blows where the loading rate is slow.

I - 3 MECHANISM OF HEAD INJURY

Only recently has man had the ability to measure the physical stresses that result from a blow to the head. To understand the magnitude of the forces involved, the dynamics of the energy transfer must be known. By knowing the dynamics of the impact, an evaluation of head protection should be possible using a headform in the simulation of the dynamic mechanism of head injury.

I - 4 TREATMENT OF HEAD INJURY

Head injury involves a very intricate organ, the brain, contained in a multilayered case, the skull. Because of the complexity and delicacy of this organ, even minor trauma can have severe complications. Because of treatment difficulties -- for example entering the skull, head injury is considered one of the most serious injuries that occur to man.

I - 5 PREVENTION OF HEAD INJURY

Due to the seriousness of head injury and the difficulties of treatment, the prevention of head injury remains as one of man's more perplexing problems.

This study will be mainly concerned with the prevention of head injury as it pertains to the use of headforms for protective headgear evaluation.

Prevention of head injury can be divided into three areas: head protection in the form of helmets, head protection in the form of safety equipment and thirdly accident awareness as shown in Figure 1.

I - 6 ACCIDENT AWARENESS

Accidents and injuries can be prevented by programmes that teach safety skills and point out hazards. Such safety programmes are now important parts of driver education, the mining and construction industries, and other sectors where head injury may be of primary concern. To increase the awareness of motorcyclists to hazardous accident situations, Newman and Webster (4) have studied the mechanisms of motorcycle accidents. Papers such as the above are made available to safety programmes for the benefit of instructors and students.

I - 7 HEAD PROTECTION (SAFETY EQUIPMENT)

To see evidence of safety equipment for head protection, one needs only to examine, for example, recent automotive and other human transport interiors. Extensive use of polymeric type foam padding has significantly reduced the possibility of head injury in many previously

hazardous locations. It is worthwhile to point out that many foams used in padding are the same as those used in current helmets.

I - 8 HEAD PROTECTION (HELMET)

Even before 1500 B.C. (5) man realized that head injury could be minimized by using head protective devices that are presently called helmets. Today's helmets are worn in the army, airforce, hockey, construction, baseball, mining, football, motorcycling, car racing, water skiing, parachuting, horse racing, lacrosse, bicycle racing, equestrian events, etc. Each of the above helmet applications has to protect the skull and its contents against a slightly different type of head impact. For instance, football helmets should protect against the low velocity but repetitive high mass type impacts. On the other hand, soldiers' helmets must protect the head against high velocity low mass impacts of projectiles like bullets and shrapnel.

As a result of these different types of impact, a soldier's helmet is not the same as a football helmet. In general, each helmet application has necessitated a design different from that of other applications.

Helmet technology has advanced considerably since ancient times. One needs only to compare helmets worn 20 years ago with current head protection.

This study will deal mainly with the motorcycle safety helmet that is also used in auto racing. Even though significant improvements have been made to this type of helmet, motorcyclists still suffer head

injuries that are often severe or fatal. It is for this reason that researchers in this area continue to look for solutions to the bio-engineering problems associated with head injury where protective head-gear is worn.

The area of head protection with helmets can be divided into three sub-areas: helmet research and development, helmet manufacturing, and thirdly, helmet standards and their revision, as shown in Figure 1.

I - 9 HELMET RESEARCH AND DEVELOPMENT

Helmet research has led to the present helmet which is composed of essentially five main parts: (1) the rigid outer shell , (2) the inner energy absorbing liner, (3) chin strap, (4) face protection shields, visors and bubbles and (5) comfort liner.

There are essentially three main shapes of motorcycle safety helmets as shown in Figure 2. The "Shorty" helmet, the "Jet Style" helmet and the full facial coverage helmet.

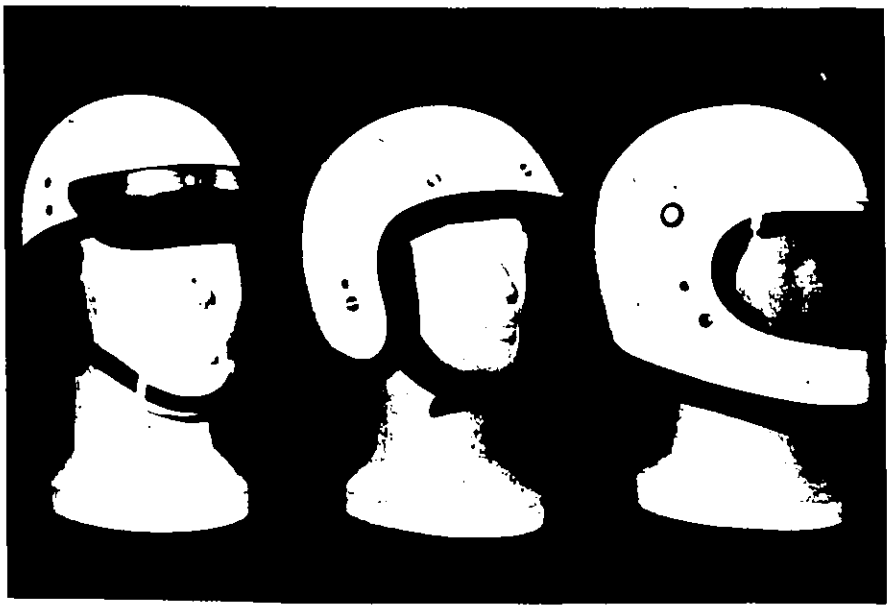

"Shorty", "Jet Style" and "Full Facial Coverage" Helmets

Figure 2

The outer shells of current helmets are usually made from fiberglass or polycarbonate. The inner liner material is usually polystyrene foam.

Snively and Chichester (6) two of the pioneers of helmet research, have listed the following considerations in protective headgear design.

Considerations in Protective Headgear Design

I Protection against penetration and abrasion.
- (A) Low coefficient of friction
- (B) Rigidity
- (C) Shatter resistance.

II Protection against impact.
- (A) Absorption of kinetic energy
  - (1) Low rotational acceleration
  - (2) Low linear acceleration
- (B) Load spreading (rigidity)
- (C) Absence of stress concentration projections

III Protection against physical factors
- (A) Flameproof
- (B) Waterproof
- (C) Weathering resistance
- (D) Electrical resistance

IV Protection against "Loss".
- (A) Harness strength
- (B) Strap strength

V Comfort factors
- (A) Weight
- (B) Bulk
- (C) Fit
- (D) Thermal
- (E) Acoustical

VI Other specialized factors ("Platform for communications, etc.")

The above considerations have proven to be a good starting point in helmet design.

(i) 10 HELMET MANUFACTURING

The fiberglass outer shell helmets are manufactured either by hand or by machine. Polycarbonate helmets are injection molded on a mass production scale. Hence they are somewhat less expensive for the consumer. Most of the manufactures do their own testing according to the various helmet standards. This helmet testing is usually employed in some aspect of quality control.

Photographs of a helmet assembly can be seen in Figure 3 where a polystyrene foam liner is ready to be placed in a polycarbonate outer shell.

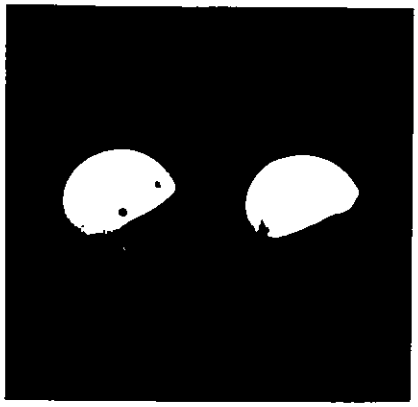

Figure 3

Outershell and Polystyrene Foam Inner Liner

One means of assuring manufacturers produce satisfactory helmets is the legal enforcement of meaningful helmet standards.

(i) 11 MOTORCYCLE HELMET STANDARDS AND THEIR REVISION

Motorcycle helmet performance standards have become law in many countries of the world. These standards require that helmets found in the retail market meet a certain minimum performance requirement. The performance requirements must be designed such that they simulate a typical motorcycle accident helmet impact.

Standards must be continually revised to keep the protective value of helmets improving as new technology and biomechanical data evolves.

One of the purposes of this study is to offer comment to the Canadian Standards Association (CSA) Standards Committee on the present headforms being used in the CSAD-230 motorcycle helmet standard. Comments will also be put forward on a multi-position helmet test apparatus, Figure 3(b) and 3(c), that has been proposed for a revision of the above standard by Newman (7).

Figure 3(b) **Multiposition Mode**

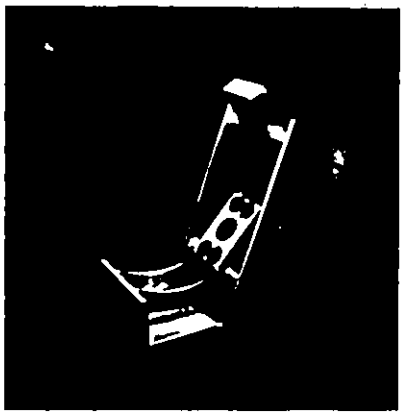

Figure 3(c) **Multiposition Apparatus**

Helmet standards can be broken down into five further subareas as seen in Figure 1: headforms, mode of testing, energy input, output

measurement, and pass fail criteria.

(i) 12 MODE OF TESTING

Whether a weight from a fixed height is dropped on a rigid headform or a headform is dropped from a fixed height onto a rigid anvil depends on the mode of testing. Both of the above modes are employed in motorcycle helmet performance standards. The first mode described is typical of the CSA-D230 standard, the second mode is used in the American National Standard Institute (ANSI) Z90.1 motorcycle helmet performance standard. The multiposition mode which has been proposed by Newman (7) allows for direct impacts to all areas of any helmet using the multiposition mode apparatus Figure 3(c)

(i) 13 THE INPUT ENERGY

The energy input refers to the amount of energy a motorcycle helmet must withstand in a given performance standard. This potential energy is calculated by multiplying the drop height by the weight of the falling mass. At present the energy input usually varies between 66 and 90 ft lbs. According to the particular standard test procedure.

(i) 14 THE OUTPUT MEASUREMENT

The output acceleration signal is usually generated from an accelerometer and the force output signal is generated from a load cell. There exists a number of methods to record such signals. This study uses a polaroid photograph record in conjunction with a storage oscilloscope.

(i) 15 THE PASS FAIL CRITERIA

This portion of the standard is probably the most important, for it determines whether the helmet attenuated the impact energy as dictated by the standard. The pass fail criteria of acceleration is usually expressed in peak g's [1] and time during which acceleration is in excess of some particular value. The load cell criteria is usually referred to as pounds or Newtons of transmitted force.

An in-depth examination of many aspects of the field of head injury that pertain to this study follows in Part(ii) of Chapter 1.

---

1 One g is defined as 32.2 ft sec^{-2}

PART (ii)

(ii) 1 PREVIEW OF PART (ii).

Part (i) has introduced the reader to the field of head injury. Part (ii) will discuss the fundamental questions that result from an investigation of the related literature.

(ii) 2 IS PROTECTIVE HEADGEAR FOR MOTORCYCLISTS NECESSARY?

Thus far it has been assumed that the use of motorcycle safety helmets reduces the chance and the severity of head injury in motorcycle accidents. This assumption has been proven to be fact in over two decades of work by such researchers as Chandler, K.N. and Thompson, J.K.L. (8), Shields, J.B. (9), Buchanan, L.S., and Bischoff, D.C. (10) and Severy, D.M. (11).

(ii) 3 THE CURRENT MAJOR HELMET STANDARDS

Having established the need for motorcycle safety helmets, the regulation of these helmets sold on the open market should next be examined. As mentioned in Part (i) of the introduction, the helmet production industry can be maintained at a certain level of adequacy by the enforcement of helmet standard laws. This study has investigated the latest versions of all the major motorcycle safety helmet standards. These standards are:

Canada 1. Canadian Standards Association (CSA D-230)
2. Quebec Standard (BNQ 1923-901)

U.S.A. 3. Snell Memorial Foundation, 1970

4. American National Standards Institute (ANSI-Z90.1)

5. Motor VEhicle Safety Standard (MVSS 218)

United Kingdom 6. British Standards Institute (BSI-2001, 1972)

International 7. International Organization For Standardization (ISO R1511)

A copy of each of these standards can be found in Appendix C of Reference 7. A summarization of the impact performance criteria of each standard has been placed in Appendix A.

The standard helmet test procedures are mainly concerned with absorption and dissipation of impact energy by a helmet. It can be seen that they also deal with penetration resistance, harness strength, water absorption, flammability, chemical attack, etc. There are also limits for peripheral vision. A further examination of the standards produces a number of fundamental questions.

(ii) 4 THE FUNDAMENTAL QUESTIONS ARISING FROM THE HELMET STANDARDS

1. Is the helmet standard performance test representative of a typical helmet impact involved in a motorcycle accident?

2. Does it matter what material a headform is constructed from?

3. Does it matter what anthropometric headform shape is used?

4. Does it matter if the headform is solid or hollow?

5. Does it matter whether the headform is moving or assumes a rigid, swing away or multiposition semi-rigid mode?

6. Is it necessary to consider the mass of the helmet?

7. Does it matter whether deceleration of the helmeted headform, deceleration of the striker, time duration of deceleration or transmitted force of the helmeted headform is measured as output?

8. Is the pass fail criteria limit representative of known biomechanical data for helmeted human beings?

(ii) 5 THE SIGNIFICANCE OF THE 8 QUESTIONS

The bio-mechanical data in the eighth question refers to the force or energy required to cause head injury. From extensive research conducted on this aspect, the Wayne State University (WSU) Cerebral Concussion Tolerance Curve (12), Figure 4, has resulted as a widely accepted tolerance criteria. This data is a result of cadaver forehead impacts on to hard flat surfaces, and animal tests involving frontal hammer blow and air blasts to the exposed brain. Cadaver skull fracture has been assumed to indicate concussion.

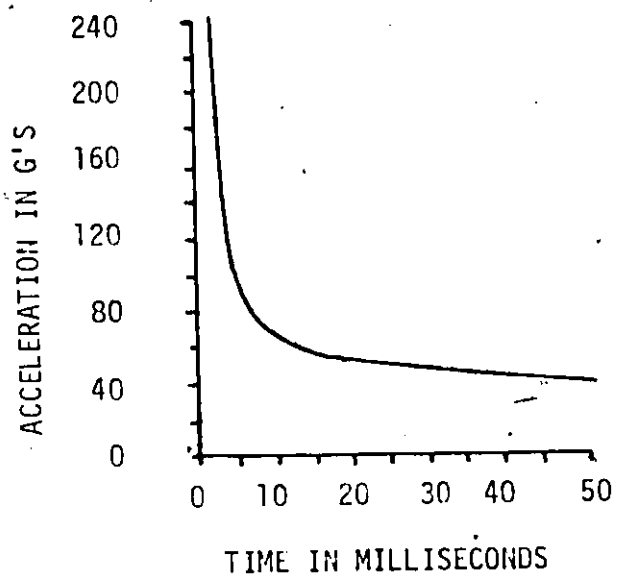

Figure 4. Wayne State University Acceleration-Time Tolerance Curve for Forehead Impact to a Hard Flat Surface.

The ordinate of the WSU Curve, Figure 4, is an indication of head linear acceleration. Effective (average) acceleration is defined as the area under the acceleration-time curve of an impact divided by the time duration of the impact.

The abscissa represents the time duration of the impact.

The figure postulates that man can tolerate average accelerations of about 50 to 60 g in the region of impact exposure above 15 msec. The curve also indicates that man may be able to withstand greater accelerations for time durations less than 5 msec. Even though the WSU tolerance curve was based on forehead tests, due to lack of better data it has been applied as a tolerance curve for the entire head.

An alternative tolerance limit criterion was proposed by Eiband (13), Figure 5, but for reasons similar to those described by Versace (14) it was never widely accepted. Gadd (15) proposed a third tolerance criterion based on the WSU curve and Eibands log-log plot, Figure 5. The Gadd criterion is represented by a straight line approximation of the data plotted in Figure 5. The Gadd Severity Index (GSI) is based on the argument that head injury severity is related to head acceleration and pulse time duration and can be expressed mathematically as

$$GSI = \int a^n \, dt$$

where

a = acceleration
n = weighting factor > 1
t = time, sec

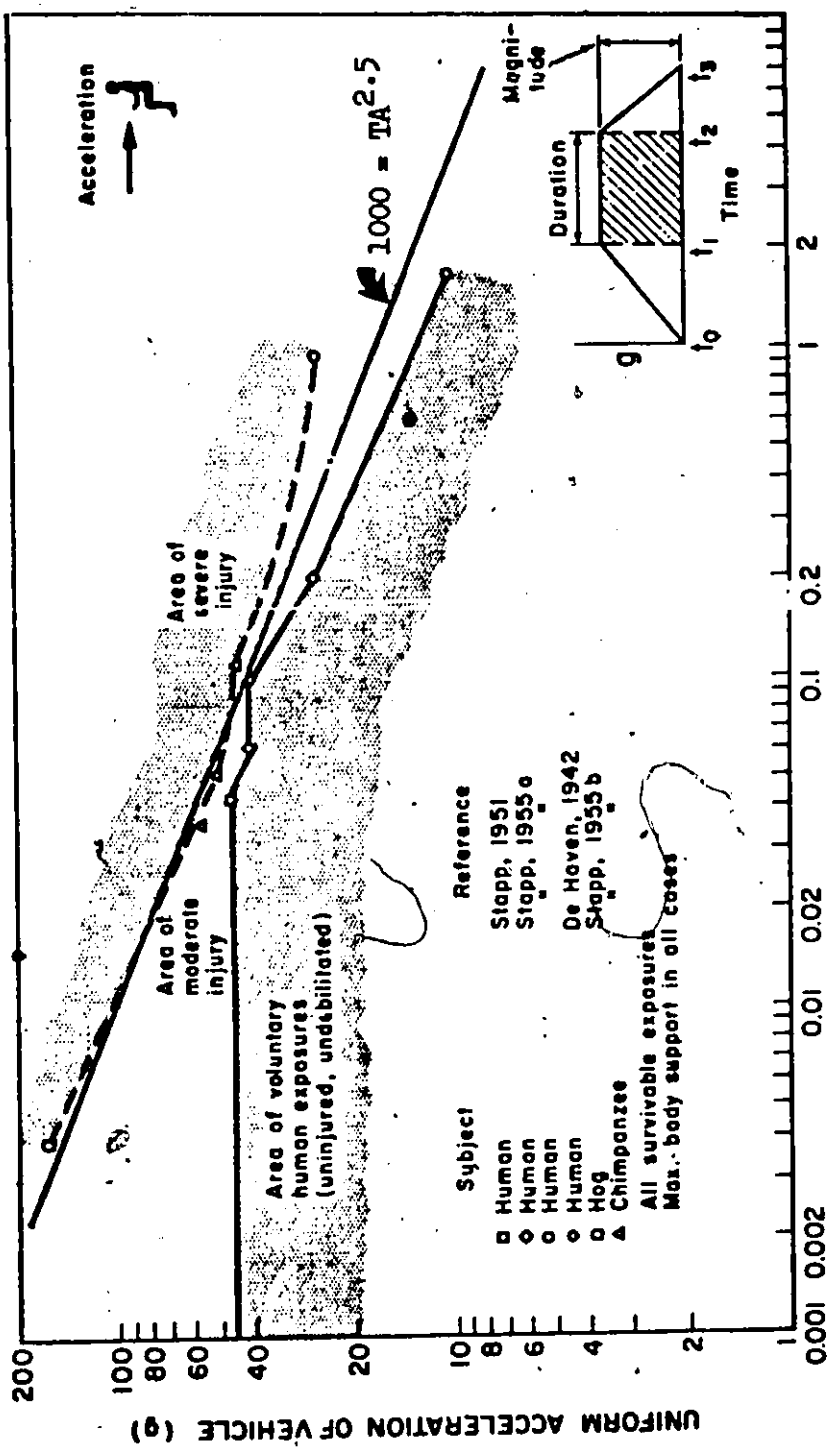

Figure 5 (Frontal Deceleration)

(Versace, J., Review of Severity Index, 15th Stapp Car Crash Conference, Pg. 774, Ref. 14)

The weighting factor n was established to be 2.5 based on the slope of the straight line in Figure 5. Gadd stated, danger to life exists, if integration of an acceleration-time pulse, of a human head model yields a value greater than 1000. Hodgson, et al. (3) stated that the Gadd severity index should be used in conjunction with a family of curves, Figure 6.

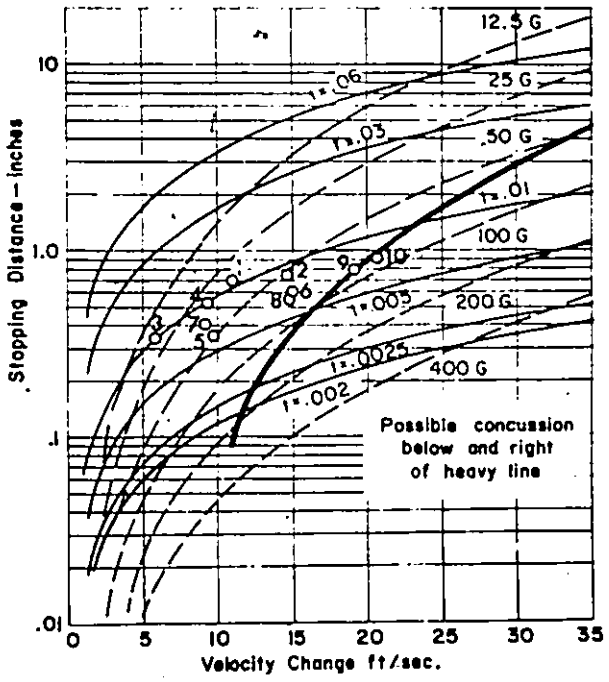

—Theoretical uniform acceleration and pulse time for combinations of velocity change and stopping distance, with superimposed WSU acceleration-time tolerance curve for cerebral concussion. Velocity change and displacement for 10 impacts to the padded or helmeted cadaver are plotted. Compare predicted effective (uniform) acceleration and pulse duration with tabulation values in Table 3 (Hodgson, V.R., et al., 14th Stapp Car Crash Conference, Pg. 181, Ref. 3)

Figure 6.

The curves shown are for uniform accelerations ranging from 12.5 - 400 G and for time durations ranging from 2.0 msec to 60 msec. for various stopping distance and velocity changes. Superimposed on this plot is the WSU tolerance curve. Hodgson considered concussion to

occur for any combination of uniform deceleration and time duration or velocity change and stopping distance to the right and below the WSU Tolerance Curve.

Once again, for reasons similar to those stated by Versace (14) the Gadd Severity index used either by itself or with Hodgson's curves has never been widely accepted as a head tolerance criterion that may be applied to the pass fail criteria of a Helmet Standard.

The Gadd severity index has become the basis of yet another Tolerance Criterion known as the head injury criterion (HIC). This criterion proposed by Versace, can be stated mathematically as

$$HIC = \left[\frac{\int_{t_1}^{t_2} a \, dt}{t_2 - t_1} \right]^{2.5} - (t_2 - t_1) \leq 1000$$

where

a is resultant head form acceleration expressed in g's

t_1 and t_2 are any two points in time which maximize HIC.

It was proposed to become the pass fail criteria of the Department of Transport of the United States for a new Helmet Standard FMVSS 208 similar to the present Z 90.1 standard.

Because of difficulties in handling the HIC equation analytically, without the use of analog to digital conversion it was changed to the present MVSS 218 Standard. Time duration over a specified acceleration is now the pass fail criteria as can be seen in Appendix A.

Slattenschek (16) introduced yet another injury criterion that is now called the Vienna Institute Index (JTI). This criterion is based

on a single degree-of-freedom vibration model.

Assuming critical damping, $\beta = 1$ with two triangular acceleration pulses determined from the Wayne State Tolerance Curve, the maximum tolerance displacement $x_{to\omega} = .092$ (2.35 mm) inches was obtained for a natural frequency value of $\omega = 635 \frac{rad}{sec}$ from the equation:

$$\ddot{x} + 2\beta\omega \dot{x} + \omega^2 x = \ddot{y}(t)$$

where

x = relative displacement of brain mass to skull

$\dot{x}$, $\ddot{x}$ = relative velocity and relative acceleration

ω = natural angular frequency of vibration 635 rad/sec

β = viscous damping coefficient at 1.0

$\ddot{y}(t)$ = acceleration pulse measured at the head

The maximum deviation between the model and the Wayne State Tolerance Curve was observed to be 4.0%

Am amplitude X_{max} which corresponded to the acceleration pulse analysed was determined from the model and compared to the maximum tolerable displacement $X_{tol_r} = .092$ inches. The ratio of these two quantities has been called the J Tolerance Index:

$$J = \frac{X_{max}}{X_{tolr}}$$

where

X_{max} = maximum X generated by the model for a given acceleration pulse

X_{tolr} = tolerable amplitude from the Wayne State Tolerance Curve .092 inches.

Impacts with $J = 1$ were said to just reach the threshold of human tolerance; $J < 1$ in the worst cases could cause cerebral concussion without permanent after-effects; $J > 1$ are considered to be hazardous to life.

Brinn and Staffield (17) proposed the effective displacement index (EDI). This criterion has been succinctly summarized by McElhaney (18). The EDI criterion was similar to the Vienna Institute model with changed damping and angular frequency.

A modification of the Vienna Institute model was introduced by Fan (19). The revised brain model (RBM) like the (JTI) is a single degree-of-freedom mass-spring-dashpot model of the brain. McElhaney has summarized the RBM as follows: "The viscous damping coefficient for this model was estimated from published values of brain material properties. With an estimated damping coefficient of 0.4, data from the Wayne State Tolerance Curve for long duration impacts,a natural frequency of 175 rad/sec and the theoretical tolerable brain deformation (S_d) of 1.25 inches was estimated. A tolerable brain velocity $\dot{S}_v$ was then calculated from the Wayne State Tolerance Curve for short pulse duration and was found to be 135.3 in/sec.

The recommended measure of brain injury potential is $\dot{x} < \dot{S}_v$ for impact pulse durations less than 20 msec and $x < S_d$ for pulse durations greater than 20 msec, as calculated from the differential equation of the Slattenshek Model with revised coefficients.

McElhaney et al. has compared the major criteria with his own criterion, the mean strain criterion (MSC) which considers the total

linear acceleration history of the head for a single injury mechanism.

McElhaney determined the dynamic structural characteristics of the skull and brain of rhesus monkeys by measuring the change in mechanical impedance (force/velocity) with frequency. The model treated the head and brains as a two mass system coupled by a spring dashpot.

McElhaney found that the predicted dynamic response of the model agreed with experimental data. Experimental impacts to the heads of various size primates showed that the dynamic model postulated on the basis of vibration studies accurately predicted head-impact injuries. It was also found for head impacts of a known magnitude, that the results could be grouped by comparing the mean strain (displacement of one side of the head relative to the other, divided by the distance across the cranium) as predicted by the theoretical model with injury levels. Using the values of predicted strain in the rhesus monkey head as a criterion of injury, a tolerance curve, Figure 8, was established that related average acceleration and time for constant levels of mean strain.

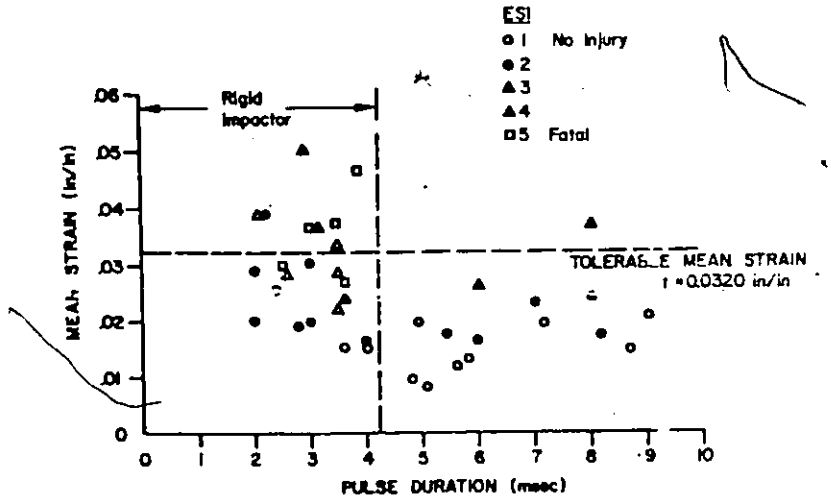

MSC strain levels for rhesus head impacts variable direction and pulse duration.

Figure 8.

(McElhaney, J.H., et al, Human Impact Response, Pg. 87, Ref. 18)

The heads of several species of subhuman primates, squirrel monkeys, rhesus monkeys, the chimpanzee and the fresh human cadaver were found to have mechanical impedance characteristics over a broad frequency band (5 to 5000 H_z) which were similar in shape but differed in mass, stiffness and damping.

These laboratory impacts using maximum predicted strain as a basis for injury formed the basis for establishing modeling relationships through which extrapolation to human heads could be made. Tests were conducted to compare the MSC to human volunteer and fresh cadaver head impacts. The results are shown in Figure 9.

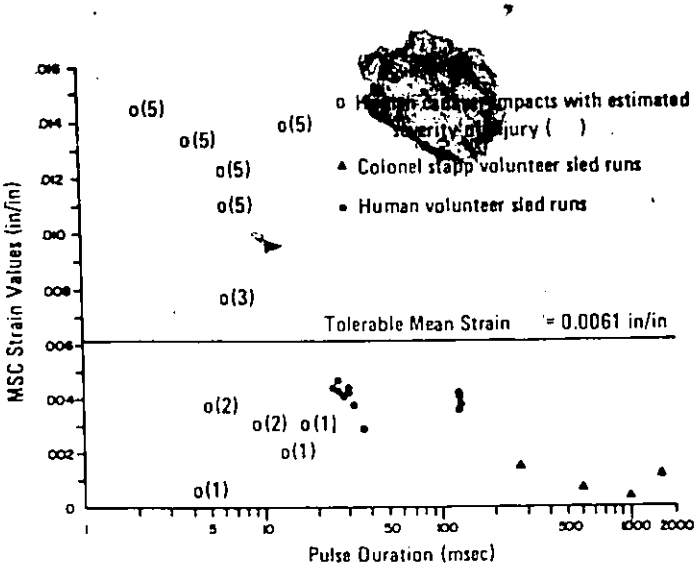

Mean strain criterion for humans vs pulse duration.

Figure 9

(McElhaney, J.H., et al, Human Impact Response, Pg. 88, Ref. 18)

Thirty rhesus monkeys were impacted at frontal, side, crown and mid-frontal. The impact levels were increased until autopsy studies determined that an estimated severity of injury (ESI) of a moderate reversible, closed type, Class 3, was obtained.

The mechanical impedance for five similar monkeys was obtained, Figure 10, for crown, side, occipital, and frontal regions of the head.

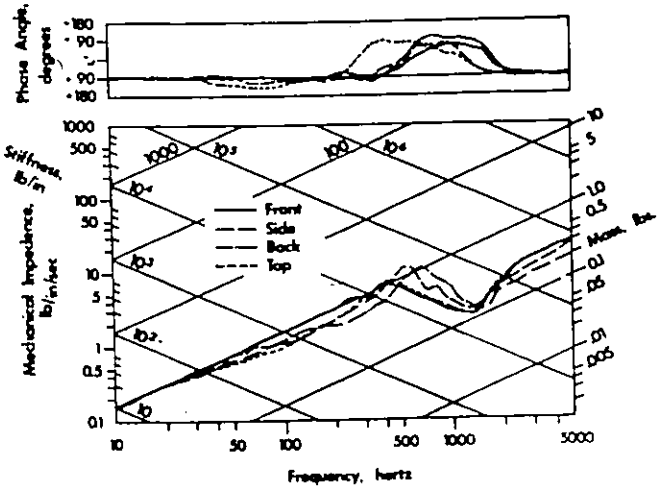

Mechanical impedance of rhesus monkey head.

(McElhaney, J.H., et al, Human Impact Response, Pg. 88, Ref. 18)
Figure 10

Widely varying accelerations were required to produce an injury level of 3 in the rhesus monkey, while the corresponding strains were approximately equal. These results were plotted by McElhaney in the form of an acceleration surface, Figure 11, and a table, Table 2 , for a strain level of .032 in/in.

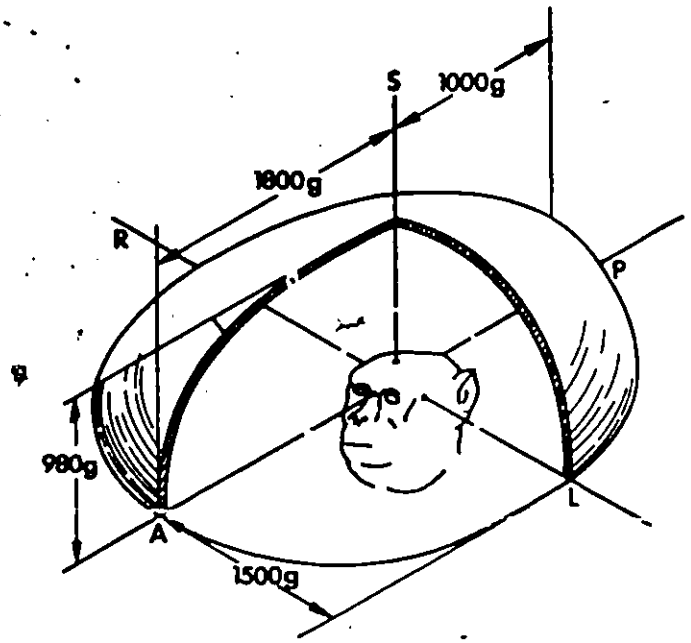

Critical acceleration surface for rhesus monkey, injury index = 3.

(McElhaney, J.H., et al, Human Impact Response, Pg. 89, Ref. 18)

Figure 11

Results of Rhesus Monkey Head Impacts and Impedance Tests

Direction of Head Impact	Acceleration (G's)	Pulse Duration (msec)	Model Constants				Mean Strain e
			w_1	k	c	w_2	
Front	1800	3.6	.051	39,000	1.6	1.1	0.032
Side	1500	2.8	.040	33,000	2.1	1.0	0.032
Top	980	7.0	.030	18,000	1.2	0.9	0.032
Back	1000	3.4	.035	20,000	2.9	1.1	0.032

(McElhaney, J.H., et al, Human Impact Response, Pg. 89, Ref. 18)

Table 2

McElhaney stated: "A sufficient number of impact tests and driving point impedance measurements have not yet been made to verify a direct extrapolation of rhesus monkey data".

McElhaney has shown (Figures 12 and 13) a mechanical impedance comparison between fresh human cadaver heads and the Sierra and Alderson headforms. Predicted and measured values of MSC for human head impacts in the sagital plane are shown in Figure 14(a).

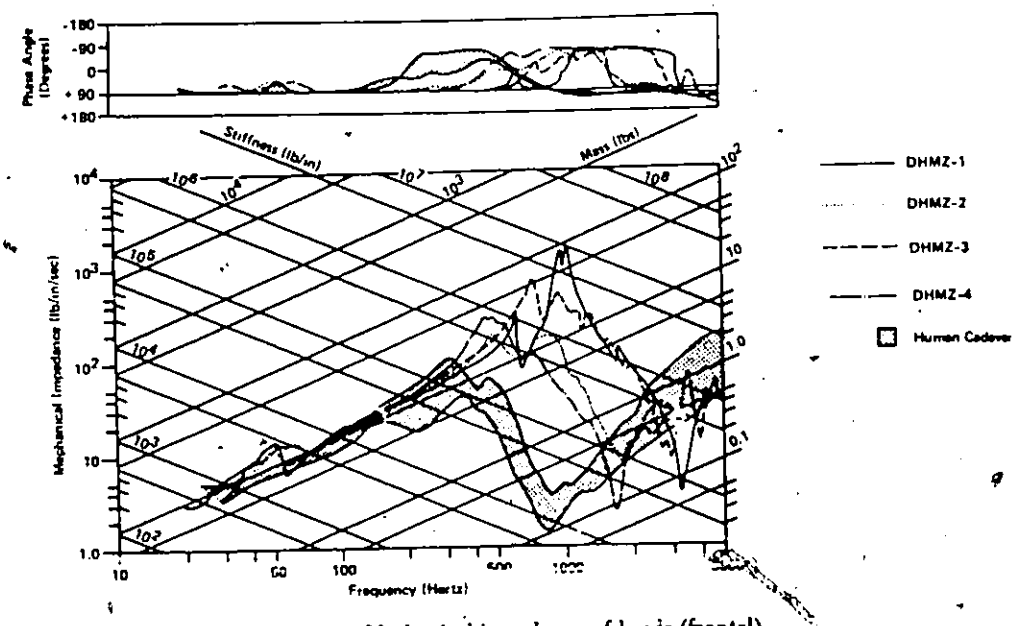

Mechanical impedance of heads (frontal).

(McElhaney, J.H., et al, Human Impact Response, Pg. 90, Ref. 18)

Figure 12

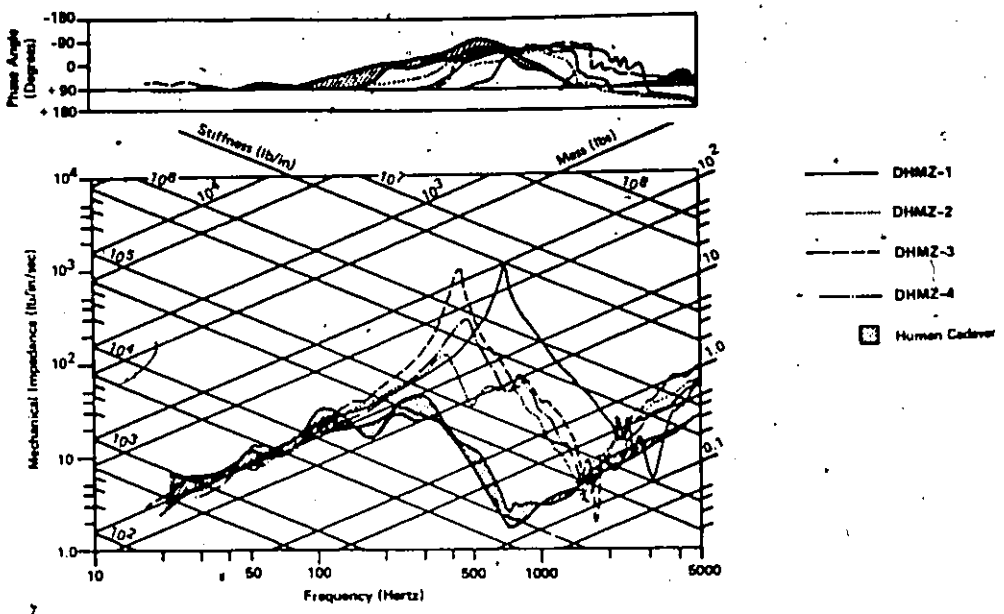

Mechanical impedance of heads (parietal).

(McElhaney, J.H., et al, Human Impact Response, Pg. 90, Ref. 18)

Figure 13

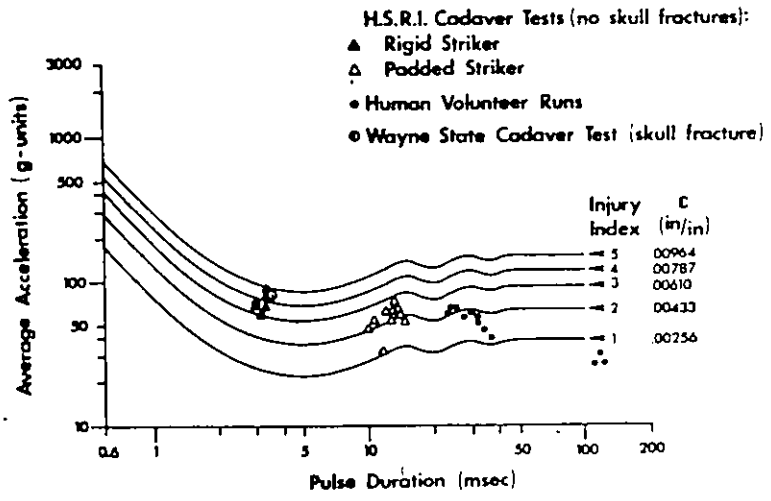

Mean strain criterion for humans, sagittal plane loading.

Figure 14 (a)

(McElhaney, J.H., et al., Human Impact Response, Pg. 91, Ref. 18)

McElhaney tabulated the results of the comparison of the major criteria in Figure 14 (b) and Table 3.

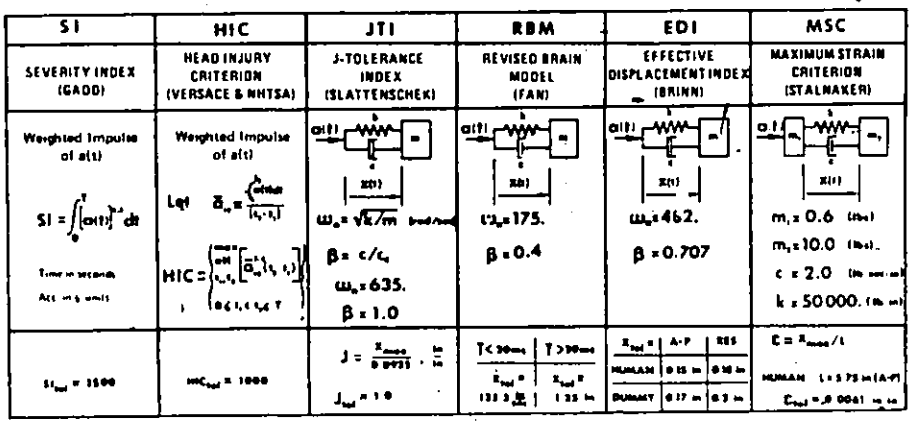

SI	HIC	JTI	RBM	EDI	MSC
SEVERITY INDEX (GADD)	HEAD INJURY CRITERION (VERSACE & NHTSA)	J-TOLERANCE INDEX (SLATTENSCHEK)	REVISED BRAIN MODEL (FAN)	EFFECTIVE DISPLACEMENT INDEX (BRINN)	MAXIMUM STRAIN CRITERION (STALNAKER)
Weighted Impulse of a(t)	Weighted Impulse of a(t)	$\omega_n = \sqrt{k/m}$	$\omega_n = 175.$	$\omega_n = 462.$	$m_1 = 0.6$
$SI = \int_0^T [a(t)]^{2.5}\,dt$		$\beta = c/c_c$	$\beta = 0.4$	$\beta = 0.707$	$m_2 = 10.0$
		$\omega_n = 635.$			$c = 2.0$
		$\beta = 1.0$			$k = 50000.$

Summary of head injury criteria.

Figure 14 (b)

(McElhaney, J.H., et al., Human Impact Response, Pg. 94, Ref. 18)

Summary of Head Injury Indice Comparisons

Pulse I.D.	Acceleration Pulse		GSI	HIC		HIC	JTI	RBM	EDI	MSC
	Duration (msec)	Peak (g's)		Duration (msec)	Aver. Accel. (g's)					
Sine	10	100	458	7.8	83	415	0.853	–	0.146	.0039
Triang	10	100	286	5.7	72	247	0.691	–	0.118	.0045
Square	10	100	1000	10.0	100	1000	1.026	–	0.172	.0061

(McElhaney, J.H., et al., Human Impact Response, Pg. 95, Ref. 18)

Table 3

The McElhaney study has shown that driving point impedance tests indicate the primate head may be modeled by a two-mass system. Injury levels associated with blunt impacts can be related to this system. The MSC model shows decreasing tolerance with pulse durations 10 times the resonant period or less. For pulses longer, then 10 times the resonant period with the MSC, EDI, JTI and RBM, a quasi-static response results that is unaffected by increasing the pulse duration. The SI and HIC indicate that a quasi-static result can never be produced.

McElhaney states "With all simple models of complex phenomena, extrapolation of model predictions beyond the range of validation or to new situations is dangerous and should be done with caution. The MSC model has been developed for blunt impacts where the amount of bone and scalp in contact with the impactor approximates that loaded by the coupling clamp during impedance tests. When the loads are applied to large sections of the head or through the neck, many of the arguments used in the model development do not apply. In addition, it is probable that the injury mechanisms change considerably with these different types of loading and a single mechanism model as are all the ones discussed in this paper would be inadequate.

The impact data provides bands of responses. The variation in these bands is due primarily to the normal inherent biological differences in cadavers". McElhaney intended that his information, "form part of a crash device performance specification that will result in a human analogue with human-like responses. The fresh cadaver has no

muscle tone, however, and the responses reported here represent a bound on human behavior with joint stiffness somewhat lower than in the anesthetized human".

In summary, with respect to the fundamental question #8, it can be said that there exists a lack of bio-mechanical data for the entire head. The existing data is not comprehensive enough to be used as a pass fail criteria for helmet standards.

The inability to use the present data as a pass fail criteria necessitated an attempt to further substantiate the WSU curve using a different approach.

To further substantiate the WSU curve, more live human testing is needed. One way of using live test subjects is through the intensive investigation of motorcycle accidents. Hence, the author has taken part in a motorcycle accident investigation team in the Ottawa and surrounding area during the summers of 1973 and 1974. This accident investigation team was headed by Dr. J.A. Newman, Associate Professor of Mechanical Engineering at the University of Ottawa. Some of the results of this continuing research can be found in references (4 and 7). During these two summers, special attention was paid to understanding the role of the motorcycle helmet in the crash dynamics of each motorcycle accident. Where helmet impacts occurred, an attempt was made to purchase these helmets from their owners. Approximately 50 helmets have been accumulated and scrutinized. It was found that studying helmet deformations with the idea of predicting the accident forces

led to inconclusive results as to how much energy the helmet absorbed. Two conclusions were drawn from this approach. Firstly, there seemed to be a need to do helmet-headform impact testing with known quantities of impact energy. The testing would use new helmets identical to those involved in each motorcycle accident where a head impact occurred. By examining deformation of the known impact energies a cross reference to the crash dynamics and original helmet deformations could be obtained. The second conclusion evolved from the first conclusion. Secondly, to use headforms in an analysis of this type meant that a great deal more knowledge would have to be obtained concerning the use of headforms. More specifically this meant to answer the fundamental question 8; answers first had to be obtained for questions 2 through 7, involving headforms. Thus again the need to study headforms becomes apparent. Furthermore, the regulation of helmet production with helmet standards only becomes meaningful when the standards use headforms that have bio-mechanical performance characteristics similar to the human head. Scalone (20) and Hodgson (3) also indicate the need for further headform testing. By answering questions 2-7 and gaining familiarity with question 8, an answer to question 1 should result.

CHAPTER II

(II) 1 PREVIEW OF CHAPTER II

In parts (i) and (ii) of the introduction, the field of head injury and the fundamental questions of the field were discussed. Chapter II will elaborate on the work done by other researchers with regard to the questions concerning testing headforms or cadaver heads. These questions deal with the mass, shape, material, mode, and response to impact. To assist the reader in following medical terminology, involving regions of the skull, a diagram showing these regions has been included in Appendix (E).

(II) 2 RELATED HEADFORM AND CADAVER HEAD RESEARCH

Hodgson, Mason and Thomas (21,22) developed a human head model to evaluate impact attenuation properties of football helmets with the additional applicability to motor vehicle safety tests. The headform model is probably one of the best approximations to a human head developed to date. Unfortunately, one of these models could not be obtained for this study. The model was molded from self-skinning urethane foam using silicon rubber molds. To simulate the brain, a rubber gel material was used. The skull and mandible were overlayed with a repairable silicon rubber skin. A flexible steel cable, fastened to the foramen magnum, gave the silicon rubber cylindrical neck an adjustable flexibility. Head response to free fall impact was obtained using a triaxial accelerometer mounted at the head, centre of gravity (C of g).

Static load-deflection and football helmeted impact tests on the models and cadaver heads led to one model that compared favourably with cadaver tests. The model was said to be, "Rugged repeatable, and practical to use in situations where either protection is worn on the head or a frangible headform is desired".

Hodgson's study has attempted to prove that, at a fixed drop height of 48 in. (1.22 m), the headform model compares closely with the cadaver head. The study investigates only one other solid metal headform at different drop heights (20 to 55 ins.). The study does not investigate a number of other headforms currently available. It may well be that other headforms would compare equally as well for helmet impact attenuation.

Hodgson states that in the 7 to 10 msec region of time duration, the effect of the neck plays a minor role. An interesting extension of this work would investigate the effect of taping the headform and helmet to the drop frame in the same manner used for the cadaver head tests. The Hodgson study does offer valuable comparative data.

Stalnaker, McElhaney and Roberts (23) compared driving point impedance (DPI) and transfer point impedance (TPI) of five dummy heads (Alderson ceramic head, Alderson VIP 50 head, Sierra wooden head, Sierra 1050 head and HSRI prototype head) with freshly embalmed cadaver heads. These investigators indicate they chose impedance as the appropriate dynamic test, "because the stiffened, effective mass and damping of the dummy's head can be compared directly to that of a human cadaver over a

wide frequency range". The investigation used an electrodynamic shaker attached successively to the parietal, frontal and occipital regions of headforms of dummies and heads of cadavers. These essentially quasi static tests were carried out for a range of peak accelerations of (5-20) g's for frequencies of 30 to 5000 Hz. The results of this investigation is more suited to the dynamic behaviour of heads on dummies used in vehicle crash simulation. The tests do not attempt to predict the performance of helmeted headforms involved in impact tests.

Hubbard and McLeod (24), described the design and development of a crash test dummy head. In this work the headforms were dropped without helmets onto a flat anvil, for impact evaluation. The results of the impacts were compared with biomechanical data established by Hodgson et al (21) for cadaver head drop tests. The results were found to be within the 225-275 g range set down by the Hodgson investigation for a 14.8" drop height. This work does not examine their test headform for drop heights between 1.0-2.5m with helmets or with other surfaces. This testing could not have been done with the set-up as it was described. The set-up dropped just the headform from 14.8". For heights greater than 14.8" the rotation of the headform before impact would become significant.

This paper (24) considers the effect of the neck. Hubbard and McLeod point out that Hodgson found the neck had little effect on the response of the head when whole cadavers were dropped onto frontal regions of the head. This is one reason why the Hubbard and McLeod

investigation did not use any portion of a neck on their model.

Nahum, Gatts, Gadd and Danforth (25) investigated the forces required for cadaver skull fracture under localized loading. They found clinically significant fractures that appeared independent of impulse duration occurring at:

Frontal Area	1100 lbs
Temporparietal Area	550 lbs
Zygomatic	225 lbs

The Nahum et al. study found no difference due to embalming for the above areas impacted using cadavers embalmed for up to one year. The study also found the cadaver neck to play a minor role at impact when the occipital region was supported by soft foam rubber pad of 4-5 inches.

The Nahum study compared force at the impact site with acceleration from an occipital mounted accelerometer. They found the g reading higher than the ($F = ma$) relation would indicate. However, when they used a rigid metal block for the head, there was agreement within a few percent.

The Nahum study found that the sex of the test subject was the most important variable they observed. The test values of the female subjects were found to be consistently at the lower end of the tolerance scale. This suggests that the female cadaver head is not as rigid or stiff as the male cadaver head.

The above paper will provide useful comparitive data for the cadaver head impact tests and data for calibration comparison of load cell and accelerometer for Newton's second law relationship ($F = ma$).

In the work mentioned, none of the investigation has offered comprehensive testing and evaluation to answer the posed fundamental questions concerning headforms.

Therefore, it is the object of this thesis to answer these questions, in an attempt to prove or disprove the null hypothesis: that it does not matter what headform combination of shape, mass, material or mode of testing is used for helmet standards.

CHAPTER III

III-1 PREVIEW OF CHAPTER III

Having examined other investigators' work regarding headforms, the position was reached enabling development of tests to provide answers to the headform questions that will prove or disprove the previously mentioned null hypothesis.

III-2 RATIONALE FOR DESIGN AND CHOICE OF BASIC EQUIPMENT

It was decided that a test apparatus would be set up to provide experience in problems associated with testing of the various helmet standards. The design criteria of this apparatus was as follows:

(1) The apparatus must test CSA Z90.1, BNQ, MVSS 218, Snell, and be adaptable in future for the ISO, and BSI-2001 standards.

(2) The apparatus must fit within the bounds of an eleven foot ceiling height.

(3) The instrumentation must also be flexible enough to be used for all of the above standards.

(4) The apparatus should also be adaptable for impact testing of various materials.

The following design, Figure 15 and Figure 16, was chosen on the basis of cost, accessibility, ease of maintenance, vibrational considerations, ease of construction, and the design criteria previously mentioned.

The apparatus as shown in Figures 15 and 16 consists of a drop frame that when released by a solenoid bolt action, falls downwards. The path of fall is guided by the guide wires. To reduce friction between the guide wires and the drop frame, nylon bushings were used. Thus if the frictional forces are small, essentially free fall conditions will exist.

The falling striker impacts the test object secured to the anvil that is in turn bolted to the floor.

In Figure 15 some of the recording equipment used to monitor the output signals is also shown.

Test Apparatus and Recording Equipment

Figure 15

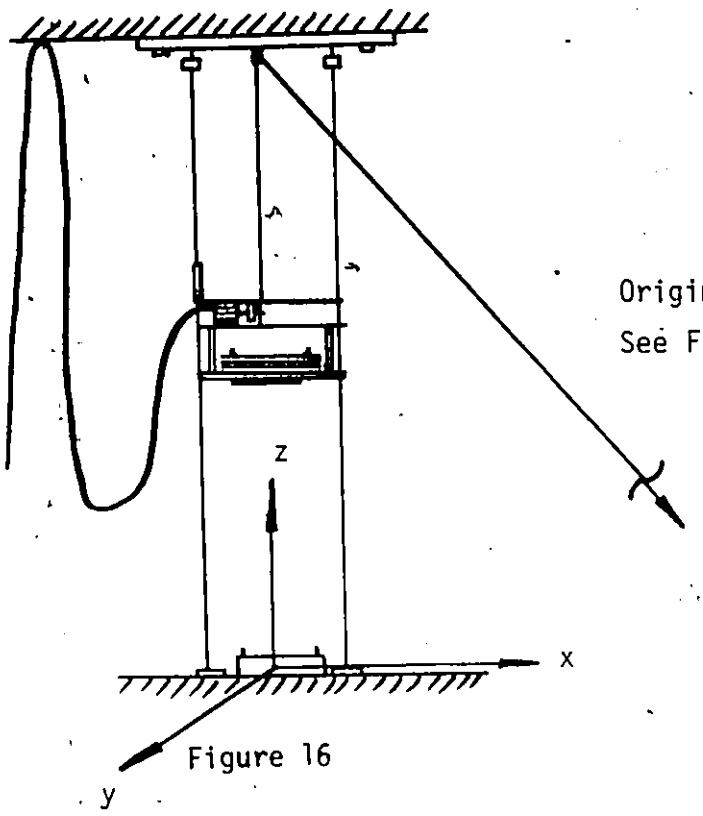

Figure 16

To comply with the CSA standard, an Endevco load cell Model #2106E, Appendix C, was obtained. To accommodate acceleration requirements of the remaining standards, an Endevco accelerometer Model #2275 M15, Appendix D, was acquired.

The load cell was mounted to a 2" hot rolled steel plate, Figures 17, 18 and 19, by a high tensile one-half inch steel bolt, torqued to a specified 70 ft. lbs. The load cell, as can be seen, was torqued between two flat, ground surfaces. The bottom plate was mounted to the floor by four lag bolts encased in lead anchors. To minimize interface problems between the cement floor and the bottom plate, a 1/8" lead sheet was used. The upper surface of the top mounting plate was also a ground surface to minimize interface problems.

Figure 17

Position of Load Cell on Bottom Plate.

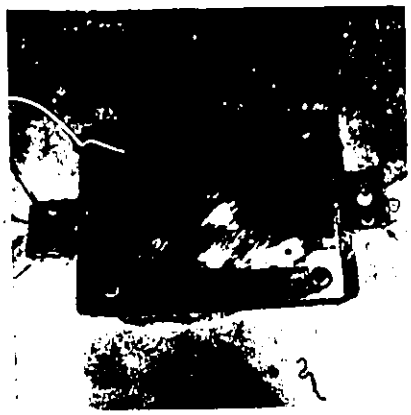

Figure 18

Top Mounting Plate Torqued to Bottom Plate.

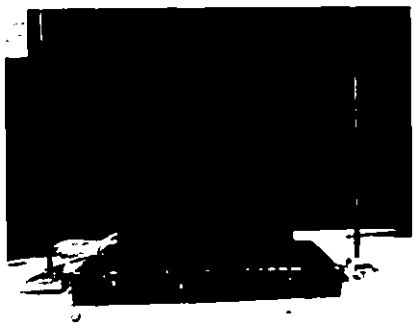

Figure 19

Front view Showing Top Mounting Plate Supported only by the Loadcell.

Three ground plates, Figure 20, to be bolted to the mounting plate were also machined. One plate is merely a flat plate, the second plate is a flat plate with a hole to accommodate the hemispherical anvil of the Z90.1 standard. The third plate has been fabricated to be used with the modular elastomer programmer (MEP)* calibration pad.

The Three Impact Plates which were fastened to the top Mounting Plate.
Figure 20

To release the drop frame, a solenoid release mechanism was contrived and fabricated; Figure 21 illustrates this feature.

---

* The comparison between the force-time traces of the load cell and of the accelerometer was made with the aid of an American elastic energy absorber known as the Modular Elastomer Programmer (MEP). It consists of a rubber-like material 152 mm in diameter and 19 mm thick at its periphery, rising to a maximum thickness of 25 mm at its centre. The material is bonded to a metal base plate. Successive blows of the same initial conditions produce repeatable force-time and acceleration-time curves.

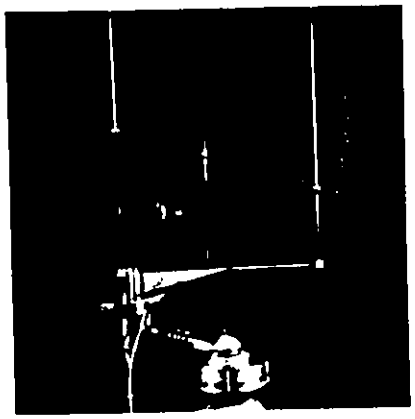

Solenoid Drop Release

Figure 21

This release mechanism has one slight fault. An activation of the solenoid produces a side thrust in the X-direction.

The accelerometer and load cell signals were relayed to a 2-channel model 5103N Tektronix oscilloscope. The oscilloscope has provisions for either internal or external triggering for storage and polaroid recording.

A drop frame, Figure 22, was built for preliminary test purposes. The frame had the accelerometer torqued to the factory specification of 18 in lb. and positioned to coincide with the Z-axis of the load cell, and the plane of the guide wires, Figure 16. The drop frame, Figure 22, also had a variable weight capability by adding or subtracting 0.5 kg bars.

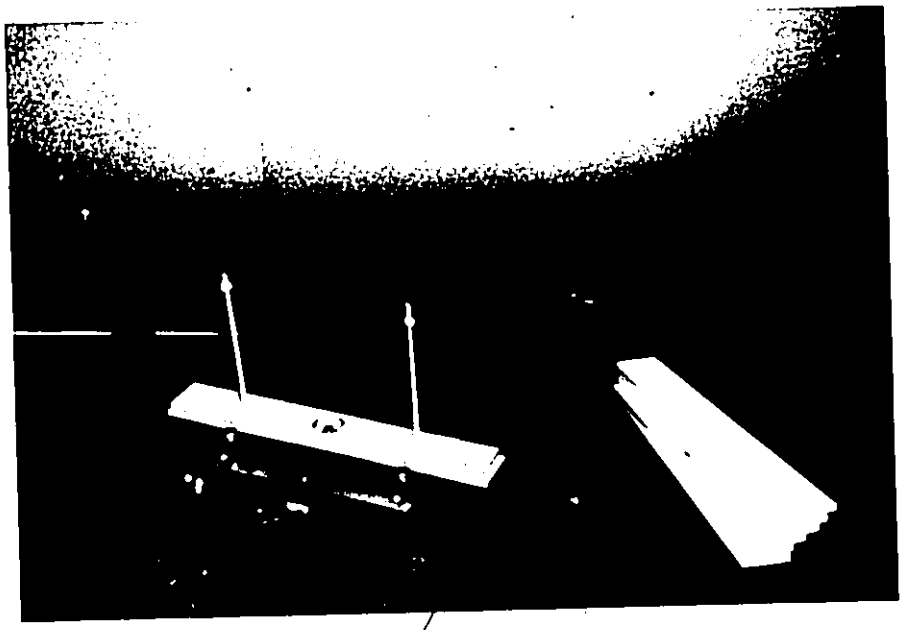

Preliminary Drop Frame and Additional Weights

Figure 22

A flat impact surface was chosen on the basis that it most closely approximated the majority of surfaces impacted by helmets during accidents.

(III) 3 PRELIMINARY TESTING

With the drop apparatus shown in Figure 16, a number of tests were carried out impacting various materials between the flat plate, Figure 20, and the drop frame plate, Figure 22.

The following problems were encountered:

(1) The input impedance of the oscilloscope was not sufficient to maintain the charge on the load cell and accelerometer after impact.

(2) There seemed to be an inconsistent D.C. offset following peak acceleration for the accelerometer signal.

(3) The drop frame, Figure 22, resonated badly upon impacting any semi-rigid or rigid material, making the accelerometer trace useless.

(4) The base plate was not flat by 1/8 in. in 12 ins. for the X-direction shown in Figure 23.

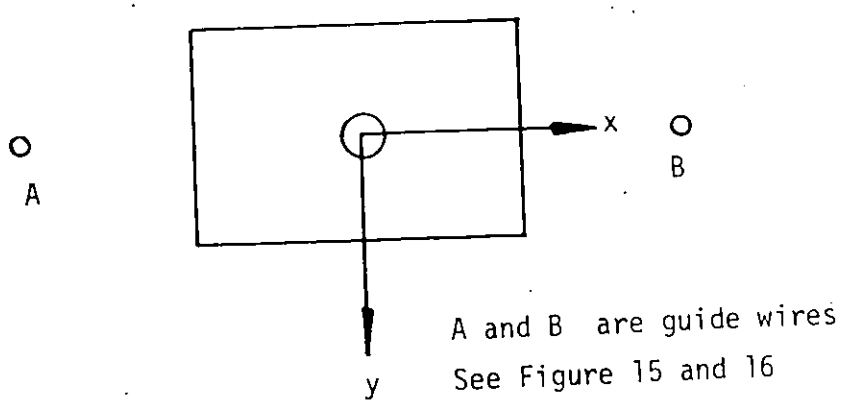

Figure 23

(5) The internal trigger of the oscilloscope could not trigger soon enough to show the important initial slope of the acceleration wave form.

(6) The solenoid on the drop release prematurely triggered both the internal and external trigger of the oscilloscope.

(7) The guide wires could not be put into sufficient tension to overcome the bending moments associated with impacts that do not have zero tangential slope with the highest point of a headform or helmeted headform and the impactor.

Each of the Problems 1-7 were solved in the following manner:

(1) Two Bruel and Kjaer amplifiers were used, one with a fixed gain of unity for the accelerometer and the second with a gain of - 100 for the load cell. The 3000 mΩ input impedance of the amplifiers was adequate in preserving the charge on the two crystal type transducers.

(2) It was found that this offset phenomenon was due to an improperly grounded accelerometer case. The case was grounded and the apparent offset disappeared.

(3) Due to the resonant effects of the drop frame, Figure 22, the apparatus was discarded. It was then decided to use the drop frame of the Z90.1 standard with its ball and socket apparatus in conjunction with aluminium discs of different weights. Four aluminium discs, Figures 24 and 25, were fabricated. From left to right they are:

The Four Impactors Used with the Z90.1 Drop Frame
Figure 24

Figure 25

(1) A disc to be used with the modular elastomer programmer (MEP) calibration pad; the total weight of disc and MEP is 5 kg (11.02 lb)

(2) A 5 kg (11.02 lb) disc with a hemispherical surface.

(3) A 5 kg (11.02 lb) disc with a flat surface.

(4) A 10 lb (4.54 kg) disc with a flat surface.

Note: The aluminium disc material was low resonance magnesium alloy from a cast aluminium ingot (magnifluxed by Alcan of Kingston).

The new drop apparatus can be seen in Figure 26 in the CSA configuration, and in Figure 27 the drop frame is shown in its original Z90.1 set-up with the hemispherical anvil in place.

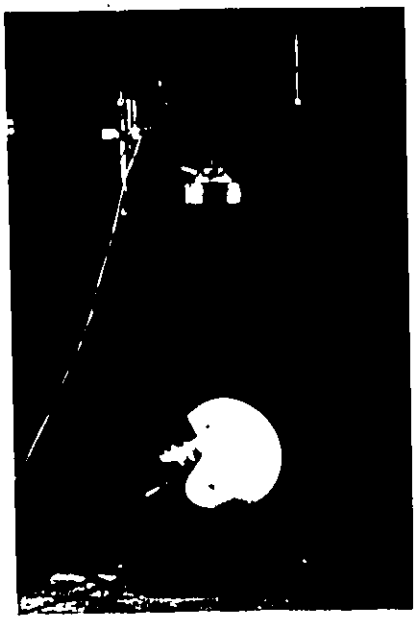

CSA Motorcycle Helmet Standard Test Mode Figure 26

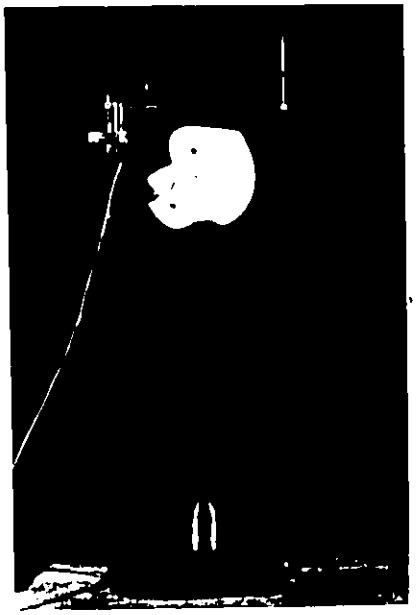

ANSI Z90.1 Motorcycle Helmet Standard Test Mode Figure 27

(4) To compensate for the non-uniform flatness of the cement floor under the base plate, the lower surface of the base plate was milled accordingly.

(5) By modifying a light sensitive photo-electric cell developed by Mr. James Kho, a height adjustable mechanical external trigger, Figure 28, for the accelerometer and load cell signals on the oscilloscope was achieved.

Photo cell Triggering Mechanism

Figure 28

(6) Aluminum foil was wrapped around the solenoid to shield the oscilloscope from the electromagnetic fields produced by the solenoid.

(7) The guide wires were replaced with 1/4 inch stainless steel bar stock. When these guide bars were placed in tension the necessary stiffness was achieved.

(III) 4 HEADFORMS OBTAINED FOR TESTING

Seven types of headforms were obtained for testing purposes. Six of these types are shown in Figures 29 and 30.

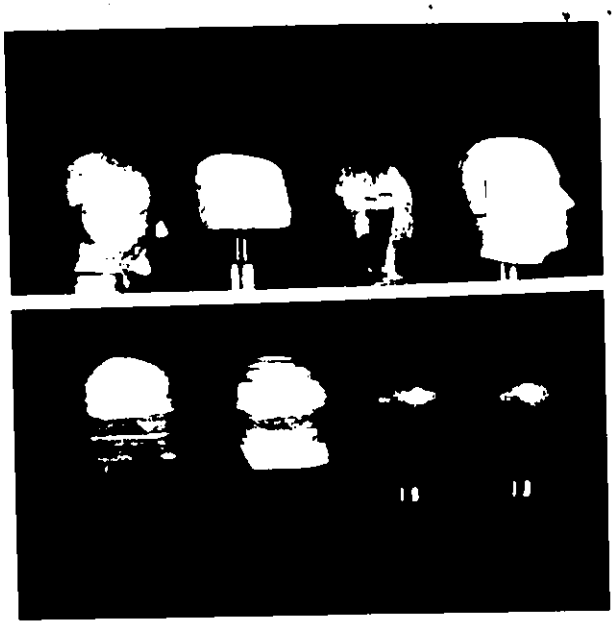

Figure 29

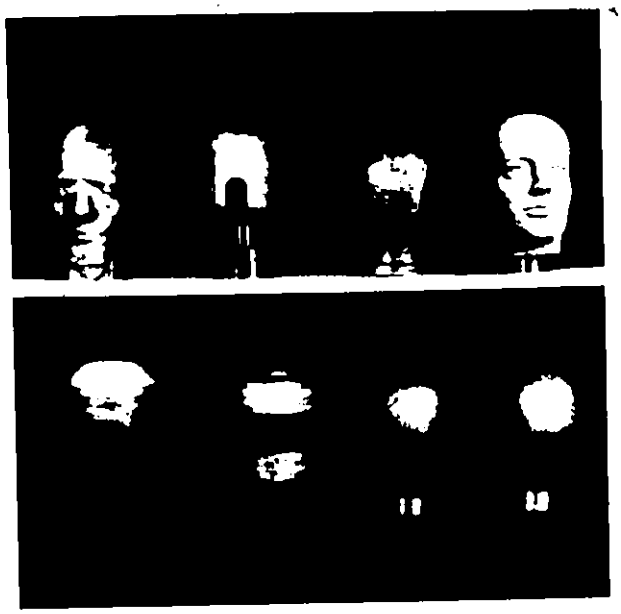

Figure 30

Headforms with steel necks

(1) From left to right, the headform in the top left is a thin cast aluminum headform with a wall thickness of approximately 5/16 inches. This headform was cast at a local casting firm from a plastic 50th percentile pattern.

(2) The second headform on the top is a Z90.1 headform with its ball and socket joint shown in Figure 31.

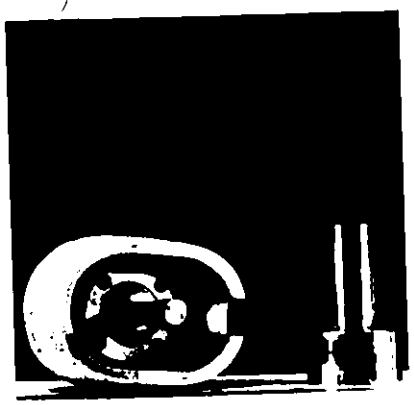

Z90.1 Headform showing ball and socket joint with steel neck.

Figure 31

(3) The third headform is a thick cast aluminum headform with wall a thickness over 1.0 in. This headform was also cast at local casting works from a polystyrene pattern.

(4) The fourth headform with the protective skin is a Sierra crash dummy head (Model #292-1650), with a cast aluminum skull beneath the 5/16 in. silicon rubber skin. The Sierra headform has a removable occipital region, Figure 32, for mounting a triaxial accelerometer block and fastening a neck.

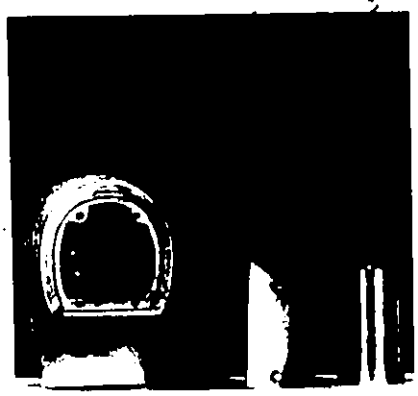

Sierra headform with removable occipital cover.

Figure 32

(5) The first two headforms in the bottom left are the CSA wooden large and small headforms. A CSA headform is about to be impacted on the brow region, Figure 33, with a flat striking surface.

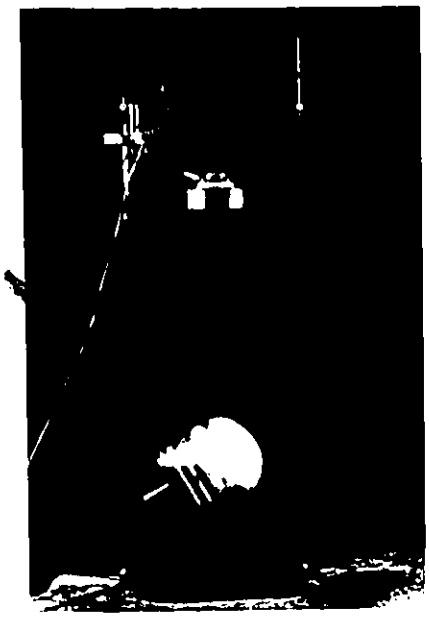

CSA mode shown without helmet
Figure 33

(6) The last two headforms in the bottom right are the large and small CSA plastic headforms used in the hockey helmet standard. (CSA-Z 262.1)

(7) The seventh headform, Figure 34, is a spherical shaped wooden headform obtained to compare impact results with Jehu (26).

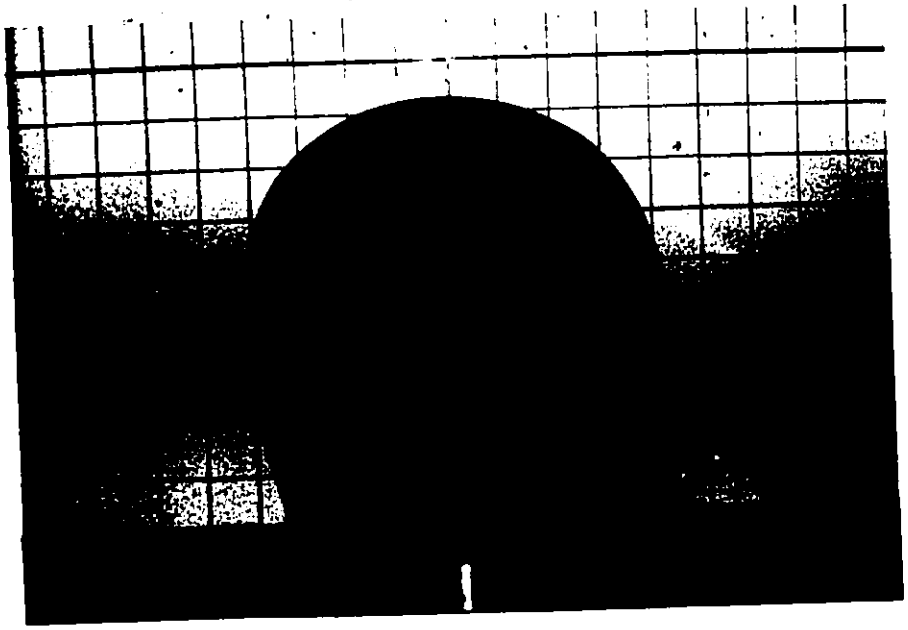

Spherical Wooden Headform
Figure 34

(III) 5 DESIGN OF TESTS AND APPARATUS FOR HEADFORM AND CADAVER RESPONSE EVALUATION

It was evident from the work of other investigators, that testing should be closely linked with the human element. For this reason, an agreement was reached to work jointly with the University of Ottawa Department of Anatomy in the Faculty of Medicine, developing techniques to test cadaver heads.

(III) 5 (i) NECK DISCUSSION

It was decided to test the headforms in a fixed mode. The fixed mode represents the worst accident situation. This situation could exist when the powerful neck muscles become tense before an expected

head impact. The fixed mode consisted of crown impacts to headforms that were securely bolted to the mounting plate using the steel necks shown in Figures 29 to 34.

Hodgson (20) illustrated with Cadavers that neck loading was not observed until a number of milliseconds after peak acceleration of the head. This fact has never been proven to be true or false with live humans expecting a head impact. Yet the absence of neck injuries for the motorcycle accident studies of reference (4,7) seems to add further evidence that the neck plays a minor role during head impacts. Whether neck injuries do not happen because the neck is not an important factor or because the neck is one of the body's larger, stronger and most used muscle groups that is able to tolerate head impacts is still open to question. If the neck muscles are stiff, the effective mass of the impacting body would increase from the 10 to 11 lbs of the head to some greater portion of the body weight. Because the greater effective mass increases the impact energy, the accident dynamics with respect to the head are worsened.

A secondary reason for using a fixed neck on the headforms, stems from the difficulties associated with measuring and repeating the stiffness with variable stiffness neck models. It was also foreseen that variable stiffness necks in the multiposition mode could create even more formidable problems.

Using a rigid neck, would, however, create problems with trying to attach a neck of this sort to the cadaver head. Consultations

with Mr. Michael Simmons and Mr. Robert Grenier from the University of Ottawa Department of Anatomy led to a solution to this problem. By using a Canus C-32 type resin, developed in work with the medical school and canus supply, a steel neck was mounted below the first and second neck vertebrae -- the atlas and axis respectively. To assist the reader, a photo copy of these two vertebrae has been placed in Appendix E. Also a copy of the mechanical properties of C-32 Canus resin has been submitted in Appendix F. A more detailed discussion of the attachments of steel necks to the cadaver heads for the fixed and multiposition modes has been left to Appendix G.

Knowing that cadaver heads could be mounted in both the fixed and multiposition modes, the straightforward mounting of necks to existing headforms was undertaken.

Cold rolled, mild steel necks were designed and fabricated, as shown in Figures 24 through 34. Another similar steel neck was devised for the thick cast aluminum headform, Figures 28. Four other steel necks were constructed for the cadaver heads: two for the fixed mode and two for the multiposition mode.

The necks in the fixed mode were to be bolted to the mounting plate, Figures 10 and 11, by the second flat plate, Figure 12. This flat plate would not allow the headform to be moved eccentrically, to insure the impact striker had zero tangential slope at the highest point of a headform or helmeted headform. Thus a fourth slotted flat plate, Figure 36, was designed and fabricated so that the above zero tangential slope requirements could be met.

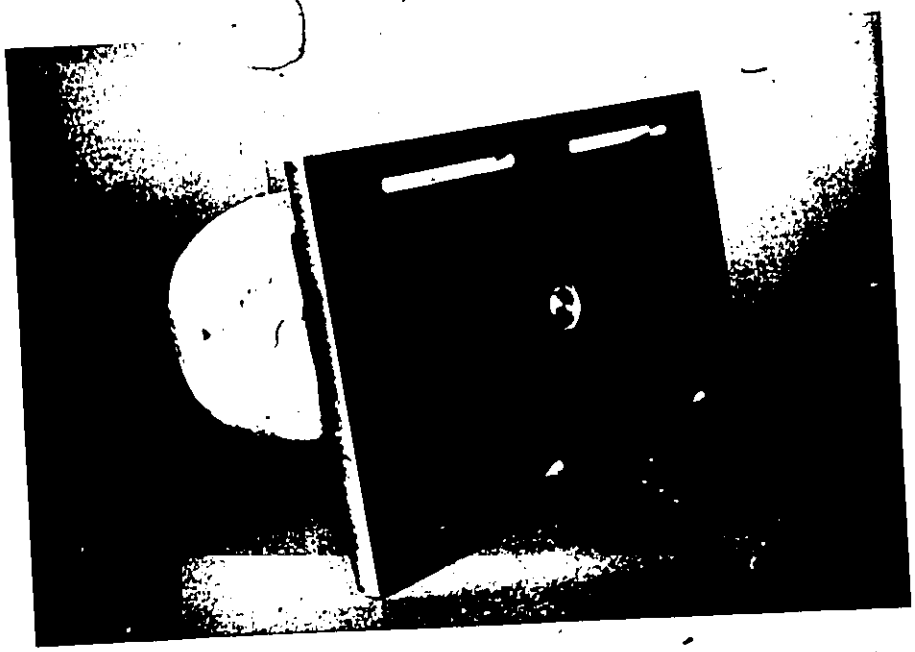

Slotted Flat Plate with Headform Bolted in Position

Figure 36

III 5 (ii) QUESTION OF COMPARISON FOR OUTPUT SIGNAL

As mentioned previously, both acceleration and transmitted force could be examined simultaneously. The significant question is what part if not all of the generated acceleration and force wave forms should be used for comparative purposes in the analysis of headform tests. From preliminary testing it was noted that the shape of the acceleration profiles was quite similar for the headforms tested with and without helmets. However, force wave forms did not compare with the same degree of similarity. It was felt that a wave form comparison could provide significant information, but the difficulty in doing so made it beyond

the scope of this study. Hence, it was decided to take the more customary path and consider the acceleration and force peaks only. The link between acceleration and force can be achieved by multiplying the peak deceleration of the striker by the mass of the striker. A force results that is in accordance with Newton's second law. This force is equal to peak transmitted force. Stated mathematically,

$$a_p M_s = (F_T)_p \text{*}$$

where

a_p is the peak acceleration

M_s is the mass of the striker

$(F_T)_p$ is the peak transmitted force

Peak acceleration and peak transmitted force are both easily discernible from the polaroid traces, Figure 37. Other means of comparison using time durations are more difficult to define. This difficulty is experienced after peak and peak acceleration occur.

---

* This equation assumes Newtonian mechanics is valid.

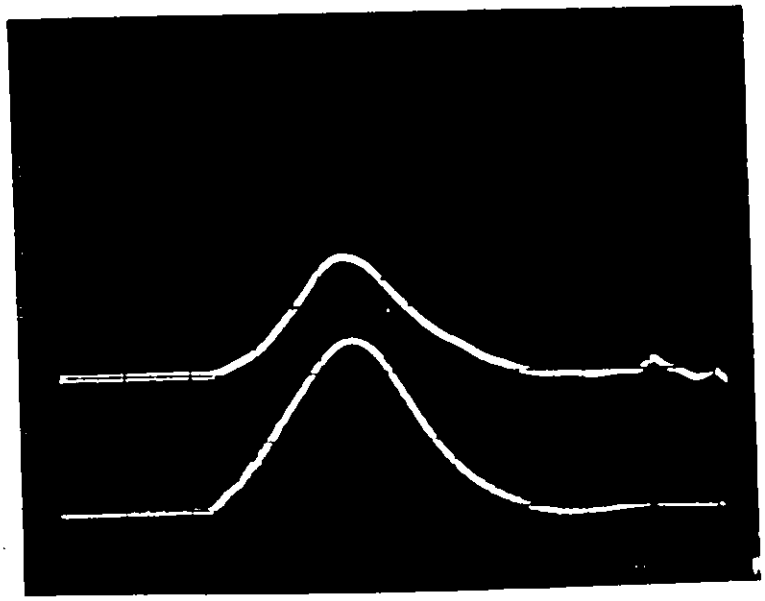

Headform Test Without Helmet

Figure 37(A)

Figure 37(B) points out the difficulty of finding the time duration of load cell trace.

Headform Test
With Helmet

Figure 37(B)

The accelerometer in certain cases of helmeted headform testing can present similar problems in discerning time durations.

It was found that vibrational induced noise on the trace due to interface problems usually did not occur until after peak readings. This means that the most reliable pact of the curve is from time $t - 0$ to the peaks or shortly thereafter.

The preliminary testing yield plots of $(F_T)_p$ and $(a_p M_s)$ against drop height. These plots yielded smooth curves through the points for impacts at various drop heights. This observation indicated that choosing the peak acceleration and transmitted force for comparative purposes was a sound choice.

III 5 (iii) STANDARD DISTANCES

Since the distance between ceiling and floor at the test rig location limited the range of drop heights, a range of 0.25 to 2.50 meters was chosen. A set of ten mild steel rods to cover this range and a stand to accommodate them, Figure 41, were fabricated.

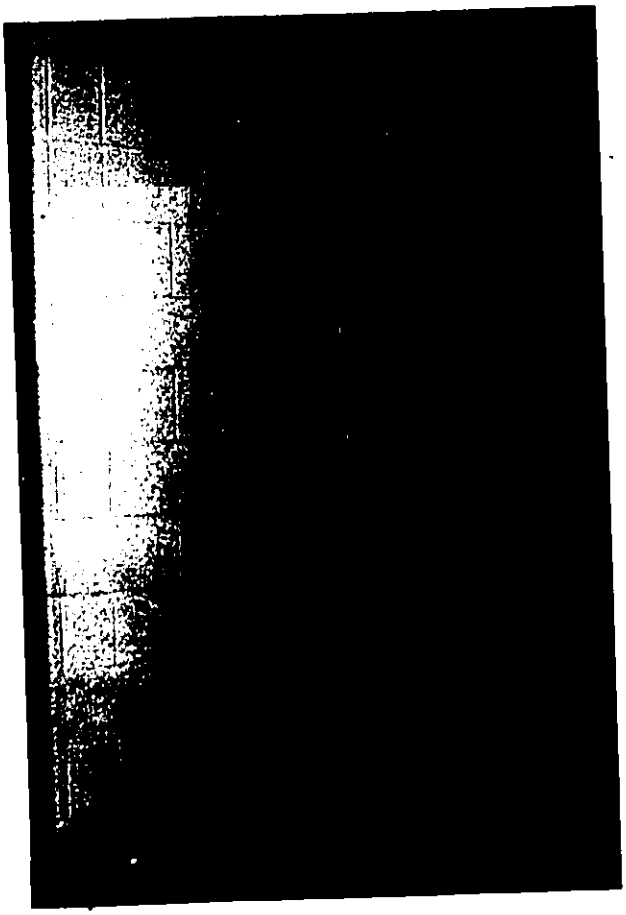

Drop Height Positioning Rods (0.25 m - 2.5 m)

Figure 41

III 5 (iv) HELMET POSITIONING INDEX (HPI)

The last problem before proposing a battery of tests was to develop a consistent means of positioning the helmets on the headforms and cadaver heads.

Three display headforms, Figure 42, (the largest is the 95th percentile, the middle is the 50th percentile and the smallest is the 5th percentile) were positioned such that their basic planes[1] were

Figure 42 Display Headforms

parallel with the reference table surface. Once the headforms were positioned properly using shims, a line was drawn on the headforms with the Vernier height gauge that indicated the basic planes. The Vernier height gauge then measured the distance (Z), Figure 43, between the zero slope tangential point of crown and the basic plane.

---

1 The basic plane is a plane on which the external ear openings and the lower floor of the eye orbitals lie.

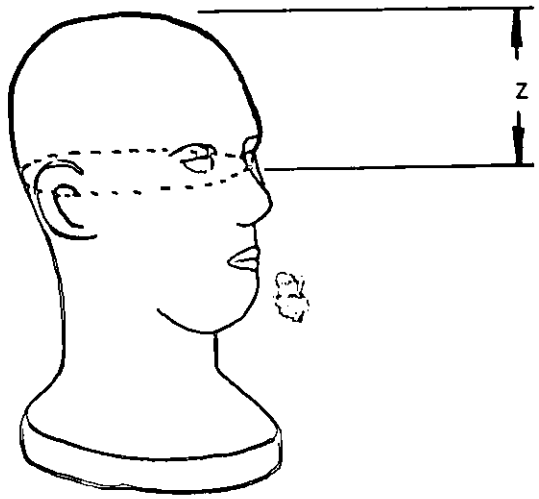

Distance Z Between Basic Plane and Crown

Figure 43

The values of Z for all three headforms were recorded.

A reference helmet as in Figure 44 was placed on each headform and positioned according to the manner in which the helmet is usually worn.

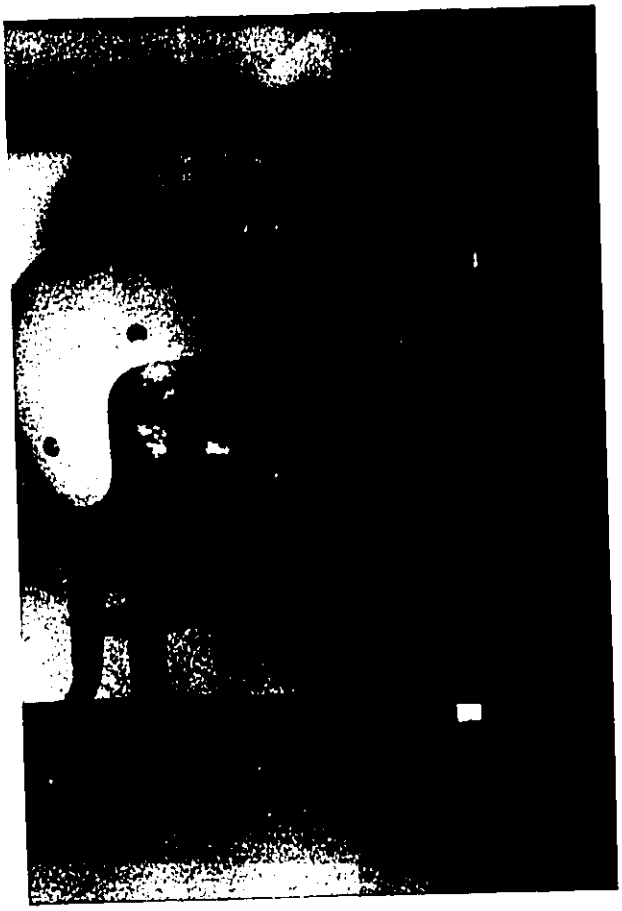

Measuring HPI With Vernier Height Gauge

Figure 44

The distance (HPI) between the brow opening and basic plane, Figure 45, was measured and recorded. These distances Z and HPI were plotted on a graph as in Graph 1 for the three reference headforms, and it was noted that a straight line was obtained. This straight line indicated that the visual guesses at positioning the helmet on the headforms were accurate. Using this straight line, the distance Z was measured for all the remaining headforms and plotted to find the HPI

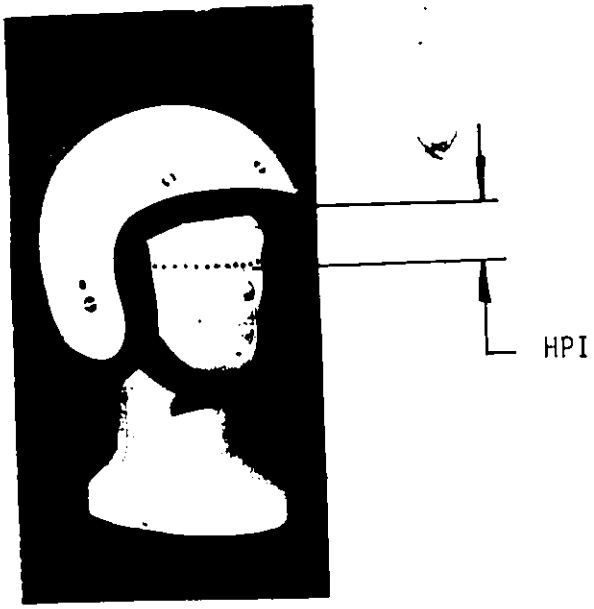

HPI Relative to a Display Headform

Figure 45

distance. These distances are shown in Table 4. The HPI distances were marked permanently on each headform so that the height positioning stand and level, Figures 46 and 47, could quickly establish the correct helmet positioning index for each helmet tested.

Figure 46

Helmet Positioning Apparatus with Reference Headform

Helmet Positioning with Z90.1 Headform

Figure 47

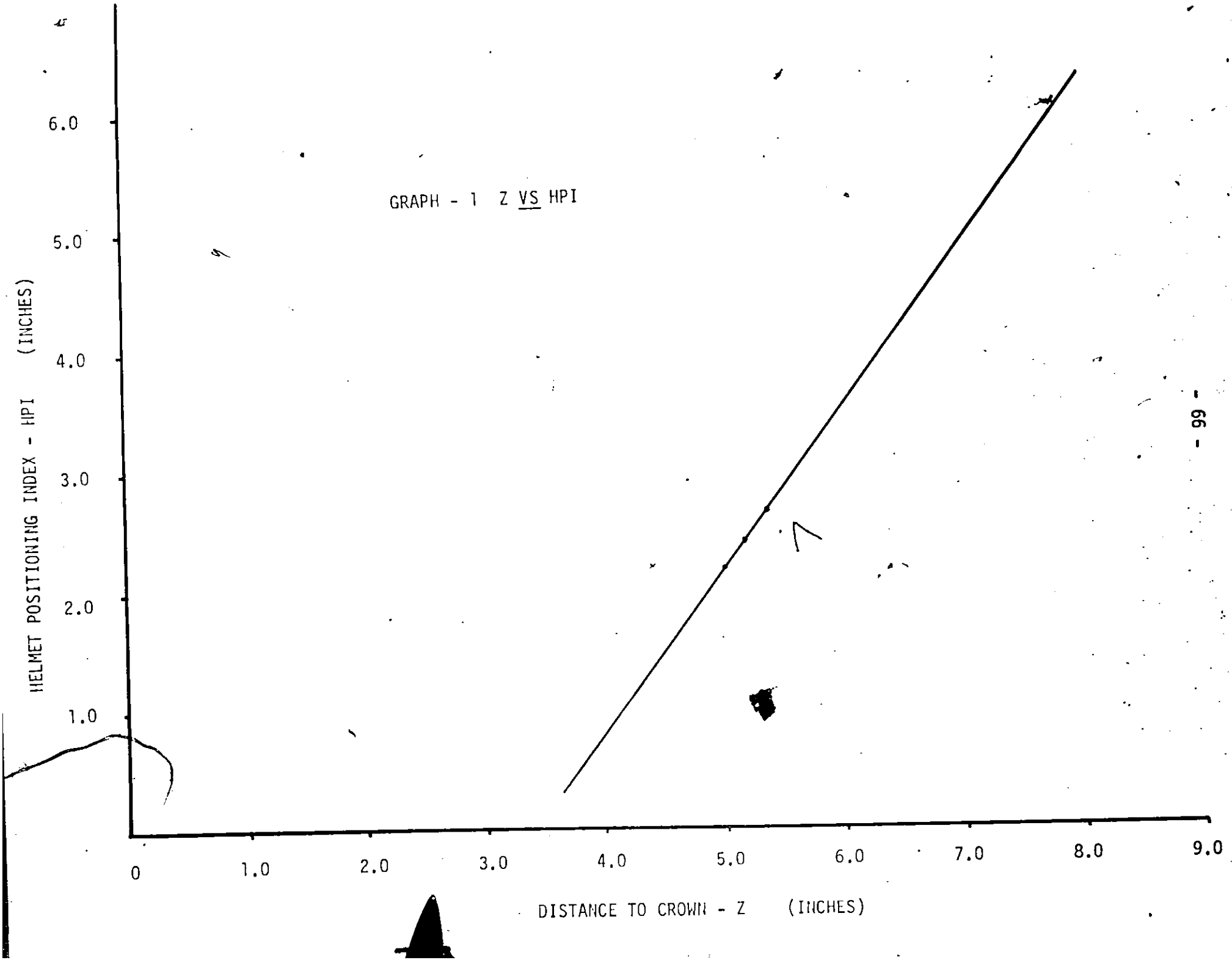
GRAPH - 1 Z VS HPI
HELMET POSITIONING INDEX - HPI (INCHES)
6.0
5.0
4.0
3.0
2.0
1.0
0
1.0
2.0
3.0
4.0
5.0
6.0
7.0
8.0
9.0
DISTANCE TO CROWN - Z (INCHES)

TABLE 4

Headform	Z (in)	HPI (in)
1. Z90.1 H.F.	4.950	2.100
2. Cast al. ref. H.F.	5.670	3.106
3. Ref H.F. (L) 95th	5.363	2.680
4. Ref H.F. (M) 50th	5.154	2.390
5. Ref H.F. (S) 5th	4.900	2.050
6. Sierra	4.710	1.800
7. Cast al. H.F. thin	5.807	2.300
8. CSA-W-L-C	5.512	2.890
9. CSA-W-S-C	5.147	2.475
10. CSA-P-L	5.354	2.675
11. CSA-P-S	4.961	2.130
12. Cast al. H.F. thick	5.197	2.475
13. Sp. wooden H.F.	4.880	2.000

The same helmet positioning index was also used for the cadaver tests.

III 5 (v) BATTERY OF TESTS

The testing that was to follow equipment calibration was divided into nine phases. The description of these phases are as follows:

Phase (i) This phase consisted of tests to all the headforms in Figures 29 through 34. The tests were conducted in the fixed mode by dropping the 5 kg MEP striker onto the headforms. The headforms were rigidly attached to the slotted mounting plate. The acceleration and transmitted forces were recorded for drop heights of 0.25 to 2.50 meters (by increments of .25 m). Peak accelerations were plotted against drop heights for comparitive purposes. The purpose of the phase (i) tests is to gain some repeatable comparitive baseline for which the helmeted headform tests can be compared.

Phase (ii) The headforms were tested in the same manner as Phase (i), except helmets (using the helmet positioning index) were placed on each headform before impact. The impactor was the 5 kg (11.02 lb) flat striker. Throughout all the helmet tests the same polycarbonate outer-shell was used. For each impact a different polystyrene liner was inserted in the outershell. The preliminary testing showed no noticeable effect between an outer shell impacted 50 times and a new outer shell. Seven polycarbonate outer shells and 50 liners with comfort padding were obtained, all the liners being of the same size, density and batch. The purpose of the Phase (ii) tests is to compare the performances of the helmeted headforms with each other as well as the

tests using no helmets and the MEP.

Phase (iii) This phase tested two cadaver heads with helmets as in Phase (ii). With this phase of testing, the headforms could be compared to the human element.

Phase (iv) This phase consisted of one series of tests to the first of the above cadaver heads without helmets using the MEP calibration pad and a second series of tests to the second of the above cadaver heads without helmets using the 5 kg(flat) striker. In both cases, testing was discontinued at the time of skull fracture.

Phase (v) This phase tested two headforms in the multiposition mode using the MEP. The tests were conducted in four locations, (1) occipital, (2) parietal right side, (3) frontal and (4) parietal left side. The two headforms were chosen on the basis of the results from the first four phases of tests.

Again, these tests would establish a comparitive baseline for the helmeted headform tests using the multiposition mode.

Phase (vi) This phase tested the same two headforms in the multiposition mode with helmets using the 5 kg (11.02 lb) flat striker.

Phase (vii) The seventh phase tested two cadaver heads in the multiposition mode using helmets as in Phase (vi), using the 5 kg (11.02 lb) flat striker.

Phase (viii) The eighth phase tested the above two cadaver heads in the multiposition mode without helmets. Testing was stopped when skull fracture occurred. The tests were conducted on the frontal

region for a further comparison with Hodgson (17). The 5 kg flat impactor was used for these tests.

Phase (ix) The ninth phase consisted of further calibration tests including tests with other testing facilities in the United States and Canada. These calibration tests were performed to compare the university test facility with other testing houses.

CHAPTER IV

IV 1 PREVIEW OF CHAPTER IV

Chapter IV contains the calibration description with sample calculations for the accelerometer and load cell. This chapter also compares the calibration tests with those of Jehu (27).

IV 2 CALIBRATION TESTS

Accelerometers are usually factory calibrated using an electrodynamic shaker. The shaker available to this study was not functioning when needed, so an alternative method was undertaken, namely 'calibration by comparison'. Levy and Bickford (26) suggest calibration by comparison be done with an accelerometer designated as a standard. Unfortunately, an accelerometer so designated could not be obtained. Hence, the Endevco Accelerometer was calibrated against five other Bruel and Kjaer (B & K) accelerometers using the 5 kg MEP striker falling on the hemispherical anvil of Z90.1 standard. This particular mode was chosen because it could be compared to similar calibration work carried out by Jehu (27). Jehu dropped the 5 kg hemispherical surface onto the MEP. In both cases, the calibration drop height was 2.0 meters. The MEP pad used by Jehu was of green code so its damping characteristics should have been comparable to the University of Ottawa MEP. The accelerometers were tested at position G of the 5 kg MEP striker, Figure 48. In Figure 49, the Endevco accelerometer can be seen on the left of the 5 kg MEP striker with the sub-miniature B & K accelerometer on the right. Peak accelerations of the accelerometers were measured for calibration comparison. The first attempt to calibrate the accelerometers was unsuccessful. Three of the factory

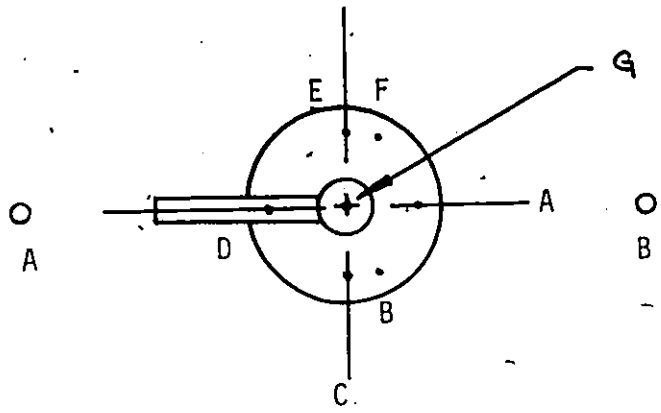

Accelerometer Positions

Figure 48

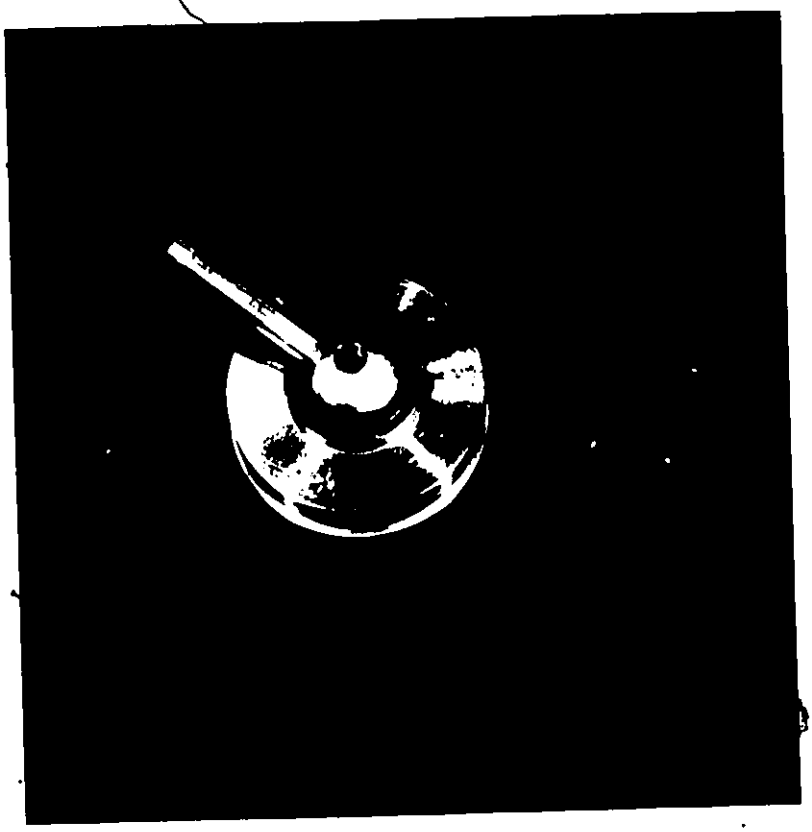

Endevco and
B & K
Accelerometers

Figure 49

specified sensitivities of the B & K accelerometers were in error. Secondly, the factory specifications of all the sensitivities did not account for an increase in capacitance of a longer output cable, and the capacitance of the amplifiers.

The accelerometers used were: (1) to (6)

TABLE 5

Accel. #		Factory sensitivity	$Q(\frac{pc}{g})$	$C_p + C_t$( )	E= Calculated sensitivity
1. B & K	399528	3.29 $\frac{mv}{g}$	3.73	1133	3.29 $\frac{mv}{g}$
2. B & K	399536	2.29	3.67	1115	3.29
3. B & K	399517	3.45	3.95	1144	3.49
4. B & K	399510	3.23	3.66	1133	3.26
5. Endevco 2271AM20	AA12	4.575	11.6	2545	4.575
6. B & K 4339	293229	9.83	10.78	1096	9.83

The factory measures the charge sensitivity (Q) and calculates the voltage sensitivity by the following equation:

$$E = \frac{Q}{C_p + C_t} \times 1000 \qquad (2)$$

where $C_p + C_t$

is the transducer capacitance (C_p)
plus the cable capacitance (C_t)
in pico farads.

This calculation was performed for each of the accelerometers as seen in Table 5. Accelerometers (3) and (4) were slightly in error with accelerometer (2) being 28% in error.

The 4-foot, 107 pF factory cable supplied with each B & K accelerometer was not long enough. A 10-foot cable with a capacitance of 306 pF was used for the B & K 4339 #6 and additional 110 pF cables were added to the subminiature B & K accelerometers #1 - 4. The calculations using the additional cable capacitance and the capacitance of the amplifier were calculated as in Table 5, using $E = \frac{Q}{C_{Total}} \times 1000.$ These new sensitivities are shown in Table 6.

TABLE 6

#	C_p	C_t	C_{amp}	C_{Total}	$E = \frac{Q}{C_{Total}} \times 1000$
1.	1026	107 110 217 pF	14 pF	1257 pF	2.97 $\frac{mv}{g}$
2.	1008	107 110 217	14	1234	2.96
3.	1037	306	14	1281	3.08
4.	1026	107 110 217	14	1257	2.91
5.	2239	306	14	2559	4.54
6.	988	306	14	1408	8.34 $\frac{mv}{g}$

where C_p is the transducer capacitance
C_t is the cable capacitance
C_{amp} is the amplifier capcitance

With the new sensitivities, the tests with MEP at 2.0 meters falling on the hemispherical anvil, were carried out with peak accelerations being recorded. Two drops were made for each accelerometer tested. The results can be seen in Table 7.

TABLE 7

Accel. #	Divisions Accel.	Divisions Load Cell	a_p
1.	AED = 2.40 div. ASF = .50 V/div.	LCD = 2.2 div. LSF = .1 μV/div.	403 g
	2.40	2.2	403
2.	2.45	2.2	413
	2.45	2.2	413
3.	2.6	2.2	421
	2.6	2.2	421
4.	2.35	2.2	403
	2.35	2.2	403
5.	3.75	2.2	413
	3.75	2.2	413
6.	6.8	2.2	408
	6.8	2.2	408
	3.8	2.2	418

Sample Calculation - For Acceleration #5

H = 2.00 m = drop height

AEP = 3.75 division = Accelerometer (Endevco) Divisions

ASF = 0.5 volts/division = Accelerometer Scale Factor

LCD = 2.2 division = Load Cell Divisions

LSF = 0.1 volts/division = Load Cell Scale Factor

$$\text{Sensitivity } A = 3.75 \text{ div} \times 0.5 \frac{V}{\text{div}} \times \frac{1}{4.54 \times 10^{-3} \frac{V}{g}}$$

$$= 412.99 \text{ g's}$$

AED and LCD - are the divisions read from the oscilloscope trace for the accelerometer and load cell channels.

ASF and LSF - are the scale factor values of the above divisions for each channel in volts/division.

The average peak acceleration is 411.29 g, Jehu had 408 g's with similar MEP pad from the same drop height. The sensitivity of the Endevco #5 accelerometer that yields 411 g's is $4.63 \frac{mv}{g}$ as compared to the calculated $4.54 \frac{mv}{g}$.

Tests were carried out at other drop heights using the new sensitivity to compare with Jehu's results listed in Table 8.

TABLE 8

Drop Height	Jehu a_p 2 readings	Jehu a_p	Webster a_p
2.5 m	500 499	500	484
2.0 m	405 411	408	411
1.5 m	323 328	326	329
1.0 m	226 232	229	242

The completion of calibration tests for the accelerometer led to the calibration of the Endevco load cell. The decision was made to calibrate the load cell in a more "violent" impact than the "soft" impact of the MEP falling on the hemispherical striker. The 5 kg MEP calibration pad falling on the flat plate was chosen to calibrate the load cell from drop heights of (.25 to 2.25) meters.

The new theoretical sensitivities of the load cell were also calculated.

$$C_{Total} \text{ @ 1000 Hz.} = (C_p + C_t + C_{amp}) \text{ pF}$$

$$= (5034(\text{@ 1000 Hz}) + 304 + 14)$$

$$= 5352 \text{ pF}$$

$$Q = 24.4 \frac{pC}{lb}$$

$$E = \frac{Q}{C_t} \times 1000 = \frac{24.4 \times 1000}{5352} = 4.56 \frac{mv}{lb}$$

$$C_{Total} \text{ @ 100 Hz} = (5359 \text{ (@ 100 Hz)} + 304 + 14) \text{ pF}$$

$$= 5667 \text{ pF}$$

$$Q = 24.4 \frac{pC}{lb}$$

$$E = \frac{Q}{C_t} \times 1000 = \frac{24.4 \times 1000}{5667} = 4.31 \frac{mv}{lb}$$

As mentioned previously, peak transmitted force can be compared to peak acceleration by Newton's second law. The drop frame, striker and accelerometer were weighed and found to be 5.0 kg (11.02 lb).

The 5.0 kg MEP was dropped onto the flat plate for drop heights of 2.50 m to 0.25 m. In each case peak acceleration and peak transmitted force were recorded from the oscilloscope trace. The accelerations were multiplied by the weight of the falling mass to determine $(Ma)_p$ in Table 9. This value was then compared to the load cell trace to establish what sensitivity in mv/lb would yield a peak load cell force $(F_{lc})_p$ equal to $(Ma)_p$. The results for these calibration tests are shown in Table 9 where an average sensitivity of 4.66 mv/lb resulted.

TABLE 9

Initial Loadcell Calibration For Random Drop Heights.

h (METERS)	a_e (g's)	ma_e	SENSITIVITY LOADCELL $(\frac{MV}{lb})$
2.00M	1101.5	12,138.7	4.61
1.75	993.52	10,948.6	4.61
1.50	885.5	9,759.1	4.66
1.25	755.9	8,330.1	4.68
1.00	626.3	6,902.0	4.70
0.75	496.8	5,474.0	4.70
0.50	356.4	3,927.0	5.00
0.25	199.8	2,202.0	5.22
		AVERAGE	4.772 $\frac{MV}{lb}$

CHAPTER V

V 1 PREVIEW OF CHAPTER V

Chapter V describes the first attempt to conduct the Phase (i) tests and the problems encountered. The solutions to these difficulties allowed Phase (i) tests to be restarted. The remainder of the chapter briefly describes the procedure used for tests of Phases (ii) to (ix). Following the description of each test phase a table listing the tests of that phase has been included.

V 2 TESTING - (1)

A battery of Phase (i) tests were carried out on all the headforms. Polaroid photographs were taken and graphs were plotted for peak transmitted force and peak acceleration against drop height. Periodical recalibration checks indicated that the sensitivity of the load cell was gradually increasing from its original sensitivity of 4.772 mv/lb. Eventually, the sensitivity change reached a value that could not be tolerated and the testing was stopped.

It was found that the lead anchors encasing the lag bolts for the bottom plate were creeping.

Truncated pyramid-shaped holes were chipped by hand in the concrete floor, Figure 50. 5/8" threaded rod combinations with ends split, jammed nuts and flat washers were cemented into the floor with cement fondue, Figure 51.

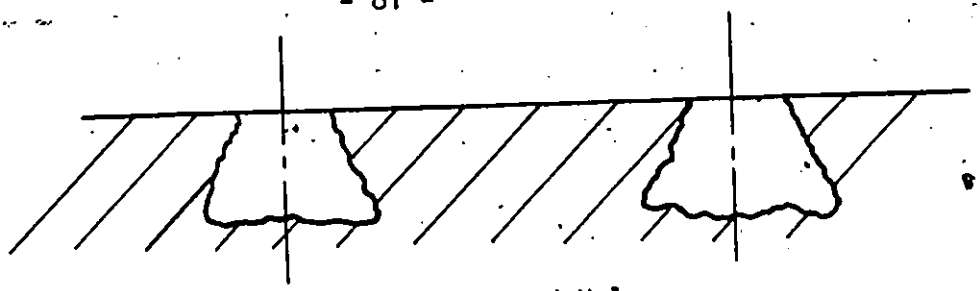

Truncated Pyramid Shaped Holes
Figure 50

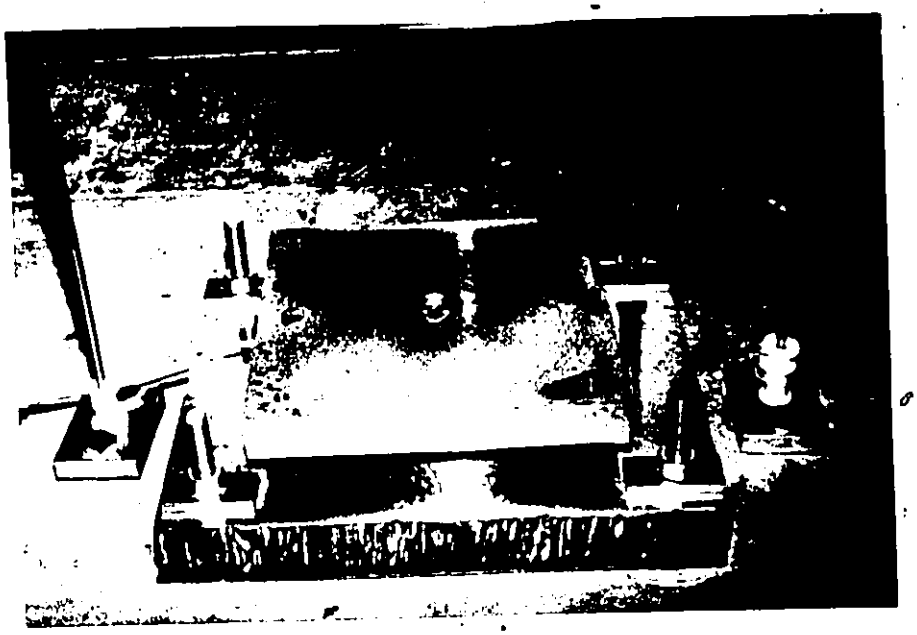

Figure 51 (Bottom Plate with Bolted Studs)

The quick-setting high strength cement fondue enabled testing to resume one week after pouring.

V-3 RECALIBRATION

The load cell was again calibrated against the accelerometer and a new sensitivity observed. Table 10 shows the resulting average sensitivity of $4.776 \frac{mv}{lb}$ for the load cell.

TABLE 10

Loadcell Calibration For Random Drop Heights

Test #31

h (METERS)	a_e (g's)	ma_e lbs	SENSITIVITY LOADCELL
2.50	1,360.7	14,994.8	4.77 $\frac{MV}{lb}$
2.00	1,123.1	12,376.7	4.72
1.50	905.0	9,972.7	4.81
1.00	647.9	7,140.3	4.76
0.50	373.6	4,117.6	4.76
2.50	1,371.5	15,113.8	4.76
		AVERAGE	4.776 $\frac{MV}{lb}$

V-4 TESTING (ii)

PHASE (i) MEP Headform Tests Fixed Mode

The first phase of tests were carried out on all headforms. The results of these tests can be found in the computer output data tables, Page 203 Section VI-3. The following Table 11, is a list of the tests in chronological order. Also an explanation of the code descriptions found in the computer output data tables is given. Phase one consists of tests 31 to 45.

MEP F → indicates that the modular elastomer programmer falls on a particular surface or headform. The MEP calibration pad assembly weighs 5.0 kg (11.02 lb).

Figure 52 shows the CSA large wooden headform about to receive a crown impact with the MEP from a drop height of one meter.

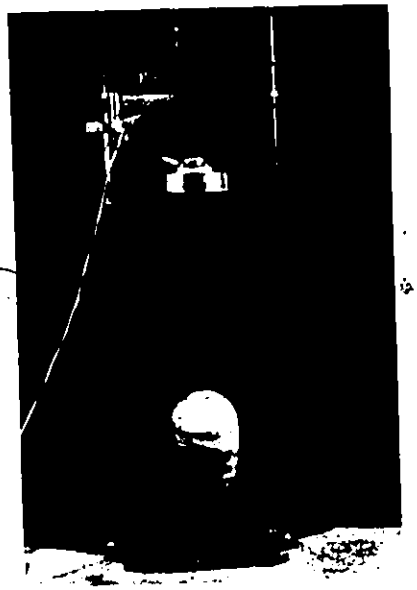

Fixed Mode MEP Falls on CSA Wooden Large Headform

Figure 52

TABLE 11

Tests for Phase (i)

Test #		
31	MEP F	Flat Plate (final load cell calibration)
32	MEP F	H.S. (Hemispherical striker)
34	MEP F	CSA - W - L - C (CSA wooden headform, large size crown impact)
35	MEP F	CSA - W - L - B (CSA wooden headform large size brow impact)
36	MEP F	CSA - W - S - C
37	MEP F	CSA - W - S - B
38	MEP F	CSA - P - L
39	MEP F	CSA - P - L
40	MEP F	CSA - P - S
41	MEP F	SP - W - H.F.
42	MEP F	SP - W - H.F.
43	MEP F	Cast Al. (thick)
44	MEP F	Sierra - H.F.
45	MEP F	Z90.1
29	MEP F	Cast Al. (thin)

PHASE (ii) Helmeted Headform Tests Fixed Mode

Upon completion of the Phase (i) tests, the Phase (ii) tests were started. Table 12 is a list of these tests. In this phase the thick cast aluminum headform and the hemispherical shaped headform could not be used due to being small headform sizes (7-7 1/8). The helmet liners used were for medium to large head sizes. Due to a limited number of helmet liners available for testing with the comfort liner, the tests

had to be carefully chosen to maximize the information with the available helmet liners.

In Figure 53, the CSA large wooden headform is shown before a helmet has been fitted for a brow impact from a one meter drop height.

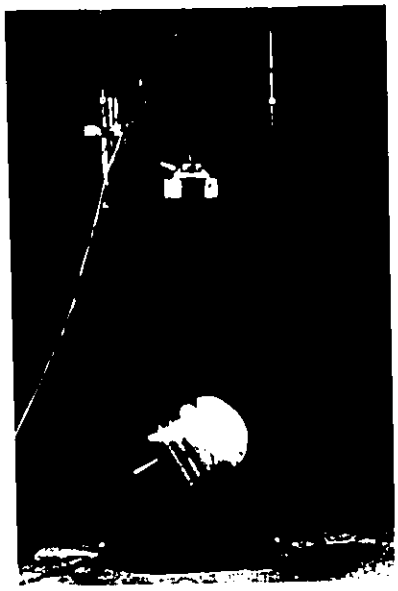

Figure 53

5 Kg Flat Striker Used for Helmet Tests Fixed Mode

TABLE 12

Tests for Phase (ii)

Test #			
46	5 kg(F)	F	Z90.1
47	5 kg(F)	F	Cast Al. H.F. (thin)
48	5 kg(F)	F	Sierra
49	5 kg(F)	F	CSA - P - L
50	5 kg(F)	F	CSA - W - L - B
51	MEP	F	Flat plate check
53	5 kg(F)	F	Z90.1
54	5 kg(F)	F	Z90.1

PHASE (iii) - Helmeted Cadaver Head Tests Fixed Mode

With the completion of Phase (ii) testing, the Phase (iii) testing was started. Table 13 lists the tests in this phase. In Figure 54, cadaver head 1 is shown just after helmet fitting in accordance with the helmet position index.

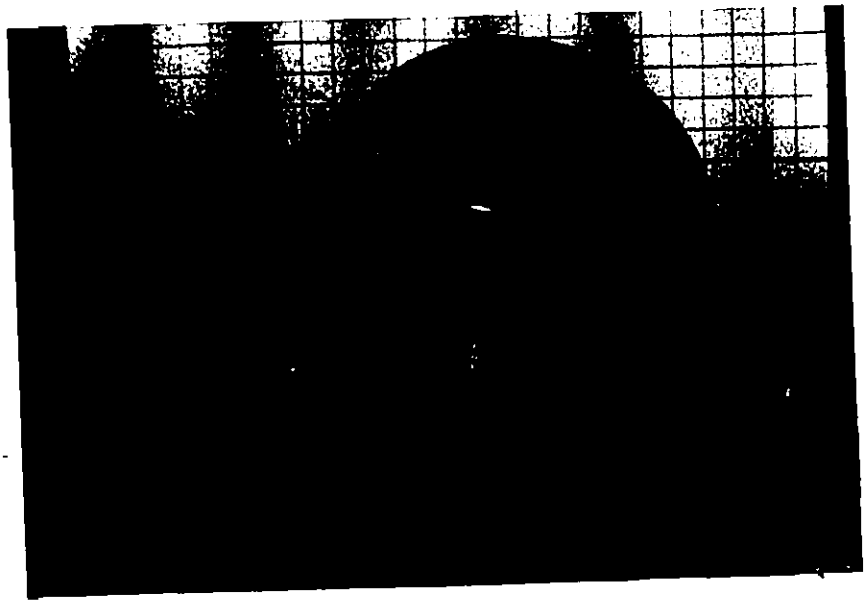

Figure 54 Cadaver Head 1

Figure 55 shows cadaver head 2 mounted on the top plate prior to receiving a crown impact to a helmet with the 5 kg flat impactor in the fixed mode.

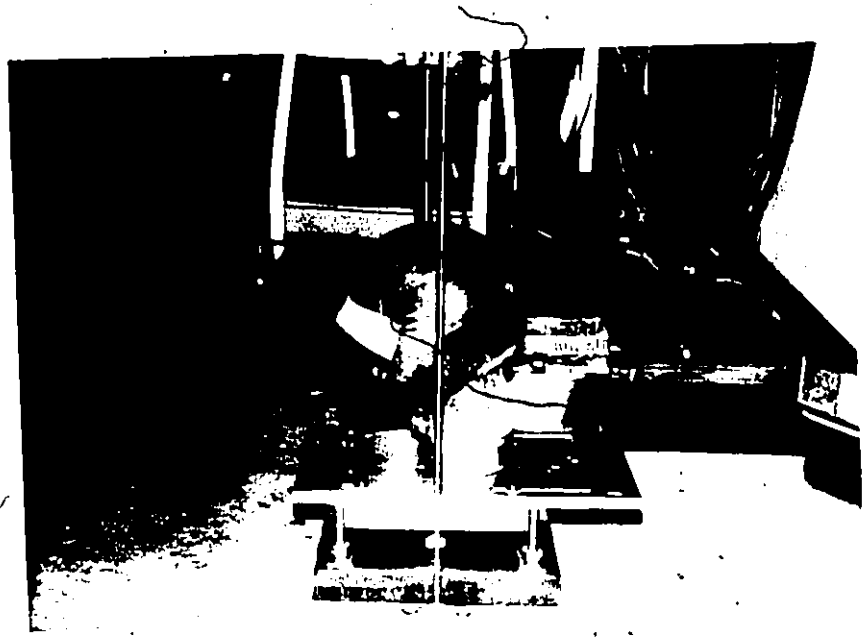

Figure 55

Slotted Plate Eccentricity of Cadaver Head 2.

Figure 55 illustrates the eccentricity of the slotted plate needed to produce a zero tangential slope impact to the crown.

Both cadaver heads were from embalmed subjects. Cadaver head 2 was moist; cadaver head 1 was dry. Cadaver head 1 was also missing part of the scalp as indicated by Figure 56.

Figure 56

Cadaver Head 1 Showing Missing Scalp Region

TABLE 13

Tests for Phase (iii)

Test #			
55	5 kg(F)	F	Cadaver 1
57	MEP	F	Flat plate check
58	5 kg(F)	F	Cadaver 2

PHASE (iv) Cadaver Head Tests without Helmets.

Phase (iv) tests followed the Phase (iii) tests for each cadaver head. This is indicated in the test numbers. Table 14 lists the Phase (iv) tests. Figure 57 shows cadaver head 2 about to receive a crown impact with the 5 kg flat plate.

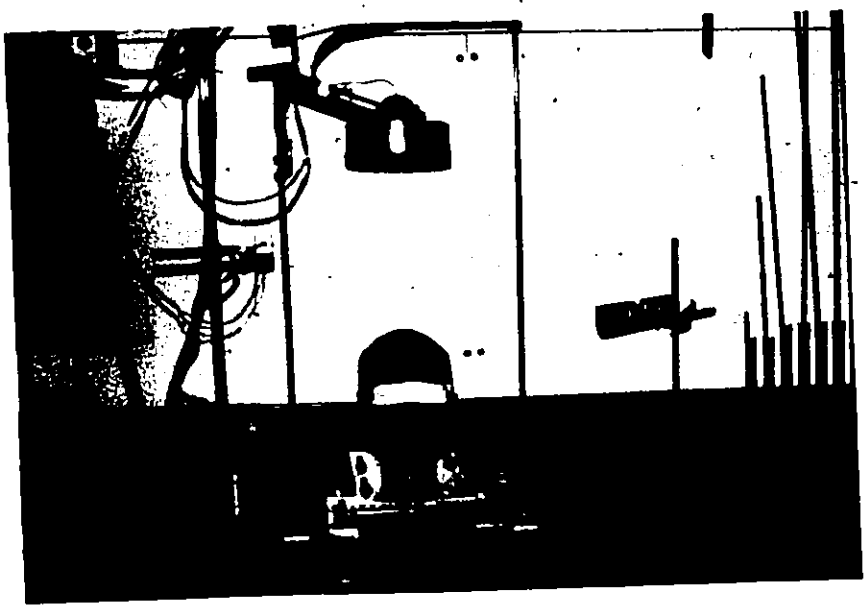

Figure 57
Cadaver Head 2 About to Receive a Crown Impact with the 5 Kg Flat Striker

TABLE 14

Tests for Phase (iv)

Test #			
56	5 kg(MEP)	F	Cadaver 1 WO Helmet
59	5 kg(F)	F	Cadaver 2 WO Helmet

PHASE (v) MEP Headform Tests Multiposition Mode

Phase (v) tests using the multi-position test rig were conducted upon the completion of Phase (iii) and (iv) tests. The Phase (v) tests are listed in Table 15.

In Figure 58 and 59, the Sierra and CSA large plastic headforms

Sierra H.F. Figure 58 Occipital Regions

Figure 59 CSA Plastic H.F

are shown respectively before receiving an impact with the MEP to the occipital region using the multi-position mode test rig.

Figure 60 shows the Sierra headform in position to receive a frontal impact. Figure 61 has the headform positioned to receive a parietal right side impact.

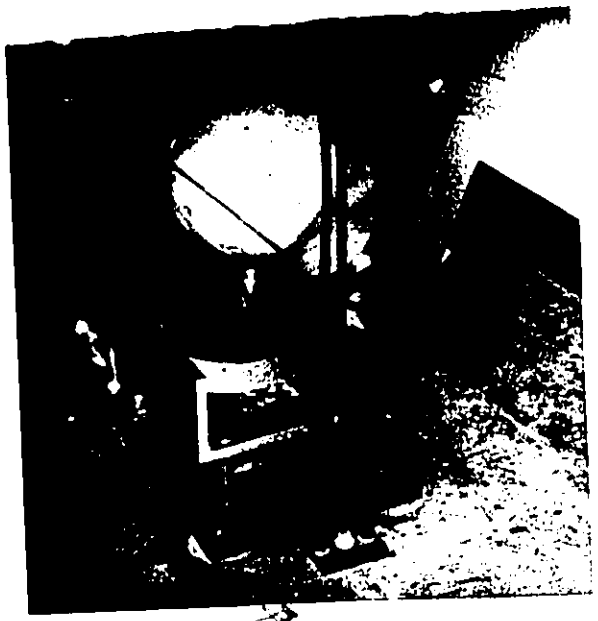

Frontal Region
Figure 60

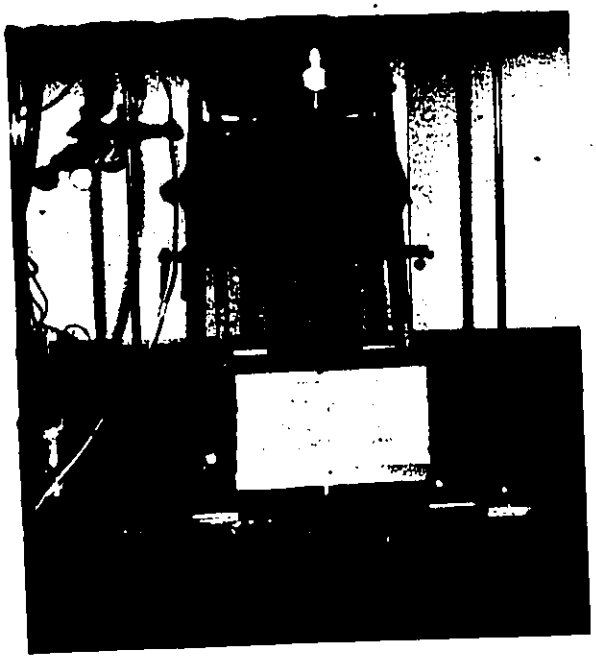

Parietal Right Side Region
Figure 61

TABLE 15

Tests for Phase (v)

Test #			
60	MEP F	Sierra	Occipital
61	MEP F	Sierra	Parietal R.S.
62	MEP F	Sierra	Parietal L.S.
63	MEP F	Sierra	Frontal
64	MEP F	CSA - P - L	Frontal
65	MEP F	CSA - P - L	Occipital
96	MEP F	Sierra	Occipital with support

PHASE (vi) Helmeted Headform Tests Multiposition Mode.

Phase (vi) tested the headforms in the multi-position mode with helmets. The Phase (vi) tests are listed in Table 16. Figure 62 has the CSA large plastic headform with a helmet prepared to receive a parietal left side impact.

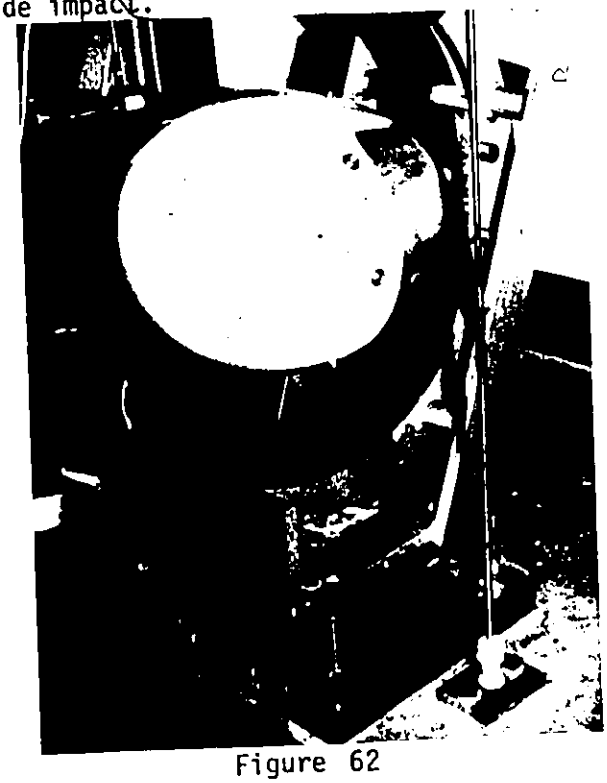

Parietal Left Side Impact to CSA Plastic Headform.

Figure 62

TABLE 16

Tests for Phase (vi)

Test #			
72	5 kg(F) F	CSA - P - L	Parietal L.S.
91	5 kg(F) F	Sierra	Frontal
93	5 kg(F) F	Sierra	Frontal
94	5 kg(F) F	CSA - P - L	Frontal
95	5 kg(F) F	Sierra	Occipital
97	5 kg(F) F	Sierra	Occipital with support

PHASE (vii) and PHASE (viii) Cadaver Head Tests Multiposition Mode

Upon completion of Phase (vi), tests on the cadaver heads were done with and without helmets in Phase (vii) and (viii) respectively. The Phase (vii) and (viii) tests are listed in Tables 17 and 18. Figure 63 depicts cadaver head 3 before receiving a frontal helmet impact, and Figure 64 shows cadaver head 3 before receiving a frontal impact without a helmet.

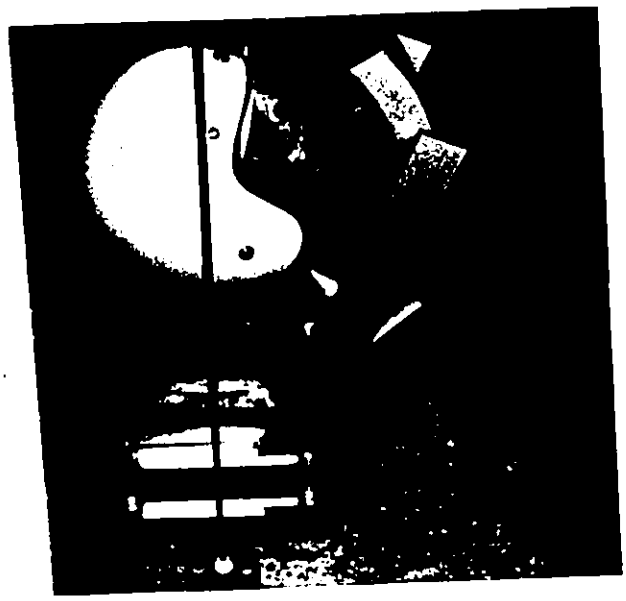

Figure 63

Frontal Impact Position of Cadaver Head 3

Figure 64 Cadaver Head 3

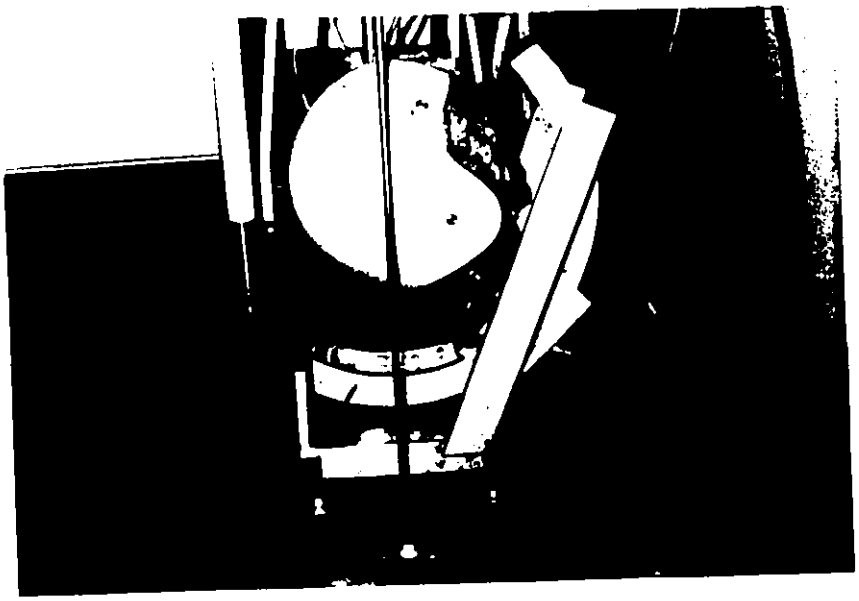

Figure 65 Cadaver Head 4 with Helmet

Figure 65 shows cadaver head 4 before receiving a frontal helmet impact. Figure 66 shows cadaver head 4 before receiving a frontal impact without a helmet.

Figure 66 Cadaver 4 Without Helmet

TABLE 17

Tests for Phase (vii)

Test #				
73	5 kg(F)	F	Cadaver 3	Frontal with helmet
90	5 kg(F)	F	Cadaver 4	Frontal with helmet
92	5 kg(F)	F	Cadaver 4	Frontal with helmet and reinforced neck 1

TABLE 18

Tests for Phase (viii)

Test #				
98	5 kg(F)	F	Cadaver 4	without helmet but with reinforced neck 2

PHASE (ix) Additional Tests

The further calibration and comparison tests of Phase (ix) are listed in Table 19, 1 to 7. These tests consisted of:

(ix) - 1. A series of tests to determine the effect of eccentric[-1] impacts to the load cell. A plate, Figure 67, was designed and constructed for these tests. This plate has a neck similar to the necks used on the headforms. Both surfaces (top and bottom) were ground to avoid interface vibrational problems. By bolting the neck to the slotted plate an impact traverse could be made across this new plate eccentric to the load cell similar to the case of eccentric headforms.

Ebar Plate to Study Eccentricity Effects
Figure 67

-1 eccentricity as shown in Figure 55 is the distance the slotted plate has to be moved to allow an impact with zero tangential slope at the highest point of a headform or helmeted headform.

The results of these tests can be found in the data tables, test #67. The plate was impacted with the 5 kg MEP calibration pad, from a drop height of 1.50 meters.

TABLE 19.0

Test #					
67	1	MEP	F	E bar	Plate, e = 0.00
67	2	MEP	F	E bar	Plate, e = 0.50
67	3	MEP	F	E bar	Plate, e = 1.00
67	4	MEP	F	E bar	Plate, e = 1.50
67	5	MEP	F	E bar	Plate, e = 0.00

Mining Helmet Tests

(ix) - 2. A battery of tests were conducted on seven miner's helmets. These tests were carried out on the spherical shaped wooden headform. The purpose of the test was to compare results with the BSA tests for miner's helmets; secondly, to examine effects of using a headform that has the point of zero tangential slope concentric with the centre of the neck; and, thirdly, to compare results with helmeted headform impacts for the web-type suspension of the miner's helmets with the styrafoam liners of the motorcycle safety helmets. The results of these tests can be found in the data tables, Test 68 and 69. Figures 68, 69 and 70 illustrate some of the helmets tested. Table 20 lists the helmets tested and their respective numbers found in the figures.

Figure 68 Helmet #1, 2, 3
L. to Right

Figure 69 Helmet #5, 6
#4 Not Shown

Figure 70 Helmet #7

TABLE 19.1

Helmet #	Description
1	(White) Fibre metal |brow brim|
2	(Yellow) Fibre metal with top pad |brow brim|
3	(Brown) Phenolic MS4 |brow brim|
4	(Brown) Phenolic MS4 |full brim| with top pad
5	(Orange) Fiberglass ultimate climbing helmet
6	(Yellow) Polyethylene Erb |brow brim|
7	(Beige) Polyethylene top guard |full brim|

The helmets were impacted from drop heights of 4 and 5 feet with the 10-lb flat impactor. The peak acceleration and force were recorded for each test.

TABLE 19.2

Test #				
69	1 to 13	10 lb	F	Mining helmets

Falling and Stationary MEP Tests

(ix) - 3. Testing was carried out on the stationary MEP with the 5 kg (11.02 lb) and the 10.00 lb impactors from drop heights of 0.25 to 2.50 meters. Peak force and peak acceleration were recorded and the results of these tests can be found in data tables. This mode of calibration is shown in Figure 71.

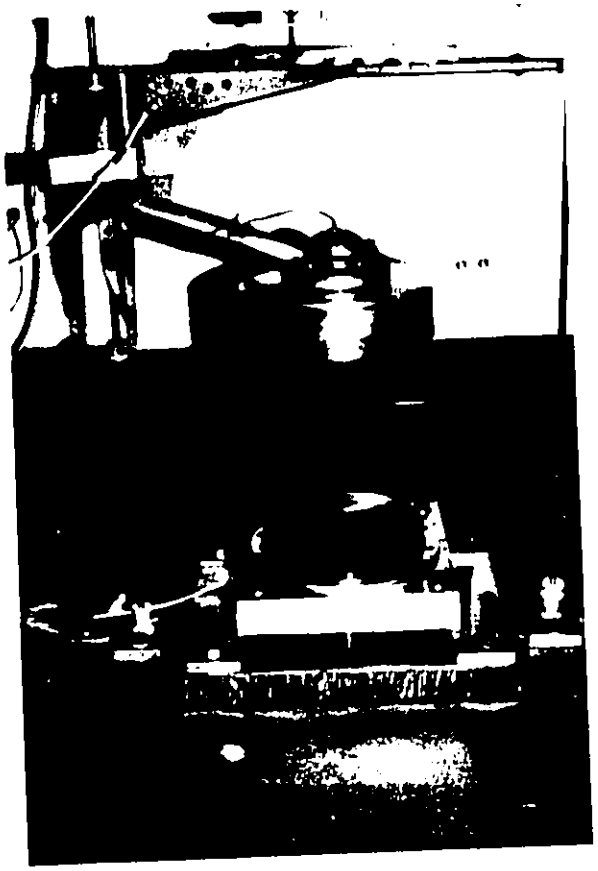

Figure 71

5 Kg Flat Impactor About the Impact MEP Pad

The object of these tests was to establish the difference, if any, between the MEP when falling and stationary. Also the effect of changing the mass can be observed.

TABLE 19.3

Test #			
76	5 kg(F)	F	MEP (Snell)
77	10 lb(F)	F	MEP (Snell)

Comparative Headform Testing with Other Researchers.

(ix) - 4. Another group of tests were performed using a Z90.1 headform that had parallel surfaces milled on the parietal left and right side. These faces were milled parallel with the mid-sagital plane, Figures 72 and 73.

Figure 72

Snell Headform, Foil Cap, and Snell MEP Level is Attached to Upper Surface.

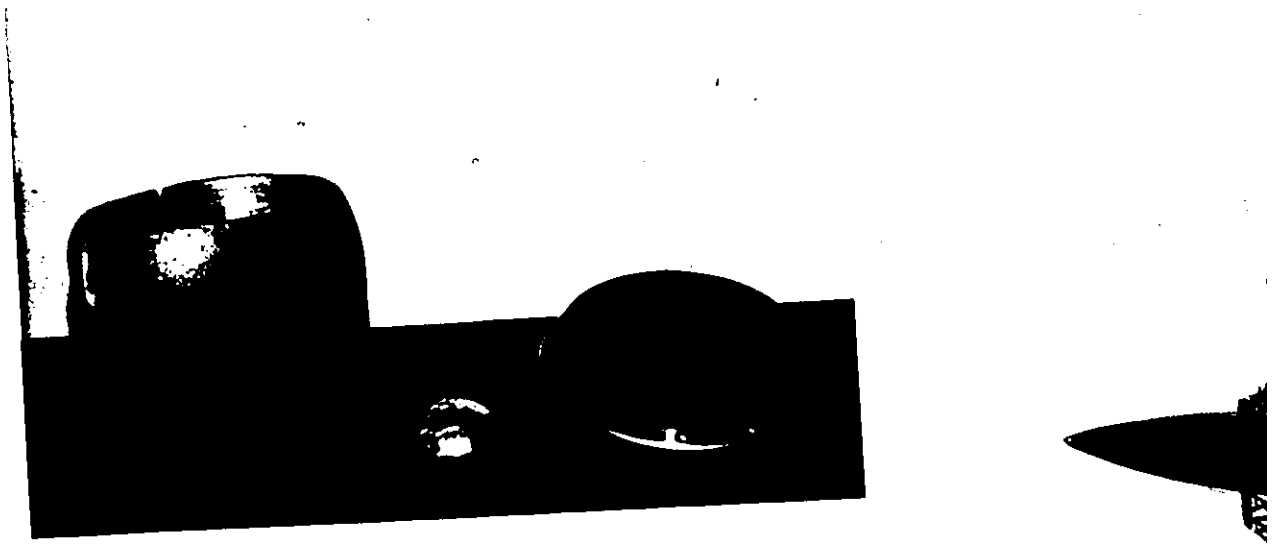

Figure 73

Note Flat Impact Surface of Z90.1 Headform (Snell)

This headform was dropped from heights of 5.0, 7.5, 10.0, 15.0, 20.0 and 25.0 inches onto the MEP pad using the MEP mounting plate, Figure 74. The results of these tests can be found in the data tables, test #75 and graph #30.

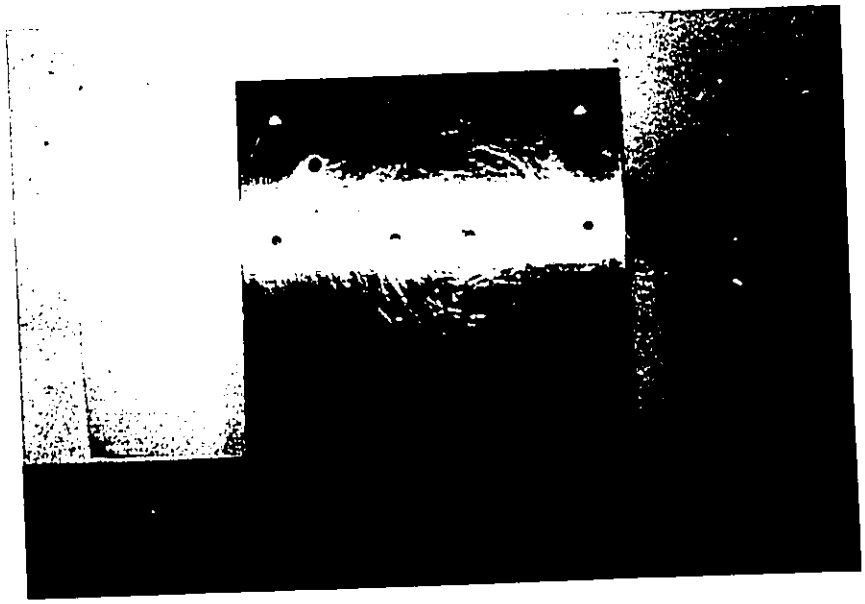

Flat Plate Snell MEP Was Attached to
Figure 74

The Z90.1 headform was the property of the Snell Memorial Foundation helmet testing facility. The headform had previously been tested by the following testing centres: Snell, Bell Helmets and the South West Research Institute.

As mentioned earlier, the purpose of these tests was to compare results between facilities.

One of the problems encountered in this testing related to the socket in the Z90.1 headform. This socket was too large to accommodate the University of Ottawa ball. To get around this problem, aluminum foil cups were made to place between the ball and socket. These cups are shown in Figure 72.

TABLE 19.4

Test #

75 5 kg (Snell H.F.) F MEP (Snell)

Velocity Calibration Check.

(ix) - 5. Another series of tests was conducted to check the freefall velocity of the drop apparatus. This was done using the 5 kg flat impactor falling on the MEP pad, from drop heights of (0.25 m to 2.50 m). The velocity measurement device was designed and constructed to measure the elapsed time of the falling blade as it passed through two light beams one inch apart.

The object of these tests was to check the drop assembly for its freefall properties and compare these results with other test facilities. The velocity measurement device is shown in Figure 75.

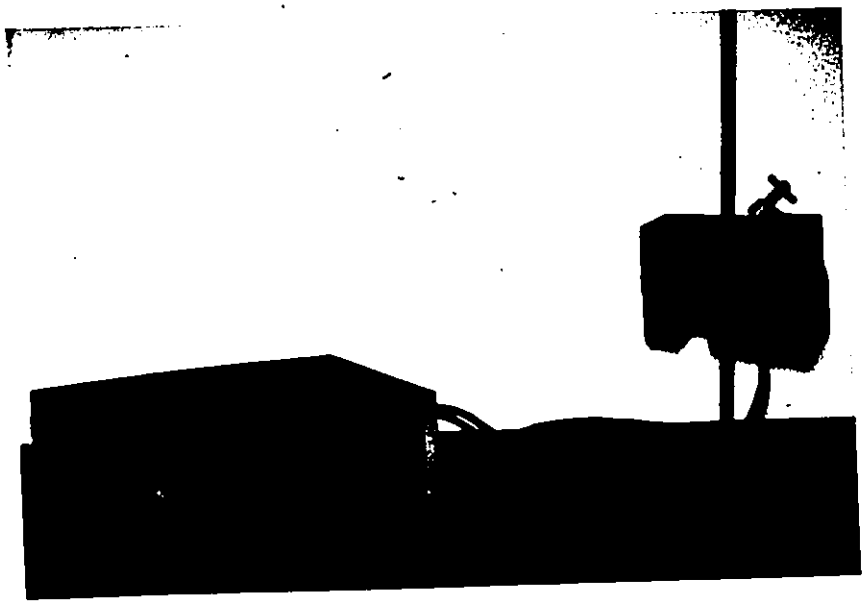

FIGURE 75

Velocity Measurement Device.

The device measures time from 0 to - 99.999 m secs. The results of these calibration tests can be found in the computer data tables.

TABLE 19.5

Test #			
99	5 kg(F)	F	MEP
100	10 lb(F)	F	MEP

Ebar Plate Tests

(ix) - 6. The results of Phase (ix) 1. led to tests of Phase (ix) 6. These tests were designed to answer the questions posed by the first battery of tests. The tests were conducted using the E bar plate at various eccentricities, Tests #79 - 83. Each eccentricity was tested from drop heights of (0.5 m to 2.0 m). Tests were also done with zero eccentricity to see the effects of having the hexagon cap screws for the slotted plate tight or loose, Test #84.

TABLE 19.6

Test #				
78	MEP	F	E bar	Plate, e = 0.0
79	MEP	F	E bar	Plate, e = 0.0
80	MEP	F	E bar	Plate, e = 0.50
81	MEP	F	E bar	Plate, e = 1.50
82	MEP	F	E bar	Plate, e = 1.75
83	MEP	F	E bar	Plate, e = 1.50
84	MEP	F	E bar	Plate, e = 1.50

Eccentricity Head Form Tests

(ix) - 7. Questions concerning the difference between eccentricity effects and problems at the headform steel neck interface resulted in a series of tests for a range of drop heights of (0.5 m to 2.00 m) with eccentricities of (0.0, 0.5, 1.0, 1.5) inches. The MEP was dropped onto the spherical wooden headform. The wooden headform was impacted with tight wood screws at the interface in question, Tests #85, 87, 88 and 89. Test #86 was conducted at 0.00" eccentricity with loose screws and a preset gap of 0.032" at each drop height. This test

was designed to illustrate the effect of interface problems in relation to eccentricity.

TABLE 19.7

Test #			
85	MEP	F	S_p - w - H.F., e = 0.00
86	MEP	F	S_p - w - H.F., e = 0.00
87	MEP	F	S_p - w - H.F., e = 0.50
88	MEP	F	S_p - w - H.F., e = 1.00
89	MEP	F	S_p - w - H.F., e = 1.50

CHAPTER VII

VII - 1 PREVIEW

This chapter deals with the analysis of the information found on the acceleration-time and force-time polaroid traces. The conclusions are stated as they occur throughout the analysis. Section 2 deals with a sample set of calculations and the correction factors used for stiffness and eccentricity effects.

Section 3 deals with the analysis of the rigid mode tests of Phases (I) to (IU).

Section 4 analyzes the tests for the multiposition mode Phase (V) to (VIII). Each of these sections 3 and 4 are followed by a conclusion summary.

Section 5 considers the analysis of the final Phase (IX) tests.

VII - 2 ANALYSIS OF DATA

The raw data from each run for each test was processed with the assistance of the computer. The calculated values of acceleration -- PA, mass x acceleration -- PMA, transmitted force -- PFLC and the percentage difference between PFLC and PMA -- P%, are shown in the data tables. As the readings were taken, the above calculations were made with a hand calculator. The calculated values of PMA and PFLC were plotted against drop height -- H before each new test drop. These plots were similar to the corrected versions, Graphs 2 and 3. By plotting and calculating during testing, errors, erroneous readings and other difficulties were spotted as they occurred.

The "P" in PA for acceleration in the data tables signifies first or premiere. In other words, the first calculated values before correction factors were taken into consideration. The "C" before the second set of calculations indicates that the first set of calculations have been corrected for eccentricity effects. The "F" in the last set of calculations indicates the use of a final correction factor for plate stiffness.

VII - 2 (i) "P"-SET OF SAMPLE CALCULATIONS

A "P"-set of calculations for test #31 will demonstrate how the raw data in the first 5 columns of the tables was processed by the computer.

H = 2.00 m — Drop Height
AED = 5.20 division — Accelerometer (Endevco) Divisions
ASF = 1.0 volts/division — Accelerometer Scale Factor
LCD = 2.95 divisions — Load Cell Division
LSF = 0.20 volts/division — Load Cell Scale Factor

Sensitivity of Accelerometer = 4.63 $\frac{mv}{g}$
Sensitivity of Load Cell = 4.776 g $\frac{mv}{lb}$

AED and LCD are the divisions read from the oscilloscope trace for the accelerometer and load cell channels.

ASF and LSF are the scale factor values of the above divisions for each channel in volts/division.

$$\text{(Acceleration)} \cdot PA = 5.20 \text{ Div} \times 0.5 \frac{\text{volts}}{\text{div}} \times \frac{1}{4.63 \times 10^{-3}} \frac{v}{g}$$

$$= 1{,}123.1 \text{ g} \times \text{Gain of } 1^*$$

$$= 1{,}123.1 \text{ g's}$$

$$\text{(Load Cell Force)} \quad FLC = 2.95 \times 0.20 \frac{\text{volts}}{\text{div}} \times \frac{1}{4.776 \times 10^{-3}} \frac{v}{lb}$$

$$= 123.534 \text{ lb} \times \text{Gain of } 100^*$$

$$= 12{,}353.4 \text{ lbs}$$

---

* The gains of 1 and 100 are for the(B and K)A.C. amplifiers for the accelerometer and load cell respectively.

VII-2-(ii) CORRECTION FACTORS

After completion of the Phase V tests there seemed to be evidence that indicated eccentricity and headform-neck interface problems were causing the large percentage differences (P%) between PMA and PFLC. It was decided, as mentioned previously, to use the Ebar plate to help understand the nature of the above problems. Tests 67(1) to 67(5) produced the results shown in the tables. The results seemed unusual, as there did not seem to be any large drop in acceleration (PA) until eccentricities (Ebar) of 1.50 inches had been reached.

After doing more Phase V, VII and IX testing, it was decided that more eccentricity testing with the Ebar plate was in order. Graphs 6 and 7 show graphically the results of Tests 79-84, Phase IX-6.

The results of these tests support Tests 67(1) - (5). The question that arose here was: why do PFLC and PMA seemingly increase from e* = 0.0 to 1.00 inches and then decrease for e = 1.50 to 1.75 inches. It was decided that to answer this question, more testing in Phase IX should be done to understand further the effects of eccentricity and the concept of effective mass. It was also hoped that this testing would lead to a correction factor to correct the large percentage differences (P%) between PMA and PFLC.

The spherical wooden headform was chosen as mentioned previously in the description of Phase (IX)-7 testing. Tests 85 and 86 illustrated dramatically in traces 85(273-274) and 86(275-278).

The effects of tight and loose screws. For loose screws Test 86,

---

* e = Ebar = slotted plate eccentricity

the load cell traces displayed jagged peaks in the region of peak force as compared to traces 273 and 274 where the load cell peaks were smooth curves for the tight screws. The reductions in PFLC and PMA are shown in Graphs 8 and 9

With this information previous and future cases of loose screws should be easily spotted.

Tests 87-89 produced the results shown in the tables, for eccentricities of 0.00", 0.50", 1.00" and 1.50" of the spherical wooden headform mounted on the slotted plate. This data was plotted in graphs 10 and 11. From the graphs, it can be seen that eccentricity affects the load cell more than the accelerometer signal. By increasing the eccentricity the load cell signal increased and the accelerometer signal decreased for any given drop height.

This information was used for the eccentricity correction factor "C", mentioned previously. Straight line graphs 12 and 13 were plotted for the increases and decreases in percent against eccentricity. The equations of these lines were obtained for the different regions of eccentricity and are summarized as follows in Table 20.

TABLE 20 Eccentricity Equations

Graph #	Region of Eccentricity (e)	Straight Line Equation	Same Straight Line Equation in Computational Fortran	Use of the Correction Factors in the Fortran Programme
PFLC Graph 12	0.00<e<0.50 0.50<e<1.50	% = 12 e % = 6.2 e + 3.0	PERF = 12.0* Ebar PERF = 6.2 * Ebar + 3.0	CFLC(I) = FLC(I) - (PERF * FLC(I))/100
PMA Graph 13	0.00<e<1.00 1.00<e<1.50	% = e % = 8.4 e - 7.4	PERMA = Ebar PERMA = 8.4 * Ebar - 7.4	CMA(I) = RMAEG(I) + (PERMA * RMAEG(I))/100

The manner in which these Fortran equations were used for eccentricity correction purposes in the computer programme is shown in the programme listing that precedes the data tables. As mentioned previously, the calculation corrections for eccentricity in the data tables are prefixed by the letter "C" for CMA, CFLC and C%.

Because all headform neck interface characteristics of other headforms were not the same as those characteristics of the spherical wooden headform (Sp - W - H.F.) the degree of tightness of the other headforms would have to be made in comparison to the spherical wooden headform. This was done by the use of an effective eccentricity relationship called "EEbar". As an example in Test #35, the actual measured eccentricity was 1.150 inches, but because the CSA wooden large headform was held by eight smaller wood screws as compared to the four larger wood screws of spherical wooden headform, the effective eccentricity was judged to be 75% of the actual eccentricity Ebar. Thus $EEbar = \frac{75}{100} \times Ebar$

$$EEbar = .75\ (1.15)$$

$$= .863 \text{ inches}$$

With the use of EEbar, the corrections were made as shown in the data tables. Table 21 lists the tests where judgements of this type

TABLE 21 EEbar Estimates

Test #	Ebar	%	EEbar	Impact Description
29	0.400	50	0.200	MEP F Cast Al. (thin)
35	1.150	75	0.863	MEP F CSA - W - L - B
37	0.720	50	0.360	MEP F CSA - W - S - B
39	1.000	75	0.750	MEP F CSA - P - L
43	0.690	50	0.345	MEP F Cast Al. (thick)
55	1.550	50	0.770	5 Kg (F) F Cadaver 1 with helmet
56	1.000	50	0.500	5 Kg (F) F Cadaver 1 without helmet

were made. In summary, the more rigid the interface, the lower the EEbar values.

These tests using the spherical wooden headform permitted the experimental correction for the large percentage differences (P%) between PMA and PFLC. The tests also supported the concept of effective mass. The concept of effective mass essentially explains the above experimental results. When the interfaces between the striker and the load cell are rigid or stiff, no P% should exist. When the interfaces are not completely rigid and permit slight movement, the impacting mass which the load cell senses, is the mass of the striker and some portion of the mass of the headform. The sum of these two masses would be the effective mass sensed by the load cell at impact.

The testing with the spherical wooden headform did not create any new information for Tests 79-84, Phase IX-6 with the Ebar plate. Thus, some other reason for the phenomena occurring in Graphs 6 and 7 would have to be found. This reason was found when the physical structures of the top mounting plate and the slotted plate were examined closely.

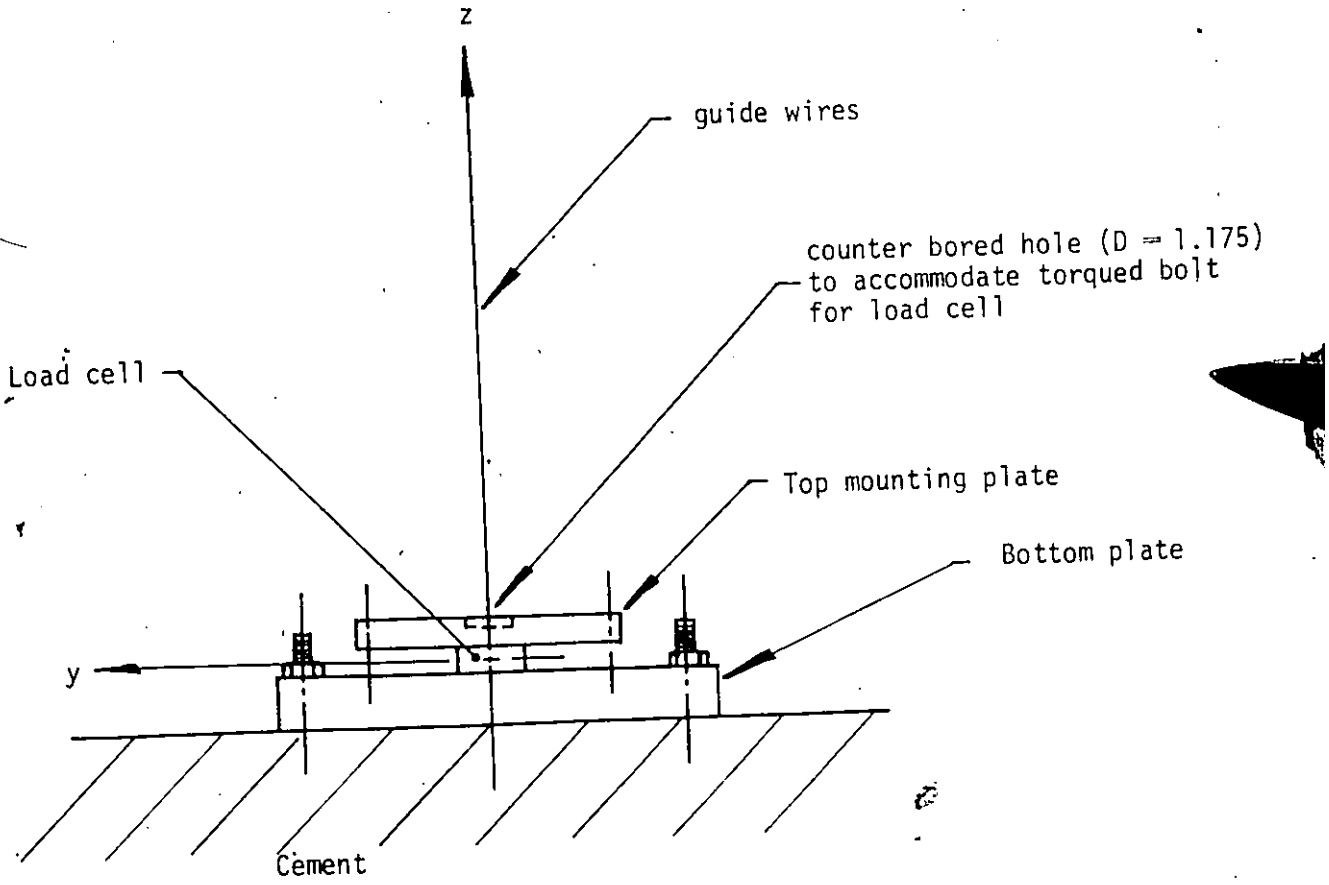

Figure 77

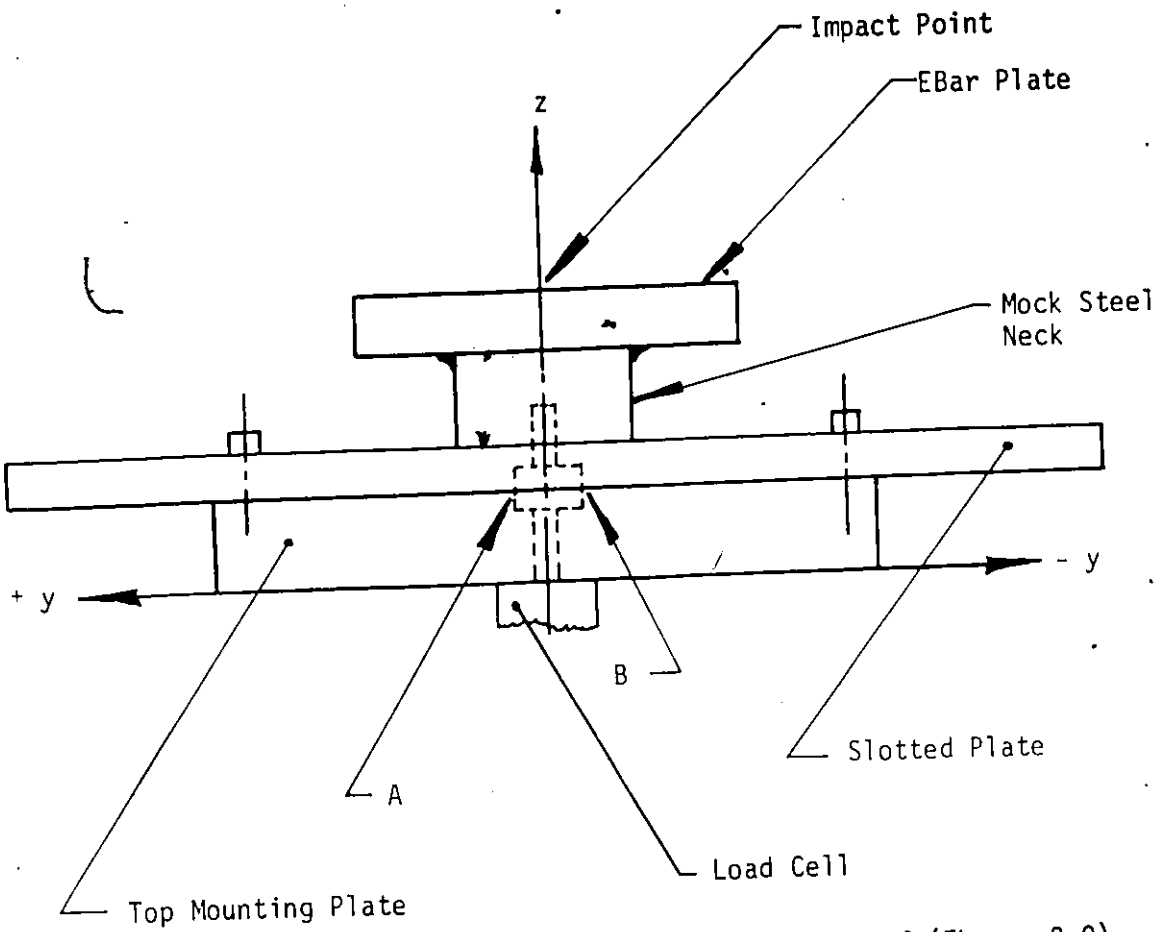

Figure 78 Shows Position of (Ebar = 0.0)

Note: Both counter bored holes have D = 1.175" and the bolts have a 1/10" clearance with the ground surfaces.

The sketch in Figure 77 shows the relationship between the top mounting plate and how it is torqued to the bottom plate by a bolt at the counter bored hole.

The sketch in Figure 78 illustrates how the counter bored hole of the slotted plate is concentric with the counter bored hole of the top mounting plate at zero eccentricity (Ebar = 0.0). As the eccen-

tricity is changed by moving the slotted plate in the positive y direction, eventually a point will be reached when the two holes no longer overlap. It was noticed that a small bur had occurred at points A and B in Figure 78. This observation along with Graphs 6 and 7 led to the conclusion that the counter bored holes were affecting the system stiffness[1]. As the slotted plate was moved in the positive y direction from Ebar = 0.00 the two holes began to overlap causing the stiffness to increase. As the eccentricity reached $Ebar_o$ = 1.00" the stiffness had reached a maximum. By increasing the eccentricity to Ebar = 1.50" the stiffness is seen in the graphs to decrease below the stiffness at Ebar = 0.0. The reason the stiffness decreases further for Ebar = 1.75 can be seen in the sketch in Figure 79. Here the major loss in stiffness is due to the absence of supporting material in the region

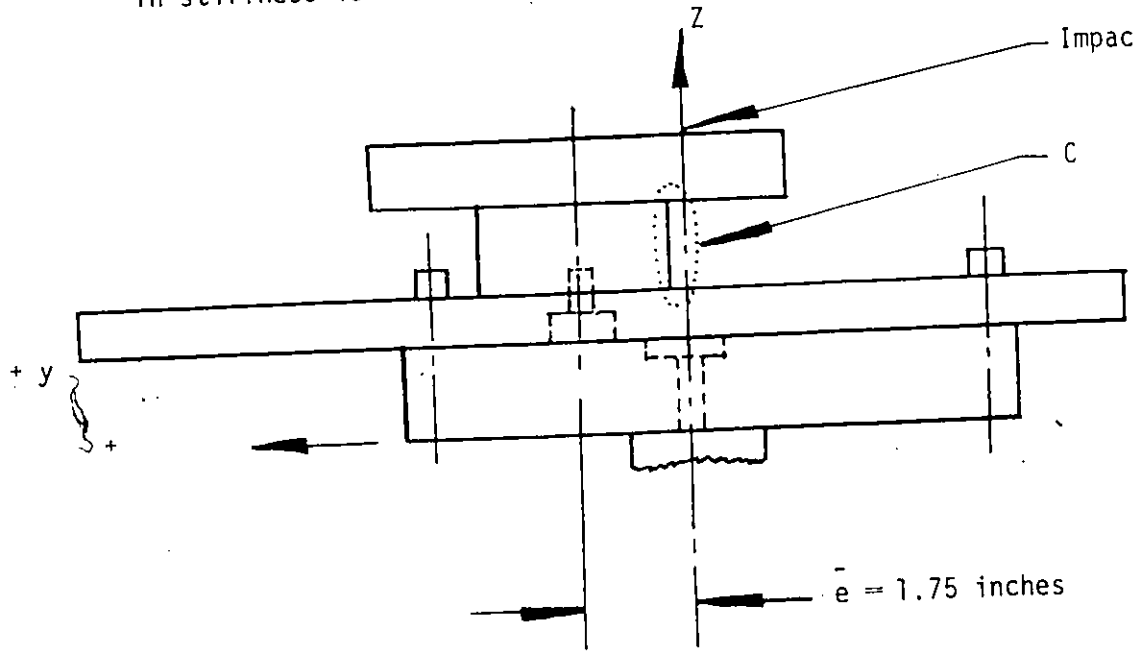

Figure 79

1 The stiffness referred to here is a function of the elastic properties of the system material or materials and the system geometry.

of C as shown. Here again the counter bored hole in the top mounting plate would result in a minor loss in stiffness. The data in Graphs 6 and 7 used to plot the straight line curves in Graphs 14 and 15. Here the stiffest condition was taken to be at Ebar = 1.00". The percentages of the stiffest condition were plotted on the ordinate with eccentricity on the abcissa. The equations of the lines in the regions of eccentricity were found and summarized as follows in Table 22.

TABLE 22 Eccentricity Equations

Graph #	Region of Eccentricity (e)	Straight line Equation	Same Straight Line Equation in Computational Fortran
PFLC Graph 14	0.00<e<1.00	% = -1.88 e + 1.88	SPERF = - 1.88 * Ebar + 1.88
	1.00<e<1.50	% = 12.84 e - 12.84	SPERF = 12.84 * Ebar - 12.84
	1.50<e<1.75+	% = 27.16 e - 34.32	SPERF = 27.16 * Ebar - 34.32
Graph 15	0.00<e<1.00	% = -1.86 e + 1.86	SPERMA = - 1.86 * Ebar + 1.86
	1.00<e<1.50	% = 7.2 e - 7.2	SPERMA = + 7.20 * Ebar - 7.2
	1.50<e<1.75+	% = 16 e - 20.4	SPERMA = +16.00 * Ebar - 20.4

The manner in which these equations were used for stiffness correction purposes in the computer programme is shown in the programme listing that precedes the data tables.

As mentioned previously, the calculation corrections for the final correction factor stiffness are prefixed by the letter "F" for FMA, FFLC and F%.

It can be noticed from the data tables that the eccentricity corrections tend to substantially reduce the percentage difference between PMA and PFLC while the stiffness correction factors tend to slightly increase the percentage difference.

VII-3 ANALYSIS OF PHASE (I),(ii),(III), and (IV) TESTS

VII-3-i PHASE (I) and (IV) MEP TESTS

Data tables for Phase (I) were plotted in Graphs 2 and 3 (H vs FFLC and FMA). The critical regions were plotted again in Graphs 4 and 5. A 5% tolerance band was drawn over the curves that came closest to cadaver 1 curve. Falling within the 5% tolerance band are the following headforms listed in Table 23(a). The headforms not falling within the tolerance band are listed in Table 23(b).

Headform Description	Test No.
Cast Al. (thin)	29
CSA - W - S - B	37
CSA - P - L	39
CSA - P - S	40
Sierra	44

Table 23(a)

Headform Description	Test No.
CSA - W - L - B	35
CSA - P - L	38
Sp - W - H.F.	42
CSA - W - L - C	34
CSA - W - S - C	36
Cast Al. (thick)	43
Z90.1	45

Table 23(b)

It is worthwhile to note that test #35 for the CSA - W - L - B was just slightly above the tolerance band. This headform would probably have fallen within the tolerance band had there not been some flattening of the headform material at the impact site due to an inadvertent drop with the flat impactor before the MEP tests.

It can be seen from Graphs 2 and 3 that the cadaver 1, Test #56 without a helmet is relatively close to the tolerance band. If cadaver 1 had a complete scalp and was less dehydrated the readings would have been somewhat lower. Repetitive impact testing with a cadaver head (scalp intact) using the MEP is not practical because of the slightly pointed nature of the MEP impact surface. This impact surface would cause the scalp tissue to break down after one impact.

The damping ability of the urethane skin of the Sierra headform was the reason it fell within the tolerance band. The thin structure of the cast aluminum headform (thin) caused it to have a fair degree of resiliency upon impact. This thickness effect is quite pronounced when comparing Test #43 for the cast aluminum (thick) with Test #29 for the cast aluminum thin. The plastic material used for the CSA hockey headforms (CSA - P - L and CSA - P - S) had sufficient resiliency for them to fall within the 5% tolerance band.

The effect of the headform shape for the MEP tests can best be realized by comparing the flat plate test 31 with test 26 incorporating the hemispherical anvil. In these tests the hemispherical (mild steel) anvil has a radius of 48 mm (1.90 inches) and the flat plate (mild steel) has an infinite radius. Graphs 2 and 3 demonstrate the large difference

in force outputs for the two impacts. The impact with the flat plate by the MEP was an extremely violent impact. Whereas the impact with the hemispherical anvil by the MEP had the smallest force output readings. Hence a headform with a larger crown radius in mid sagital plane* would have higher force and acceleration output readings assuming both were of the same material and hence of the same stiffness.

This headform shape effect was most pronounced for the Z90.1 headform. To avoid ball rotation, the Z90.1 headform was tilted slightly (6^0) and impacted with zero eccentricity. This meant that the MEP impactor would be falling on an essentially flat surface. It was concluded that this flat surface was mainly responsible for the high output force readings, for the Z90.1 headform. It could be argued that stiffness was also a factor but to a lesser degree, because the Z90.1 headform was probably slightly stiffer than the cast aluminum (thick) headform. It should be pointed out, however, that the cast aluminum thick headform was a small size and had the most pronounced radius at the impact site.

The grouping in Graphs 4 and 5 lead to the following conclusions. From the MEP tests of Phase (I) and (IV) it can be said two factors governed the performance of the headforms:

(1) The stiffness, which depended on the material and headform wall thickness.

(2) The anthropometric shape of the headform.

---

* Mid sagital plane - a longitudinal or fore and aft, plane passing through the vertex or crown of the headform, perpendicular to the basic plane *-1 , which geometrically bisects the headform.

* - 1 A plane at the level of the external opening of the ear and the floor of the bony rim or orbital of the eye.

VII - 3 (ii) PHASE (II) AND (III) HELMET TESTS

The helmeted tests of Phase (II) and (III) were plotted in Graphs 2 and 3. The critical regions between 1.5 and 2.5 meters were plotted again in Graphs 4 and 5. Here it can be seen that with a helmet the Sierra headform, Test 48, is closest to the cadaver results. The fact that cadaver 2, as was described in the cadaver information tables, was an embalmed moist cadaver head with an intact scalp accounts for different results from cadaver head 1.

Graph 4 shows the results of the helmet tests grouped less closely than the acceleration results of Graph 5. This implies that even though the helmets felt similar, acceleration effects the energy transmitted to the load cell was different.

Anthropometric shape and stiffness were found to be the essential factors governing the results of the headform MEP tests of Phase (I) and (IV). It is unlikely that the stiffness is as great a factor for the helmet tests. A general reduction in stiffness would reduce both the peak acceleration and the peak force, but reducing the stiffness would do little in reducing the difference (F%) between FMA and FFLC.

The anthropometric headform shape affects the F% more directly by either increasing or decreasing the permanent deformation of the styrafoam liner of the helmet.

The amount of permanent deformation in the polystyrene liner depends highly on the contact area between the headform and the polystyrene foam liner. If the contact area is small the permanent deformation should increase. This is true for the headforms without a skin. In the case

of the Sierra headform, had the yielding skin not been present, the polystyrene foam liner would have had to deform to a greater degree. The question still is present, "Then why is the F% low for the Sierra headform?" The answer lies in the nature of the impact and how the energy is transferred to the load cell. In the case of the Sierra headform a certain amount of the wave of energy passing through the skin tangential to the surface of the headform cannot get to the load cell because there is no physical attachment other than friction between the skin and the aluminum skull of the headform.

It seemed a little surprising at first that the Z90.1 headform was as close to the Sierra and cadaver head responses when they were so far apart for the MEP tests. The reason that explains this phenomenon lies in the anthropometric shape of the Z90.1 headform relative to the test helmet as shown in Figure 80.

Air Space at Z90.1 Headform-Helmet Interface
Figure 80

Figure 80 shows a helmet identical to the test helmet sectioned along the mid-sagital plane and resting on the Z90.1 headform. The large air gap is very much apparent. This air gap and absence of material acted to improve the performance of the helmeted Z90.1 headform. Instead of crushing the polystyrene foam liner in the region of impact, crushing and sliding have been shifted to a smaller area annulus around the point of impact. The combination compressing of the air space and increased permanent deformation caused the accelerometer to see a softer deceleration and the load cell not to see the energy lost in permanent deformation of the liner.

What has been said so far does not explain why this percentage difference (F%) exists. When the load cell was calibrated, there was only a flat plate between the load cell and the MEP striker. The impacting mass is essentially the mass of the striker. By placing a headform and then a helmet between the striker and the load cell, the system has been changed considerably. The real mass that the load cell sees is that of an effective mass. The effective mass depends on the mass of the striker and the mass of the helmet. Hence it can be seen if the acceleration values were multiplied by a greater mass the FMA values would be closer to the FFLC values, thus reducing the F%. One might argue that the effective mass is even larger than the sum of the mass of the helmet and striker. Since at impact (for the cast aluminum thin headform, the headforms with interface problems the CSA-W-L-B and the CSA-P-L) there was headform wall or headform movement this tends to

increase the effective mass still further by some portion of the headform weight.

It was suggested earlier that headform stiffness would not play as great a part in the helmet tests as it did in the MEP tests. The reasoning behind this statement assumes that the headforms are a great deal stiffer than the helmets. Comparing the helmet tests of the Sierra with the cadaver heads 1 and 2 illustrates that the cadaver heads are not as stiff and rigid as the headforms. This suggests the aluminum skull thickness of the Sierra headform could be reduced for more favourable performance relative to the cadaver heads.

VII - 3 - (iii) OUTER SHELL EFFECTS

It is of interest to note that Test #53 and 54 were carried out to see the effects of using a new outer shell relative to the test outer shell. In Test #53, the yellow J.C.B. plastics outer shell (polycarbonate) was tested at the 2.00 meters drop height. This yellow outer shell was the same outer shell used in all previous helmet impacts in Phase (II) and (III). This outer shell had also been used for 10 impacts during preliminary testing. Test #54 used an identical new blue outer shell with the usual new liner at the same drop height (peak acceleration and peak transmitted force) of 2.0 meters. The results of the new outer shell were 4.5% higher. One might ask if this is not going to have a slight effect on these results. The answer is no; since the helmet had been impacted in preliminary testing, the initial stiffness of the new helmet had been removed. Comparing Test #53 at the end of the

fixed mode helmet tests with Test #46 at the beginning, both using the Z90.1 headform with the same outer shell, it can be seen that the results are within 2.27%.

The procedure of placing the liners into the outer shell left no room for error. Each liner application was performed by two people and checked by both before impact.

Spot checks on the polystyrene foam liners for weight assured that they were all from the same batch, and hence had the same density.

The reason the Z90.1 headform was used for these tests was illustrated in a previous discussion and Figure 80. This air gap between the top of the headform and comfort liner would allow for considerable deflection of the outer shell. The Z90.1 headform was judged to accentuate this deflection more than any of the other headform. In other words, the Z90.1 headform would have been the most likely headform to bring out any helmet outer shell stiffness problems should they have existed.

VII - 3 - (iv) MEP COMPARISON TESTS

Test #41 of the MEP tests was performed on the spherical wooden headform (Sp-W-H.F.). At a drop height of 1.66 meters to compare results with Jehu (27). These results are compared in Table 24. Jehu used a similar MEP (Code Green) calibration pad.

Table 24

Researcher	Impact Energy	M x a	FLC	% Diff.
Jehu	8.3 m kg f	25.6 knt	27.6 knt	7.25 %
Webster	8.3 m kg f	5,176.5 lb 23.023 knt	5226.3 lb 23.24 knt	0.96 %
	% Diff.	10.06 %	15.79 %	

$$M \times a = 5,176.1 \text{ lb} \times \frac{4.448}{1 \text{ lb}} \text{ nt}$$

$$= 23,023 \text{ nt}$$

$$= 23.023 \text{ knt}$$

Jehu accounts for his 7.25% difference in a stepped onset of force which he postulates is a frequency characteristic of the load cell. This stepped onset he described is shown in Figure 81.

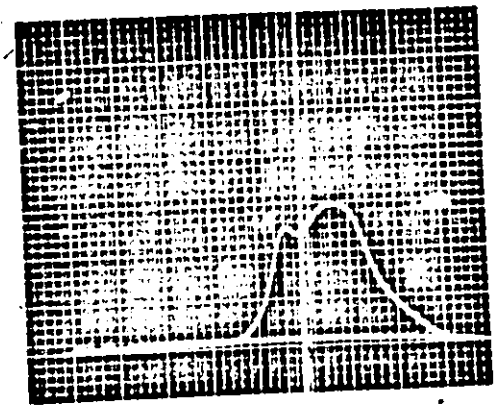

Figure 81

This stepped onset looks suspiciously like interface problems that occurred in many time traces #132, 142 and the loose screw tests of traces 275, 276, 277 and 278. In all cases, there were smooth acceleration curves, paralleling Jehu's observations. Perhaps the reason Jehu's stepped onset is before the peak has something to do with the physical distance between impact point and the load cell. From Jehu's apparatus diagrams our distance looks considerably greater. Hence, this wave phenomenon takes longer to be sensed by the load cell. One might ask the question, "How can the 15.79% and 10.06% differences in Table 24 be accounted for?" This difference can best be accounted for by considering the stiffness of the headforms. Both headforms had relatively the same crown radii and thus the same shape. However, Jehu's headform was carefully constructed from hardwood, whereas the spherically-shaped headform used here was constructed from a soft wood - pine. Hence it is the author's opinion that the softer material reduced the acceleration and load cell readings. It is also believed that the speculated interface problems Jehu encountered increased the effective mass of that system, thereby increasing that percentage difference (%Diff) to 7.25%. In other words, the two tests should have both differed by 10.6%, not 15.79% and 10.06%.

VII - 3 (v) PERIODIC CALIBRATION TESTS

Before and after each phase of testing, calibration checks were made using the MEP impacting the flat plate or the hemispherical anvil. Some of these checks have been included in the tables. Tests 32, 51 and 57. This practice became less frequent as it became apparent that the calibration sensitivities of the load cell and accelerometer were remaining constant with not the slightest variation.

VII - 3 -(vi) DISCUSSION OF CADAVER SKULL FRACTURES

Returning to the cadaver head tests without a helmet, the testing for cadaver 1, Test #56, with the MEP was stopped at 1.50 m. At this drop height, skull fracture occurred. The fracture shown in Figure 82 started at the point of impact and descended the parietal right side to 1/2" below the level of the ear opening.

Figure 82(a) Fracture Location

The time trace #206 clearly indicates skull fracture. With a large disturbance shown by the accelerometer trace slightly after peak acceleration similar disturbances have also been reported by other researchers. This author observed that the audibly different noise produced at impact for fracture also proved to be an accurate indicator.

The trace #213 illustrates the same disturbance. Phenomena for the skull fracture of cadaver head 2, shown in Figure 82(b). Cadaver head 2, Test #59 fractured at a lower drop height with the 5 kg flat striker

Figure 82(b) Fracture Location

even though cadaver 2 had a moist intact scalp. Cadaver 2 was impacted only twice to minimize the breakdown of the scalp and fatigue of the skull. For both cadaver head tests, the neck mounting arrangement

remained secure. The cadaver 1 base of the skull -- plastic interface loosened at the fracture-impact. This was due to the fact that cadaver 1 did not incorporate the use of the first two neck vertebrae -- the atlas and axis -- in the plastic neck portion. By using these two vertebrae in the plastic section of the neck, a stronger interface was found to occur.

The more serious skull fracture of cadaver head 1 was accompanied by a substantial increase in the F%, whereas the minor skull fracture of cadaver head 2 was accompanied by only a slight increase.

Because there is no fracture impact data for the crown region, comparisons of force cannot be made. However, these two tests will yield relevant future data. The MEP tests for cadaver head 1 should aid in further development of frangible headforms.

With regard to frangible headforms, it was mentioned previously that if the cast aluminum skull of Sierra headform were made of comparable wall thickness to the cast aluminum (thin) headform, the results may have been considerably lower in both the MEP and helmet tests. Hence, comparing even more favourably with the cadaver head tests.

VII - 3 - (vii) ANALYSIS OF ACCELERATION AND LOAD CELL TRACES

In order to understand and explain the meaning of any acceleration trace, Trace #185 of Test #48 was re-plotted in Graph 24. Using the rectangular rule for integration the acceleration curve $\ddot{x}(t)$ was

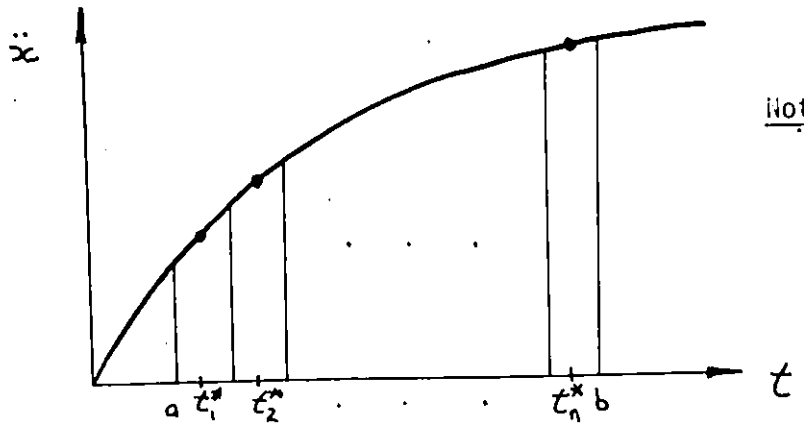

Note: Graph 24 real t=0 occurs A t=.4 m sec according to scales on Graphs 24-27

$$\Delta t = \frac{b - a}{n}$$

$$(1) \quad \int_a^b f(t)dt \quad \Delta t[f(t_1^*) + f(t_2^*) + \quad + f(t_n^*)]$$

integrated from 0.0 to 10.5 m.sec. The integral of the acceleration curve $\ddot{x}(t)$ produces a velocity curve $\dot{x}(t)$.

$$(2) \quad \int_a^b f(t)\,dt = \int_a^b x(t)\,dt = x(t)\Big|_a^b$$

The reference datum to establish a sign convention for displacement $x(t)$, velocity $\dot{x}(t)$ and acceleration $\ddot{x}(t)$ was taken at time $t = 0$.

The sign convention for the falling striker shortly before impact ($t = 0^-$) and shortly after impact ($t = 0^+$) would be as follows:

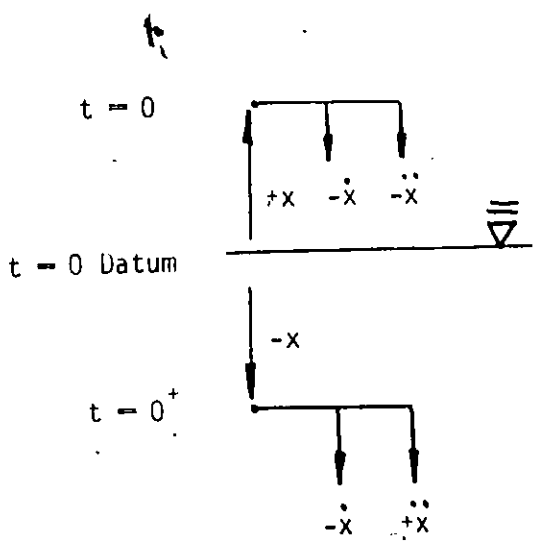

Displacement Sign Convention

Displacement x positive away from the centre of the earth

Velocity Sign Convention

$+\dot{x}$ if in + x direction

$-\dot{x}$ if in - x direction

Acceleration Sign Convention

$+\ddot{x}$ if + x increases

or $-\ddot{x}$ if - x increases

The velocity curve $\dot{x}(t)$ has been plotted in Graph 25, curve (1). When $a = 0 = t$ in equation (2), the initial condition for $\dot{x}(0)$ must be used. From Graph 28 which is a plot of drop height versus ideal velocity for free fall conditions the initial conditions for the 2.50 meter drop height can be seen to be $\dot{x}(0) = 23$ ft.sec^{-1}. Thus Equation

(2) becomes

$$(3)\quad \int_0^{t=n} f(t)\,dt = \int_{t=0}^{t=n} \ddot{x}(t)\,dt = \dot{x}(t)\Big|_0^n = [\dot{x}(n) - \dot{x}(0)]$$

$$= -\dot{x}(0) + \dot{x}(n)$$

$$= -23.0\ \text{ft.sec}^{-1} + \dot{x}(n)$$

To show the integration procedure the first integration has been performed for Graph 24.

$$(4)\quad \int_0^{t=n=4^{SDIV}} f(t)\,dt = \int_0^{4^{SDIV}} -\ddot{x}(t)\,dt \approx -23.0 + 0.1\ \text{msec}$$

$$[(.25 + 5 + 10 + 15)\ \text{large divisions}]$$

$$\Delta t = \frac{b-a}{n} = \frac{(.4-0)}{4}\ \text{msec} = 0.1\ \text{msec}$$

$$\approx -23.0 + 0.1\ \text{msec}\left[(30.25)\text{Sdiv} \times \frac{1\ \text{Ldiv}}{20\ \text{Sdiv}} \times \frac{43.2\text{g}}{1\ \text{Ldiv}}\right]$$

$$\approx -23.0 + 0.1\ \text{msec}\left[65.2\ \text{g} \times 32.2\ \frac{\text{ft sec}^{-2}}{1\ \text{g}}\right]$$

$f(t_1^*) = 0.25$	20 large div = 2 m sec	$\approx (-23.0 + 0.21)\ \text{ftsec}^{-1}$
$f(t_2^*) = 5.00$	1 large div = .1 msec	
$f(t_3^*) = 10.00$	large div = Ldiv	$\approx -22.79\ \text{ftsec}^{-1}$
$f(t_4^*) = 15.00$	small div = Sdiv	

This procedure was carried out for $t = 0$ to 10.5 msec.

From Graph 25 it can be seen that $\dot{x}(t) = 0$ at $t = 5.72$ msec. The corresponding point on the acceleration curve is pointed out on Graph 24 for the third acceleration peak. It also can be seen that the velocity reaches its positive maximu of $\dot{x}(t) = +8.4 \text{ft sec}^{-1}$ for $\ddot{x}(t) = 0$ at 9.60 msec.

The velocity curve $\dot{x}(t)$ in Graph 25 was integrated again from 0 to 10.5 msec. The integral of the velocity curve $\dot{x}(t)$ produces a displacement curve $x(t)$.

$$(5) \quad \int_a^b \dot{x}(t)\, dt = x(t) \Big|_a^b$$

The displacement curve has been plotted in Graph 26. To show the integration procedure, the first integration of the $\dot{x}(t)$ curve for Graph 25 has been performed, Equation (6).

$$(6) \quad \int_0^{t=n=4\text{Sdiv}} f(t)\, dt = \int_0^{4\text{Sdiv}} -\dot{x}(t)\, dt \approx 0.1 \text{ msec} | 23.00 + 22.93 + 29.90 + 22.71 | \text{ ftsec}^{-1}$$

$$\Delta t = \frac{b - a}{n} = \frac{(.4 - 0)}{4} \text{msec} \quad \text{or} \quad \dot{x}(5.72 \text{ msec}) \approx -0.009054 \text{ ft}$$

$= 0.1$ msec
$f(t_1^*) = 23.00 \text{ ft sec}^{-1}$
$f(t_2^*) = 22.93 \text{ ft sec}^{-1}$
$f(t_3^*) = 22.90 \text{ ft sec}^{-1}$
$f(t_4^*) = 22.70 \text{ ft sec}^{-1}$

The preceding procedure was carried out for $t = 0$ to 10.5 msec.

From Graph 26 it can be seen that maximum displacement is reached at $x(t) = 0.09$ ft which corresponds to $t = 5.72$ msec, $\dot{x}(t) = 0$ or $\ddot{x}(t) = 188$ g. It is interesting to note how little the three acceleration peaks of Graph 24 affect the velocity and displacement curves of Graphs 25 and 26.

The load cell signal for trace 185 was also replotted on Graph 27. There is a 0.7 msec delay between the time the accelerometer first senses a deceleration and the load cell senses any force. The three well defined force peaks need not correspond to the three acceleration peaks. The wave phenomena and damping characteristics of the helmet and headform have altered their occurrence in time so that the force peaks are not in phase with the acceleration peaks. Interestingly, the force goes to zero at the same time the acceleration is zero. The examination of other traces for helmet and MEP tests shows that the above phenomenon is coincidental.

The three acceleration peaks can be thought of as the striker overcoming three barriers of resistance, before assuming maximum displacement and zero velocity. The first two force peaks represent sharp increases and decreases in force that pose a likely hazard should they be transmitted to the brain of the helmeted human.

In the integral calculations of the acceleration curve for Graph 25, the ideal velocity of -23.0 ft sec^{-1} was used. Since guide wire friction and air frictional resistance exist the real velocity will

be less than -23.0 ftsec^{-1}. If one supposes that the maximum velocity occurred at peak acceleration then from Graph 24, this would occur at peak (2) for 4.2 msecs. If $\dot{x}(t) = 0$ at 4.2 msecs then curve (2), Graph 25 would result. Curve (3) illustrates a further shifting of the velocity curve.

For curve (2) the real velocity at impact would have been 13.6 ftsec^{-1}. This is a 41% difference than the ideal velocity. Throughout the testing, visual tests were carried out to monitor free fall conditions. The visual tests consisted of dropping a steel nut and the striker from the drop release and visually observing their impacts from a 2.0 m drop height. In all checks throughout testing the guided striker appeared to fall at the same velocity as the steel nut.

The periodic calibration checks for force and acceleration at standard drop heights illustrated that the free fall velocity remained consistent throughout the testing programme. It was also assumed that the visual velocity checks could guarantee velocities which were within 10% to 15% of the ideal velocity.

Considering the crudity of this method of visually monitoring striker velocity, an attempt was made to have a velocity measurement device fabricated. Unfortunately, this device could not be obtained until well after testing had been completed.

If visual velocity comparison indicates actual velocities are within 15% of the ideal velocity, and if zero velocity occurs at peak acceleration which dictates that the actual velocity is 41% from ideal,

what explains this discrepancy?

This discrepancy may be partially explained by considering wave phenomena, damping characteristics and the surface contour of the medium being impacted. The physical time it takes for the wave to travel through the helmet and headform to the load cell would tend to move the force curve to the right in Graph 27. The damping characteristics of the helmet and headform would tend to make the force curve move to the left. What this means is that peak force need not necessarily occur at peak acceleration. The matter is further complicated by the spherical shape of the helmet as it is impacted by the flat impactor, this will tend to make the stress time curve non linear. Still further complications arise when the plastic deformation of polystyrene or the anelasticity of the MEP calibrating pad are considered. From this discussion it is evident that there is a need for more work to be done in this aspect of helmet-headform testing before more precise explanations can be made.

VII - 3 - (viii) COMPARISON OF ACCELERATION AND LOAD CELL TRACES FOR MEP AND HELMET TESTS

In general the MEP tests tend to have very well defined load cell and acceleration traces similar to a half sine wave. For example, trace #163 for the MEP falling on the Sierra headform Test #44. Here it can be seen that peak force and peak acceleration occur at nearly identical times. We would expect the $\ddot{x}(t)$, $\dot{x}(t)$ and $x(t)$ curves to be similar to those shown in Figure 83.

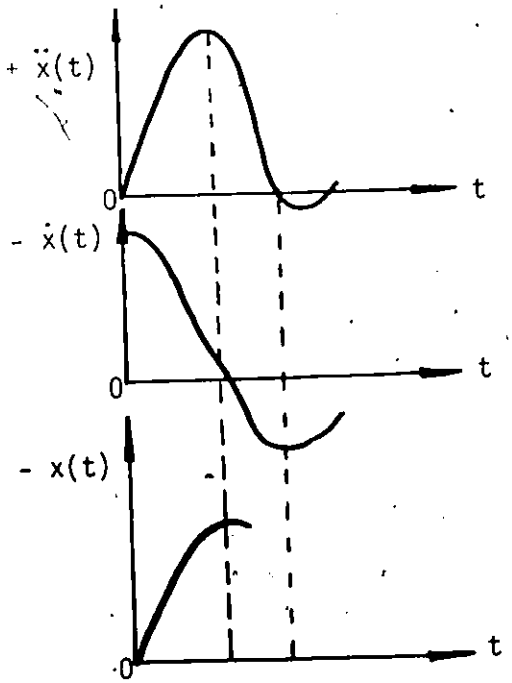

Figure 83

These MEP traces are very much different from the helmet traces for the same headform Graphs, 24-27. The MEP traces are still more different compared to the traces for cadaver 1 with a helmet, trace #204. Here the accelerometer exhibits a trace somewhat similar to Sierra trace Graph 24, but the load cell displays three peaks of force of nearly equal magnitude. This load cell Trace #204 for cadaver 1 illustrates the undesirable force increases and decreases of the three peaks. Since Trace #205 and 206 for the MEP falling on cadaver 1 show similar force peaks, the peaks in Trace #204 may have been somewhat a manifestation of cadaver head-neck interface problems. The force peaks for cadaver 2, Trace #211 were not as pronounced as those of cadaver 1. The helmet load cell and accelerometer traces will require a fairly exhaustive study before detailed explanations concerning their shape can be given.

VII - 3 (ix) SUMMARY OF CONCLUSIONS

1. From the MEP and helmet tests of phases (I) to (IV) the Sierra headform compared most closely with the cadaver heads and is consequently recommended as the headform to be used for the multi position mode tests of Phases (V) to (VIII). It is proposed to compare the Sierra headform performance with the CSA-P-L headform. It was deemed desirable to test one of the headforms that came close to the Sierra in performance for the MEP and helmet tests as well as permitting a rigid neck mount free from interface problems. The CSA-P-L headform filled these criteria best. By testing this headform the added advantage of gaining information for the CSA Hockey Helmets Standards Committee was achieved.

2. For the MEP tests of Phases (I) and (IV) the main factors governing headform performance were found to be (i) anthropometric shape and (ii) stiffness.

3. For the helmet tests of Phases (II) and (III) the main factors governing headform performance were (i) anthropometric shape, (ii) concept of effective mass and (iii) stiffness.

4. It seems quite apparent that the load cell does not err. It describes precisely what is sees. Thus far the load cell used in conjunction with the accelerometer has been a valuable tool in deciphering what happened during and after the impact.

VII - 4 ANALYSIS OF PHASE (V), (VI), (VII) and (VIII)

VII - 4 (i) PHASE (V)

These tests involved the use of the multiposition mode (MPM) test apparatus with the previously recommended Sierra headform and the CSA plastic large headform (CSA-P-L). This CSA hockey helmet headform was chosen on the basis of the headform's relative closeness in performance to the Sierra headform for the MEP tests and the ease of fastening a rigid steel neck for tests with the multiposition test rig.

The manner in which the steel neck height for the cadaver heads and the plastic headforms was determined is shown in Figure 84. An

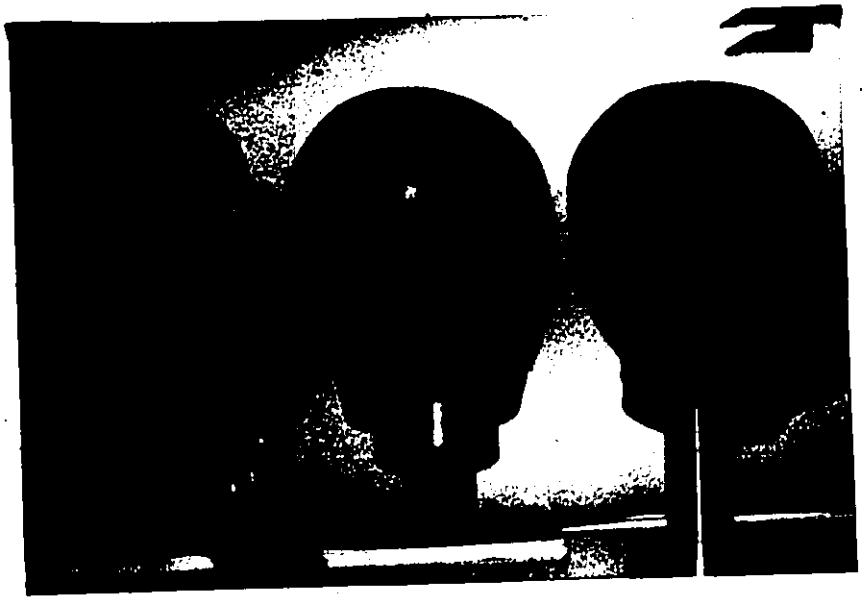

Determination of Steel Neck Size and Location
Figure 84

attempt was made to have relatively the same neck length and height from the crown to the base for each headform. The neck arrangement for the CSA plastic head form is shown in Figure 85A. The steel neck

Pressfitted Steel Neck

Figure 85A

was press fitted into a 1 1/2" d hole to a depth of 2 inches, thus making the neck - headform interface extremely rigid.

The results of the multiposition mode testing can be found in the tables and Graphs 16-23.

The heights of both headforms were measured with a Vernier height gauge. The distances (h) from the base of the neck stock to the crown are shown in Table 25.

	h
Sierra	13.775 inches
CSA - P - L	15.417 inches
Difference	1.642 inches

Neck Position
Table 25

In order to insure the impact striker had zero tangential slope at the point of impact the headforms had to be positioned differently in the aluminum neck clamp that secures the headforms to the curved positioning rails, Figure 85B.

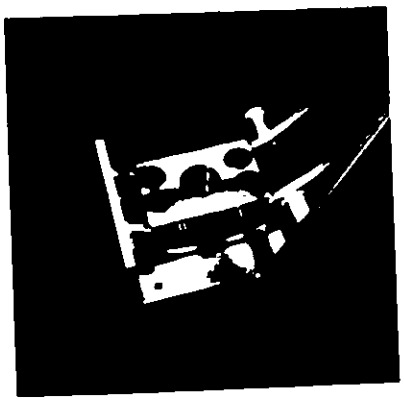

Aluminum Neck Clamp
Figure 85B

The distance of penetration by the headform neck stocks beyond the neck clamp was observed and recorded for each impact position of both headforms. This distance, labelled stock extension, varied only slightly considering the 8.75 inch cantilevered length between the point of impact and the neck clamp, R*, Figure 87. The measured values of stock extension are listed in Table 26.

Table 26 (Stock Extension)

	Stock Extension (inches)				
Headform	Parietal Left Side	Parietal Right Side	Occipital	Frontal	Weight (kg)
Sierra	.265	.265	.325	0.00	9.043 kg
CSA-P-L	1.907	1.907	1.967	1.642	8.758 kg

The above distances take into consideration the fact that the neck stock of the CSA-P-L headform is 1.642 inches longer than the Sierra.

Figure 87 illustrates that increases in stock extension increase the stiffness of the headform-neck beam by shifting the centre of mass towards the neck clamp. The weights of the headforms as shown in Table 26 were within 3.0% and the centres of gravity were crudely found to be within about 5.0% of each other for the y-direction of Figure 87.

Graphs 16, 17, 18 and 19 show the results for each headform when impacted by the 5.0 kg MEP striker. It can be seen that both headforms occupy the same regions and respond very similarly. In both headforms

---

* R is the fixed radius about which the neck clamp rotates.

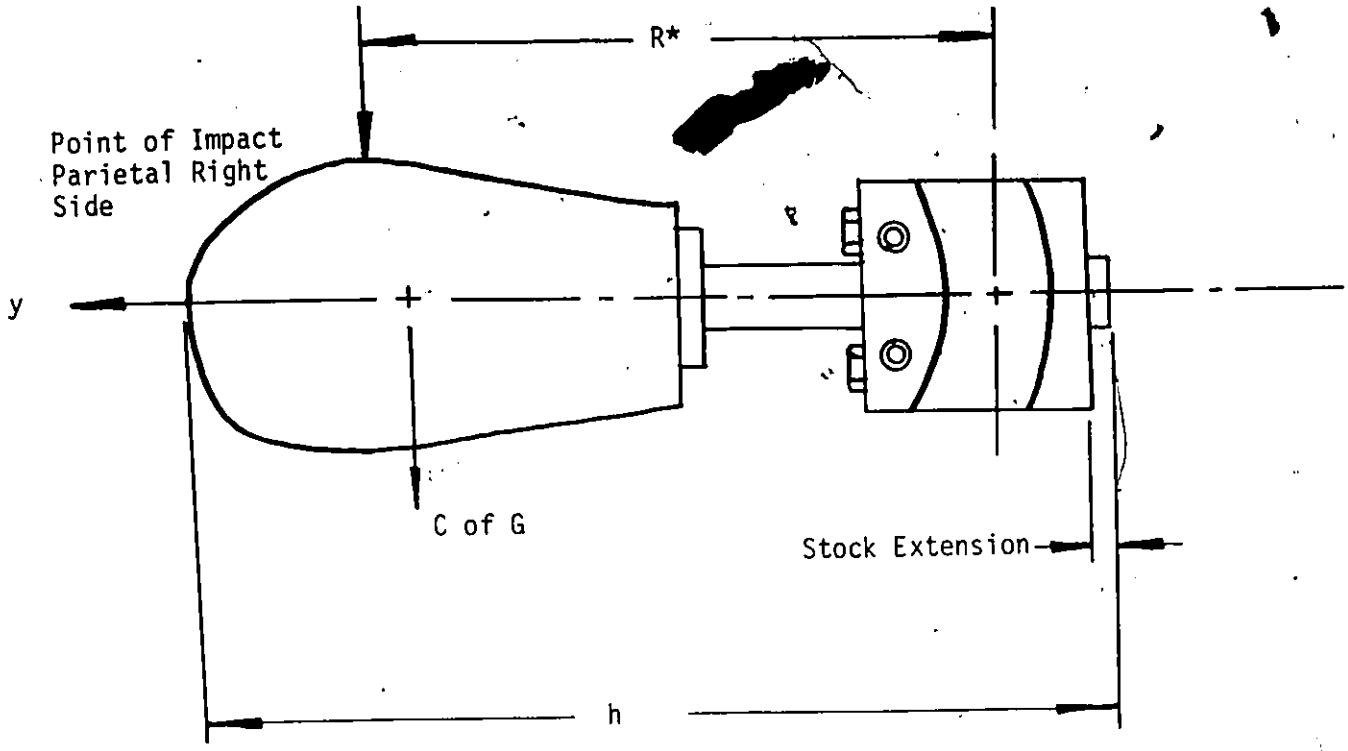

Relationship Between R* and Stock Extension

Figure 87

the parietal positions seem to have higher load cell and acceleration readings. This is probably due to the flatter impact surface of the headform when in position for parietal impacts.

The general good agreement between the two headforms for the multiposition mode MEP tests reinforces their good agreement in the fixed mode MEP tests. Comparing Graphs 16 and 18 with Graph 4 of the fixed mode it can be seen that the regions occupied are very similar for the two headforms. However, when looking at the FMA values of Graphs 17 and 19 it can be seen that these values are about 1000 lbs

or 20% lower than the corresponding fixed mode values in Graph 5.

The reason this phenomenon occurs is essentially a stiffness reason similar to the case of the fixed mode, only in this case the apparent lack of stiffness of the multiposition test apparatus is considerably greater than in the fixed mode. This lack of stiffness results from the cantilevered beam (headform-neck arrangement) and the elastic properties of the test apparatus itself. The decreased stiffness may increase the effective mass which, as seen previously, increases the percentage difference (P%) between PMA and PFLC. An attempt to establish this loss of stiffness was made in tests 66 and 96. The first four impacts of Test 66 of the tables were without any support. The fifth impact used a machinist's jack as a support but with the jack just touching the parietal left side as in Figure 88.

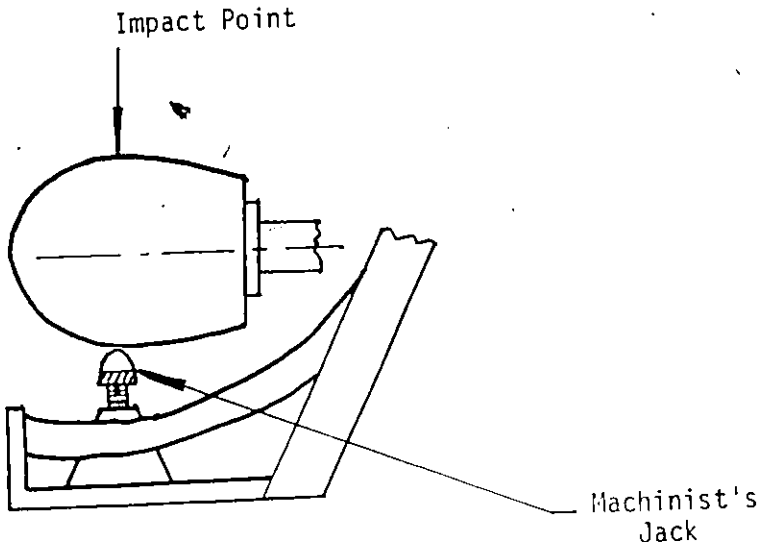

Figure 88

The sixth impact increased the contact area between the jack and headform with the use of a large flat washer. The seventh impact was a control impact like the initial four without the support.

From the tables and traces 229, 230 and 235 a number of interesting observations can be made.

Trace #229 for test 66-1 shows a considerably lengthened acceleration and load cell signal. This effect is due to the striker decelerating to a peak value upon initial impact and again decelerating to another peak as the test apparatus reaches the end of its elastic deflection.

For Trace 230, the identical wave forms as in 229 can be seen for Test 66-4. The 2nd set of signals for Test 66-5 shows how the support has flattened out the second acceleration pulse and shortened its time duration. It is worthwhile to note that the addition of the support did not change the slope of the initial acceleration pulse, just the magnitude of the peak slightly.

For the load cell signal the addition of the support caused the load cell to sense the impact approximately 0.4 msec earlier. The initial slope of the force increase changed to a uniform slope. The addition of the support also reduced the pulse time duration by reducing the flattened plateau after peak force occurred. Comparing Trace 231 for Test 67-1 (for the MEP falling on a flat plate from 1.5 m) with Trace 229 and 230 it can be seen that it takes about 1.5 msec for load cell to sense peak force in the multiposition mode.

It was noticed after the fifth impact that the ball had penetrated the headform after impact causing plastic deformation of the headform. It was hoped for the sixth impact this could be avoided by increasing the contact area and preloading the jack to 10 ft lbs.

The pulses labelled (1) in Trace 235 indicates the sixth impact of Test #66 and (2) indicates the seventh impact.

For the seventh impact the trigger was advanced slightly to avoid signal overlap.

As before, the addition of the support served only to increase the peak acceleration without changing the initial slope. The support shortened the time duration by 2.6 msec and completely removed the second acceleration peak leaving only a slight bump at 1 msec after peak acceleration.

The support increased the slope and peak magnitude of the force pulse and shortened the time duration by removal of the plateau portion after peak force occurred. The addition of the support also caused the load cell to achieve peak force about 2.1 msec earlier.

From the tables with the support there is a P% of 37.75% compared to 24.22% without the support. This implies that the concept of effective mass is not the major factor it was in the fixed mode. It seems that the addition of the support has transmitted the force faster and more efficiently to the load cell. This explanation seems reasonable when the forces in the apparatus after impact are considered. For instance, the energy absorbed by the neck clamp in resisting the bending

of the headform neck cannot be passed on to the load cell.

It can also be said that the 2.0% loss for impact five for P% was due to the energy required to plastically deform the headform at the support not being passed on to the load cell.

Comparing traces 307 to 311 for Test #96 (where the MEP impacts the Sierra occipital region with the support jack)with traces 214 to 219 for Test #60 (for the same impact as above without the support) observations similar to the CSA plastic headform can be found.

Looking specifically at Traces 310 and 215 for 2.0m drop heights, it can be seen that the use of the support increased the slope of the force signal and shortens the time duration of both the accelerometer and load cell signals. The only evidence of the plateaus after the peaks, occurs for the load cell where there is a slight step after the peak. This is probably due to the headform's urethane skin bottoming out at the support. It should be pointed out that to assess the slopes as mentioned above, the traces had to be replotted taking into account the different scale factors.

The new support that was constructed for Test 96 that would allow for an increased contact area at the support-headform interface is shown in Figure 89.

From the tests for the two headforms with and without a support, it can be said that when both headforms were supported, the P% was not substantially reduced through a decrease in effective mass. This may have been also due to a still too small contact area for the CSA head-

form and the fact that using the support with the Sierra headform necessitated having compressed urethane skin between the support and the cast aluminum skull.

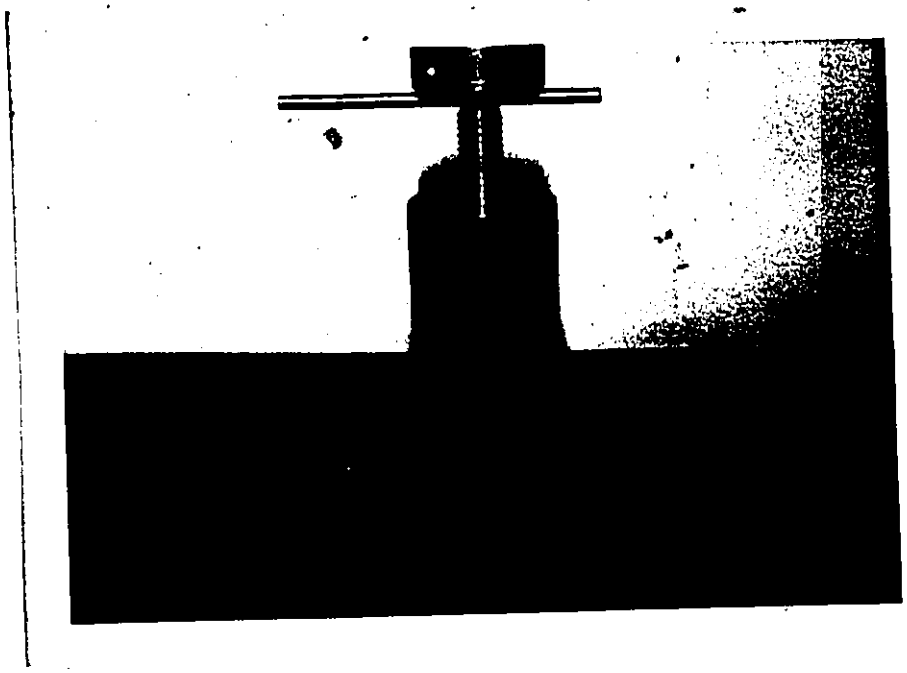

Figure 89

Multiposition Mode Headform Support

Even though energy is thought to be lost to the load cell primarily at the neck clamp, the multiposition apparatus still provides a valuable means of headform or helmet comparison using the load cell in conjunction with the accelerometer.

It can be seen that further support testing should provide the necessary information to calibrate the apparatus for use in any helmet standard.

VII - 4 (ii) PHASE (VI and (VII)

With the use of the helmet positioning index, the CSA plastic, the Sierra and one cadaver head were tested in the multi-position mode. For each impact a new liner was prepared with a comfort liner and inserted into the same yellow outer shell previously used in the fixed mode. The results can again be seen in the tables and Graphs 16 to 23.

Test 94 tested the CSA plastic headform for the frontal region and Test 90 and 92 tested cadaver head 4 in the same area. Test 93 completed the frontal tests with the Sierra headform. Graphs 20 and 21 show these comparisons.

In Graph 20 (H vs PFLC) the CSA headform is closest to cadaver head 4 (prior to fracture of the plastic neck at a drop height of 1.5 m) while the Sierra is about 40% higher. This probably means that some impact energy for the CSA and cadaver head 4 was lost in plastically deforming the polystyrene liner. For the case of the Sierra headform the elasticity of the skin allowed the striker to compress the skin and then eventually pass some of the signal to the load cell a few milliseconds later without doing as much plastic deformation to the liner.

In Graph 21, the Sierra and the CSA perform similarly, but both are about 17% higher than cadaver head 4 at the 2.0 m height. Further testing here with cadaver heads will validate the relative closeness of the Sierra headform to cadaver heads. It is the author's speculation again that had the wall thickness of the Sierra headform been thinner

it would have behaved more closely to cadaver head 4. This fact could be proven if the thin walled cast aluminum headform could be mounted in the multiposition mode.

It can also be said from the behaviour of the Sierra headform in Graph 20, that there seems to be further evidence that the skin thickness of the Sierra could be decreased.

It should be noted that cadaver head 4 belonged to a female specimen. From the previous discussion of reference (25) the fact that cadaver head 4 was female suggests a decreased skull stiffness should be expected relative to the male cadaver heads tested in the fixed mode. Hence, the cadaver head curve in Graph 21 may have been closer to the Sierra headform had a male cadaver head been tested.

The dotted lines in Graphs 18 and 20 for the helmeted cadaver head 4, Tests 90 and 92, indicate the effect of breakage at the plastic neck. This breakage also dramatically illustrates the concept of effective mass. Here the acceleration signal remains constant with a near doubling of the force signal. The same effect could be seen when breakage occurred at 1.50 m for Test 90, Figure 90. After Test 90 the plastic neck portion was enlarged as shown in Figure 91. After the plastic fractured again at 2.00 m for Test 92, Figure 92, the plastic portion was dismantled and repoured using a fiberglass aggregate to strengthen the plastic neck further for Test 98.

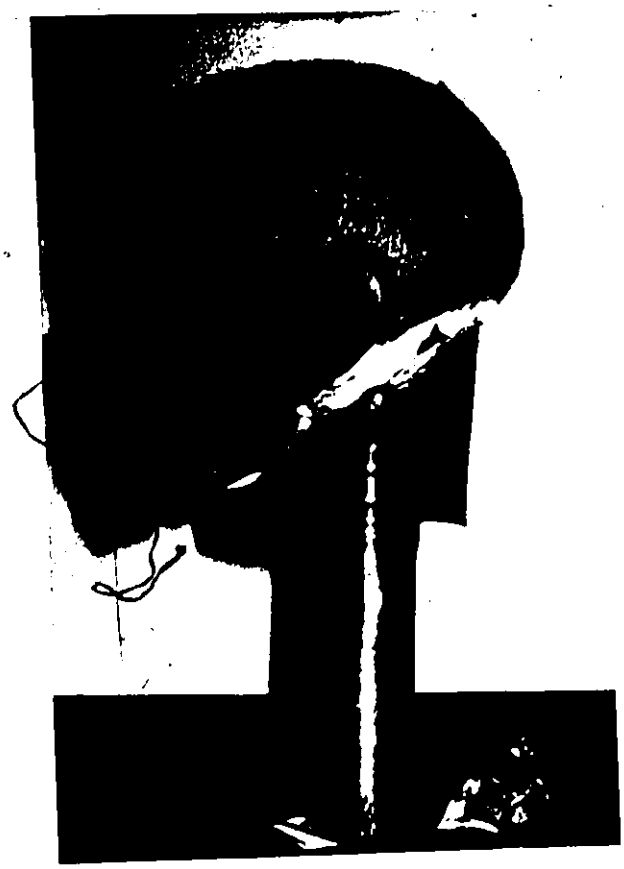

Figure 90

Breakage of Plastic
Neck Portion
Test #90

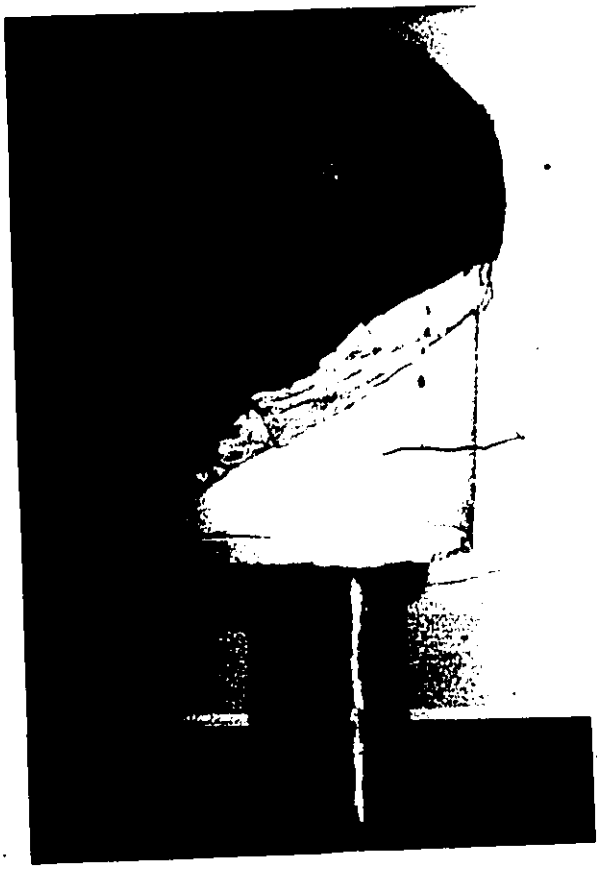

Figure 91

Enlarged Plastic
Neck
Test #92

Cracking of Enlarged Plastic Neck
Figure 92

Tests 95 and 97 were carried out to evaluate system stiffness with helmets. The same support used in Test 96, Figure 89, was used for Test 97.

The graphical results for these two tests are illustrated in Graphs 18 and 19. Test 97 is with the support and Test 95 is without the support. These results are also shown in Graphs 22 and 23. The support makes the accelerometer sense an eighteen percent stiffer impact medium for the PMA calculations. The load cell detected an 87% increase in force transmitted to it with the support. Comparing traces for the 2.0 m drop height, the acceleration signal in Trace 306 for Test 95 has a longer time duration and flatter peak than Trace 312 for Test 97.

Both traces have identical slopes before the peak. This agrees with what was seen in the MEP tests.

The addition of the support increased the slope of initial rise in transmitted force of the load cell. The support shortened the time duration and caused a double spike. The peak force also occurred several milliseconds sooner. These observations also agree with the MEP tests.

The most significant observation for these two tests can be seen in Graph 22. At the 2.25 m drop height there is a significant drop in the transmitted force. This drop in force resulted from a crack in the polystyrene foam liner that opened up slightly at 2.00 m and became fully developed at 2.25 m. The energy to cause this permanent deformation was not able to be transmitted to the load cell. No evidence of this phenomenon appears on the acceleration trace which reinforces the author's opinion of the desirability of using both accelerometer and load cell for monitoring helmet testing.

VII - 4 (iii) PHASE (VII)

Using the new neck with the fiberglass aggregate, cadaver 4 was tested in the frontal position without a helmet using the 5.0 kg flat striker. Graph 18 and 19 show the results for Test 98. Cadaver head 4 was impacted at .15, .25, .30, .38 and .46 m with a skull fracture occurring at .46 m as shown in Figure 93.

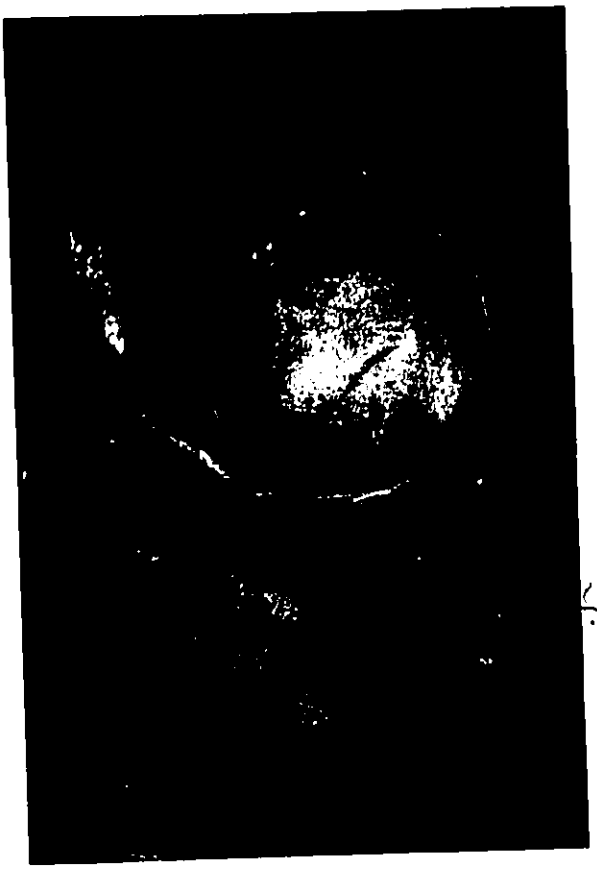

Frontal Skull Fracture

Figure 93

As indicated by Trace 316, the skull fracture was highly identifiable similar to previous tests. The fracture was also accompanied by the characteristic noise. The fracture, Figure 93, was similar to those photographed by Hodgson (21) and Nahum (25). It started due to the stress concentration created by the upper orbital of the eye.

Table 27 compares the results with Hodgson's results. Hodgson dropped the cadaver heads onto a flat plate supported on a load cell. The accelerometers were mounted on the side of the head to measure frontal impact accelerations.

Hodgson impacted the cadavers usually once unless fracture did not occur. The reason for this as mentioned previously, was to minimize the breakdown of the soft tissue at the impact site.

Table 27

Cad No.		Drop Ht. in.	Drop Ht m	Peak a-p G	Mass lbs.	M_a lbs.	Peak Force PFLC	P%	Sex
4	A	18	.46	212.	11.02	2330	2198.5	-6.10	F
1717	B	10	.25	195	10.0	2300	1600	-30.43%	M
1701	B	10	.25	345	8.0	2960	1450	-51.0	M
1699	B	10	.25	220	10.0	2700	1700	-37.0	M
1805	B	10	.25	150	10.0	1900	1450	-23.7	M
1873	B	25	.64	195	10.0	2400	2100	-12.5	M
1857	B	30	.76	220	11.8	2596	2000	-23.0	M

A - Cadaver heads tested by Webster.

B - Cadaver heads tested by Hodgson.

Test 98 contained more than one impact in order to establish the effects of fatigue caused by the previous helmet tests. After 5 impacts with a helmet and 4 impacts without a helmet, the cadaver head 4 still had high force and acceleration readings compared with the heads tested by Hodgson. It can then be concluded that the helmet tests did not significantly fatigue cadaver head 4.

The reason behind the large P% for Hodgson in Table 27 was probably due to the accelerometers seeing more of the resonance type vibration than the load cell which was the opposite of the University of Ottawa's case. Another observation of these tests is that the female sex of cadaver 4 doesn't seem to have lowered the fracture load as would be expected.

4. Testing a variety of headforms in the multiposition mode with the MEP and with helmets should give conclusions identical to those in the rigid mode with respect to factors affecting headform performance.

VII - 4 - (iv) SUMMARY OF CONCLUSIONS FOR THE MULTIPOSITION MODE TESTING FOR PHASES V - VIII

1. From Graph 21 it was seen that the Sierra headform compared most closely with cadaver head 4, but in Graph 20 the CSA headform compared most closely with cadaver head 4. It was suggested that this may have been due to the elasticity of the Sierra's urethane skin and due to the stiffness of the female cadaver head 4 being less than the male cadaver heads tested in the rigid mode. To verify the explanation of this anomaly, further testing is recommended to understand more completely the multiposition mode test apparatus. Despite this minor point, the Sierra headform is believed by the author to be the headform that should be used in the helmet standard proposed by Newman for the Canadian Standards Association. Continued headform and cadaver head testing should be carried out to investigate the possibilities of using new generation frangible headforms for use in future versions of CSA Standards.

2. The multiposition mode test apparatus has proven to be an extremely useful tool for evaluation of the performance of headforms and helmets in many positions. It is believed that further testing of headforms and cadaver heads will reinforce the above statement.

3. The multiposition mode tests established further the need to use both the accelerometer and the load cell in the helmet standard proposal, rather than just the accelerometer.

4. Testing a variety of headforms in the multiposition mode with the MEP and with helmets should give conclusions identical to those in the fixed mode with respect to factors affecting headform performance.

VII - 5 ANALYSIS OF PHASE (IX) TESTS

VII - 5 (i) PHASE (IX) - 1 and 6

The results of the Phase (IX) -1 and 6 tests have already been discussed in this Chapter (VII - 2) in connection with Ebar plate tests for the stiffness correction factor.

VII - 5 - (ii) PHASE (IX) - 2 MINERS' HELMETS

Test 68 consisted of three impacts to a prototype mining helmet with an ensolite and web suspension using the CSA-W-L-C headform in the fixed mode. The traces (not shown here) had the accelerometer reaching a peak then going back to zero before reaching a larger peak after which zero acceleration had been maintained. To further understand this phenomenon, regular mining web type suspension helmets were tested with the spherical wooden headform, Test 69.

This zero acceleration between the two peaks can be seen for Trace 69-1 which follows Trace 235. The steep acceleration and load cell peaks to the extreme right of the trace illustrate the effect of the striker bottoming out on the headform. The first peak occurs when the striker first impacts the helmet. The deceleration decreases to zero while the striker and the helmet move down at constant velocity for 1.2 m sec towards the headform. As the suspension begins to stretch, it starts to decelerate again. Table 28 lists the helmets tested in cross-reference to the tables and traces. Helmets were positioned visually.

TABLE 28

Impact No.	Trace No.	Helmet No.	Trace t_d	Helmet Description
69-1	1	1	1 msec/div	(White) Fibre metal |Brow brim|
69-2	2 curve 1	2	2	(Yellow) Fibre metal with top pad |Brow brim|
69-3	2 curve 2	2		(Yellow) Fibre metal with top pad |Brow brim|
69-4	3	3	5	(Brown) Phenolic MSA |Brow brim|
69-5	4	3	5	(Brown) Phenolic MSA |Brow brim|
69-6	5	4	5	(Brown) Phenolic MSA with top pad |Full brim|
69-7	6	4	5	(Brown) Phenolic MSA with top pad |Full Brim|
69-8	7	5	5	(Orange) Fibreglass ultimate climbing Helmet
69-9	8	5	5	(Orange) Fibreglass ultimate climbing Helmet
69-10	9	7	5	(Beige) Polyethylene Top Guard |Full brim|
69-11		7	5	(Beige) Polyethylene Top Guard |Full brim|
69-12	10	6	5	(Yellow) Polyethylene Erb |Brow brim|
69-13	11	6	5	(Yellow) Polyethylene Erb |Brow brim|

Top Pad - Refers to a piece of 1/2 inch thick ensolite glued to the outside of the outer shell of the helmet.

In Test 68 for impact three the suspension and ensolite pad bottomed out as shown in Figure 94.

Figure 94

The peaks of the force and acceleration were recorded for calculations. From the tables it can be seen that the F% was 45% less than for the first two impacts. The reason for this is again effective mass. For the first two impacts the effective mass is the mass of the striker plus the mass of the helmet. For the third impact the mass of the helmet cannot be added since it was essentially stationary against the headform.

For Tests 69-1, rivets popped in the suspension and a vinyl drawstring in the suspension snapped for Test 69-5. In both of these impacts the F% was noticeably lower due to energy not being transmitted to the load cell. These tests provided valuable insights into the behaviour of a different type of head protection on a headform mounted with zero eccentricity ($e = 0$).

VII - 5 - (iii) PHASE (IX) - 3 CHANGE OF FALLING MASS TESTS

Test 76 dropped the 5 kg(11.02 lb) flat striker onto a stationary MEP pad. For test 76 and 77 the MEP calibration pad was supplied by the Snell testing facility for comparitive testing purposes. Test 77 dropped the 10 lb (4.54 kg) flat striker onto the stationary MEP pad. The results from the tables were plotted in Graph 30. The results are as expected. The smaller mass has reduced acceleration and load cell readings. From the traces it can also be seen that the pulse time duration is shorter for the 10 lb mass which is to be expected. Curve #1 in Graph 30 compares the results of Test 24 (for MEP falling on the flat plate). The curves are of the same shape as expected and as touching the Snell MEP indicated it is not as stiff as the University of Ottawa calibration pad.

VII - 5 - (iv) PHASE (IX) - 4 OTHER TESTING HOUSE COMPARISON TESTS

Test 75 had the Snell Z.90.1 headform falling on to the stationary Snell MEP calibration pad. The results were compared with the findings from Bell Helmets Corp. and the South West Research Institute (S.W.R.I.) in Graph 31. (28)

It can be seen that the University of Ottawa results compare fairly closely with the S.W.R.I. results. Both curves, however, differ by approximately 25% with the Bell Helmets curve.

The higher readings by Bell Helmets may have been due to higher impact velocity resulting from lower guide wire friction, the use of an impact mass greater than the 11.02 lbs used by the University of Ottawa, errors in accelerometer output measurement, or errors in velocity measurement.

Table 29 lists the Bell and S.W.R.I. ideal and actual elapsed times for a 1.00 inch blade to open and close a light beam-photo cell circuit just before impact.

From the elapsed times shown in Table 29, the average percentage difference differed for the S.W.R.I. and Bell Helmets by 1.68%. This seems to imply that velocity is not the cause of the discrepancy in Graph 31 between Bell and S.W.R.I. testing facilities. The above implication would only be true if the times recorded over the 1.00 inch displacement were correct due to previous calibration.

Further discussion concerning Graph 31 and Table 29 will follow the velocity tests of the next section (VII - 5 - (v)).

Table 29

Drop (m) Height	Drop " Height	Ideal M Sec	Bell M Sec	% Diff	SWRI M Sec	% Diff	U of O Graph 32 M Sec	% Diff
.0508	2"		29.09					
.1270	5"		16.66					
.254	10"	11.20	11.77	5.08	12.272	9.57		
.381	15"	9.55	9.27	- 1.88	9.728	1.88	11.25	15.11
.508	20"	8.06	8.49	5.33	8.389	4.08	9.75	17.33
.635	25"	7.25	7.42	2.34	7.458	2.87	8.16	11.15
1.1176	44"	5.46	5.63	3.11	5.60	2.56	5.97	8.54
1.2192	48"	5.20	5.29	1.73	5.45	4.80	5.72	7.52
1.3208	52"	5.00	5.13	2.60	5.43	8.06	5.50	9.09
				3.15%		4.83%		11.51%
					1.68%			
						8.36%		

VII - 5 - (v) PHASE (IX) - 5 VELOCITY TESTS

The velocity tests were carried out with the velocity measurement device shown in Figure 75, for the 5.0 kg flat impactor falling on the MEP calibration pad.

Tests were carried out in Test 99 for drop heights of 0.25 M to 2.50 m. These results, Table 30, were plotted for Graph 32 to 35.

Table 30

(1)	(2)	(3)		
h_v * (meters)	time - t * (M secs)	Velocity Actual ($ft.sec^{-1}$)	Velocity Ideal ($ft.sec^{-1}$)	% Difference
2.45	4.194	19.86	22.70	12.50%
2.20	4.256	19.57	21.52	9.06
1.95	4.453	18.71	20.30	7.83
1.70	4.734	17.60	18.93	7.03
1.45	5.222	15.95	17.50	8.85
1.20	5.766	14.45	15.90	9.12
0.95	6.421	12.97	14.15	8.34
0.70	7.429	11.21	12.10	7.36
0.45	9.181	9.07	9.65	6.01
0.20	13.858	6.01	6.51	7.68
			Average	8.378%

h_v* - Velocity drop height

h - actual drop height between MEP and impact surface

$h = (h_v + 0.05)$ m.

Column 1 in Table 30 lists the drop height - h_v for each test. The drop was measured from the lower edge of the blade to a point midway

between the two light beams. Column 2 lists the elapsed time in m secs for the moving blade on the striker, Figure 28, to fall the distance h_v. By dividing distance between the two light beams by the elapsed time an expression for average velocity is obtained.

$$V = \frac{x}{t} = \frac{1.0 \text{ in}}{12 \text{ in}} \times \frac{1 \text{ ft}}{4.194 \text{ m sec}}$$

$$= 19.86 \text{ ft sec}^{-1}$$

Column 3 lists the actual velocity while column 4 lists the ideal velocity for ideal conditions (zero guide frictional resistance and zero air frictional resistance). Column 5 lists the percentage difference between actual and ideal velocity.

Graph 32 plots the drop height against the elapsed time between the 1.0 inch beams. Curve 1 is the ideal and curve 2 is the actual. From this graph the elapsed times were taken for the drop heights of Table 29 and percentage comparisons were made between Bell, SWRI and the University of Ottawa results.

It should be pointed out that no rigorous calibration of the University of Ottawa velocity measurement apparatus was performed. It is not known to what extent the other devices at Bell and SWRI were calibrated. An attempt was made to calibrate the University of Ottawa device using a falling golf ball that was dropped simultaneously with the 5 kg MEP onto the slotted plate. It was hoped that this would yield two spikes on the load cell trace and the distance between them a measure of the reduction in velocity due to guide wire friction and the greater air frictional

resistance of the striker. This idea did not work as well as expected, but did seem to indicate there was up to about a 10% difference between actual and relatively ideal velocity. This method proved to be a little better than usual comparing the free fall of a steel nut with the 5 kg MEP striker mentioned previously.

Further testing and calibration of the University of Ottawa device should indicate if the 8.4% average in Table 30 is correct. The device is supposed to be accurate to within 1.0% if the light beam photo cell circuits are properly set up and maintained.

Graph 33 is an extension of Graph 32. Here drop height is plotted against velocity of the 5 kg MEP striker. Curve 1 is the ideal velocity, curve 2 is the actual velocity.

Graph 34 plots drop height against transmitted force. Curve 1 is for the 5 kg flat plate falling on the MEP calibrating pad. Curve 2 is for the 5 kg MEP falling on the flat plate. Graph 35 plots drop height against impact force - m x a. Curve 3 in both these graphs is from Test 31.

Comparing Test 100 with Test 31 for Graph 35, it can be concluded that the accelerometer calibration has remained constant over approximately the one year between Test 31 and 100.

Graph 34 illustrates that the load cell sensitivity may have changed slightly when comparing Tests 31 and 100. The author believes the load cell sensitivity has remained constant but the interface condition of the top mounting plate and the flat plate has deteriorated and surface re-grinding is necessary. Because of a deteriorated interface condition

the effective mass has increased thus increasing the load cell signal.

Graph 34 for Test 100 and 99 indicates that the load cell appears to sense little difference, whether the MEP is on the striker or top mounting plate. The accelerometer in Graph 35 does detect a difference. The explanation of this occurrence also is effective mass. The load cell senses an additional interface for Test 99 when the MEP is mounted on the flat plate that is in turn bolted on the top mounting plate. This additional (now ground) interface increases the effective mass thus increasing the load cell signal.

In essence the conclusion of this is that there is a difference between mounting the MEP on the striker to mounting the MEP on the top mounting plate.

VIII - 1 PREVIEW OF CONCLUSIONS

This chapter lists in summary the major conclusions and recommendations in order of importance in Section 2 and the conclusions with respect to the eight fundamental questions in Section 3. These conclusions have previously been stated in greater detail throughout the text.

VIII - 2 MAJOR CONCLUSIONS AND RECOMMENDATIONS

1. Conclusion and Recommendation

The performance of the Sierra headform has been found to compare closest to the cadaver head tests. On this basis the headform is being recommended for use in the new CSA motorcycle helmet standard proposed by Newman (7). The proposed use of the Sierra Headform and the multiposition test Apparatus were conditional upon the results of this thesis.

2. Conclusion and Recommendation

The multiposition test apparatus has proven to be a useful tool for comprehensive testing of helmets, headforms and cadaver heads. With proper calibration it is recommended as the test apparatus to be used in the new CSA Motorcycle Helmet Standard.

3. Conclusion and Recommendation

It can be concluded from the test results that the load cell used in conjunction with the accelerometer provides a better means of monitoring helmet tests than either of the transducers used alone. The author believes that any revision to the CSA Motorcycle Helmet Standard should incorporate the use of both transducers to evaluate helmet performance.

4. Conclusions

For the MEP tests of phases (I) and (IV) the main factors governing headform performance were found to be (1) anthropometric shape and (2) stiffness.

For the helmet tests of Phase (II) and Phase (III) the main factors governing headform performance were (1) anthropometric shape, (2) effective mass and (3) stiffness.

If tests similar to those above were carried out with the same headforms in the multiposition mode similar results should be expected.

5. Conclusion and Recommendation

The falling Z90.1 drop frame and ball used with the 5.0 kg flat striker is a suitable device for use as a striker with the means of attaching the accelerometer. It is thus recommended that this type of striker adaptation to the Z90.1 drop frame be used for the CSA Motorcycle Helmet Standard. This should prove to be little inconvenience to helmet test facilities since most have the Z90.1 drop frame.

6. Discussion, Conclusion and Recommendation

Figure 100 shows one example of a polystyrene liner from accident Case #61 where the damage incurred was a great deal more severe than any damage created by the 5.0 kg flat striker at 2.25 m. For purposes of demonstration, Case #61 has been chosen because it is an extreme case of helmet damage.

Figure 100

Figure 101 shows a typical liner impacted in the occipital region at 2.25 m with the 5.0 kg flat striker. It is plainly seen that no evidence of damage comparable to Figure 100 exists. Both liners were weighed and found to be 98.0 g (Figure 100) and 84.5 g (Figure 101). Thus it can be assumed that they are relatively close in their densities, with the damaged liner having the greater density.

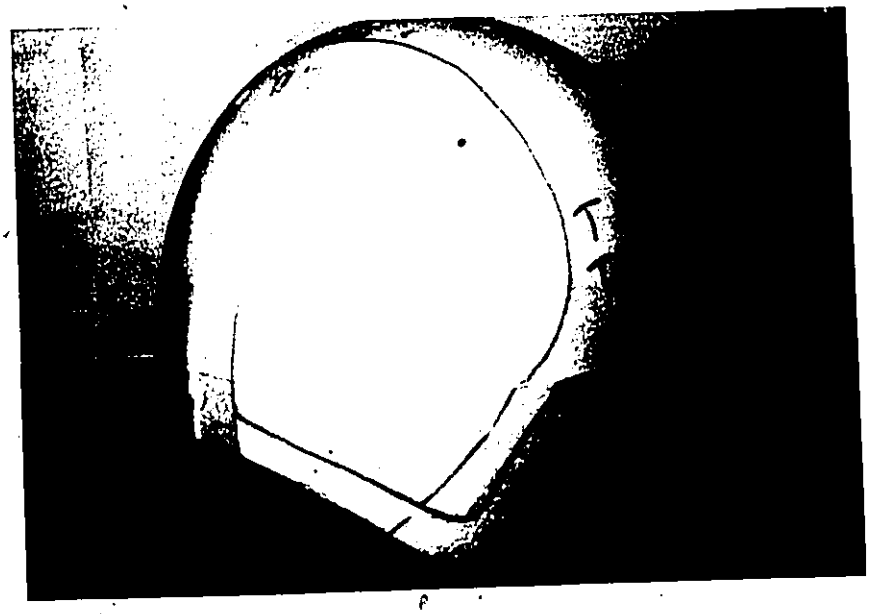

Figure 101

It can thus be concluded that the performance test is not severe enough to duplicate one of a number of accident situations. Thus it is proposed that further testing be carried out to establish the extent of velocity increases, mass increases and or shape changes to the falling striker that will produce a more severe helmet performance standard. These shape changes might consist of changing the flat impact surface to a hemispherical surface of a particular radius.

7. Conclusion and Recommendation

With the use of a headform that compares favourably with cadaver heads, namely the Sierra, it is now possible to continue pursuing the question of the specific loading conditions that caused head injury in the accident cases for the helmets collected.

This may be done by attempting to duplicate the permanent deformation of the polystyrene liners from the accident cases, with the multiposition test apparatus.

8. Conclusion and Recommendation

From a high speed motion picture at Bell Helmets of the Z90.1 helmeted headform impacting flat and hemispherical surfaces, the advantages of using guide bars instead of guide wires was clearly evident. After impact the wires and drop frame with helmeted headform flopped around with whiplash-like effects.

The preliminary testing for this work led to the same observation, hence 1/4 inch guide bars under tension were used instead of the conventional 1/8 inch strand wire in tension.

9. Conclusion and Recommendation

The development of plastic necks (see Appendix G) for testing the cadaver heads in the fixed and multiposition mode has proven to be a major accomplishment. The use of this type of neck for further cadaver head testing by the University of Ottawa and other researchers should significantly add to the bio-mechanical data on head injury.

It is recommended that further cadaver head testing of both sexes in the fixed and multiposition mode be carried out to begin adding to and comparing bio-mechanical data for head injury.

10. Conclusion and Recommendation

The measurement of the recorded peak force and peak acceleration for calculation and comparison purposes has proven to be a suitable choice. The use of the velocity measurement device has made the impact information package even more comprehensive. However, it is recommended that the integral of the acceleration pulse (the velocity curve) and the integral of the velocity signal (the displacement curve) also be displayed and recorded. This should give a very complete perspective of any impact of interest.

11. Conclusion and Recommendation

The observance of multiple force spikes exhibited by the load cell for helmet tests was not expected. This indicates that a helmeted human head would be in effect receiving multiple impacts. It is thus recommended that this phenomenon be studied more closely with more polycarbonate and fibreglass helmet testing.

12. Conclusion

The calibration of the accelerometer and load cell has proven successful on the basis of comparison tests with other test facilities.

13. Conclusion

The helmet positioning index proved to be a fast, reliable means of helmet positioning using headforms or cadaver heads.

14. Conclusion

The use of various cross-sections of helmet outer shells to measure polystyrene liner deformation after impact proved to be a useful tool. It is also believed that a clear plastic helmet shell would be useful for examining further helmets obtained from the accident investigation.

15. Conclusion

The ability to recognize interface problems should prove extremely helpful for future testing.

16. Conclusion and Recommendation

On the basis of preliminary tests using variable frequency electronic filtering, significant alterations to the acceleration and load cell signals were observed. It is thus recommended that filtering be avoided where possible. No filters were seen necessary for these tests.

17. Conclusion

The impact test facility developed for this work has proven to be efficient, repeatable and versatile. The fact that it is being used for further dynamic testing of polystyrene foam illustrates its

versatility as an impact facility used for testing impacts other than helmets or headforms.

18. Conclusion

The tests with the impact facility developed for this thesis have proven that the 300 lb block in the present CSA standard for mounting the impact surface is not necessary when rigid concrete floors are available. However, the impact surface must be bolted to the floor by studs that are cemented with concrete in the floor itself. The advantage of using a concrete floor becomes most obvious when low laboratory ceiling heights are present.

19. Conclusion

The impact test facility and conclusions developed for this thesis have produced a basis by which answers to fundamental questions in the field of head injury may be derived.

VIII - 3 CONCLUSION SUMMARY WITH RESPECT TO THE EIGHT FUNDAMENTAL QUESTIONS FROM THE FIELD OF HEAD INJURY

Question 1. Is the helmet standard performance test representative of a typical helmet impact involved in a motorcycle accident?

Conclusion for 1. Based on accident investigation and liner deformations from laboratory tests the author believes that the present standards should be modified to increase the input energy and/or change the shape of the falling striker. (See conclusion 6, Chapter VIII - 2).

Question 2. Does it matter from what material a headform is constructed?

Conclusion for 2. It has been established that the headform material had a minor effect on the impact response of the helmeted headform.

Question 3. Does it matter what headform shape is used?

Conclusion for 3. It has been shown that the head form shape especially headform radii of curvatures was the major factor affecting the response of the helmeted headforms. One implication of this conclusion is that for various headform sizes (e.g. CSA-wooden-large and small headform) it may be necessary to have different performance requirements in the helmet standard. This, as mentioned previously is due to the smaller sized headforms having smaller radii of curvatures and hence causing different deformation processes to occur to the helmet liners.

Question 4. Does it matter if the headform is solid or hollow?

Conclusion for 4. For headforms of the same material it was found that solid headforms were stiffer than hollow headforms.

Question 5. Does it matter whether the headform is moving or assumes a fixed, swing-away or multiposition semi rigid mode?

Conclusion for 5. The tests indicated that the factors governing helmeted headform response were the same in the fixed and multiposition headform modes. Further testing is necessary before the above statement could be made for the falling or swingaway headform modes.

Question 6. Is it necessary to consider the mass of the helmet?

Conclusion for 6. The concept of effective mass illustrates that the helmet mass should be considered.

Question 7. Does it matter whether deceleration of the helmeted headform, deceleration of the striker, time duration of deceleration or transmitted force of the helmeted headform is measured as output?

Conclusion for 7. The author believes the best configuration for testing is in the multiposition mode monitoring striker peak deceleration, load cell peak force, and striker velocity just before impact. As previously mentioned, the acceleration integrals would be a useful cross-reference to the above measurements.

Question 8. Is the pass fail criteria limit representative of known bio-mechanical data for helmeted human beings?

Conclusion for 8. The present pass fail criteria limit in the CSA D-230 standard is not representative of newest bio-mechanical data. The standard will pass all helmets that do not exceed 5,000 lb of transmitted force when impacted with a 10-lb flat impactor from a drop height of 9.0 ft. The 5,000 lbs comes from the (mass x acceleration) relationship where ($\frac{10\ lb}{g}$ x 500 g = 5000 lb). In other words, the headform is not supposed to sense an acceleration of greater than 500 g. This 500 g, according to Patrick (29), was taken from the fact cadaver heads were found to be subjected to average accelerations of 400 to 600 g. The British standard was supposed to have adopted the 500 g limit in their standard. The CSA D-230 standard is a modified version of former BSI standard. More recent bio-mechanical data suggests the 500 g or 5,000 lb is too high, (except perhaps for very short duration loading). The fact that helmeted people are receiving head injury from moderate blows further indicates that this limit should be lowered. Extended helmet testing using the multiposition mode with cadaver heads and headforms should establish such a limit more rigorously.

REFERENCES

1. Delaporte, Louis Joseph, "Mesopotamia (The Babylonian and Assyrian Civilization)"Translated by Childe, U. Gordon, Published 1925, Barnes & Noble Inc., N.Y., Reprint 1970, pp. 69-73.

2. Walker, A. Earl, "Introduction", Paper #1, Proceedings of the Head Injury Conference, 1966, pp. 12-25.

3. Hodgson, V.R., Thomas, L.M., and Prasad, P., "Testing the Validity and Limitations of the Severity Index", Paper 700901, Proceedings of the Fourteenth Stapp Car Crash Conference, 1970, pp. 169-187.

4. Newman, James A., and Webster, Gary D., "Mechanics of Motorcycle Accidents", Proceedings of the 18th Conference of the American Association for Automotive Medicine, Sep. 1974, pp. 265-302.

5. Hencken, Hugh O'Neill, "The Earliest European Helmets", Published 1902, Volume Number 28, pp. 97-122.

6. Snively, George G., and Chichester, C.O., "Evaluation and Design Criteria of Protective Headgear", Paper #14 , Proceedings of the Fifth Stapp Car Crash Conference, 1961, pp. 182-190.

7. Newman, James A., "Motorcycle Accident Investigation, Ottawa-Hull, Canada", unpublished report to the Ministry of Transport, Canada, 1974.

8. Chandler, K.N. and Thompson, J.K.L., "Effectiveness of Present-Day Crash Helmets for Motorcyclists", Vol. 8, No. 2, June 1957.

9. Shields, J.B., "Fatal Motorcycle Accidents", Dec. Quarterly Issue, American Association for Automotive Medicine, Safety News, December 1972, pp. 21-22, Item #25.

10. Buchanan, L.S., Bischoff, D.C., and Richardson, H.A., "Preliminary Analysis of Safety Helmet Effectiveness", Paper #73013, Proceedings of the 2nd International Congress on Automotive Safety, 1973, Session #4, Volume 1.

11. Severy, D.M., Brink, H.M., and Blaisdell, D.M., "Motorcycle Collision Experiments", Paper 700897, Proceedings of the Fourteenth Stapp Car Crash Conference, 1970, pp. 115-116.

12. Hirsch, A.E., "Current Problems in Head Protection", Paper #3, Proceedings of the Conference on Head Injury, February 1966, pp. 37-40.
Note: The original paper containing the Wayne State University (WSU) Curve could not be obtained, the original, Hirsch refers to is:

Gurojian, E.S., et al.: Protection of the Head and Neck in Sports. JAMA 182: 509-512, (Nov.), 1962.

13. Eiband, A.M., "Human Tolerance to Rapidly Applied Acceleration, A Summary of the Literature", NASA Memo 5-19-59E.
Note: This paper could not be obtained so the photocopy of the original paper used by Versace (14) was recopied for Figure 5.

14. Versace, Joh, "A Review of the Severity Index", Paper # 710881, Proceedings of the Fifteenth STAPP Car Crash Conference, 1971, pp. 771-796.

15. Gadd, C.W., "Use of Weighted-Impulse Criterion for Estimating Injury Hazard", Proceedings of tenth STAPP Car Crash Conference Proceedings, Paper #660793, 1966, pp. 95-100.

16. Slattenschek, A., Tauffkirchen, W., "Critical Evaluation of Assessment Methods for Head Impact Applied in Appraisal of Brain Injury Hazard, In Particular in Head Impact on Windshields", International Automobile Safety Compendium, 1970, Paper 700426, pp. 280-301, New York: Society of Automotive Engineers, Inc., 1971.

17. Brinn, J., Staffeld, S.L., "Evaluation of Impact Test Accelerations: A Damage Index For The Head and Torso", 14th STAPP Car Crash and Field Demonstration Conference Proceedings, November 17-18, 1970, Paper 700902, pp. 188-202, New York: Society of Automotive Engineers, Inc., 1971.

18. McElhaney, J.H., Stalnaker, U.L. and Roberts, V.L., "Biomechanical Aspects of Head Injury", Symposium Human Impact Response, 1972, Human Impact Response Measurement and Simulation, Plenum Press, 1973, pp. 85-112.

19. Fan, W.R.S., "Internal Head Injury Assessment", 15th Stapp Car Crash Conference Proceedings, November 17-19, 1971, Paper 710870, pp. 645-665, New York: Society of Automotive Engineers, Inc., 1972.

20. Scalone, A.A., "Developments in Motorcycle Helmet Testing and Their Effects on Future Designs", 2nd International Congress on Automotive Safety, Motorcycle and Recreational Vehicle Safety, July 16-18, 1973, Paper 73015, pp. 1-19, Vol. I, Washington, D.C.: National Motor Vehicle Safety Advisory Council, U.S. Dept. of Transportation.

21. Hodgson, V.R., Mason, M.W., and Thomas, L.M., "Head Model for Impact", 16th Stapp Car Crash Conference Proceedings, November 8-10, 1972, Paper 720969, pp. 1-13, New York: Society of Automotive Engineers, Inc., 1972.

22. Hodgson, V.K., "Head Model for Impact Tolerance", Symposium Human Impact Response, 1972, Human Impact Response Measurement and Simulation, Plenum Press, 1973, pp. 113-128.

23. Stalnaker, R.L., McElhaney, J.H., and Roberts, V.L., "Mechanical Impedence Response of Prototype and Production Anthropometric Dummy Heads", ASME Meeting, November 11-15, 1973, Paper 73-WA/Bio-13.

24. Hubbard, R.P., and McLeod, D.G., "Definition and Development of A Crash Dummy Head", 18th Stapp Car Crash Conference Proceedings, December 4-5, 1974, Paper 741193, pp. 599-628, New York: Society of Automotive Engineers, Inc., 1974.

25. Nahum, A.M., Gatts, J.D., Gadd, C.W., and Danforth, J., "Impact Tolerance of the Skull and Face", 12th Stapp Car Crash Conference Proceedings, pp. 302-316, Paper 680785, New York: Society of Automotive Engineers, Inc., 1968.

26. Levy, S. and Bickford, R.H., "Calibration Pickups", Shock and Vibration Handbook, Volume I, Section 18, pp. 1-39, Harris and Crede, McGraw-Hill 1961.

27. Jehu, V.J., "Swing-away Helmet Testing Apparatus", Road Research Laboratory, Crowthorne and Berkshire England, RRL Report LR 407, 1971.

28. The Bell Helmets and South West Research Institutes Results were obtained through mutual correspondence.

29. Patrick, L.M., Head Impact, Paper #4, Proceedings of the Head Injury Conference, 1966, pp. 41-48.

APPENDIX A

A COMPARISON OF STANDARD IMPACT PERFORMANCE CRITERIA

COMPARISON OF VARIOUS HELMET SHOCK ABSORPTION TEST METHODS

METHOD	INPUT	HEADFORM	OUTPUT	LIMIT
CSA D230	90 ft.lb Moving striker	Stationary Laminated birch	Force transmitted to headform	Peak force must be less than 5,000 lbf.
BSI 2001 1972 a	122.6 J (90 ft.lb.) Moving striker	Stationary, Unspecified material	Force transmitted to headform	Peak force must be less than 19.6 kN (4420 lbf.)
BSI 2001 1972 b & ISO-1S11	$\frac{k}{k+1}$ x 122.6J* Moving striker	Unspecified material Headform mounted on pendulum arm.	Deceleration of striker.	Max striker deceleration shall not exceed 400 g.
Snell	88 ft.lb-1st blow 66 ft.lb-2nd blow	Moving headform of K1A magnesium	Deceleration of headform	Max headform deceleration shall not exceed 300g.
MVSS 218	45 ft.lb approx. hemi anvil 66 ft.lb approx. flat anvil	Moving headform of magnesium alloy	Deceleration and time duration of deceleration of headform	(a) Peak accelerations shall not exceed 400g; (b) Accelerations in excess of 200g shall not exceed a cumulative duration of 2 milliseconds; and (c) Accelerations in excess of 150g shall not exceed a cumulative duration of 4 milliseconds.
ANSI Z90	Same as MVSS 218 except			200 g < 3 msec; 150g < 6 msec
BNQ 1923-901	Same as MVSS 218 except			200 g < 3 msec; 150g< 4 msec.

* $k = \frac{\text{mass of helmeted headform}}{\text{mass of striker}}$

APPENDIX B

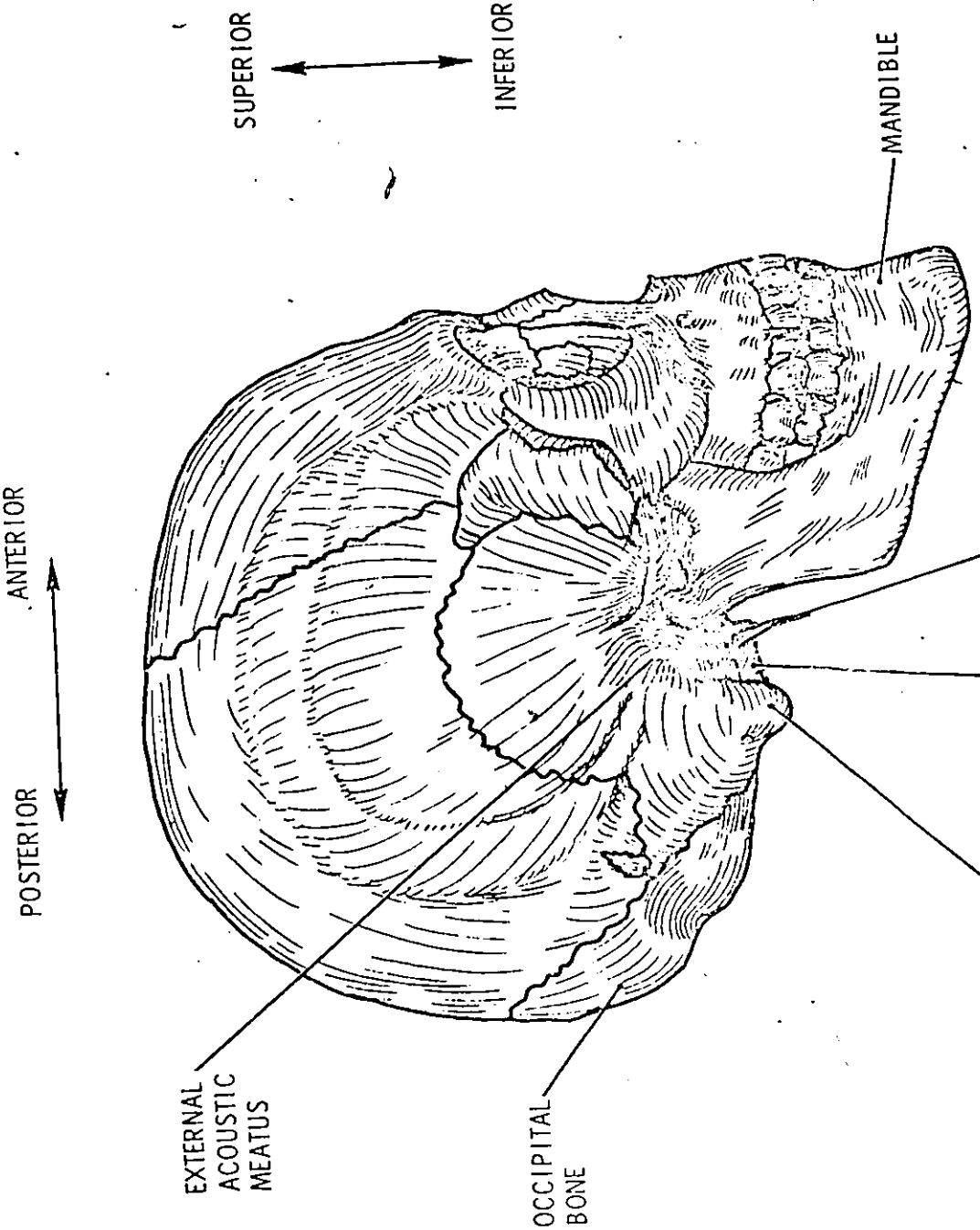

FIG. 2 POSITION OF THE OCCIPITAL CONDYLES RELATIVE TO LANDMARKS OF THE SKULL (Reference 3)

APPENDIX C

ENDEVCO PRODUCT DATA

MODEL 2106E

High Dynamic Forces
Wide Frequency Range

DYNAMIC FORCE GAGE

The Model 2106E Force Gage is a new approach in dynamic force measurement. It incorporates three force transducers in the same plane which accurately simulate point loading. This Endevco development gives high force sensitivity while permitting the convenience of the center mounting hole. It also permits a more stable design in which the height is small compared to the diameter. This "flat" configuration practically eliminates concern about shear loads.

The entire top and bottom surfaces are used as load bearing members, and this large area results in a gage with stiffness of 2.7 × 10⁷ lb/in. High gage stiffness results in high natural frequency which permits accurate force measurements at high frequencies. High frequency response, high sensitivity, center mounting hole and "flat" configuration are benefits of the three transducer concept.

The transducers used in the Model 2106E Force Gage utilize self-generating piezoelectric elements requiring no external source of electrical excitation.

Specifications for Model 2106E Force Gage
(According to ASA and ISA Standards)

DYNAMIC

CHARGE SENSITIVITY	15 pC/lb., ±50%
VOLTAGE SENSITIVITY[1]	2.5 mV/lb., nom.
AMPLITUDE LINEARITY	Sensitivity increases approximately 1% per 250 lb., 0 - 5000 lb.
FREQUENCY RESPONSE (±5%)	2 to 5000 Hz[2]
ALLOWABLE COMPRESSIVE LOAD[3]	25,000 lb., maximum (Static)
STIFFNESS	2.7 × 10⁷ lb./in., nominal, with mounting bolt removed.
EFFECTIVE END MASS	0.3 lb., nominal
TRANSDUCER CAPACITANCE	5700 pF, nominal
RESISTANCE	20,000 MΩ, minimum, output to signal ground.
	10 MΩ, minimum, signal ground to case ground.

NOTES

[1] With 300 pF external capacitance

[2] Use ENDEVCO® Model 2710B Series or 2718 Charge Amplifier, or voltage amplifier with high input resistance. See curves below.

[3] Compressive preload must exceed dynamic tensile load by 1000 lb. or more

TYPICAL FREQUENCY RESPONSE

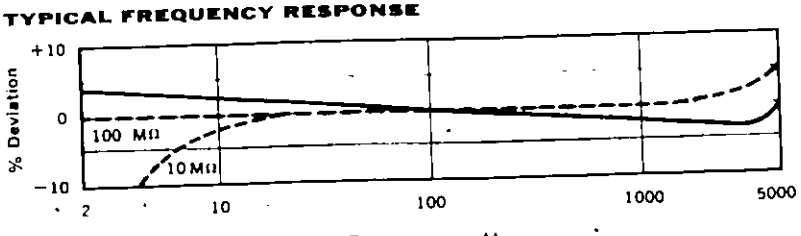

The solid line shows the response when using a charge amplifier. The broken line shows the frequency response with 300 pF external capacitance and when using a voltage amplifier. The low frequency response depends on the input resistance of the voltage amplifier, as indicated by the curves.

Specifications for Model 2106E

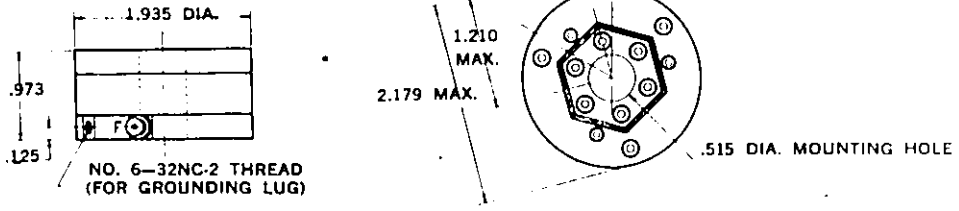

Dimensions in inches

PHYSICAL

WEIGHT	200 grams (7.1 oz.), nominal.
CRYSTAL MATERIAL	Piezite® Element Type P-8.
CASE MATERIAL	Stainless Steel and Aluminum.
CONNECTOR TYPE	Coaxial, 10-32 thread, mates with accessory cable.
MOUNTING	Hole provided for ½" bolt. High strength steel bolt recommended for high force applications. Recommended mounting torque: 30 ft.-lb. to measure up to ±1000 pk lb.; 125 ft.-lb. to measure up to ±5000 pk lb.
GROUNDING	Signal ground insulated from case.
ACCESSORIES INCLUDED	Model 3090A-120 Low Noise Cable Assembly, 10 ft., 300 pF, nominal. Model 10063 Tapered Adapter Block (173 grams). Ground Lug and Screw.
ACCESSORIES AVAILABLE	Model 2953 Force Generator (±1 lb.).

ENVIRONMENTAL

ACCELERATION LIMITS	±1000 g, sinusoidal ±5000 g, shock
FORCE LIMIT	Limited by strength of mounting bolt
TEMPERATURE RANGE	-30°F to +200°F (-35°C to +94°C)
ALTITUDE	Not affected
HUMIDITY	Will withstand normal laboratory environmental conditions.
SALT SPRAY	Meets MIL-E-5272C (with sealed connector)

APPLICATIONS

The excellent design configuration of the ENDEVCO® Model 2106E brings new possibilities and conveniences in dynamic force measurement. The Model 2106E may be used to measure forces transmitted by liquid or solid fuel rocket engines; turbines of all kinds; or any rotating device, such as a generator, where the forces caused by unbalance must be measured.

When electrodynamic shakers are used as drivers of a complex structure, such as a wing section or automobile, the Model 2106E Force Gage may be used to monitor the input force. It can be used in measuring thrust forces in hydraulic, pneumatic, or explosive actuators. Other applications are the determination of dynamic loading characteristics of plastics and fibers, bulk modulus studies of plastic materials, and measurement of forces generated by ball bearings.

For mechanical impedance studies, the ENDEVCO® Model 2110E Impedance Head is recommended.

Continuing product improvement necessitates that Endevco Corporation reserve the right to modify these specifications and/or prices without notice

RELIABILITY: Endevco maintains a program of constant surveillance over all products to ensure a high level of reliability. This program includes attention to reliability factors during product design, the support of stringent Quality Control requirements, and compulsory corrective action procedures. These measures, together with conservative specifications, have made the name Endevco synonymous with reliability.

CALIBRATION: Each force gage is dynamically calibrated for sensitivity with sinusoidal forces and its capacitance is measured and recorded. Other calibrations are available; see Calibration Service Bulletin No. 301.

PRICE: (F.O.B. Pasadena) $425.00 in any quantity

Prices of ENDEVCO® products for export or purchased with intent to export beyond the territorial limits of the United States are subject to special quotation.

ENDEVCO CORPORATION · 801 SO. ARROYO PARKWAY · PASADENA, CALIF. 91109 · TELEPHONE 213 795-0271
Akron, Ohio · Albuquerque, New Mexico · Boston, Massachusetts · Chicago, Illinois · Houston, Texas · Huntsville, Alabama · Mountain View, California
Palo Alto, California · Philadelphia, Pennsylvania · Washington, D.C. · West Palm Beach, Florida
Representatives: Australia · Belgium · Canada · Denmark · England · France · Germany · Holland · Italy · India · Israel · Japan · Norway · S.Africa · Sweden · Switzerland
TWX: 910 588-3272 Cable: Endevco

PRINTED IN U.S.A. 3/67

APPENDIX U

ENDEVCO PRODUCT DATA

MODELS 2271A 2275

Low Strain Sensitivity
Flat Charge-Temperature Response
Electrical Insulation

PRECISION ISOBASE® ACCELEROMETER

The Models 2271A and 2275 Accelerometers featuring the new ISOBASE® construction represent a major breakthrough in the state of the art of transducer development. ISOBASE® construction provides mechanical isolation of the seismic element from the base, resulting in very low strain sensitivity heretofore available only in shear-type construction.

The Models 2271A and 2275 are precision accelerometers for use in the laboratory or in airborne applications. They feature extremely flat charge-temperature response over a broad temperature range, from −185°C to +260°C, and excellent stability with time. Their high internal capacitance permits operation directly into oscilloscopes or voltmeters.

In the Model 2271A, the signal ground is insulated from the case; in the Model 2275, signal ground is connected to the case. The Models 2271AM20 and 2275M15 with dynamic characteristics identical to the above, respectively, feature top connectors.

These accelerometers are self-generating piezoelectric transducers, require no external power for operation, and may be used with either charge or voltage amplifiers.

2271AM20
2275M15

ACTUAL SIZE

SPECIFICATIONS FOR MODEL 2271A AND 2275 ACCELEROMETERS
(According to ANSI and ISA Standards)

DYNAMIC

CHARGE SENSITIVITY	11.5 pC/g, nominal 10 pC/g, minimum
VOLTAGE SENSITIVITY[1]	5.0 mV/g, nominal
MOUNTED RESONANCE FREQUENCY	27,000 Hz ± 3 kHz
FREQUENCY RESPONSE (±5%)[2]	2 to 5500 Hz, see curves below[3]
TRANSVERSE SENSITIVITY	2% maximum; 1% on special selection
AMPLITUDE LINEARITY, RANGE	Sensitivity increases approximately 1% per 1000 g, 0 to 10,000 g
TRANSDUCER CAPACITANCE	2000 pF, nominal
TRANSDUCER RESISTANCE	20,000 MΩ, minimum at +75°F (24°C); 100 MΩ, minimum at +500°F (260°C)
INSULATION RESISTANCE (2271A)	10 MΩ minimum

NOTES

[1] With 300 pF external capacitance

[2] In shock measurement, minimum pulse duration for half-sine or triangular pulses should exceed 0.20 msec to avoid high frequency ringing. See Endevco Piezoelectric Instruction Manual

[3] Use ENDEVCO® Charge Amplifier Series 2700 or 2640

TYPICAL TEMPERATURE RESPONSE

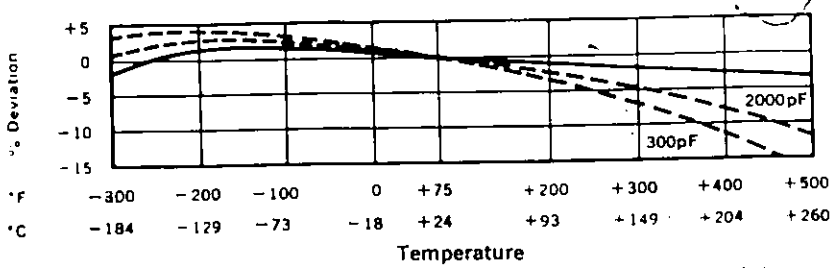

The solid line shows the nominal charge-temperature response. The broken lines show the nominal voltage-temperature response with the cable supplied and also with an external capacitance of 2000 pF.

TYPICAL FREQUENCY RESPONSE

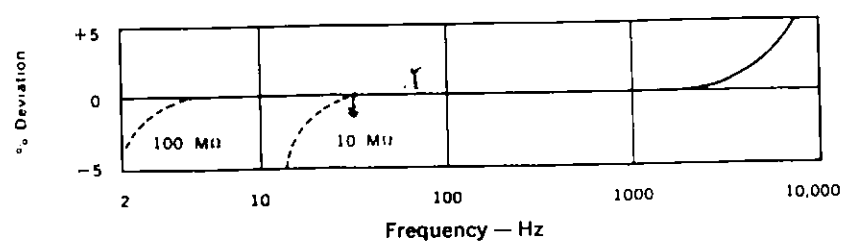

The solid curve shows the charge-frequency response. The broken lines show the voltage-frequency response with the loads shown and cable as supplied.

Estimated Calibration Errors:
5 to 900 Hz: ±1.5%
900 to 10,000 Hz: ±2.5%

Specifications for Models 2271A and 2275

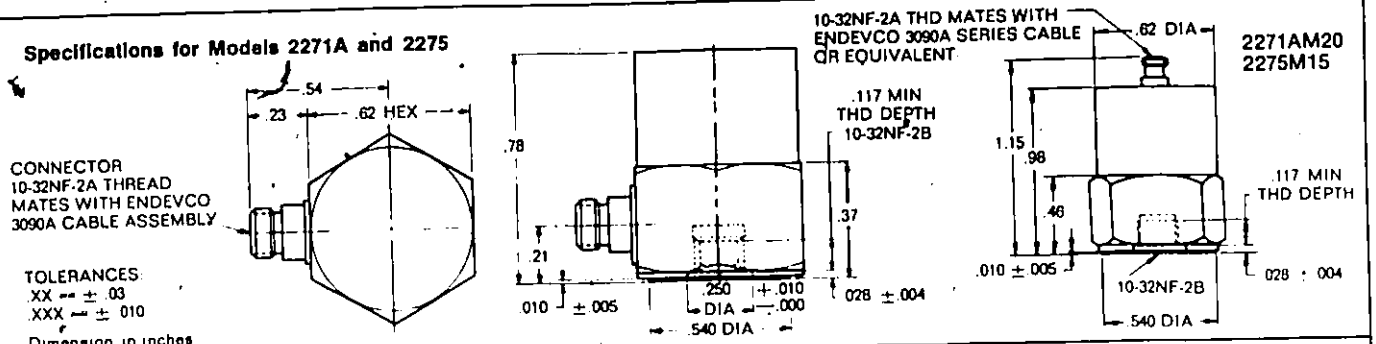

PHYSICAL

DESIGN		Single-ended compression, ISOBASE®
WEIGHT		27 grams (1 ounce), nominal
CRYSTAL MATERIAL		Piezite® Element Type P-10
CASE MATERIAL		Stainless Steel
CONNECTOR TYPE		Coaxial, 10-32 thread, mates with accessory cable
MOUNTING		Base tapped for 10-32x⅛" ENDEVCO® Mounting Stud. Recommended mounting torque: 18 in.-lb. (20 kg-cm)
GROUNDING	2271A: 2275:	Signal ground is isolated from case by 10 MΩ, minimum Signal ground connected to case.
ACCESSORIES INCLUDED		Model 2981-3 Mounting Stud (10-32), or Model 2981-4 (M5 metric). Model 3090A-120 Low Noise Cable Assembly, 10 ft., 300 pF nominal capacitance
OPTIONS AVAILABLE		Model 2271AM20 with top connector. Model 2275M15 with top connector.

ENVIRONMENTAL

ACCELERATION LIMITS	Vibration: Shock:	1000 pk g, sinusoidal, in any direction 10,000 pk g, in any direction
TEMPERATURE		−270°C to +260°C (−450°F to +500°F). Short connector during storage at extreme temperatures.
BASE STRAIN SENSITIVITY		0.5 equivalent g, nominal, at 250 μin./in. strain
MAGNETIC SENSITIVITY		0.03 equivalent g, nominal, at 100 gauss, 60 Hz
STRAY VOLTAGE SENSITIVITY	(2271A)	Typically, 0.1 g/V applied between signal ground and case
ALTITUDE		Not affected
HUMIDITY		All welded hermetic seal
CHARGE SENSITIVITY STABILITY		Within calibration accuracy over 12-month period.[1]

NOTE: [1]Endevco warrants only the free recalibration of this accelerometer if the sensitivity deviates beyond the normal ±1.5% accuracy of the original calibration

Continued product improvement necessitates that Endevco reserve the right to modify these specifications and/or prices without notice

RELIABILITY: Endevco maintains a program of constant surveillance over all products to ensure a high level of reliability. This program includes attention to reliability factors during product design, the support of stringent Quality Control requirements, and compulsory corrective action procedures. These measures, together with conservative specifications, have made the name Endevco synonymous with reliability.

CALIBRATION: Each unit is calibrated at room temperature for charge and voltage sensitivity, capacitance of both transducer and cable, transverse sensitivity, and frequency response from 20 to 4000 Hz. Temperature calibration at −300°F, +75°F, +350°F and +500°F, and other calibrations are supplied on special order. See Calibration Service Bulletin No. 301.

PRICES: F.O.B. Pasadena

Model	1 only	2 to 5	6 or more
2271A	$225.00	$215.00	$200.00
2275	$215.00	$205.00	$190.00
2271AM20	$235.00	$225.00	$210.00
2275M15	$225.00	$215.00	$200.00

Prices of ENDEVCO® products to be exported or purchased with intent to export beyond the territorial limits of the United States and Canada are subject to special quotation

ENDEVCO DYNAMIC INSTRUMENT DIVISION
801 S. ARROYO PARKWAY • PASADENA, CALIF. 91109 • PHONE (213) 795-0271
AKRON, OHIO • BOSTON, MASSACHUSETTS • CHICAGO, ILLINOIS • DALLAS, TEXAS • PALO ALTO, CALIFORNIA • PHILADELPHIA, PENNSYLVANIA • WASHINGTON, D.C. • WEST PALM BEACH, FLORIDA
AUSTRALIA • BELGIUM • CANADA • DENMARK • ENGLAND • FINLAND • FRANCE • GERMANY • INDIA • ISRAEL • ITALY • JAPAN • NETHERLANDS • NORWAY • S. AFRICA • SPAIN • SWEDEN • SWITZERLAND
TWX 910 588 3272 CABLE ENDEVCO

PRINTED IN U.S.A. 7/70

APPENDIX E

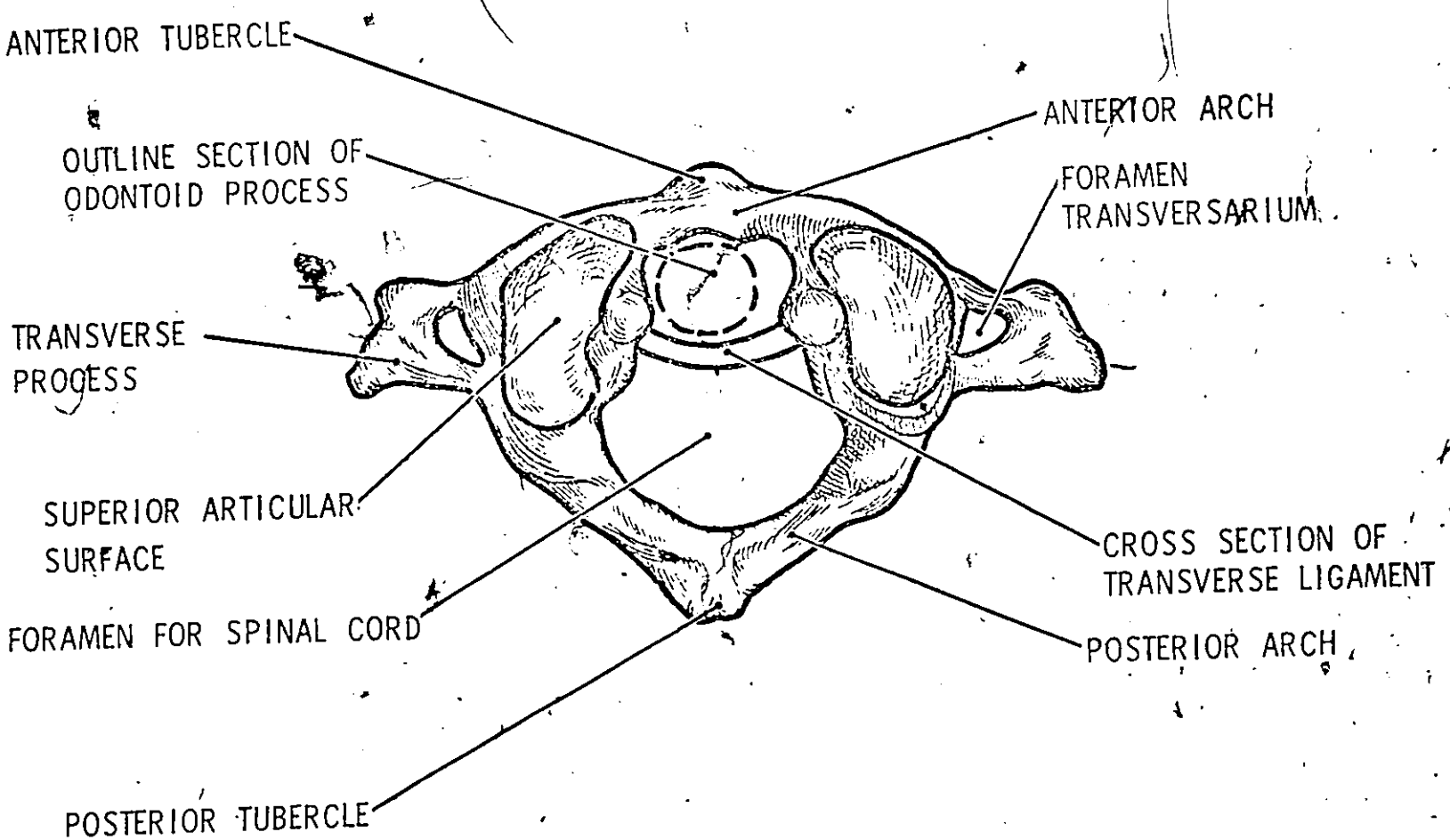

FIG. 3 SUPERIOR VIEW OF THE FIRST CERVICAL VERTEBRA, THE ATLAS (Reference 3)

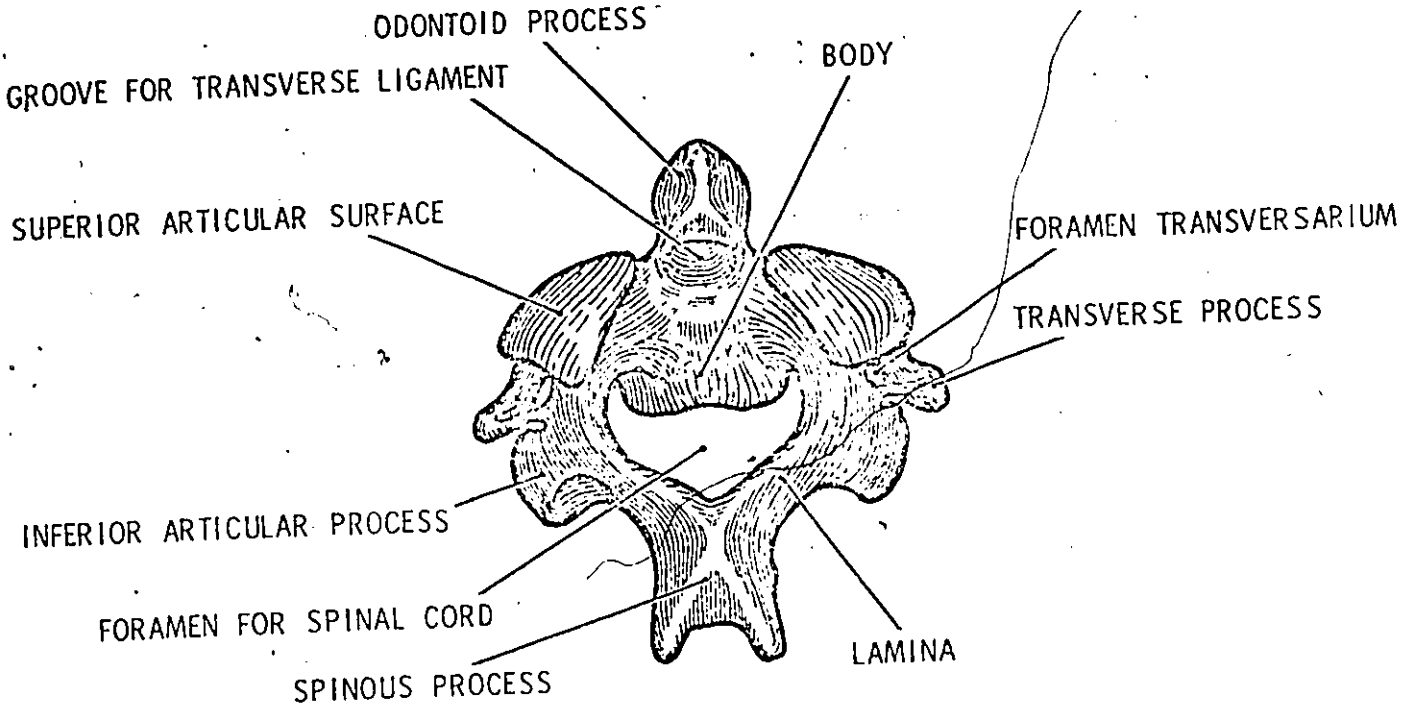

POSTEROSUPERIOR VIEW

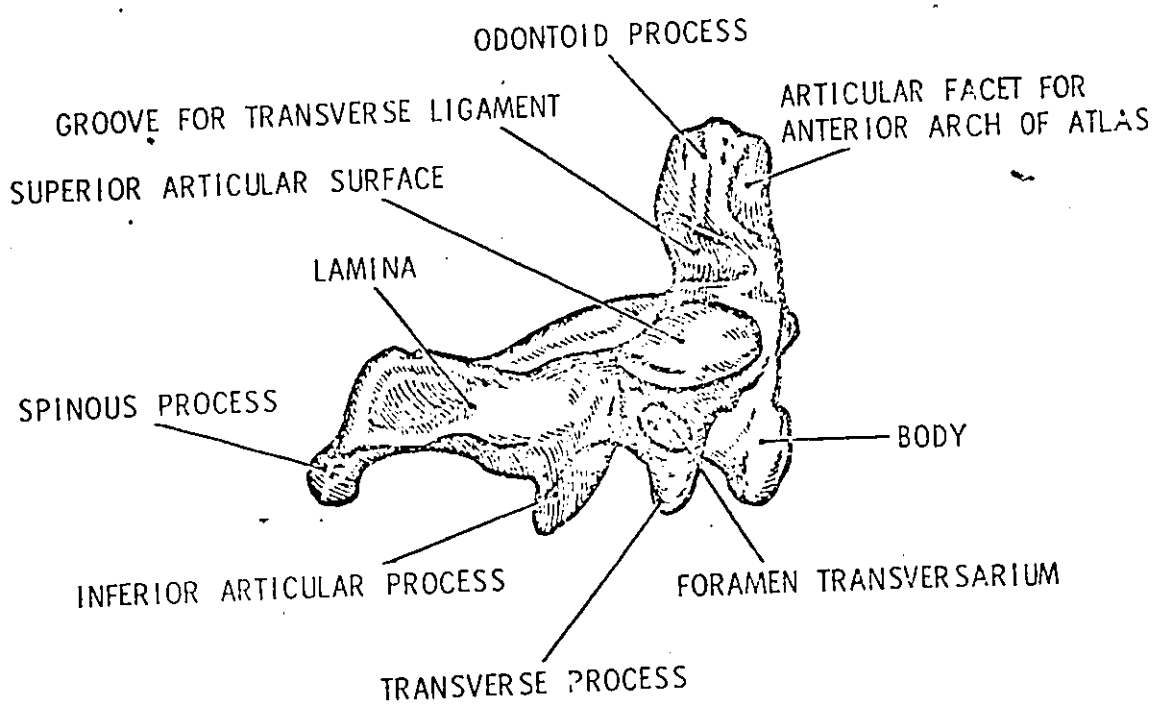

LATERAL VIEW

FIG. 4 THE SECOND CERVICAL VERTEBRA, THE AXIS
(Reference 3)

APPENDIX F

CANUS C-32 CLEAR CASTING RESIN

This resin was designed primarily for use as a clear, water-white, casting resin. Among its uses are potting or encapsulating biological, botanical and geological specimens. Its extreme clarity makes it ideally suited for encapsulating applications and for castings incorporating decorative media.

Other applications for which C-32 is well suited are encasing transistor radio components, impregnating capacitors, embedding hearing aid assemblies, molding terminal blocks, large filled castings and for casting such decorative items as table tops, lamp bases and the like.

C-32 can be modified as much as 50% with fillers. Fillers can be added for special mechanical or electrical properties or to reduce cost and shrinkage.

Physical Properties of Liquid C-32

Viscosity, Cps. @ 77°F	320-340
Acid Number, Max	20
Monomer Content, %	36-38
Specific Gravity	1.120

Handling Characteristics at 77°F
When Catalyzed with MEK peroxide "60"

	(Weight in Grams)			
C-32	100	100	100	100
MEK Peroxide "60"	1.5	1.0	0.75	0.5
	(Minutes)			
Gel Time	11	14	16	21
Cure Time	46	60	90	165

Typical Physical Properties of C-32
(Determined on Cured unfilled 1/8" casting)

Tensile Strength, psi	9500
Flexural Strength, psi	13,500
Flexural Modulus, psi	5.92 x 105
Compressive Strength, psi	22,500
Heat Distortion Point	163°F
Barcol Hardness	42-43

Electrical property values on a 1/8" casting of C-32

Dielectric Strength, S/T	429
Dielectric Constant, 60 cycles	3.34
Dielectric Constant, 1 Megacycle	2.96
Power Factor 60 Cycles	0035
Power Factor 1 Megacycle	0015
Loss Factor, 1 Megacycle	0044
Loss Factor, 60 Cycles	0117

APPENDIX G

A joint effort between the author, Associate Professor C. Cotton from the Department of Kinanthropology, Dr. V.J. Sistek, Mr. M. Simmons and Mr. R. Grenier of the Department of Anatomy, all from the University of Ottawa, led to the development of plastic necks for the rigid and multiposition mode tests. This part of the appendix will briefly describe the format necessary to fabricate a neck of this type for testing.

The cadaver head was decapitated below the second cervical vertebra, the axis. These two vertebrae left attached to the base of the skull will form a strong anchor for securing the plastic to the base of the skull.

The region surrounding the two vertebrae was dissected with the ultimate goal of removing fat and tissue down to the bone of the skull. The tendons, ligaments and muscle attached to the two remaining vertebrae, the atlas and axis were left intact.

The cadaver head was positioned such that the neck vertebrae were vertical and the crown supported as in Figure 95.

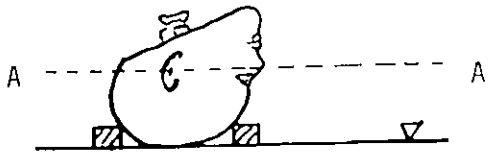

Figure 95

The cadaver head was supported so a line A-A that passed through the ear opening and the floor of the lower orbital of the eye would be parallel with the level datum.

A retort stand was then used to position the steel neck over the vertebrae as in Figure 96.

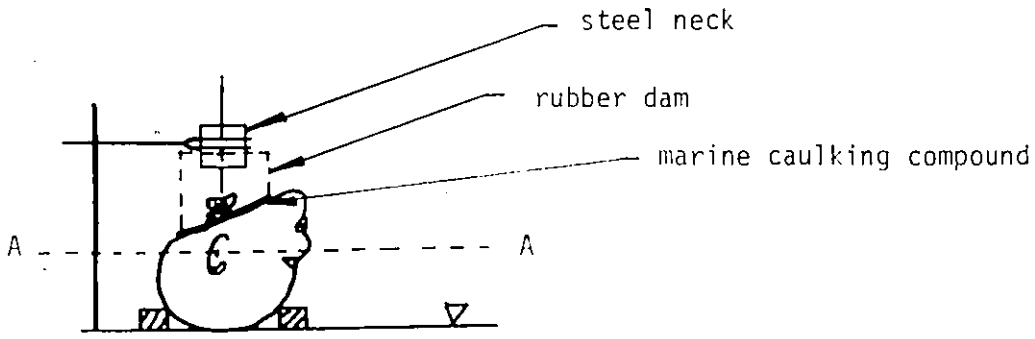

Figure 96

The cylindrical rubber dam was sealed with caulking compound to permit the pouring of the C-32 Canus resin around the steel neck.

The completed specimen cadaver head 2 is shown in Figure 97, for the rigid mode. Here holes were drilled and wood screws inserted to insure a rigid steel to plastic interface. The centre hole in Figure 97 was tapped to accommodate mounting to the slotted plate.

Figure 97

The plastic necks for the multiposition mode were made in much the same manner, except the steel necks were positioned directly on top of the vertebrae as in Figure 98.

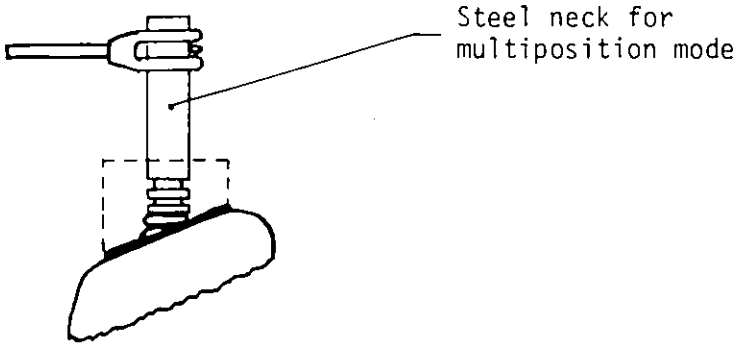

Figure 98

The completed specimen cadaver head 4 is shown in Figure 99 with the steel neck ready for inserting into the neck clamp of the multi-position mode apparatus.

Figure 99

VOLUME II

VI-I PREVIEW OF CHAPTER VI

Chapter VI is Volume II of this thesis and has been designed in this manner to assist the reader in referring to the data when necessary. Section 2 and 3 contain the computer output Tables, Section 4 consists of 35 graphs, Section 5 contains the Accelerometer and Loadcell Time Traces and Section 6 is an information table for the Cadaver Heads used in the testing programme.

VI-2 DATA TABLE TEST INDEX

TEST #			
24	MEP	F	FLAT PLATE
26	MEP	F	H.S. SLOTTED PLATE
27	MEP	F	H.S. LEAD DISC, SLOTTED PLATE
28	MEP	F	SLOTTED PLATE
29	MEP	F	CAST AL. (H.F.) THIN
30	5Kg	F	CAST AL. (H.F.) THIN WITH HELMET
31	MEP	F	FLAT PLATE
32	MEP	F	H.S. CHECK
34	MEP	F	CSA-W-L-C
35	MEP	F	CSA-W-L-B
36	MEP	F	CSA-W-S-C
37	MEP	F	CSA-W-S-B
38	MEP	F	CSA-P-L
39	MEP	F	CSA-P-L
40	MEP	F	CSA-P-S
41	MEP	F	SP-W-H.F.
42	MEP	F	SP-W-H.F.
43	MEP	F	CAST AL. (THICK)
44	MEP	F	SIERRA
45	MEP	F	Z90.1
46	5Kg(F)	F	Z90.1
47	5Kg(F)	F	CAST AL (THIN)
48	5Kg(F)	F	SIERRA
49	5Kg(F)	F	CSA-P-L
50	5Kg(F)	F	CSA-W-L-B
51	MEP	F	H.S.
52	MEP	F	FLAT PLATE CHECK
53	5Kg(F)	F	Z90.1 H.F.
54	5Kg(F)	F	Z90.1
55	5Kg(F)	F	CADAVER 1
56	5Kg(MEP)	F	CADAVER 1 WO HELMET
57	MEP	F	FLAT PLATE CHECK
58	5Kg(F)	F	CADAVER 2
59	5Kg(F)	F	CADAVER 2 WO HELMET
60	MEP	F	SIERRA OCCIPITAL
61	MEP	F	SIERRA PARIETAL R.S.
62	MEP	F	SIERRA PARIETAL L.S.
63	MEP	F	SIERRA FRONTAL
64	MEP	F	CSA-P-L FRONTAL
65	MEP	F	CSA-P-L OCCIPITAL

TEST #			
66	MEP	F	CSA-P-L PARIETAL R.S.
67-1	MEP	F	EBAR PLATE , $\bar{e}$ = 0.00
67-2	MEP	F	EBAR PLATE , $\bar{e}$ = 0.50
67-3	MEP	F	EBAR PLATE , $\bar{e}$ = 1.00
67-4	MEP	F	EBAR PLATE , $\bar{e}$ = 1.50
67-5	MEP	F	EBAR PLATE , $\bar{e}$ = 0.00
68	5Kg(F)	F	MINING HELMET
69	10lb(F)	F	MINING HELMETS
70	MEP	F	CSA-P-L P.L.S.
71	MEP	F	CSA-P-L P.R.S.
72	5Kg(F)	F	CSA-P-L P.L.S.
73	5Kg(F)	F	CADAVER 3 FRONTAL
75	5Kg(*)	F	MEP (* - SNELL HEAD FORM)
76	5Kg(F)	F	MEP (SNELL)
77	10lb(F)	F	MEP (SNELL)
78	MEP	F	EBAR PLATE , ($\bar{e}$ = 0.00)
79	MEP	F	EBAR PLATE , ($\bar{e}$ = 0.00)
80	MEP	F	EBAR PLATE , ($\bar{e}$ = 0.50)
81	MEP	F	EBAR PLATE , ($\bar{e}$ = 1.00)
82	MEP	F	EBAR PLATE , ($\bar{e}$ = 1.50)
83	MEP	F	EBAR PLATE , ($\bar{e}$ = 1.75)
84	MEP	F	EBAR PLATE , ($\bar{e}$ = 1.50)
85	MEP	F	SP-W-H.F. , ($\bar{e}$ = 0.00)
86	MEP	F	SP-W-H.F. , ($\bar{e}$ = 0.00)
87	MEP	F	SP-W-H.F. , ($\bar{e}$ = 0.50)
88	MEP	F	SP-W-H.F. , ($\bar{e}$ = 1.00)
89	MEP	F	SP-W-H.F. , ($\bar{e}$ = 1.50)
90	5Kg(F)	F	CADAVER 4 FRONTAL WITH HELMET
91	5Kg(F)	F	SIERRA FRONTAL
92	5Kg(F)	F	CADAVER 4 WITH HELMET AND REINFORCED NECK 1
93	5Kg(F)	F	SIERRA FRONTAL
94	5Kg(F)	F	CSA-P-L FRONTAL
95	5Kg(F)	F	SIERRA OCCIPITAL
96	MEP	F	SIERRA OCCIPITAL WITH SUPPORT
97	5Kg(F)	F	SIERRA OCCIPITAL WITH SUPPORT AND HELMET
98	5Kg(F)	F	CADAVER 4 WITHOUT HELMET BUT WITH REINFORCED NECK 2
99	5Kg(F)	F	MEP
100	5Kg(MEP)	F	FLAT PLATE

VI-3

TABLES OF DATA WITH COMPUTER PROGRAMME LISTING FOR CALCULATIONS

HEADING ABBREVIATIONS

H - DROP HEIGHT

AED - DIVISIONS ON ACCELERATION - TIME TRACE

ASF - ACCELERATION SCALE FACTOR - VOLTS/DIVISION

LCD - DIVISIONS ON FORCE - TIME TRACE

LSF - FORCE (LOADCELL) SCALE FACTOR

AEG - ACCELERATION (NEGATIVE) - G'S

MAEG - MASS OF STRIKER TIMES ACCELERATION - LBS.

FLC - TRANSMITTED FORCE SEEN BY LOADCELL - LBS.

$$\% = \frac{MAEG - FLC}{FLC} \times 100$$

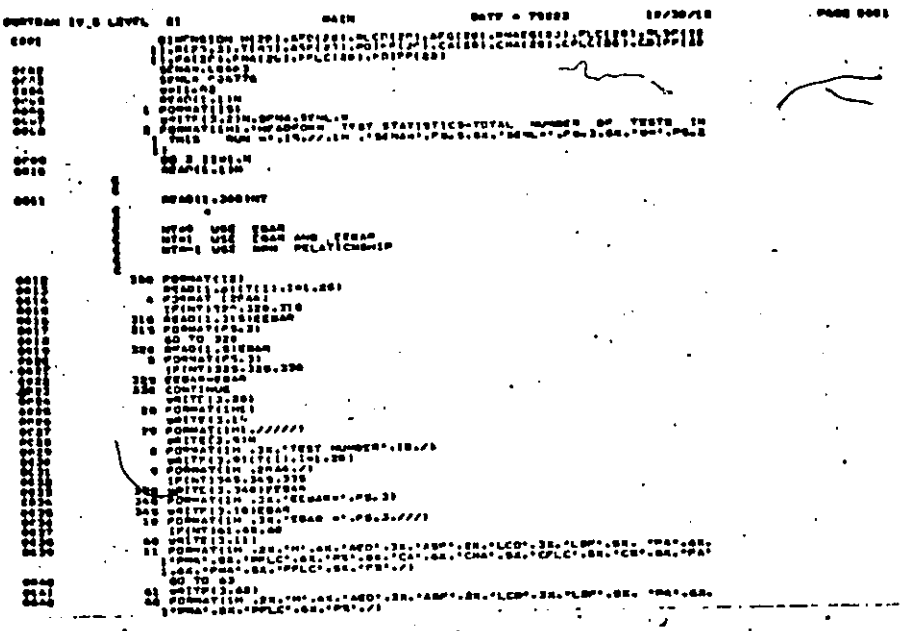

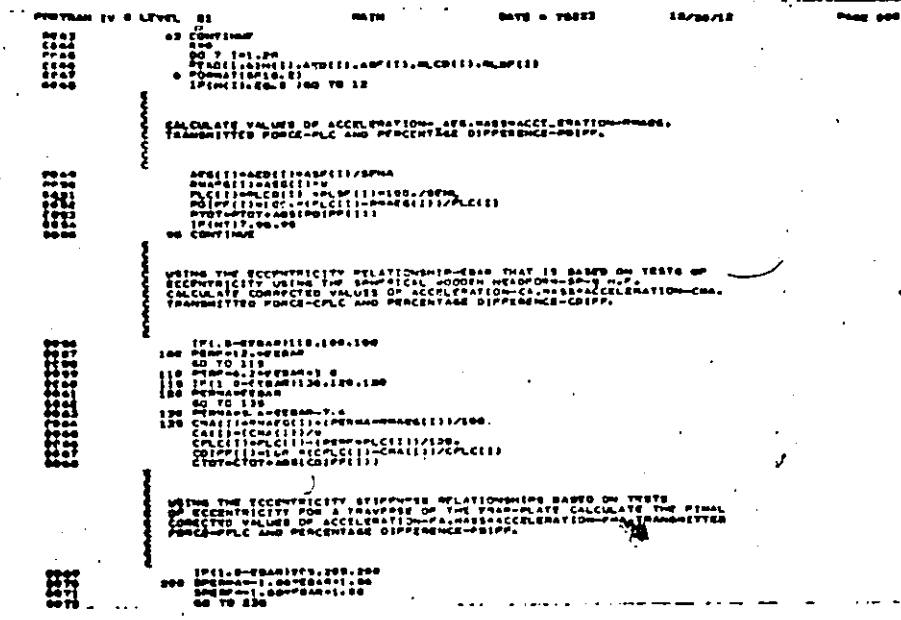

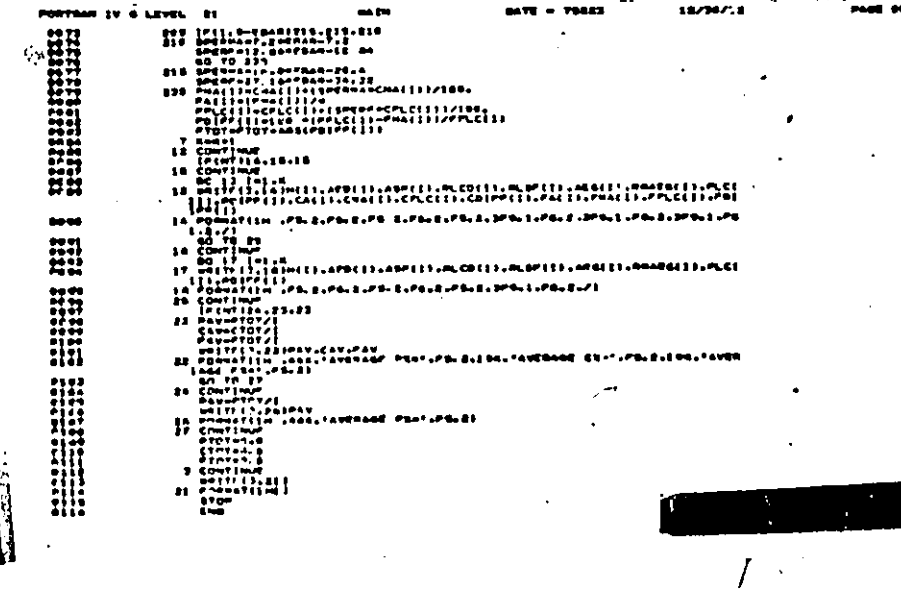

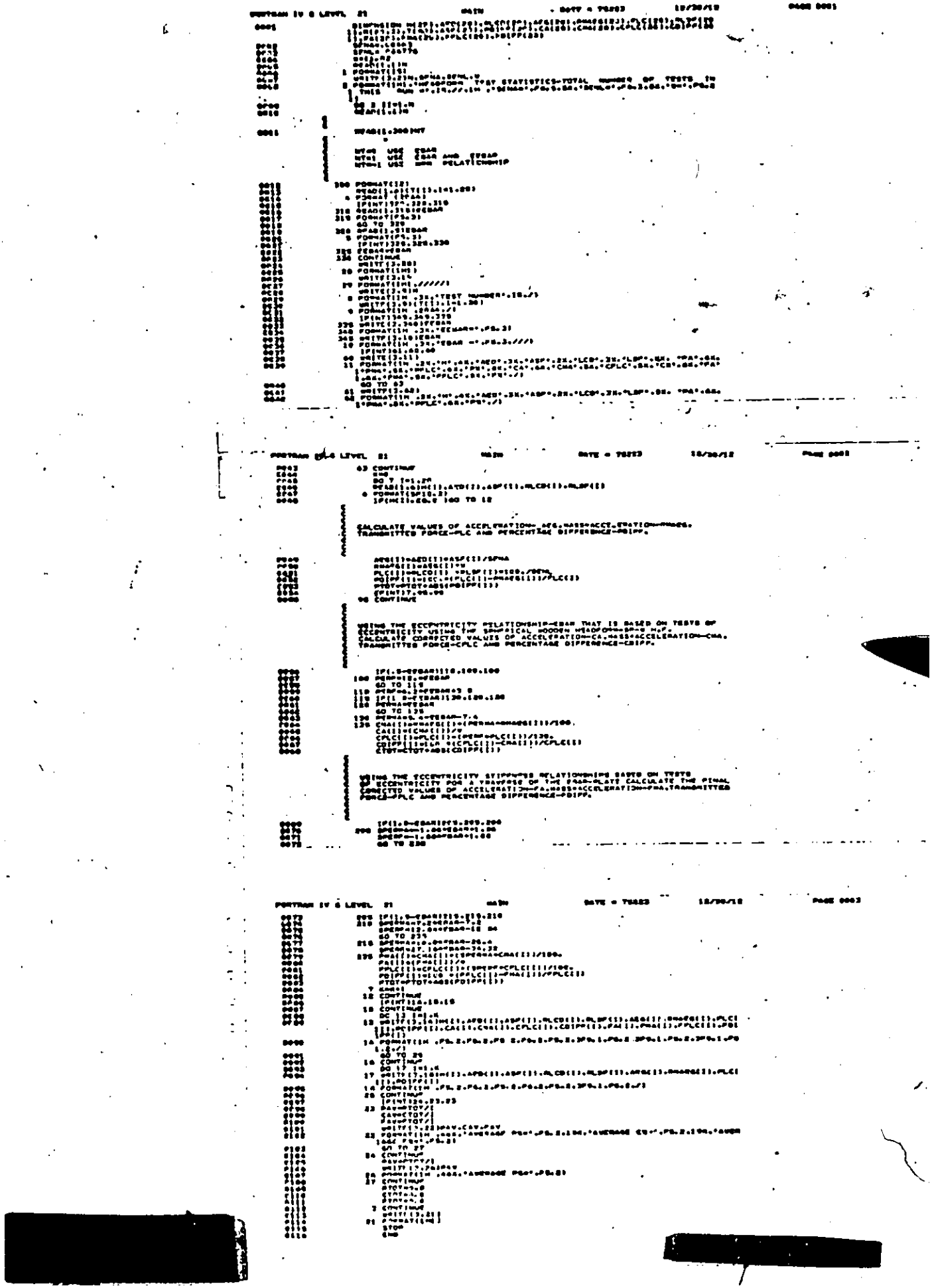

TEST NUMBER 24

MEP F FLAT PLATE

EBAR =0.0

H	AED	ASF	LCD	LSF	PA	PMA	PFLC	P%	CA	CMA	CFLC	C%	FA	FMA	FFLC	F%
2.00	5.30	1.00	6.00	0.10	1144.7	12614.7	12562.8	-0.41	1144.7	12614.7	12562.8	-0.41	1166.0	12849.3	12799.0	-0.39
1.75	4.75	1.00	5.45	0.10	1025.9	11305.6	11411.2	0.93	1025.9	11305.6	11411.2	0.93	1045.0	11515.9	11625.8	0.94
1.50	4.35	1.00	4.90	0.10	939.5	10353.6	10259.6	-0.92	939.5	10353.6	10259.6	-0.92	957.0	10546.1	10452.5	-0.90
1.25	3.65	1.00	4.25	0.10	788.3	8687.5	8898.7	2.37	788.3	8687.5	8898.7	2.37	803.0	8849.1	9065.9	2.39
1.00	3.07	1.00	3.58	0.10	663.1	7307.0	7495.8	2.52	663.1	7307.0	7495.8	2.52	679.4	7442.9	7636.7	2.54
0.75	2.40	1.00	2.85	0.10	518.4	5712.3	5967.3	4.27	518.4	5712.3	5967.3	4.27	528.0	5818.6	6079.5	4.27
0.50	1.75	1.00	2.10	0.10	378.0	4165.2	4397.0	5.27	378.0	4165.2	4397.0	5.27	385.0	4242.7	4476.6	5.29

AVERAGE P%= 2.49 AVERAGE C%***** AVERAGE F%*****

TEST NUMBER 26

MEP F H.S. SLOTTED PLATE

EBAR =0.0

H	AED	ASF	LCD	LSF	PA	PMA	PFLC	P%	CA	CMA	CFLC	C%	FA	FMA	FFLC	F%
2.25	4.08	0.50	2.43	0.10	440.6	4855.5	5087.9	4.57	440.6	4855.5	5087.9	4.57	448.8	4945.8	5183.6	4.59
2.00	3.78	0.50	2.25	0.10	408.2	4498.4	4711.1	4.51	408.2	4498.4	4711.1	4.51	415.8	4582.1	4799.6	4.53
1.75	3.45	0.50	2.08	0.10	372.6	4105.7	4355.1	5.73	372.6	4105.7	4355.1	5.73	379.5	4182.1	4437.0	5.74
1.50	3.10	0.50	1.90	0.10	334.8	3689.2	3978.2	7.27	334.8	3689.2	3978.2	7.27	341.0	3757.8	4053.0	7.28
1.25	2.76	0.50	3.38	0.05	298.1	3284.6	3538.5	7.18	298.1	3284.6	3538.5	7.18	303.6	3345.7	3605.0	7.19
1.00	2.30	0.50	2.95	0.05	248.4	2737.1	3088.4	11.37	248.4	2737.1	3088.4	11.37	253.0	2788.1	3146.4	11.39
0.75	1.80	0.50	2.37	0.05	194.4	2142.1	2481.2	13.66	194.4	2142.1	2481.2	13.66	198.0	2182.0	2527.8	13.68
0.50	1.38	0.50	1.80	0.05	149.0	1642.3	1884.4	12.85	149.0	1642.3	1884.4	12.85	151.8	1672.8	1919.8	12.87
0.25	0.84	0.50	1.15	0.05	90.7	999.7	1203.9	16.97	90.7	999.7	1203.9	16.97	92.4	1018.2	1226.6	16.98

AVERAGE P%= 9.34 AVERAGE C%= 9.34 AVERAGE F%= 9.36

TEST NUMBER 27

MEP F H.S. LEAD DISC . SLOTTED PLATE

EBAR =0 0

H	AED	ASF	LCD	LSF	PA	PMA	PFLC	PX	CA	CMA	CFLC	CX	FA	FMA	FFLC	FX
2.25	4.08	0.50	2.40	0.10	440.6	4855.5	5025.1	3.38	440.6	4855.5	5025.1	3.38	448.8	4945.8	5119.6	3.40
2.00	3.78	0.50	2.25	0.10	408.2	4498.4	4711.1	4.51	408.2	4498.4	4711.1	4.51	415.8	4582.1	4799.6	4.53
1.50	3.05	0.50	1.85	0.10	329.4	3629.7	3873.5	6.29	329.4	3629.7	3873.5	6.29	335.5	3697.2	3946.4	6.31
1.00	2.24	0.50	2.85	0.05	241.9	2665.7	2983.7	10.66	241.9	2665.7	2983.7	10.66	246.4	2715.3	3039.8	10.67
0.50	1.38	0.50	1.80	0.05	149.0	1642.3	1884.4	12.85	149.0	1642.3	1884.4	12.85	151.8	1672.8	1919.8	12.87

AVERAGE PX= 7.64 AVERAGE CX= 7.64 AVERAGE FX= 7.64

TEST NUMBER 28

MEP F SLOTTED PLATE CHECK

EBAR =0.0

H	AED	ASF	LCD	LSF	PA	PMA	PFLC	P%	CA	CMA	CFLC	C%	FA	FMA	FFLC	F%
0.25	0.95	1.00	1.19	0.10	205.2	2261.1	2491.6	9.25	205.2	2261.1	2491.6	9.25	209.0	2303.2	2538.5	9.27
2.00	5.50	1.00	6.40	0.10	1187.9	13090.7	13400.3	2.31	1187.9	13090.7	13400.3	2.31	1210.0	13334.2	13652.3	2.33
2.00	5.30	1.00	3.02	0.20	1144.7	12614.7	12646.6	0.25	1144.7	12614.7	12646.6	0.25	1166.0	12849.3	12884.3	0.27
							AVERAGE P%=	3.94			AVERAGE C%=	3.94			AVERAGE F%=	3.96

TEST NUMBER 29

MEP F CAST AL.(THIN)

EEBAR=0.200
EBAR =0.400

H	AED	ASF	LCD	LSF	PA	PMA	PFLC	P%	CA	CMA	CFLC	C%	FA	FMA	FFLC	F%
2.25	4.90	0.50	2.95	0.10	529.2	5831.3	6176.7	5.59	530.2	5843.0	6028.5	3.08	536.1	5908.2	6096.5	3.09
2.00	4.50	0.50	2.65	0.10	486.0	5355.3	5548.6	3.48	486.9	5366.0	5415.4	0.91	492.4	5425.9	5476.5	0.92
1.75	4.10	0.50	2.45	0.10	442.8	4879.3	5129.8	4.88	443.6	4889.0	5006.7	2.35	448.8	4943.6	5063.2	2.36
1.50	3.64	0.50	2.20	0.10	393.1	4331.8	4606.4	5.96	393.9	4340.5	4495.8	3.45	398.3	4388.9	4546.5	3.47
1.25	3.20	0.50	1.95	0.10	345.6	3808.2	4082.9	6.73	346.3	3815.8	3984.9	4.24	350.1	3858.4	4029.9	4.25
1.00	2.70	0.50	1.67	0.10	291.6	3213.2	3496.6	8.11	292.2	3219.6	3412.7	5.66	295.4	3255.5	3451.2	5.67
0.75	5.40	0.20	2.80	0.05	233.3	2570.5	2931.3	12.31	233.7	2575.7	2861.0	9.97	236.3	2604.4	2893.2	9.98
0.50	4.02	0.20	2.20	0.05	173.7	1913.6	2303.2	16.91	174.0	1917.5	2247.9	14.70	175.9	1938.8	2273.3	14.71
0.25	2.50	0.20	1.40	0.05	108.0	1190.1	1465.7	18.80	108.2	1192.4	1430.5	16.64	109.4	1205.8	1446.6	16.65

AVERAGE P%= 9.20 AVERAGE C%= 6.78 AVERAGE F%= 6.79

TEST NUMBER 30

CAST AL, (THIN) WITH HELMET

EBAR =0.880

H	AED	ASF	LCD	LSF	PA	PHA	PFLC	P%	CA	CHA	CFLC	C%	FA	FHA	FFLC	F%
2.00	2.00	0.50	1.45	0.10	216.0	2380.1	3036.0	21.60	217.9	2401.1	2779.3	13.61	218.4	2406.4	2785.6	13.61
							AVERAGE P%=21.60				AVERAGE C%=13.61				AVERAGE F%=13.61	

TEST NUMBER 31

MEP F FLAT PLATE CHECK

EBAR =0.0

H	AED	ASF	LCD	LSF	PA	PMA	PFLC	P%	CA	CMA	CFLC	C%	FA	FMA	FFLC	F%
2.50	6.30	1.00	3.58	0.20	1360.7	14994.8	14991.6	-0.02	1360.7	14994.8	14991.6	-0.02	1386.0	15273.7	15273.5	-0.00
2.00	5.20	1.00	2.95	0.20	1123.1	12376.7	12353.4	-0.19	1123.1	12376.7	12353.4	-0.19	1144.0	12606.9	12585.7	-0.17
1.50	4.19	1.00	4.80	0.10	905.0	9972.7	10050.3	0.77	905.0	9972.7	10050.3	0.77	921.8	10158.2	10239.2	0.79
1.00	3.00	1.00	3.40	0.10	647.9	7140.4	7118.9	-0.30	647.9	7140.4	7118.9	-0.30	660.0	7273.2	7252.8	-0.28
0.50	1.73	1.00	1.96	0.10	373.6	4117.6	4103.8	-0.34	373.6	4117.6	4103.8	-0.34	380.6	4194.2	4181.0	-0.32

AVERAGE P%= 0.32 AVERAGE C%= 0.32 AVERAGE F%= 0.31

TEST NUMBER 32

MEP F HEMISPHERICAL ANVIL

FBAR =0.0

H	AED	ASF	LCD	LSF	PA	PMA	PFLC	P%	CA	CMA	CFLC	C%	FA	FMA	FFLC	F%
2.00	3.73	0.50	2.25	0.10	402.8	4438.9	4711.1	5.78	402.8	4438.9	4711.1	5.78	410.3	4521.5	4799.6	5.79
2.00	3.78	0.50	2.25	0.10	408.2	4498.4	4711.1	4.51	408.2	4498.4	4711.1	4.51	415.8	4582.1	4799.6	4.53
2.50	4.48	0.50	2.58	0.10	483.8	5331.5	5402.0	1.31	483.8	5331.5	5402.0	1.31	492.8	5430.7	5503.6	1.32
2.00	4.41	0.50	2.58	0.10	476.2	5248.2	5402.0	2.85	476.2	5248.2	5402.0	2.85	485.1	5345.8	5503.6	2.87
							AVERAGE P%= 3.61				AVERAGE C%= 3.61				AVERAGE F%= 3.63	

TEST NUMBER 34

MEP F CSA-W-L-C

EBAR =0.230

H	AED	ASF	LCD	LSF	PA	PMA	PFLC	P%	CA	CMA	CFLC	C%	FA	FMA	FFLC	F%
2.25	5.20	0.50	3.25	0.10	561.6	6188.3	6804.9	9.06	562.8	6202.6	6617.0	6.26	570.9	6291.4	6712.8	6.28
2.00	4.73	0.50	2.95	0.10	510.8	5629.0	6176.7	8.87	512.0	5641.9	6006.2	6.07	519.3	5722.8	6093.2	6.08
1.75	4.33	0.50	2.67	0.10	467.6	5153.0	5590.4	7.83	468.7	5164.8	5436.1	4.99	475.4	5238.8	5514.8	5.01
1.50	3.85	0.50	2.40	0.10	415.8	4581.7	5025.1	8.82	416.7	4592.3	4886.4	6.02	422.7	4658.1	4957.2	6.03
1.25	3.40	0.50	2.10	0.10	367.2	4046.2	4397.0	7.98	368.0	4055.5	4275.6	5.15	373.3	4113.6	4337.5	5.16
1.00	2.90	0.50	1.78	0.10	313.2	3451.2	3727.0	7.40	313.9	3459.1	3624.1	4.55	318.4	3508.7	3676.6	4.57
0.75	2.35	0.50	1.50	0.10	253.8	2796.7	3140.7	10.95	254.4	2803.1	3054.0	8.22	258.0	2843.2	3098.2	8.23
0.50	4.45	0.20	2.25	0.05	192.2	2118.3	2355.5	10.07	192.7	2123.2	2290.5	7.31	195.4	2153.6	2323.7	7.32
0.25	2.80	0.20	1.50	0.05	121.0	1332.9	1570.4	15.12	121.2	1335.9	1527.0	12.51	123.0	1355.1	1549.1	12.53

AVERAGE P%= 9.57 AVERAGE C%= 6.79 AVERAGE F%= 6.80

TEST NUMBER 35

MEF F CSA-W-L-B

EEBAR=0.863
EBAR =1.150

H	AED	ASF	LCD	LSF	PA	PMA	PFLC	P%	CA	CMA	CFLC	C%	FA	FMA	FFLC	F%
2.25	5.30	0.50	3.25	0.10	572.4	6307.3	6804.9	7.31	577.3	6361.8	6236.6	-2.01	583.5	6430.5	6356.7	-1.16
2.00	4.78	0.50	2.95	0.10	516.2	5688.5	6176.7	7.90	520.7	5737.6	5660.9	-1.35	526.3	5799.6	5769.9	-0.51
1.75	4.38	0.50	2.64	0.10	473.0	5212.5	5527.6	5.70	477.1	5257.5	5066.0	-3.78	482.2	5314.2	5163.6	-2.92
1.50	3.81	0.50	2.40	0.10	411.4	4534.1	5025.1	9.77	415.0	4573.3	4605.5	0.70	419.5	4622.7	4694.2	1.52
1.25	3.35	0.50	2.12	0.10	361.8	3986.7	4438.9	10.19	364.9	4021.1	4068.2	1.16	368.8	4064.5	4146.5	1.98
1.00	7.10	0.20	3.60	0.05	306.7	3379.8	3768.8	10.32	309.3	3408.9	3454.1	1.31	312.7	3445.8	3520.6	2.13
0.75	5.70	0.20	2.95	0.05	246.2	2713.3	3088.4	12.14	248.3	2736.8	2830.5	3.31	251.0	2766.3	2885.0	4.11
0.50	4.30	0.20	2.25	0.05	185.7	2046.9	2355.5	13.10	187.3	2064.6	2158.8	4.37	189.4	2086.9	2200.4	5.16
0.25	2.65	0.20	1.40	0.05	114.5	1261.5	1465.7	13.93	115.5	1272.4	1343.3	5.28	116.7	1286.1	1369.1	6.07

AVERAGE P%=10.04 AVERAGE C%= 2.58 AVERAGE F%= 2.84

TEST NUMBER 36

MEP F CSA-W-S-C

EBAR =0.150

H	AED	ASF	LCD	LSF	PA	PMA	PFLC	P%	CA	CMA	CFLC	C%	FA	FMA	FFLC	F%
2.25	5.30	0.50	3.25	0.10	572.4	6307.3	6804.9	7.31	573.2	6316.8	6682.4	5.47	582.3	6416.7	6789.1	5.49
2.00	4.77	0.50	2.95	0.10	515.1	5676.6	6176.7	8.10	515.9	5685.1	6065.5	6.27	524.0	5775.0	6162.5	6.29
1.75	4.38	0.50	2.78	0.10	473.0	5212.5	5820.8	10.45	473.7	5220.3	5716.0	8.67	481.2	5302.8	5807.3	8.69
1.50	3.85	0.50	2.51	0.10	415.8	4581.7	5255.4	12.82	416.4	4588.6	5160.8	11.09	423.0	4661.2	5243.3	11.10
1.25	3.40	0.50	2.17	0.10	367.2	4046.2	4543.5	10.95	367.7	4052.3	4461.8	9.18	373.5	4116.4	4533.1	9.19
1.00	2.90	0.50	1.90	0.10	313.2	3451.2	3978.2	13.25	313.6	3456.4	3906.6	11.53	318.6	3511.0	3969.0	11.54
0.75	2.30	0.50	1.58	0.10	248.4	2737.1	3308.2	17.26	248.8	2741.3	3248.7	15.62	252.7	2784.6	3300.6	15.63
0.50	4.30	0.20	2.40	0.05	185.7	2046.9	2512.6	18.53	186.0	2050.0	2467.3	16.92	189.0	2082.4	2506.8	16.93
0.25	2.62	0.20	1.45	0.05	113.2	1247.2	1518.0	17.84	113.3	1249.1	1490.7	16.21	115.1	1268.8	1514.5	16.22

AVERAGE P%=12.95 AVERAGE C%=11.22 AVERAGE F%=11.23

TEST NUMBER 37

MEP F CSA-W-S-B

EEBAR=0.360
EBAR =0.720

H	AED	ASF	LCD	LSF	PA	PMA	PFLC	P%	CA	CMA	CFLC	C%	FA	FMA	FFLC	F%
2.25	4.90	0.50	2.86	0.10	529.2	5831.3	5988.3	2.62	531.1	5852.3	5729.6	-2.14	533.8	5882.8	5759.7	-2.14
2.00	4.52	0.50	2.63	0.10	488.1	5379.1	5506.7	2.32	489.9	5398.5	5268.8	-2.46	492.4	5426.6	5296.5	-2.45
1.75	4.16	0.50	2.45	0.10	449.2	4950.7	5129.8	3.49	450.9	4968.5	4908.2	-1.23	453.2	4994.4	4934.0	-1.22
1.50	3.62	0.50	2.15	0.10	390.9	4308.0	4501.7	4.30	392.3	4323.5	4307.2	-0.38	394.4	4346.1	4329.9	-0.37
1.25	3.20	0.50	1.90	0.10	345.6	3808.2	3978.2	4.27	346.8	3821.9	3806.4	-0.41	348.6	3841.8	3826.4	-0.40
1.00	2.73	0.50	1.63	0.10	294.8	3248.9	3412.9	4.81	295.9	3260.6	3265.5	0.15	297.4	3277.6	3282.6	0.16
0.75	2.18	0.50	1.36	0.10	235.4	2594.3	2847.6	8.89	236.3	2603.7	2724.6	4.44	237.5	2617.2	2738.9	4.44
0.50	1.63	0.50	1.02	0.10	176.0	1939.8	2135.7	9.17	176.7	1946.8	2043.4	4.73	177.6	1956.9	2054.2	4.73
0.25	2.50	0.20	1.30	0.05	108.0	1190.1	1361.0	12.56	108.4	1194.3	1302.2	8.28	108.9	1200.6	1309.0	8.29

AVERAGE P%= 5.83 AVERAGE C%= 2.69 AVERAGE F%= 2.69

TEST NUMBER 38

MEP F CSA-P-L

EBAR =0.540

H	AED	ASF	LCD	LSF	PA	PMA	PFLC	P%	CA	CMA	CFLC	C%	FA	FMA	FFLC	F%
2.25	4.95	0.50	3.25	0.10	534.6	5890.8	6804.9	13.43	537.4	5922.6	6372.9	7.07	542.0	5973.3	6428.0	7.07
2.00	4.52	0.50	2.95	0.10	488.1	5379.1	6176.7	12.91	490.8	5408.1	5784.6	6.51	495.0	5454.4	5834.6	6.52
1.75	4.15	0.50	2.66	0.10	448.2	4938.8	5569.5	11.32	450.6	4965.4	5216.0	4.80	454.4	5007.9	5261.1	4.81
1.50	3.60	0.50	2.35	0.10	388.8	4284.2	4920.4	12.93	390.9	4307.4	4608.1	6.53	394.2	4344.2	4647.9	6.53
1.25	3.20	0.50	2.10	0.10	345.6	3808.2	4397.0	13.39	347.4	3828.8	4117.9	7.02	350.4	3861.5	4153.5	7.03
1.00	2.65	0.50	1.75	0.10	286.2	3153.7	3664.2	13.93	287.7	3170.7	3431.6	7.60	290.2	3197.8	3461.2	7.61
0.75	2.20	0.50	1.45	0.10	237.6	2618.1	3036.0	13.76	238.9	2632.3	2843.3	7.42	240.9	2654.8	2867.9	7.43
0.50	4.09	0.20	2.21	0.05	176.7	1946.9	2313.7	15.85	177.6	1957.5	2166.8	9.66	179.1	1974.2	2185.5	9.67
0.25	2.50	0.20	1.40	0.05	108.0	1190.1	1465.7	18.80	108.6	1196.5	1372.6	12.83	109.5	1206.7	1384.5	12.84

AVERAGE PX=14.04 AVERAGE CX= 7.72 AVERAGE FX=-7.72

TEST NUMBER 39

MEP F CSA-P-L

EEBAR=0.750
EBAR =1.000

H	AED	ASF	LCD	LSF	PA	PMA	PFLC	PX	CA	CMA	CFLC	CX	FA	FMA	FFLC	FX
2.25	4.95	0.50	3.11	0.10	534.6	5890.8	6511.7	9.54	538.6	5935.0	6013.6	1.31	538.6	5935.0	6013.6	1.31
2.00	4.59	0.50	2.78	0.10	495.7	5462.4	5820.8	6.16	499.4	5503.4	5375.5	-2.38	499.4	5503.4	5375.5	-2.38
1.75	4.18	0.50	2.55	0.10	451.4	4974.5	5339.2	6.83	454.8	5011.8	4930.7	-1.64	454.8	5011.8	4930.7	-1.64
1.50	3.70	0.50	2.25	0.10	399.6	4403.2	4711.1	6.53	402.6	4436.3	4350.7	-1.97	402.6	4436.3	4350.7	-1.97
1.25	3.24	0.50	2.00	0.10	349.9	3855.8	4187.6	7.92	352.5	3884.7	3867.3	-0.45	352.5	3884.7	3867.3	-0.45
1.00	2.75	0.50	1.73	0.10	297.0	3272.7	3622.3	9.65	299.2	3297.2	3345.2	1.43	299.2	3297.2	3345.2	1.43
0.75	2.20	0.50	1.47	0.10	237.6	2618.1	3077.9	14.94	239.4	2637.8	2842.4	7.20	239.4	2637.8	2842.4	7.20
0.50	1.65	0.50	1.19	0.10	178.2	1963.6	2491.6	21.19	179.5	1978.3	2301.0	14.02	179.5	1978.3	2301.0	14.02
0.25	2.45	0.20	1.58	0.05	105.8	1166.3	1654.1	29.49	106.6	1175.0	1527.6	23.08	106.6	1175.0	1527.6	23.08

AVERAGE PX=12.47 AVERAGE CX= 5.94 AVERAGE FX= 5.94

TEST NUMBER 40

MEP F CSA-P-S

EBAR =0.465

H	AED	ASF	LCD	LSF	PA	PMA	PFLC	P%	CA	CMA	CFLC	C%	FA	FMA	FFLC	F%
2.25	4.60	0.50	2.90	0.10	496.8	5474.3	6072.0	9.84	499.1	5499.7	5733.2	4.07	504.0	5554.5	5790.9	4.08
2.00	4.20	0.50	2.65	0.10	453.6	4998.3	5548.6	9.92	455.7	5021.5	5239.0	4.15	460.2	5071.5	5291.7	4.16
1.75	3.84	0.50	2.42	0.10	414.7	4569.8	5067.0	9.81	416.6	4591.1	4784.3	4.04	420.8	4636.8	4832.4	4.05
1.50	3.40	0.50	2.18	0.10	367.2	4046.2	4564.5	11.35	368.9	4065.0	4309.8	5.68	372.5	4105.5	4353.1	5.69
1.25	3.00	0.50	1.95	0.10	324.0	3570.2	4082.9	12.56	325.5	3586.8	3855.1	6.96	328.7	3622.5	3893.9	6.97
1.00	2.55	0.50	1.69	0.10	275.4	3034.7	3538.5	14.24	276.7	3048.8	3341.1	8.75	279.4	3079.1	3374.7	8.76
0.75	2.05	0.50	1.40	0.10	221.4	2439.6	2931.3	16.77	222.4	2451.0	2767.8	11.45	224.6	2475.4	2795.6	11.45
0.50	3.75	0.20	2.10	0.05	162.0	1785.1	2198 5	18.80	162.7	1793.4	2075.8	13.61	164.4	1811.2	2096.7	13.61
0.25	2.35	0.20	1.38	0.05	101.5	1118.7	1444.7	22.57	102.0	1123.9	1364.1	17.61	103.0	1135.0	1377.8	17.62

AVERAGE PX=13.99

AVERAGE CX= 8.48

AVERAGE FX= 8.49

TEST NUMBER 41

MEP F SP-W-H,F.

EBAR =0.0

H	AED	ASF	LCD	LSF	PA	PMA	PFLC	P%	CA	CMA	CFLC	C%	FA	FMA	FFLC	F%
1.66	4.27	0.50	2.45	0.10	461.1	5081.6	5129.8	0.94	461.1	5081.6	5129.8	0.94	469.7	5176.1	5226.3	0.96
							AVERAGE P%=	0.94			AVERAGE C%=	0.94			AVERAGE F%=	0.96

TEST NUMBER 42

MEP F SP-W-H.F.

EBAR =0.0

H	AED	ASF	LCD	LSF	PA	PMA	PFLC	P%	CA	CMA	CFLC	C%	FA	FMA	FFLC	F%
2.25	5.40	0.50	3.05	0.10	583.2	6426.3	6386.1	-0.63	583.2	6426.3	6386.1	-0.63	594.0	6545.9	6506.1	-0.61
2.00	4.93	0.50	2.78	0.10	532.4	5867.0	5820.8	-0.79	532.4	5867.0	5820.8	-0.79	542.3	5976.1	5930.2	-0.77
1.75	4.30	0.50	2.45	0.10	464.4	5117.3	5129.8	0.24	464.4	5117.3	5129.8	0.24	473.0	5212.5	5226.3	0.26
1.50	3.93	0.50	2.25	0.10	424.4	4676.9	4711.1	0.72	424.4	4676.9	4711.1	0.72	432.3	4763.9	4799.6	0.74
1.25	3.40	0.50	1.95	0.10	367.2	4046.2	4082.9	0.90	367.2	4046.2	4082.9	0.90	374.0	4121.5	4159.7	0.92
1.00	2.87	0.50	1.64	0.10	309.9	3415.5	3433.8	0.53	309.9	3415.5	3433.8	0.53	315.7	3479.0	3498.4	0.55
0.75	2.32	0.50	1.42	0.10	250.5	2760.9	2973.2	7.14	250.5	2760.9	2973.2	7.14	255.2	2812.3	3029.1	7.16
0.50	1.75	0.50	1.02	0.10	189.0	2082.6	2135.7	2.48	189.0	2082.6	2135.7	2.48	192.5	2121.3	2175.8	2.50
0.25	2.62	0.20	1.33	0.05	113.2	1247.2	1392.4	10.43	113.2	1247.2	1392.4	10.43	115.3	1270.4	1418.6	10.45

AVERAGE P%= 2.65 AVERAGE C%= 2.65 AVERAGE F%= 2.66

TEST NUMBER 43

MEP F CAST AL. (THICK)

EEBAR=0.345
EBAR =0.690

H	AED	ASF	LCD	LSF	PA	PMA	PFLC	P%	CA	CMA	CFLC	C%	FA	FMA	FFLC	F%
2.25	6.20	0.50	3.64	0.10	669.5	7378.4	7621.4	3.19	671.9	7403.9	7305.9	-1.34	675.7	7446.5	7348.5	-1.33
2.00	5.61	0.50	3.31	0.10	605.8	6676.3	6930.5	3.67	607.9	6699.3	6643.6	-0.84	611.4	6737.9	6682.3	-0.83
1.75	5.14	0.50	3.05	0.10	555.1	6116.9	6386.1	4.21	557.0	6138.0	6121.7	-0.27	560.2	6173.4	6157.4	-0.26
1.50	4.51	0.50	2.70	0.10	487.0	5367.2	5653.3	5.06	488.7	5385.7	5419.2	0.62	491.5	5416.8	5450.8	0.62
1.25	3.74	0.50	2.25	0.10	403.9	4450.8	4711.1	5.52	405.3	4466.2	4516.0	1.10	407.6	4491.9	4542.3	1.11
1.00	3.14	0.50	1.96	0.10	339.1	3736.8	4103.8	8.94	340.3	3749.7	3933.9	4.68	342.2	3771.3	3956.9	4.69
0.75	2.60	0.50	1.62	0.10	280.8	3094.2	3392.0	8.78	281.7	3104.8	3251.5	4.51	283.4	3122.7	3270.5	4.52
0.50	5.02	0.20	2.53	0.05	216.8	2389.6	2648.7	9.78	217.6	2397.9	2539.0	5.56	218.8	2411.7	2553.8	5.56
0.25	3.12	0.20	1.62	0.05	134.8	1485.2	1696.0	12.43	135.2	1490.3	1625.8	8.33	136.0	1498.9	1635.2	8.34

AVERAGE P%= 6.84 AVERAGE C%= 3.03 AVERAGE F%= 3.03

TEST NUMBER 44

MEP F SIERRA

EBAR =0.0

H	AED	ASF	LCD	LSF	PA	PMA	PFLC	P%	CA	CMA	CFLC	C%	FA	FMA	FFLC	F%
2.25	4.80	0.50	2.80	0.10	518.4	5712.3	5862.6	2.56	518.4	5712.3	5862.6	2.56	528.0	5818.6	5972.9	2.58
2.00	4.40	0.50	2.54	0.10	475.2	5236.3	5318.3	1.54	475.2	5236.3	5318.3	1.54	484.0	5333.7	5418.2	1.56
1.75	3.94	0.50	2.26	0.10	425.5	4688.9	4732.0	0.91	425.5	4688.9	4732.0	0.91	433.4	4776.1	4820.9	0.93
1.50	3.53	0.50	2.05	0.10	381.2	4200.9	4292.3	2.13	381.2	4200.9	4292.3	2.13	388.3	4279.1	4373.0	2.15
1.25	3.05	0.50	1.74	0.10	329.4	3629.7	3643.2	0.37	329.4	3629.7	3643.2	0.37	335.5	3697.2	3711.7	0.39
1.00	6.45	0.20	3.02	0.05	278.6	3070.4	3161.6	2.89	278.6	3070.4	3161.6	2.89	283.8	3127.5	3221.1	2.91
0.75	5.20	0.20	2.46	0.05	224.6	2475.3	2575.4	3.88	224.6	2475.3	2575.4	3.88	228.8	2521.4	2623.8	3.90
0.50	4.00	0.20	1.90	0.05	172.8	1904.1	1989.1	4.27	172.8	1904.1	1989.1	4.27	176.0	1939.5	2026.5	4.29
0.25	2.00	0.20	1.00	0.05	86.4	952.1	1046.9	9.06	86.4	952.1	1046.9	9.06	88.0	969.8	1066.6	9.08
							AVERAGE P%=	3.07			AVERAGE C%=	3.07			AVERAGE F%=	3.09

TEST NUMBER 45

MEP F Z90.1

EBAR =0.0

R	AED	ASF	LCD	LSF	PA	PMA	PFLC	PX	CA	CMA	CFLC	CX	FA	FMA	FFLC	FX
2.25	6.40	0.50	3.87	0.10	691.1	7616.4	8103.0	6.01	691.1	7616.4	8103.0	6.01	704.0	7758.1	8255.4	6.02
2.00	5.86	0.50	3.48	0.10	632.8	6973.8	7286.4	4.29	632.8	6973.8	7286.4	4.29	644.6	7103.5	7423.4	4.31
1.75	5.29	0.50	3.14	0.10	571.3	6295.4	6574.5	4.25	571.3	6295.4	6574.5	4.25	581.9	6412.5	6698.1	4.26
1.50	4.65	0.50	2.75	0.10	502.2	5533.8	5758.0	3.89	502.2	5533.8	5758.0	3.89	511.5	5636.7	5866.2	3.91
1.25	4.10	0.50	2.47	0.10	442.8	4879.3	5171.7	5.65	442.8	4879.3	5171.7	5.65	451.0	4970.0	5268.9	5.67
1.00	3.47	0.50	2.08	0.10	374.7	4129.5	4355.1	5.18	374.7	4129.5	4355.1	5.18	381.7	4206.3	4437.0	5.20
0.75	2.75	0.50	1.65	0.10	297.0	3272.7	3454.8	5.27	297.0	3272.7	3454.8	5.27	302.5	3333.5	3519.7	5.29
0.50	2.02	0.50	1.22	0.10	218.1	2403.9	2554.4	5.89	218.1	2403.9	2554.4	5.89	222.2	2448.6	2602.5	5.91
0.25	3.13	0.20	1.60	0.05	135.2	1490.0	1675.0	11.05	135.2	1490.0	1675.0	11.05	137.7	1517.7	1706.5	11.07

AVERAGE PX= 5.72 AVERAGE CX= 5.72 AVERAGE FX= 5.74

TEST NUMBER 46

5KG.(F) F Z90.1

EBAR =0.0

H	AED	ASF	LCD	LSF	PA	PMA	PFLC	P%	CA	CMA	CFLC	C%	FA	FMA	FFLC	F%
2.50	2.21	0.50	0.59	0.20	238.7	2630.0	2470.7	-6.45	238.7	2630.0	2470.7	-6.45	243.1	2679.0	2517.1	-6.43
2.00	4.90	0.20	2.25	0.05	211.7	2332.5	2355.5	0.98	211.7	2332.5	2355.5	0.98	215.6	2375.9	2399.8	1.00
1.50	4.05	0.20	1.95	0.05	174.9	1927.9	2041.5	5.56	174.9	1927.9	2041.5	5.56	178.2	1963.8	2079.8	5.58
1.00	3.40	0.20	1.80	0.05	146.9	1618.5	1884.4	14.11	146.9	1618.5	1884.4	14.11	149.6	1648.6	1919.8	14.13
0.50	2.05	0.20	1.10	0.05	88.6	975.9	1151.6	15.26	88.6	975.9	1151.6	15.26	90.2	994.0	1173.2	15.28

AVERAGE P%= 8.47 AVERAGE C%= 8.47 AVERAGE F%= 8.48

TEST NUMBER 47

5KG(F) F CAST AL (THIN)

EBAR =0.900

H	AED	ASF	LCD	LSF	PA	PMA	PFLC	PX	CA	CMA	CFLC	C%	FA	FMA	FFLC	F%
2.50	5.65	0.20	3.38	0.05	244.1	2689.5	3538.5	23.99	246.3	2713.8	3234.9	16.11	246.7	2718.8	3241.0	16.11
2.00	4.80	0.20	2.75	0.05	207.3	2284.9	2879.0	20.63	209.2	2305.5	2632.0	12.40	209.6	2309.8	2636.9	12.41
1.50	4.75	0.20	2.65	0.05	205.2	2261.1	2774.3	18.50	207.0	2281.5	2536.3	10.05	207.4	2285.7	2541.0	10.05
1.00	3.90	0.20	2.15	0.05	168.5	1856.5	2250.8	17.52	170.0	1873.2	2057.7	8.97	170.3	1876.7	2061.6	8.97
0.50	2.15	0.20	1.19	0.05	92.9	1023.5	1245.8	17.85	93.7	1032.7	1138.9	9.33	93.9	1034.6	1141.1	9.33

AVERAGE PX=19.70 AVERAGE C%=11.37 AVERAGE F%=11.37

TEST NUMBER 48

5KG(F) F SIERRA

EBAR =0.500

H	AED	ASF	LCD	LSF	PA	PMA	PFLC	P%	CA	CMA	CFLC	C%	FA	FMA	FFLC	F%
2.50	5.10	0.20	2.80	0.05	220.3	2427.7	2931.3	17.18	221.4	2439.9	2755.4	11.45	223.5	2462.6	2781.3	11.46
2.00	4.20	0.20	2.26	0.05	181.4	1999.3	2366.0	15.50	182.3	2009.3	2224.0	9.66	184.0	2028.0	2244.9	9.66
1.50	3.75	0.20	5.30	0.02	162.0	1785.1	2219.4	19.57	162.8	1794.0	2086.3	14.01	164.8	1810.7	2105.9	14.02
1.00	3.20	0.20	4.40	0.02	138.2	1523.3	1842.5	17.33	138.9	1530.9	1732.0	11.61	140.2	1545.1	1748.3	11.62
0.50	1.75	0.20	1.00	0.05	75.6	833.0	1046.9	20.43	76.0	837.2	984.1	14.93	76.7	845.0	993.3	14.93

AVERAGE P%=18.00 AVERAGE C%=12.33 AVERAGE F%=12.34

TEST NUMBER 49

5KG(F) F CSA-P-L

EBAR =0.480

H	AED	ASF	LCD	LSF	PA	PMA	PFLC	PX	CA	CMA	CFLC	CX	FA	FMA	FFLC	FX
2.50	5.63	0.20	3.70	0.05	243.2	2680.0	3873.5	30.81	244.4	2692.9	3650.4	26.23	246.7	2718.9	3686.1	26.24
2.00	4.90	0.20	2.95	0.05	211.7	2332.5	3088.4	24.47	212.7	2343.7	2910.5	19.47	214.7	2366.4	2938.9	19.48
1.50	4.20	0.20	2.86	0.05	181.4	1999.3	2994.1	33.23	182.3	2008.9	2821.7	28.80	184.1	2028.3	2849.3	28.81
1.00	3.65	0.20	2.35	0.05	157.7	1737.5	2460.2	29.38	158.4	1745.8	2318.5	24.70	160.0	1762.7	2341.2	24.71
0.50	2.19	0.20	1.58	0.05	94.6	1042.5	1654.1	36.98	95.1	1047.5	1558.8	32.80	96.0	1057.6	1574.1	32.81

AVERAGE PX=30.97

AVERAGE CX=26.40

AVERAGE FX=26.41

TEST NUMBER 50

5KG(F) F CSA-W-L-B

EBAR =0.110

H	AED	ASF	LCD	LSF	PA	PMA	PFLC	P%	CA	CMA	CFLC	C%	FA	FMA	FFLC	F%
2.50	5.90	0.20	3.55	0.05	254.9	2808.6	3716 5	24.43	255.1	2811·6	3667.4	23.34	259.4	2858.2	3728.8	23.35
2.00	4.05	0.20	3.10	0.05	174.9	1927.9	3245.4	40.60	175.1	1930.0	3202.6	39.73	178.0	1962.0	3256.1	39.75
1.50	3.90	0.20	1.92	0.05	168.5	1856.8	2010.0	7.64	168.7	1858.5	1983.5	6.30	171.4	1889.3	2016.7	6.32
1.00	3.35	0.20	1.85	0.05	144.7	1594.7	1936.8	17.66	144.9	1596.4	1911.2	16.47	147.3	1622.9	1943.2	16.48
0.50	1.61	0.20	0.80	0.05	69.5	766.4	837.5	8.49	69.6	767.2	826.5	7.17	70.8	779.9	840.3	7.18

AVERAGE P%=19.76

AVERAGE C%=18.60

AVERAGE F%=18.62

TEST NUMBER 51

MEP F H.S. CHECK

EBAR =0.0

H	AED	ASF	LCD	LSF	PA	PMA	PFLC	PX	CA	CMA	CFLC	CX	FA	FMA	FFLC	FX
2.00	3.75	0.50	2.25	0.10	405.0	4462.7	4711.1	5.27	405.0	4462.7	4711.1	5.27	412.5	4545.7	4799.6	5.29
2.00	3.78	0.50	2.25	0.10	408.2	4498.4	4711.1	4.51	408.2	4498.4	4711.1	4.51	415.8	4582.1	4799.6	4.53
							AVERAGE PX=	4.89			AVERAGE CX=	4.89			AVERAGE FX=	4.91

TEST NUMBER 52

MEP F FLAT PLATE CHECK

EBAR =0.0

H	AED	ASF	LCD	LSF	PA	PMA	PFLC	PX	CA	CMA	CFLC	C%	FA	FMA	FFLC	F%
2.00	5.30	1.00	3.10	0.20	1144.7	12614.7	12981.6	2.83	1144.7	12614.7	12981.6	2.83	1166.0	12849.3	13225.6	2.85
							AVERAGE PX=	2.83			AVERAGE C%=	2.83			AVERAGE F%=	2.85

TEST NUMBER 53

5KG(F) F Z90.1

EBAR =0.0

H	AED	ASF	LCD	LSF	PA	PMA	PFLC	P%	CA	CMA	CFLC	C%	FA	FMA	FFLC	F%
2.00	1.85	0.50	0.55	0.20	199.8	2201.6	2303.2	4.41	199.8	2201.6	2303.2	4.41	203.5	2242.6	2346.5	4.43
							AVERAGE P%=	4.41			AVERAGE C%=	4.41			AVERAGE F%=	4.43

TEST NUMBER 54

5KG(F) F Z90.1

EBAR =0.0

H	AED	ASF	LCD	LSF	PA	PMA	PFLC	PX	CA	CMA	CFLC	CX	FA	FMA	FFLC	FX
2.00	4.85	0.20	2.10	0.05	209.5	2308.7	2198.5	-5.01	209.5	2308.7	2198.5	-5.01	213.4	2351.7	2239.8	-4.99
							AVERAGE PX=	5.01			AVERAGE CX=	5.01			AVERAGE FX=	4.99

TEST NUMBER 55

5KG(F) F CADAVER 1 WITH HELMET

EEBAR=0.770
EBAR =1.550

H	AED	ASF	LCD	LSF	PA	PMA	PFLC	P%	CA	CMA	CFLC	C%	FA	FMA	FFLC	F%
2.50	4.80	0.20	2.45	0.05	207.3	2284.9	2564.9	10.92	208.9	2302.5	2365.5	2.66	218.1	2403.8	2549.5	5.71
2.00	4.20	0.20	2.20	0.05	181.4	1999.3	2303.2	13.19	182.8	2014.7	2124.1	5.15	190.9	2103.3	2289.3	8.12
1.50	3.62	0.20	1.85	0.05	156.4	1723.2	1936.8	11.03	157.6	1736.5	1786.2	2.78	164.5	1812.9	1925.1	5.83
1.00	3.10	0.20	1.40	0.05	133.9	1475.7	1465.7	-0.68	134.9	1487.0	1351.7	-10.01	140.9	1552.5	1456.9	-6.56
0.50	1.95	0.20	0.84	0.05	84.2	928.3	879.4	-5.56	84.9	935.4	811.0	-15.33	88.6	976.6	874.1	-11.72
							AVERAGE P%= 8.27				AVERAGE C%= 7.19				AVERAGE F%= 7.59	

TEST NUMBER 56

5KG(MEP) F CADAVER 1 WITH OUT HELMET

EEBAR=0.500
EBAR =1.000

H	AED	ASF	LCD	LSF	PA	PMA	PFLC	PX	CA	CMA	CFLC	CX	FA	FMA	FFLC	FX
1.50	2.90	0.50	1.90	0.10	313.2	3451.2	3978.2	13.25	314.7	3468.4	3739.5	7.25	314.7	3468.4	3739.5	7.25
1.00	6.05	0.20	2.95	0.05	261.3	2880.0	3088.4	6.75	262.6	2894.4	2903.1	0.30	262.6	2894.4	2903.1	0.30
0.50	3.90	0.20	1.95	0.05	168.5	1856.5	2041.5	9.06	169.3	1865.8	1919.0	2.77	169.3	1865.8	1919.0	2.77
							AVERAGE PX=	9.69			AVERAGE CX=	3.44			AVERAGE FX=	3.44

TEST NUMBER 57

MFP F FLAT PLATE CHECK

EBAR =0.0

H	AED	ASF	LCD	LSF	PA	PMA	PFLC	PX	CA	CMA	CFLC	CX	FA	FMA	FFLC	FX
2.00	5.35	1.00	3.10	0.20	1155.5	12733.7	12981.6	1.91	1155.5	12733.7	12981.6	1.91	1177.0	12970.5	13225.6	1.93
							AVERAGE PX=	1.91			AVERAGE CX=	1.91			AVERAGE FX=	1.93

TEST NUMBER 58

5KG(F) F CADAVER 2 WITH HELMET

EEBAR=0.625
EBAR =1.250

H	AED	ASF	LCD	LSF	PA	PMA	PFLC	PX	CA	CMA	CFLC	CX	FA	FMA	FFLC	FX
2.50	4.25	0.20	2.60	0.05	183.6	2023.1	2721.9	25.67	184.7	2035.8	2534.8	19.69	188.1	2072.4	2616.2	20.79
2.00	3.94	0.20	1.92	0.05	170.2	1875.5	2010.0	6.69	171.3	1887.3	1871.9	-0.82	174.3	1921.2	1931.9	0.55
1.50	3.35	0.20	1.50	0.05	144.7	1594.7	1570.4	-1.55	145.6	1604.7	1462.4	-9.73	148.2	1633.5	1509.3	-8.23
1.00	2.83	0.20	1.30	0.05	122.2	1347.2	1361.0	1.02	123.0	1355.6	1267.4	-6.96	125.2	1380.0	1308.1	-5.50
0.50	1.85	0.20	1.00	0.05	79.9	880.6	1046.9	15.88	80.4	886.2	974.9	9.11	81.9	902.1	1006.2	10.35

AVERAGE PX=10.16 AVERAGE CX= 9.26 AVERAGE FX= 9.08

TEST NUMBER 59

5KG(F) F CADAVER 2 WITH OUT HELMET

EBAR =1.250

H	AED	ASF	LCD	LSF	PA	PMA	PFLC	P%	CA	CMA	CFLC	C%	FA	FMA	FFLC	F%
0.30	4.00	0.10	3.25	0.02	86.4	952.1	1361.0	30.05	89.1	981.6	1214.7	19.19	90.7	999.2	1253.7	20.29
0.15	3.00	0.10	2.40	0.02	64.8	714.0	1005.0	28.95	66.8	736.2	897.0	17.93	68.0	749.4	925.8	19.05

AVERAGE P%=29.50 AVERAGE C%=18.56 AVERAGE F%=19.67

TEST NUMBER 60

MEP F SIERRA OCCIPITAL

EBAR =0.0

H	AED	ASF	LCD	LSF	PA	PMA	PFLC	PX
2.25	1.50	1.00	2.68	0.10	324.0	3570.2	5611.4	36.38
2.00	1.41	1.00	2.61	0.10	304.5	3356.0	5464.8	38.59
1.75	2.58	0.50	2.30	0.10	278.6	3070.4	4815.7	36.24
1.50	2.32	0.50	2.00	0.10	250.5	2760.9	4187.6	34.07
1.00	1.75	0.50	1.30	0.10	189.0	2082.6	2721.9	23.49
0.50	1.10	0.50	0.68	0.10	118.8	1309.1	1423.8	8.06

AVERAGE PX=29.47

TEST NUMBER 61

MEP F SIERRA PARIETAL RS

EBAR =0.0

H	AED	ASF	LCD	LSF	PA	PMA	PFLC	P%
2.25	3.40	0.50	3.00	0.10	367.2	4046.2	6281.4	35.58
2.00	3.10	0.50	2.85	0.10	334.8	3689.2	5967.3	38.18
1.50	2.60	0.50	2.20	0.10	280.8	3094.2	4606.4	32.83
1.00	2.00	0.50	1.50	0.10	216.0	2380.1	3140.7	24.22
0.50	1.25	0.50	0.75	0.10	135.0	1487.6	1570.4	5.27

AVERAGE P%=27.22

TEST NUMBER 62

MEP F SIBPA PARIETAL LS

EBAR =0.0

H	AED	ASF	LCD	LSF	PA	PMA	PFLC	P%
2.25	3.50	0.50	2.91	0.10	378.0	4165.2	6093.0	31.64
2.00	3.18	0.50	2.86	0.10	343.4	3784.4	5988.3	36.80
1.50	2.60	0.50	2.18	0.10	280.8	3094.2	4564.5	32.21
1.00	2.00	0.50	1.40	0.10	216.0	2380.1	2931.3	18.80
0.50	1.28	0.50	0.83	0.10	138.2	1523.3	1737.9	12.35

AVERAGE P%=26.36

TEST NUMBER 63

MEP F SIERRA FRONTAL

EBAR =0.0

H	AED	ASF	LCD	LSF	PA	PMA	PFLC	P%
2.25	3.25	0.50	2.30	0.10	351.0	3867.7	4815.7	19.69
2.00	3.00	0.50	2.25	0.10	324.0	3570.2	4711.1	24.22
1.50	2.50	0.50	1.92	0.10	270.0	2975.2	4020.1	25.99
1.00	1.91	0.50	1.49	0.10	206.3	2273.0	3119.8	27.14
0.50	1.20	0.50	0.97	0.10	129.6	1428.1	2031.0	29.69

AVERAGE P%=25.34

TEST NUMBER 64

MEP F CSA-P-L FRONTAL

FBAR =0.0

H	AED	ASF	LCD	LSF	PA	PMA	PFLC	PX
2.25	3.92	0.50	2.52	0.10	423.3	4665.1	5276.4	11.59
2.00	3.60	0.50	2.30	0.10	388.8	4284.2	4815.7	11.04
1.50	2.92	0.50	1.68	0.10	315.3	3475.0	3517.6	1.21
1.00	2.21	0.50	1.25	0.10	238.7	2630.0	2617.3	-0.49
0.50	1.43	0.50	0.82	0.10	154.4	1701.8	1716.9	0.88

AVERAGE PX= 5.04

TEST NUMBER 65

MEP F CSA-P-L OCCIPTAL

FBAR =0.0

H	AED	ASF	LCD	LSF	PA	PMA'	PFLC	PX
2.25	3.30	0.50	2.65	0.10	356.4	3927.2	5548.6	29.22
2.00	3.00	0.50	2.41	0.10	324.0	3570.2	5046.1	29.25
1.50	2.50	0.50	1.90	0.10	270.0	2975.2	3978.2	25.21
1.00	1.80	0.50	1.33	0.10	194.4	2142.1	2784.8	23.08
0.50	1.18	0.50	0.59	0.10	127.4	1404.3	1235.3	-13.67

AVERAGE PX=24.09

TEST NUMBER 66

MEP F CSA-P-L PARIETAL RS

EBAR =0.0

H	AED	ASF	LCD	LSF	PA	PMA	PFLC	PX
2.25	4.00	0.50	2.90	0.10	432.0	4760.3	6072.0	21.60
2.25	4.00	0.50	2.90	0.10	432.0	4760.3	6072.0	21.60
2.25	4.00	0.50	2.95	0.10	432.0	4760.3	6176.7	22.93
2.25	4.00	0.50	3.00	0.10	432.0	4760.3	6281.4	24.22
2.25	4.15	0.50	3.00	0.10	448.2	4938.8	6281.4	21.37
2.25	4.60	0.50	4.20	0.10	496.8	5474.3	8794.0	37.75
2.25	4.00	0.50	3.00	0.10	432.0	4760.3	6281.4	24.22

AVERAGE PX=24.81

TEST NUMBER 671

MEP ,F EBAR PLATE

FBAR =0.0

H	AED	ASF	LCO	LSF	PA	PMA	PFLC	P%	CA	CMA	CFLC	C%	FA	FMA	FFLC	F%
1.50	4.27	1.00	5.02	0.10	922.2	10163.1	10510.9	3.31	922.2	10163.1	10510.9	3.31	939.4	10352.2	10708.5	3.33
							AVERAGE P%=	3.31			AVERAGE C%=	3.31			AVERAGE F%=	3.33

TEST NUMBER 672

MEP F EBAR PLATE

EBAR =0.500

H	AED	ASF	LCD	LSF	PA	PMA	PFLC	PX	CA	CMA	CFLC	CX	FA	FMA	FFLC	FX
1.50	4.27	1.00	5.07	0.10	922.2	10163.1	10615.6	4.26	926.9	10214.0	9978.6	-2.36	935.5	10308.9	10072.4	-2.35
							AVERAGE PX=	4.26			AVERAGE CX=	2.36			AVERAGE FX=	2.35

TEST NUMBER 673

MEP F EBAR PLATE

EBAR =1.000

H	AED	ASF	LCD	LSF	PA	PMA	PFLC	P%	CA	CMA	CFLC	C%	FA	FMA	FFLC	F%
1.50	4.25	1.00	5.10	0.10	917.9	10115.5	10678.4	5.27	927.1	10216.7	9696.0	-5.37	927.1	10216.7	9696.0	-5.37

AVERAGE P%= 5.27

AVERAGE C%= 5.37

AVERAGE F%= 5.37

TEST NUMBER 674

MEP F EBAR PLATE

EBAR =1.500

H	AED	ASF	LCD	LSF	PA	PMA	PFLC	P%	CA	CMA	CFLC	C%	FA	FMA	FFLC	F%
1.50	4.10	1.00	4.90	0.10	885.5	9758.5	10259.6	4.88	931.6	10266.0	8997.7	-14.10	965.1	10635.5	9575.3	-11.07

AVERAGE P%= 4.88

AVERAGE C%=14.10

AVERAGE F%=11.07

TEST NUMBER 675

MFP. F EBAR PLATE

EBAR =0.0

H	AED	ASF	LCD	LSF	PA	PMA	PFLC	P%	CA	CMA	CFLC	C%	FA	FMA	FFLC	F%
1.50	4.25	1.00	5.01	0.10	917.9	10115.5	10489.9	3.57	917.9	10115.5	10489.9	3.57	935.0	10303.7	10687.2	3.59
							AVERAGE P%=	3.57			AVERAGE C%=	3.57			AVERAGE F%=	3.59

TEST NUMBER 68

5KG(F) F MINING HELMETS

EBAR =0.0

H	AED	ASF	LCD	LSF	PA	PMA	PFLC	P%	CA	CMA	CFLC	C%	FA	FMA	FFLC	F%
1.11	1.65	0.20	1.80	0.05	71.3	785.4	1884.4	58.32	71.3	785.4	1884.4	58.32	72.6	800.1	1919.8	58.33
1:11	1.65	0.20	1.90	0.05	71.3	785.4	1989.1	60.51	71.3	785.4	1989.1	60.51	72.6	800.1	2026.5	60.52
2.00	3.00	0.50	2.00	0.10	324.0	3570.2	4187.6	14.74	324.0	3570.2	4187.6	14.74	330.0	3636.6	4266.3	14.76
							AVERAGE P%=44.53				AVERAGE C%=44.53				AVERAGE F%=44.54	

TEST NUMBER 69

ICLB(F) F MINING HELMETS

EBAR =0.0

H	AED	ASF	LCD	LSF	PA	PMA	PFLC	P%	CA	CMA	CFLC	C%	FA	FMA	FFLC	F%
1.52	0.90	1.00	1.00	0.10	194.4	1943.8	2093.8	7.16	194.4	1943.8	2093.8	7.16	198.0	1980.0	2133.2	7.18
1.52	0.60	1.00	0.80	0.10	129.6	1295.9	1675.0	22.63	129.6	1295.9	1675.0	22.63	132.0	1320.0	1706.5	22.65
1.52	0.60	1.00	0.80	0.10	129.6	1295.9	1675.0	22.63	129.6	1295.9	1675.0	22.63	132.0	1320.0	1706.5	22.65
1.22	2.00	0.20	2.20	0.02	86.4	863.9	921.3	6.22	86.4	863.9	921.3	6.22	88.0	880.0	938.6	6.24
1.22	2.00	0.20	2.20	0.02	86.4	863.9	921.3	6.22	86.4	863.9	921.3	6.22	88.0	880.0	938.6	6.24
1.22	1.40	0.20	1.80	0.02	60.5	604.8	753.8	19.77	60.5	604.8	753.8	19.77	61.6	616.0	767.9	19.79
1.22	1.40	0.20	1.80	0.02	60.5	604.8	753.8	19.77	60.5	604.8	753.8	19.77	61.6	616.0	767.9	19.79
1.22	2.70	0.20	2.45	0.02	116.6	1166.3	1026.0	-13.68	116.6	1166.3	1026.0	-13.68	118.8	1188.0	1045.3	-13.66
1.22	2.70	0.20	2.45	0.02	116.6	1166.3	1026.0	-13.68	116.6	1166.3	1026.0	-13.68	118.8	1188.0	1045.3	-13.66
1.22	1.75	0.20	1.95	0.02	75.6	755.9	816.6	7.43	75.6	755.9	816.6	7.43	77.0	770.0	831.9	7.44
1.22	1.75	0.20	1.95	0.02	75.6	755.9	816.6	7.43	75.6	755.9	816.6	7.43	77.0	770.0	831.9	7.44
1.22	1.70	0.20	1.80	0.02	73.4	734.3	753.8	2.58	73.4	734.3	753.8	2.58	74.8	748.0	767.9	2.60
1.22	1.70	0.20	1.80	0.02	73.4	734.3	753.8	2.58	73.4	734.3	753.8	2.58	74.8	748.0	767.9	2.60

AVERAGE P%=11.68 AVERAGE C%=11.68 AVERAGE F%=11.69

TEST NUMBER 70

MEP F CSA-P-L PARIETAL LS

EBAR =0.0

H	AED	ASF	LCD	LSF	PA	PMA	PFLC	PX
2.25	4.00	0.50	2.93	0.10	432.0	4760.3	6134.8	22.41
2.00	3.65	0.50	2.70	0.10	394.2	4343.7	5653.3	23.16
1.50	3.00	0.50	2.15	0.10	324.0	3570.2	4501.7	20.69
1.00	2.21	0.50	1.48	0.10	238.7	2630.0	3098.8	15.13
0.50	1.38	0.50	0.70	0.10	149.0	1642.3	1465.7	-12.05

AVERAGE PX=18.69

TEST NUMBER 71

MEP F CSA-P-L PARIETAL RS

EBAR =0.0

H	AED	ASF	LCD	LSF	PA	PMA	PFLC	PX
2.25	4.00	0.50	3.00	0.10	432.0	4760.3	6281.4	24.22
2.00	3.63	0.50	2.75	0.10	392.0	4319.9	5758.0	24.97
1.50	2.95	0.50	2.23	0.10	318.6	3510.7	4669.2	24.81
1.00	2.20	0.50	1.60	0.10	237.6	2618.1	3350.1	21.85
0.50	1.35	0.50	0.82	0.10	145.8	1606.6	1716.9	6.43

AVERAGE PX=20.46

TEST NUMBER 72

5KG(F) F CSA-P-L PARIETAL LS

EBAR =0.0

H	AED	ASF	LCD	LSF	PA	PMA	PFLC	P%
2.25	3.80	0.20	2.50	0.05	164.1	1808.9	2617.3	30.89
2.00	3.60	0.20	2.25	0.05	155.5	1713.7	2355.5	27.25
1.50	2.70	0.20	1.60	0.05	116.6	1285.3	1675.0	23.27
1.00	2.30	0.20	1.20	0.05	99.4	1094.9	1256.3	12.85
0.50	1.60	0.20	0.90	0.05	69.1	761.6	942.2	19.16

AVERAGE P%=22.68

TEST NUMBER 73

5KG(F) F CADAVER 3 FRONTAL WITH HELMET

EBAR =0.0

H	AED	ASF	LCD	LSF	PA	PMA	PFLC	PX
0.50	1.40	0.20	0.74	0.05	60.5	666.4	774.7	13.98

AVERAGE PX=13.98

TEST NUMBER 75

5KG(SNELL H.F.) F MEP (SNELL)

EBAR =0.0

H	AED	ASF	LCD	LSF	PA	PMA	PFLC	PX	CA	CMA	CFLC	CX	FA	FMA	FFLC	FX
0.25	1.60	0.50	5.16	0.02	172.8	1904.1	2160.8	11.88	172.8	1904.1	2160.8	11.88	176.0	1939.5	2201.4	11.90
0.25	1.60	0.50	5.16	0.02	172.8	1904.1	2160.8	11.88	172.8	1904.1	2160.8	11.88	176.0	1939.5	2201.4	11.90
0.25	1.60	0.50	5.16	0.02	172.8	1904.1	2160.8	11.88	172.8	1904.1	2160.8	11.88	176.0	1939.5	2201.4	11.90
0.19	1.39	0.50	3.98	0.02	150.1	1654.2	1666.7	0.75	150.1	1654.2	1666.7	0.75	152.9	1685.0	1698.0	0.77
0.19	1.39	0.50	3.98	0.02	150.1	1654.2	1666.7	0.75	150.1	1654.2	1666.7	0.75	152.9	1685.0	1698.0	0.77
0.19	1.39	0.50	3.98	0.02	150.1	1654.2	1666.7	0.75	150.1	1654.2	1666.7	0.75	152.9	1685.0	1698.0	0.77
0.13	0.65	0.50	0.90	0.05	70.2	773.5	942.2	17.90	70.2	773.5	942.2	17.90	71.5	787.9	959.9	17.92
0.38	2.36	0.50	2.85	0.05	254.9	2808.6	2983.7	5.87	254.9	2808.6	2983.7	5.87	259.6	2860.8	3039.8	5.89
0.38	2.36	0.50	2.85	0.05	254.9	2808.6	2983.7	5.87	254.9	2808.6	2983.7	5.87	259.6	2860.8	3039.8	5.89
0.38	2.38	0.50	2.92	0.05	257.0	2832.4	3057.0	7.35	257.0	2832.4	3057.0	7.35	261.8	2885.0	3114.4	7.37
0.51	3.07	0.50	3.73	0.05	331.5	3653.5	3904.9	6.44	331.5	3653.5	3904.9	6.44	337.7	3721.5	3978.4	6.46
0.51	3.05	0.50	3.73	0.05	329.4	3629.7	3904.9	7.05	329.4	3629.7	3904.9	7.05	335.5	3697.2	3978.4	7.07
0.51	3.05	0.50	3.73	0.05	329.4	3629.7	3904.9	7.05	329.4	3629.7	3904.9	7.05	335.5	3697.2	3978.4	7.07
0.64	3.63	0.50	4.40	0.05	392.0	4319.9	4606.4	6.22	392.0	4319.9	4606.4	6.22	399.3	4400.3	4693.0	6.24
0.64	3.62	0.50	4.50	0.05	390.9	4308.0	4711.1	8.55	390.9	4308.0	4711.1	8.55	398.2	4388.2	4799.6	8.57
0.64	3.80	0.50	4.75	0.05	410.4	4522.2	4972.8	9.06	410.4	4522.2	4972.8	9.06	418.0	4606.4	5066.3	9.08
0.64	3.80	0.50	4.80	0.05	410.4	4522.2	5025.1	10.01	410.4	4522.2	5025.1	10.01	418.0	4606.4	5119.6	10.02

AVERAGE PX= 7.60 AVERAGE CX= 7.60 AVERAGE FX= 7.62

TEST NUMBER 76
SKG(F) F MEP(SNELL)
EBAR =0.0

H	AED	ASF	LCD	LSF	PA	PMA	PFLC	P%	CA	CMA	CFLC	C%	FA	FMA	FFLC	F%
2.00	4.95	1.00	2.95	0.20	1069.1	11781.6	12353.4	4.63	1069.1	11781.6	12353.4	4.63	1089.0	12000.8	12585.7	4.65
1.50	4.00	1.00	4.80	0.10	863.9	9520.5	10050.3	5.27	863.9	9520.5	10050.3	5.27	880.0	9697.6	10239.2	5.29
1.00	2.90	1.00	3.41	0.10	626.3	6902.4	7139.9	3.33	626.3	6902.4	7139.9	3.33	638.0	7030.8	7274.1	3.35
0.50	1.58	1.00	1.90	0.10	341.3	3760.6	3978.2	5.47	341.3	3760.6	3978.2	5.47	347.6	3830.6	4053.0	5.49
							AVERAGE P%=	4.67			AVERAGE C%=	4.67			AVERAGE F%=	4.69

TEST NUMBER 77

10LB(F) F MEP(SNELL)

EBAR =0.0

H	AED	ASF	LCD	LSF	PA	PMA	PFLC	P%	CA	CMA	CFLC	C%	FA	FMA	FFLC	F%
2.00	4.85	1.00	5.50	0.10	1047.5	10475.2	11515.9	9.04	1047.5	10475.2	11515.9	9.04	1067.0	10670.0	11732.4	9.06
1.50	4.00	1.00	4.50	0.10	863.9	8639.3	9422.1	8.31	863.9	8639.3	9422.1	8.31	880.0	8800.0	9599.2	8.33
1.00	2.90	1.00	3.20	0.10	626.3	6263.5	6700.2	6.52	626.3	6263.5	6700.2	6.52	638.0	6380.0	6826.1	6.54
0.50	1.65	1.00	1.79	0.10	356.4	3563.7	3747.9	4.91	356.4	3563.7	3747.9	4.91	363.0	3630.0	3818.4	4.93

AVERAGE P%= 7.19 AVERAGE C%= 7.19 AVERAGE F%= 7.21

TEST NUMBER 78

MEP F EBAR PLATE

EBAR =0.0

H	AED	ASF	LCD	LSF	PA	PMA	PFLC	PX	CA	CMA	CFLC	CX	FA	FMA	FFLC	FX
2.00	5.20	1.00	6.20	0.10	1123.1	12376.7	12981.6	4.66	1123.1	12376.7	12981.6	4.66	1144.0	12606.9	13225.6	4.68
1.50	4.17	1.00	5.00	0.10	900.6	9925.1	10469.0	5.20	900.6	9925.1	10469.0	5.20	917.4	10109.7	10665.8	5.21
1.00	2.95	1.00	3.58	0.10	637.1	7021.4	7495.8	6.33	637.1	7021.4	7495.8	6.33	649.0	7152.0	7636.7	6.35
0.50	1.70	1.00	2.08	0.10	367.2	4046.2	4355.1	7.09	367.2	4046.2	4355.1	7.09	374.0	4121.5	4437.0	7.11
							AVERAGE PX= 5.82				AVERAGE CX= 5.92				AVERAGE FX= 5.84	

TEST NUMBER 79

MEP F EBAR PLATE

EBAR =0.0

H	AED	ASF	LCD	LSF	PA	PMA	PFLC	P%	CA	CMA	CFLC	C%	FA	FMA	FFLC	F%
2.00	5.10	1.00	3.10	0.20	1101.5	12138.7	12981.6	6.49	1101.5	12138.7	12981.6	6.49	1122.0	12364.4	13225.6	6.51
1.50	4.17	1.00	5.00	0.10	900.6	9925.1	10469.0	5.20	900.6	9925.1	10469.0	5.20	917.4	10109.7	10665.8	5.21
1.00	2.95	1.00	3.64	0.10	637.1	7021.4	7621.4	7.87	637.1	7021.4	7621.4	7.87	649.0	7152.0	7764.7	7.89
0.50	1.70	1.00	2.18	0.10	367.2	4046.2	4564.5	11.35	367.2	4046.2	4564.5	11.35	374.0	4121.5	4650.3	11.37
							AVERAGE P%=	7.73			AVERAGE C%=	7.73			AVERAGE F%=	7.75

TEST NUMBER 80

MEP F EBAR PLATE

EBAR =0.500

H	AED	ASF	LCD	LSF	PA	PMA	PFLC	P%	CA	CMA	CFLC	C%	FA	FMA	FFLC	F%
2.00	5.10	1.00	3.10	0.20	1101.5	12138.7	12981.6	6.49	1107.0	12199.3	12202.7	0.03	1117.3	12312.8	12317.4	0.04
1.50	4.20	1.00	5.13	0.10	907.1	9996.5	10741.2	6.93	911.7	10046.5	10096.7	0.50	920.1	10140.0	10191.6	0.51
1.00	2.95	1.00	3.66	0.10	637.1	7021.4	7663.3	8.38	640.3	7056.5	7203.5	2.04	646.3	7122.1	7271.2	2.05
0.50	1.70	1.00	2.18	0.10	367.2	4046.2	4564.5	11.35	369.0	4066.4	4290.6	5.22	372.4	4104.3	4330.9	5.23

AVERAGE P%= 8.29 AVERAGE C%= 1.95 AVERAGE F%= 1.96

TEST NUMBER 81

MEP F EBAR PLATE

EBAR =1.000

H	AED	ASF	LCD	LSF	PA	PMA	PFLC	P%	CA	CMA	CFLC	C%	FA	FMA	FFLC	F%
2.00	5.18	1.00	3.18	0.20	1118.8	12329.1	13316.6	7.42	1130.0	12452.4	12091.5	-2.98	1130.0	12452.4	12091.5	-2.98
1.50	4.20	1.00	5.10	0.10	907.1	9996.5	10678.4	6.39	916.2	10096.5	9696.0	-4.13	916.2	10096.5	9696.0	-4.13
1.00	2.98	1.00	3.68	0.10	643.6	7092.8	7705.2	7.95	650.1	7163.7	6996.3	-2.39	650.1	7163.7	6996.3	-2.39
0.50	1.70	1.00	2.14	0.10	367.2	4046.2	4480.7	9.70	370.8	4086.7	4068.5	-0.45	370.8	4086.7	4068.5	-0.45

AVERAGE P%= 7.86 AVERAGE C%= 2.49 AVERAGE F%= 2.49

TEST NUMBER 82
MEP F EBAR PLATE
EBAR =1.500

H	AED	ASF	LCD	LSF	PA	PMA	PFLC	PX	CA	CMA	CFLC	CX	FA	FMA	FFLC	FX
2.00	5.00	1.00	5.90	0.10	1079.9	11900.6	12353.4	3.67	1136.1	12519.5	10834.0	-15.56	1177.0	12970.2	11529.5	-12.50
1.50	4.10	1.00	4.88	0.10	885.5	9758.5	10217.8	4.49	931.6	10266.0	8961.0	-14.56	965.1	10635.5	9536.3	-11.53
1.00	2.90	1.00	3.59	0.10	626.3	6902.4	7516.8	8.17	658.9	7261.3	6592.2	-10.15	682.6	7522.7	7015.4	-7.23
0.50	1.70	1.00	2.13	0.10	367.2	4046.2	4459.8	9.27	386.3	4256.6	3911.2	-8.83	400.2	4409.9	4162.3	-5.95
							AVERAGE PX=	6.40			AVERAGE CX=	12.28			AVERAGE FX=	9.30

'TEST NUMBER 83
MEP F EBAR PLATE
EBAR =1.750

H	AED	ASF	LCD	LSF	PA	PMA	PFLC	P%	CA	CMA	CFLC	C%	FA	FMA	FFLC	F%
2.00	4.80	1.00	5.50	0.10	1036.7	11424.6	11515.9	0.79	1112.4	12258.6	9921.0	-23.56	1196.9	13190.3	11231.5	-17.44
1.50	3.92	1.00	4.55	0.10	846.7	9330.1	9526.8	2.06	908.5	10011.2	8207.3	-21.98	977.5	10772.0	9291.5	-15.93
1.00	2.80	1.00	3.45	0.10	604.8	6664.4	7223.6	7.74	648.9	7150.9	6223.1	-14.91	698.2	7694.3	7045.2	-9.21
0.50	1.65	1.00	2.09	0.10	356.4	3927.2	4376.0	10.26	382.4	4213.9	3770.0	-11.78	411.4	4534.1	4268.0	-6.24
							AVERAGE P%= 5.21				AVERAGE C%=18.06				AVERAGE F%=12.21	

TEST NUMBER 84

MEP F EBAR PLATE

EBAR =1.500

H	AED	ASF	LCD	LSF	PA	PMA	PFLC	P%	CA	CMA	CFLC	C%	FA	FMA	FFLC	F%
2.00	5.00	1.00	5.83	0.10	1079.9	11900.6	12206.9	2.51	1136.1	12519.5	10705.4	-16.95	1177.0	12970.2	11392.7	-13.85
2.00	5.00	1.00	5.83	0.10	1079.9	11900.6	12206.9	2.51	1136.1	12519.5	10705.4	-16.95	1177.0	12970.2	11392.7	-13.85
2.00	5.00	1.00	5.90	0.10	1079.9	11900.6	12353.4	3.67	1136.1	12519.5	10834.0	-15.56	1177.0	12970.2	11529.5	-12.50
2.00	5.00	1.00	5.83	0.10	1079.9	11900.6	12206.9	2.51	1136.1	12519.5	10705.4	-16.95	1177.0	12970.2	11392.7	-13.85
							AVERAGE P%= 2.80				AVERAGE C%=16.60				AVERAGE F%=13.51	

TEST NUMBER 85

MEP F SP-W-H: F.

EBAR =0.0

H	AED	ASF	LCD	LSF	PA	PMA	PFLC	P%	CA	CMA	CFLC	C%	FA	FMA	FFLC	F%
2.00	4.82	0.50	2.75	0.10	520.5	5736.1	5758.0	0.38	520.5	5736.1	5758.0	0.38	530.2	5842.8	5866.2	0.40
1.50	3.88	0.50	2.25	0.10	419.0	4617.4	4711.1	1.99	419.0	4617.4	4711.1	1.99	426.8	4703.3	4799.6	2.01
1.00	2.89	0.50	1.70	0.10	312.1	3439.3	3559.5	3.38	312.1	3439.3	3559.5	3.38	317.9	3503.3	3626.4	3.40
0.50	1.75	0.50	1.11	0.10	189.0	2082.6	2324.1	10.39	189.0	2082.6	2324.1	10.39	192.5	2121.3	2367.8	10.41

AVERAGE P%= 4.03 AVERAGE C%= 4.03 AVERAGE F%= 4.05

TEST NUMBER 86

MEP F SP-W-H.F.

EBAR =0.0

H	AED	ASF	LED	LSF	PA	PMA	PFLC	PX	CA	CMA	CFLC	CX	FA	FMA	FFLC	FX
2.00	4.60	0.50	2.40	0.10	496.8	5474.3	5025.1	-8.94	496.8	5474.3	5025.1	-8.94	506.0	5576.1	5119.6	-8.92
1.50	3.66	0.50	1.90	0.10	395.2	4355.6	3978.2	-9.49	395.2	4355.6	3978.2	-9.49	402.6	4436.6	4053.0	-9.47
1.00	2.78	0.50	1.58	0.10	300.2	3308.4	3308.2	-0.01	300.2	3308.4	3308.2	-0.01	305.8	3369.9	3370.4	0.01
0.50	1.50	0.50	0.90	0.10	162.0	1785.1	1884.4	5.27	162.0	1785.1	1884.4	5.27	165.0	1818.3	1919.8	5.29

AVERAGE PX= 5.93 AVERAGE CX= 5.93 AVERAGE FX= 5.92

TEST NUMBER 87

MEP F SP-W-H.Fe -

EBAR =0.500

H	AED	ASF	LCD	LSF	PA	PMA	PFLC	P%	CA	CMA	CFLC	C%	FA	FMA	FFLC	F%
2.00	4.80	0.50	2.90	0.10	518.4	5712.3	6072.0	5.92	520.9	5740.9	5707.7	-0.58	525.8	5794.3	5761.4	-0.57
1.50	3.80	0.50	2.38	0.10	410.4	4522.2	4983.2	9.25	412.4	4544.9	4684.3	2.98	-16.3	4587.1	4728.3	2.99
1.00	2.80	0.50	1.79	0.10	302.4	3332.2	3747.9	11.09	303.9	3348.8	3523.0	4.94	306.7	3380.0	3556.1	4.95
0.50	1.70	0.50	1.13	0.10	183.6	2023.1	2366.0	14.49	184.5	2033.2	2224.0	8.58	186.2	2052.1	2244.9	8.59
							AVERAGE P%=10.19				AVERAGE C%= 4.27				AVERAGE F%= 4.27	

TEST NUMBER 88

MEP F SP-W-H.F.

EBAR =1.000

H	AED	ASF	LCD	LSF	PA	PMA	PFLC	P%	CA	CMA	CFLC	C%	FA	FMA	FFLC	F%
2.00	4.72	0.50	2.98	0.10	509.7	5617.1	6239.5	9.98	514.8	5673.3	5665.5	-0.14	514.8	5673.3	5665.5	-0.14
1.50	3.80	0.50	2.45	0.10	410.4	4522.2	5129.8	11.84	414.5	4567.5	4657.9	1.94	414.5	4567.5	4657.9	1.94
1.00	2.81	0.50	1.80	0.10	303.5	3344.1	3768.8	11.27	306.5	3377.5	3422.1	1.30	306.5	3377.5	3422.1	1.30
0.50	1.70	0.50	1.11	0.10	183.6	2023.1	2324.1	12.95	185.4	2043.3	2110.3	3.17	185.4	2043.3	2110.3	3.17

AVERAGE P%=11.51 AVERAGE C%= 1.64 AVERAGE F%= 1.64

TEST NUMBER 69

MEP, F SP-W-H F.

FBAR =Y.500

H	AED	ASF	LCD	LSF	PA	PMA	PFLC	P%	CA	CMA	CFLC	C%	FA	FMA	FFLC	F%
2.00	4.60	0.50	2.90	0.10	496.8	5474.3	6072.0	9.84	522.6	5759.0	5325.2	-8.15	541.4	5966.3	5667.0	-5.28
1.50	3.70	0.50	2.45	0.10	399.6	4403.2	5129.8	14.16	420.3	4632.2	4498.8	-2.96	435.5	4799.0	4787.7	-0.24
1.00	2.75	0.50	1.90	0.10	297.0	3272.7	3978.2	17.74	312.4	3442.9	3488.9	1.32	323.7	3566.8	3712.9	3.93
0.50	1.68	0.50	1.15	0.10	181.4	1999.3	2407.9	16.97	190.9	2103.3	2111.7	0.40	197.7	2179.0	2247.3	3.04

AVERAGE P%=14.68 AVERAGE C%= 3.21 AVERAGE F%= 3.12

TEST NUMBER 290

5KG(F) F CADAVER 4 FRONTAL WITH HELMET

EBAR =0.40

H	AED	ASF	LCD	LSF	PA	PMA	PFLC	PX
1.50	2.70	0.20	1.95	0.05	116.6	1285.3	2041.5	37.04
1.00	2.40	0.20	1.95	0.05	103.7	1142.5	2041.5	44.04
0.50	1.60	0.20	0.90	0.05	69.1	761.6	942.2	19.16

AVERAGE PX=33.41

TEST NUMBER 91

SKG(F) F SIERRA FRONTAL

EBAR =0.0

H	AED	ASF	LCD	LSF	PA	PMA	PFLC	PX
2.00	4.20	0.20	2.20	0.05	181.4	1999.3	2303.2	13.19
1.50	3.65	0.20	-2.10	0.05	157.7	1737.5	2198.5	20.97
1.00	2.60	0.20	1.60	0.05	112.3	1237.7	1675.0	26.11
0.50	1.75	0.20	1.19	0.05	75.6	833.0	1245.8	33.13

AVERAGE PX=23.35

TEST NUMBER 92

5KG(F) F CADAVER 4 FRONTAL WITH HELMET AND REINFORCED NECK 1

EBAR =0.0

H	AED	ASF	LCD	LSF	PA	PMA	PFLCF	PX
2.00	3.13	0.20	3.58	0.05	135.2	1490.0	3747.9	60.25
1.50	2.80	0.20	1.40	0.05	121.0	1332.9	1465.7	9.06

AVERAGE PX=34.65

TEST NUMBER 93

5KG(F) F SIERRA FRONTAL

EBAR =0.0

H	AED	ASF	LCD	LSF	PA	PMA	PFLC	P%
2.00	3.65	0.20	2.10	0.05	157.7	1737.5	2198.5	20.97
1.50	3.00	0.20	1.77	0.05	129.6	1428.1	1853.0	22.93
1.00	2.63	0.20	1.62	0.05	113.6	1251.9	1696.0	26.18
0.50	1.95	0.20	1.40	0.05	84.2	928.3	1465.7	36.67

AVERAGE P%=26.69

TEST NUMBER 94

SKG(F) F CSA-P-L FRONTAL

EBAR =0.0

H	AED	ASF	LCD	LSF	PA	PMA	PFLC	P%
2.00	3.75	0.20	1.60	0.05	162.0	1785.1	1675.0	-6.57
1.50	3.38	0.20	1.44	0.05	146.0	1609.0	1507.5	-6.73
1.00	2.73	0.20	1.20	0.05	117.9	1299.6	1256.3	-3.44
0.50	2.20	0.20	1.10	0.05	95.0	1047.3	1151.6	9.06

AVERAGE P%= 6.45

TEST NUMBER 95

SKG(F) F SIERRA OCCIPITAL

FBAR =0.0

H	AED	ASF	LCD	LSF	PA	PMA	PFLC	P%
2.25	3.65	0.20	1.40	0.05	157.7	1737.5	1465.7	-18.55
2.00	3.45	0.20	1.45	0.05	149.0	1642.3	1518.0	-8.19
1.50	2.90	0.20	0.98	0.05	125.3	1380.5	1026.0	-34.55
1.00	2.45	0.20	0.95	0.05	105.8	1166.3	994.6	-17.26
0.50	1.75	0.20	0.75	0.05	75.6	833.0	785.2	-6.10

AVERAGE P%=16.93

TEST NUMBER 96

MEP F SIERRA OCCIPITAL WITH SUPPORT

EBAR =C-0

H	AED	ASF	LCD	LSF	PA	PMA	PFLC	PX
2.25	3.90	0.50	3.00	0.10	421.2	4641.3	6281.4	26.11
2.00	3.60	0.50	2.80	0.10	388.8	4284.2	5862.6	26.92
1.50	3.00	0.50	2.45	0.10	324.0	3570.2	5129.8	30.40
1.00	5.75	0.20	3.40	0.05	248.4	2737.1	3559.5	23.10
0.50	3.50	0.20	2.30	0.05	151.2	1666.1	2407.9	30.81

AVERAGE PX=27.47

TEST NUMBER 97

5KG(F) F SIERRA OCCIPITAL WITH SUPPORT

EBAR =0.0

H	AED	ASF	LCD	LSF	PA	PHA	PFLC	Px
2.25	1.65	0.50	1.20	0.10	178.2	1963.6	2512.6	21.85
2.00	4.00	0.20	2.64	0.05	172.8	1904.1	2763.8	31.11
1.50	3.40	0.20	1.95	0.05	146.9	1618.5	2041.5	20.72
1.00	2.80	0.20	1.38	0.05	121.0	1332.9	1444.7	7.74

AVERAGE Px=20.35

TEST NUMBER 98

SKG(F) F CADAVER & FRONTAL WITH OUT HELMET AND REINFORCED NECK 2

EBAR =0.0

H	AED	ASF	LCD	LSF	PA	PMA	PFLC	PX
0.46	4.90	0.20	2.10	0.05	211.7	2332.5	2198.5	-6.10
0.38	3.60	0.20	2.10	0.05	155.5	1713.7	2198.5	22.05
0.30	3.30	0.20	2.05	0.05	142.5	1570.9	2146.1	26.80
0.23	2.94	0.20	1.65	0.05	127.0	1399.5	1727.4	18.98
0.15	2.10	0.20	1.34	0.05	90.7	999.7	1402.8	28.74

AVERAGE PX=20.53

TEST NUMBER 99

SXG(F) F MEP

EBAR =0.0

H	AED	ASF	LCD	LSF	PA	PMA	PFLC	P%	CA	CMA	CFLC	C%	FA	FMA	FFLC	F%
2.50	5.90	1.00	3.80	0.20	1274.3	14042.8	15912.9	11.75	1274.3	14042.8	15912.9	11.75	1298.0	14304.0	16212.1	11.77
2.25	5.40	1.00	3.48	0.20	1166.3	12852.7	14572.9	11.80	1166.3	12852.7	14572.9	11.80	1188.0	13091.8	14846.8	11.82
2.00	5.00	1.00	3.20	0.20	1079.9	11900.6	13400.3	11.19	1079.9	11900.6	13400.3	11.19	1100.0	12122.0	13652.3	11.21
1.75	4.58	1.00	5.75	0.10	989.2	10901.0	12039.4	9.46	989.2	10901.0	12039.4	9.46	1007.6	11103.8	12265.7	9.47
1.50	4.00	1.00	5.10	0.10	863.9	9520.5	10678.4	10.84	863.9	9520.5	10678.4	10.84	880.0	9697.6	10879.1	10.86
1.25	3.50	1.00	4.39	0.10	755.9	8330.4	9191.8	9.37	755.9	8330.4	9191.8	9.37	770.0	8485.4	9364.6	9.39
1.00	2.92	1.00	3.68	0.10	630.7	6950.0	7705.2	9.80	630.7	6950.0	7705.2	9.80	642.4	7079.2	7850.0	9.82
0.75	2.36	1.00	2.95	0.10	509.7	5617.1	6176.7	9.06	509.7	5617.1	6176.7	9.06	519.2	5721.6	6292.8	9.08
0.50	1.75	1.00	2.20	0.10	378.0	4165.2	4606.4	9.58	378.0	4165.2	4606.4	9.58	385.0	4242.7	4693.0	9.59
0.25	0.96	1.00	1.34	0.10	207.3	2284.9	2805.7	18.56	207.3	2284.9	2805.7	18.56	211.2	2327.4	2858.4	18.58

AVERAGE P%=11.14 AVERAGE C%=11.14 AVERAGE F%=11.16

TEST NUMBER 100

MFR F FLAT PLATE

EBAR =0.0

H	AED	ASF	LCD	LSF	PA	PMA	PFLC	PX	CA	CMA	CFLC	CX	FA	FMA	FFLC	FX
2.50	6.25	1.00	3.78	0.20	1349.9	14875.8	15829.1	6.02	1349.9	14875.8	15829.1	6.02	1375.0	15152.5	16126.7	6.04
2.00	5.30	1.00	3.20	0.20	1144.7	12614.7	13400.3	5.86	1144.7	12614.7	13400.3	5.86	1166.0	12849.3	13652.3	5.88
1.50	4.20	1.00	5.18	0.10	907.1	9996.5	10845.9	7.83	907.1	9996.5	10845.9	7.83	924.0	10182.5	11049.8	7.85
1.00	3.00	1.00	3.80	0.10	647.9	7140.4	7956.4	10.26	647.9	7140.4	7956.4	10.26	660.0	7273.2	8136.0	10.27
0.50	1.74	1.00	2.25	0.10	375.8	4141.4	4711.1	12.09	375.8	4141.4	4711.1	12.09	382.8	4218.4	4799.6	12.11

AVERAGE PX= 8.41 AVERAGE CX= 8.41 AVERAGE FX= 8.43

VI-4 GRAPHS OF DATA

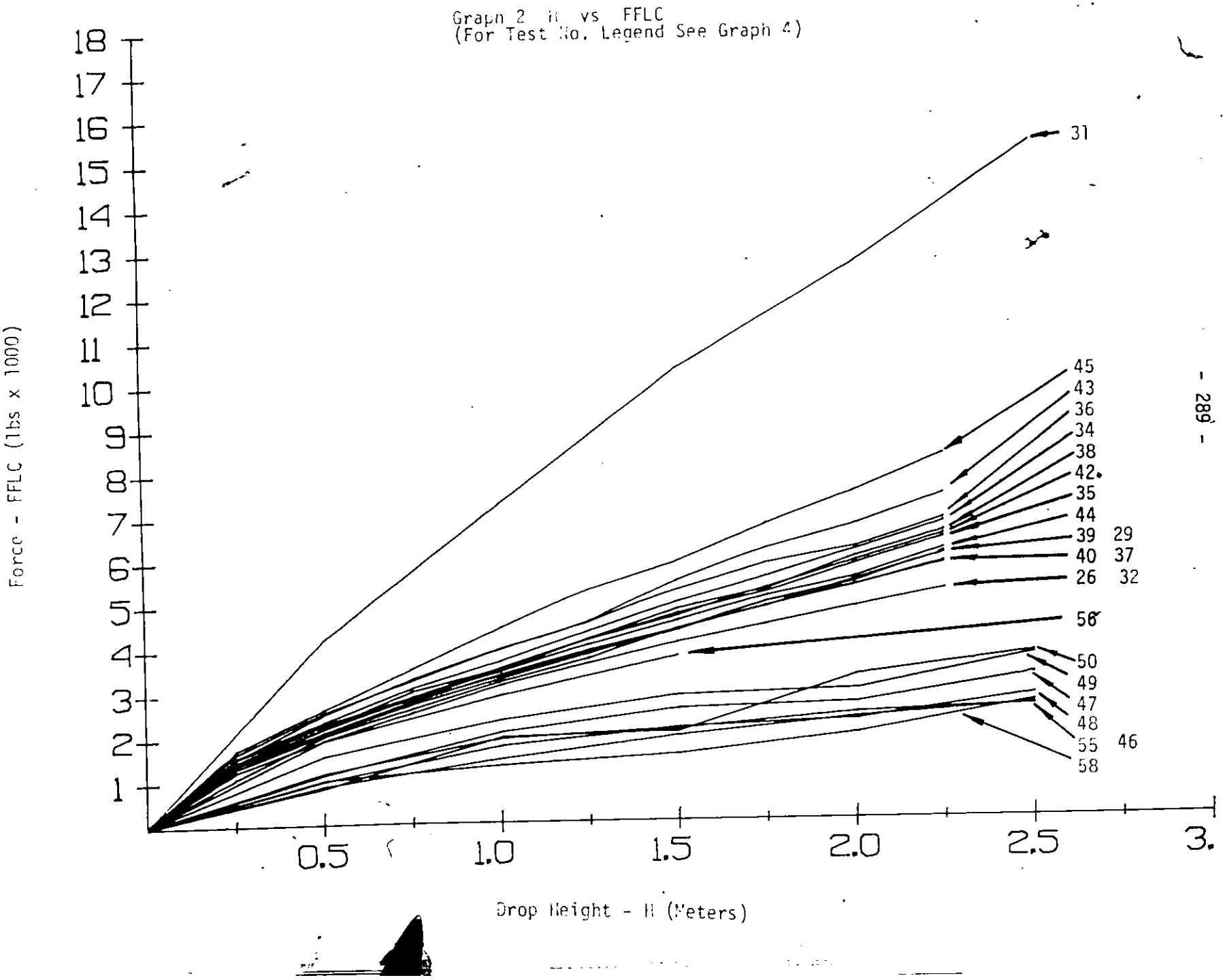
Graph 2 H vs FFLC
(For Test No. Legend See Graph 4)
Force - FFLC (lbs x 1000)
Drop Height - H (Meters)
18
17
16
15
14
13
12
11
10
9
8
7
6
5
4
3
2
1
0.5
1.0
1.5
2.0
2.5
3.
31
45
43
36
34
38
42
35
44
39
29
40
37
26
32
56
50
49
47
48
55
46
58

Graph 3 H vs FMA
(For Test No. Legend See Graph 5)

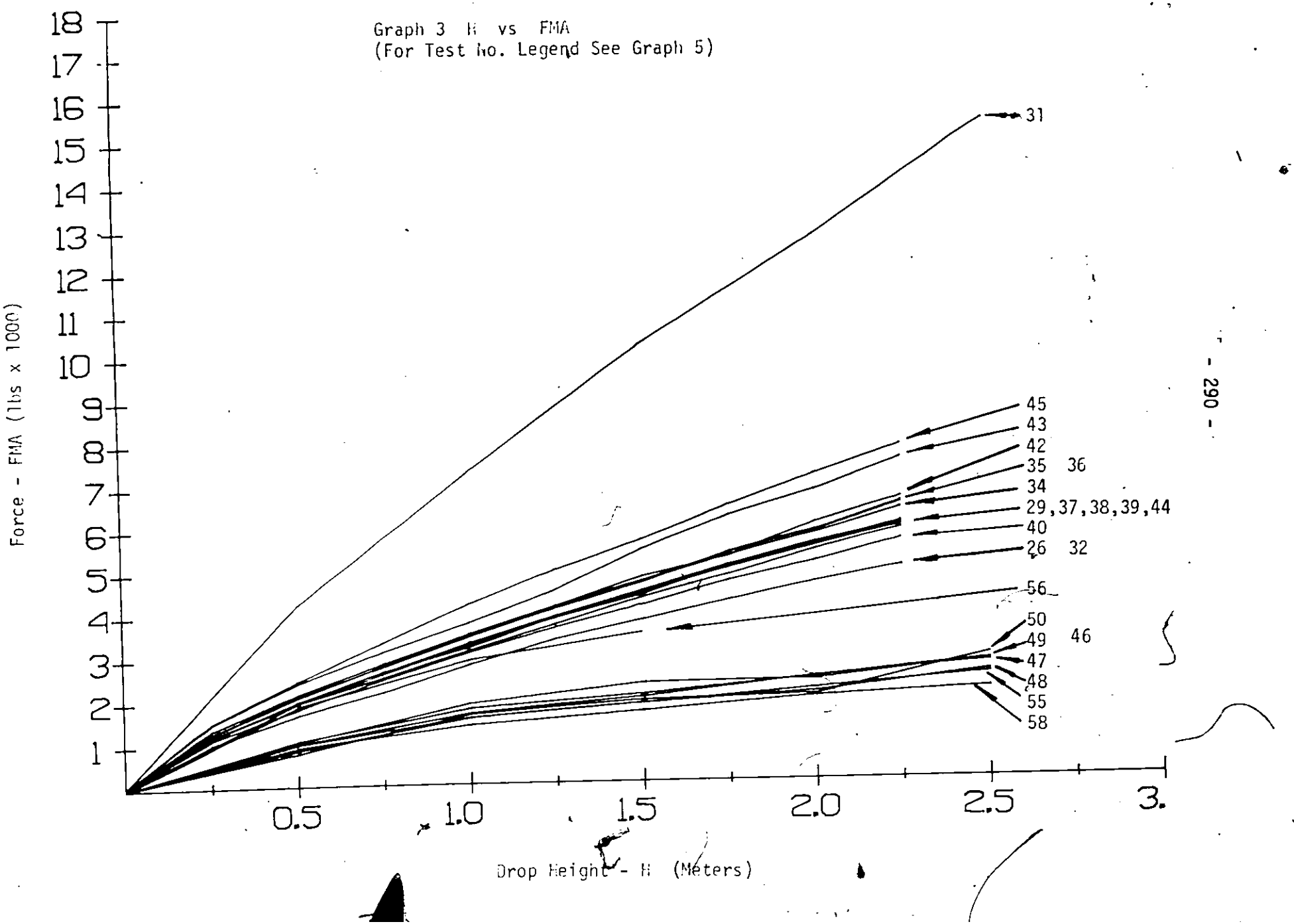

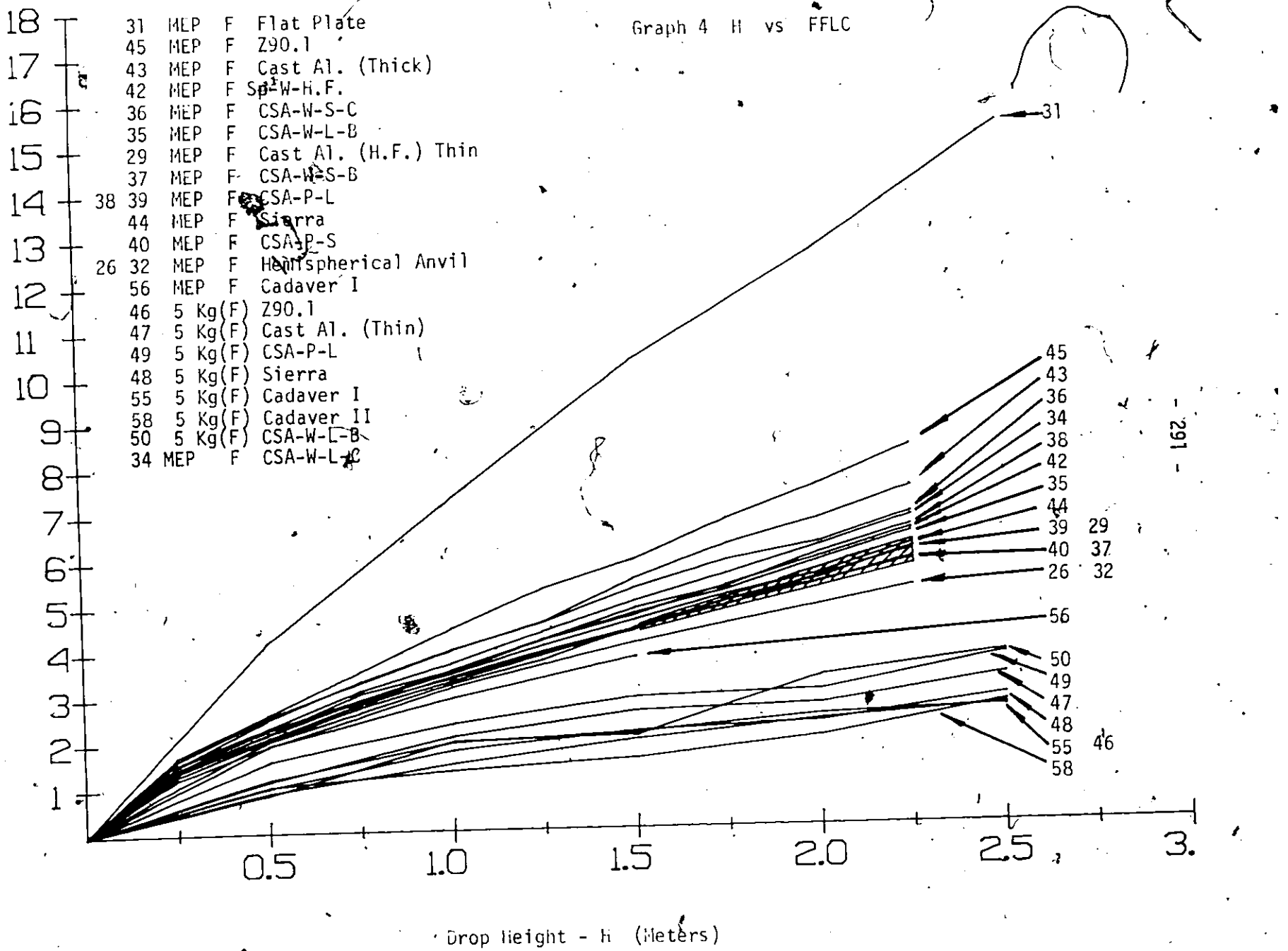
Graph 4 H vs FFLC
31 MEP F Flat Plate
45 MEP F Z90.1
43 MEP F Cast Al. (Thick)
42 MEP F Sp-W-H.F.
36 MEP F CSA-W-S-C
35 MEP F CSA-W-L-B
29 MEP F Cast Al. (H.F.) Thin
37 MEP F CSA-W-S-B
38 39 MEP F CSA-P-L
44 MEP F Sierra
40 MEP F CSA-P-S
26 32 MEP F Hemispherical Anvil
56 MEP F Cadaver I
46 5 Kg(F) Z90.1
47 5 Kg(F) Cast Al. (Thin)
49 5 Kg(F) CSA-P-L
48 5 Kg(F) Sierra
55 5 Kg(F) Cadaver I
58 5 Kg(F) Cadaver II
50 5 Kg(F) CSA-W-L-B
34 MEP F CSA-W-L-C
Force - FFLC(lbs x 1000)
Drop Height - H (Meters)
18
17
16
15
14
13
12
11
10
9
8
7
6
5
4
3
2
1
0.5
1.0
1.5
2.0
2.5
3.
31
45
43
36
34
38
42
35
44
39 29
40 37
26 32
56
50
49
47
48
55 46
58

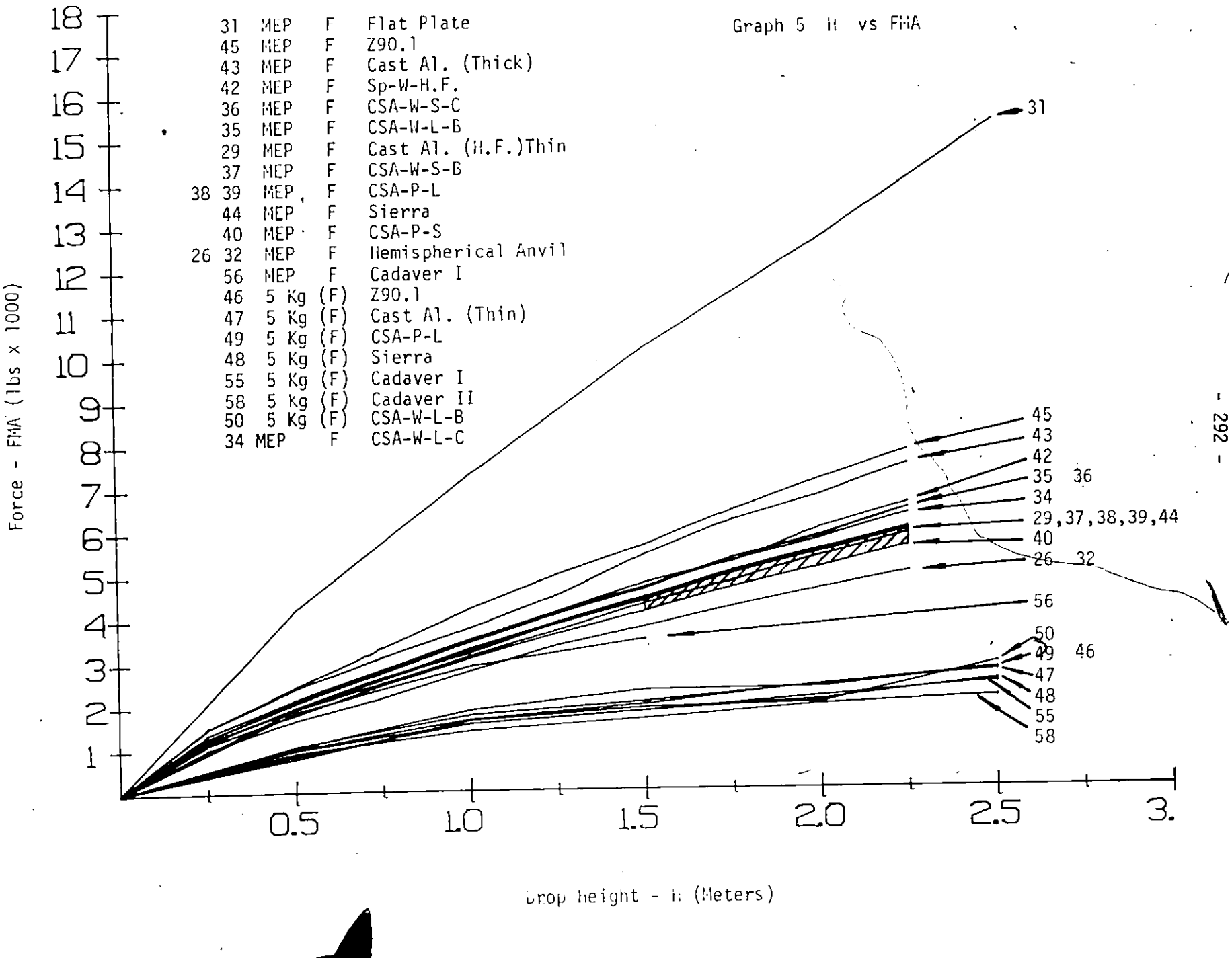
Graph 5 H vs FMA
31 MEP F Flat Plate
45 MEP F Z90.1
43 MEP F Cast Al. (Thick)
42 MEP F Sp-W-H.F.
36 MEP F CSA-W-S-C
35 MEP F CSA-W-L-B
29 MEP F Cast Al. (H.F.)Thin
37 MEP F CSA-W-S-B
38 39 MEP F CSA-P-L
44 MEP F Sierra
40 MEP F CSA-P-S
26 32 MEP F Hemispherical Anvil
56 MEP F Cadaver I
46 5 Kg (F) Z90.1
47 5 Kg (F) Cast Al. (Thin)
49 5 Kg (F) CSA-P-L
48 5 Kg (F) Sierra
55 5 Kg (F) Cadaver I
58 5 Kg (F) Cadaver II
50 5 Kg (F) CSA-W-L-B
34 MEP F CSA-W-L-C
Force - FMA (lbs x 1000)
Drop Height - H (Meters)
18
17
16
15
14
13
12
11
10
9
8
7
6
5
4
3
2
1
0.5
1.0
1.5
2.0
2.5
3.
31
45
43
42
35 36
34
29,37,38,39,44
40
26 32
56
50
49 46
47
48
55
58

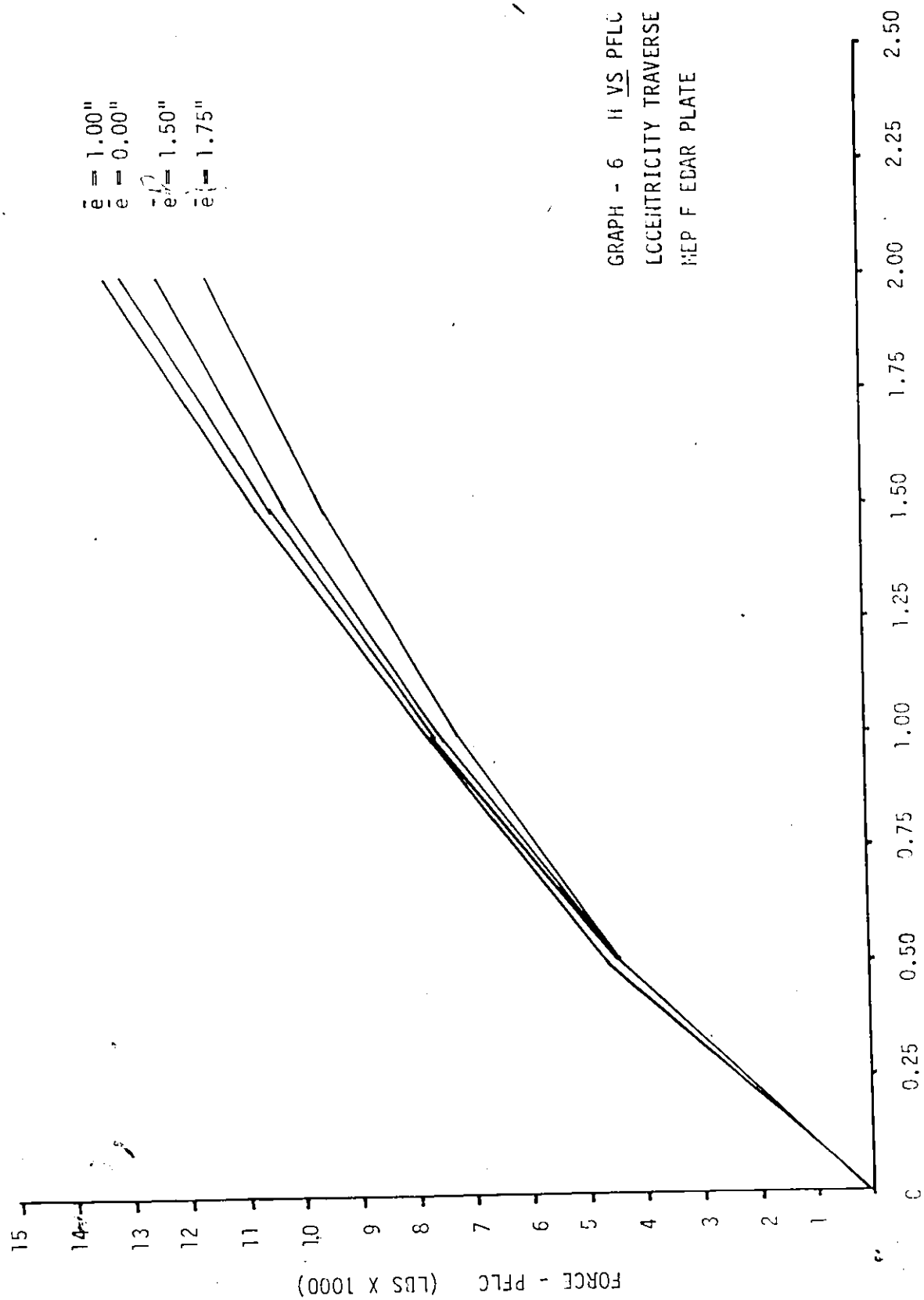
GRAPH - 6 H VS PFLC
ECCENTRICITY TRAVERSE
MEP F EDAR PLATE
ē = 1.00"
ē = 0.00"
ē = 1.50"
ē = 1.75"
FORCE - PFLC (LBS X 1000)
DROP HEIGHT - h (METERS)
0
0.25
0.50
0.75
1.00
1.25
1.50
1.75
2.00
2.25
2.50
1
2
3
4
5
6
7
8
9
10
11
12
13
14
15

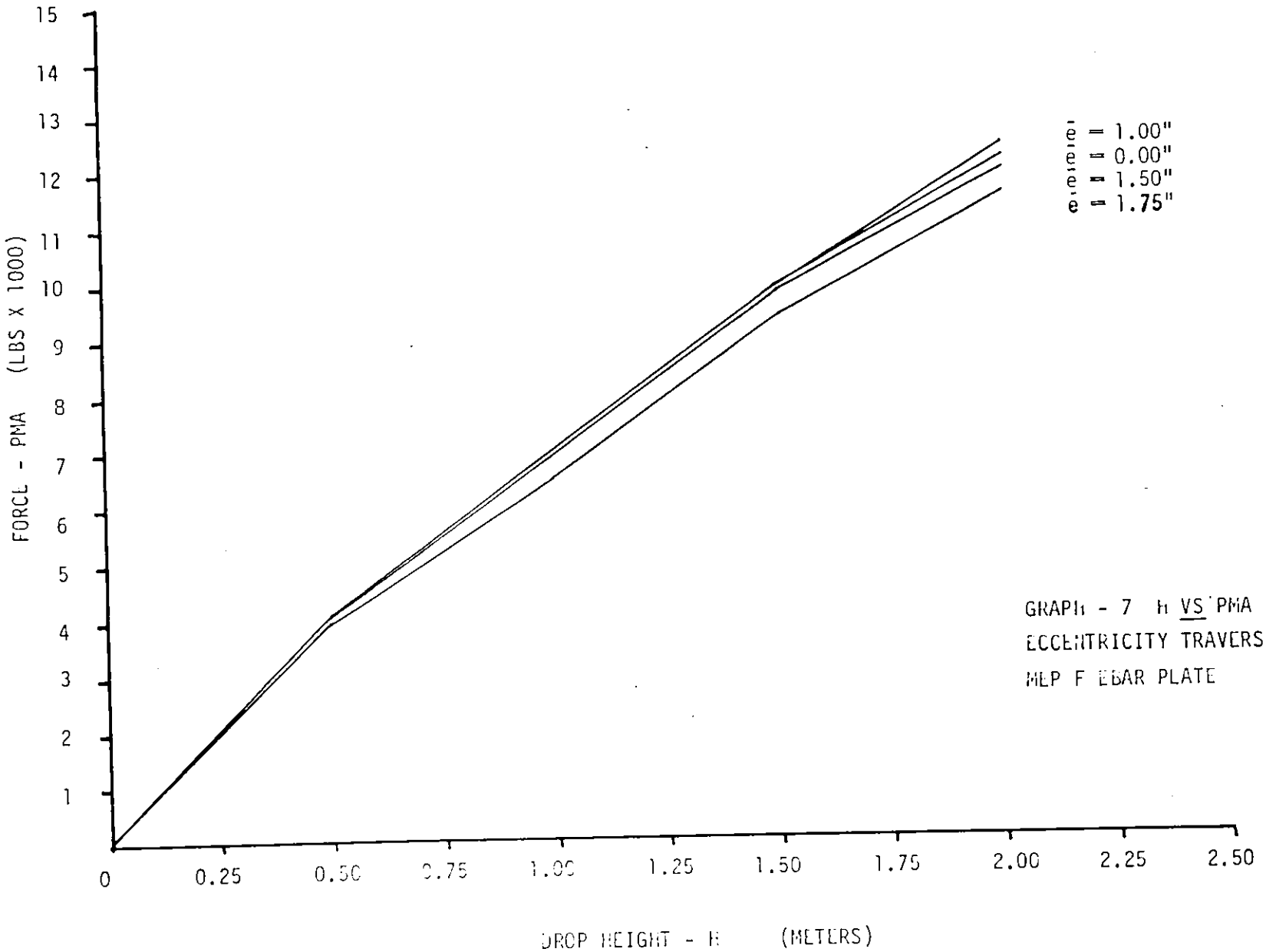

GRAPH - 7 H VS PMA
ECCENTRICITY TRAVERSE
MLP F EBAR PLATE

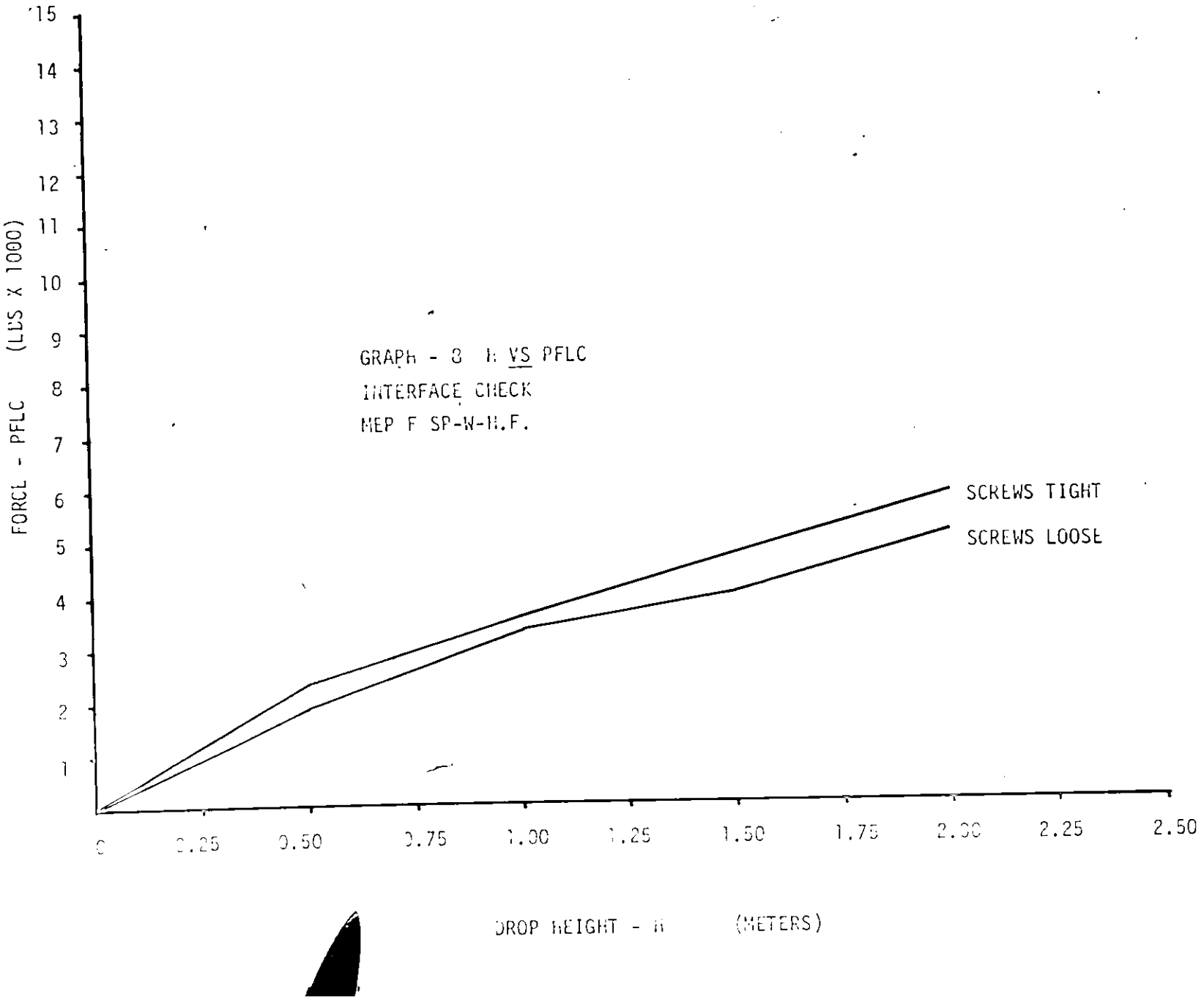
GRAPH - 8 H VS PFLC
INTERFACE CHECK
MEP F SP-W-H.F.
FORCE - PFLC (LBS X 1000)
15
14
13
12
11
10
9
8
7
6
5
4
3
2
1
0
0.25
0.50
0.75
1.00
1.25
1.50
1.75
2.00
2.25
2.50
SCREWS TIGHT
SCREWS LOOSE
DROP HEIGHT - H (METERS)

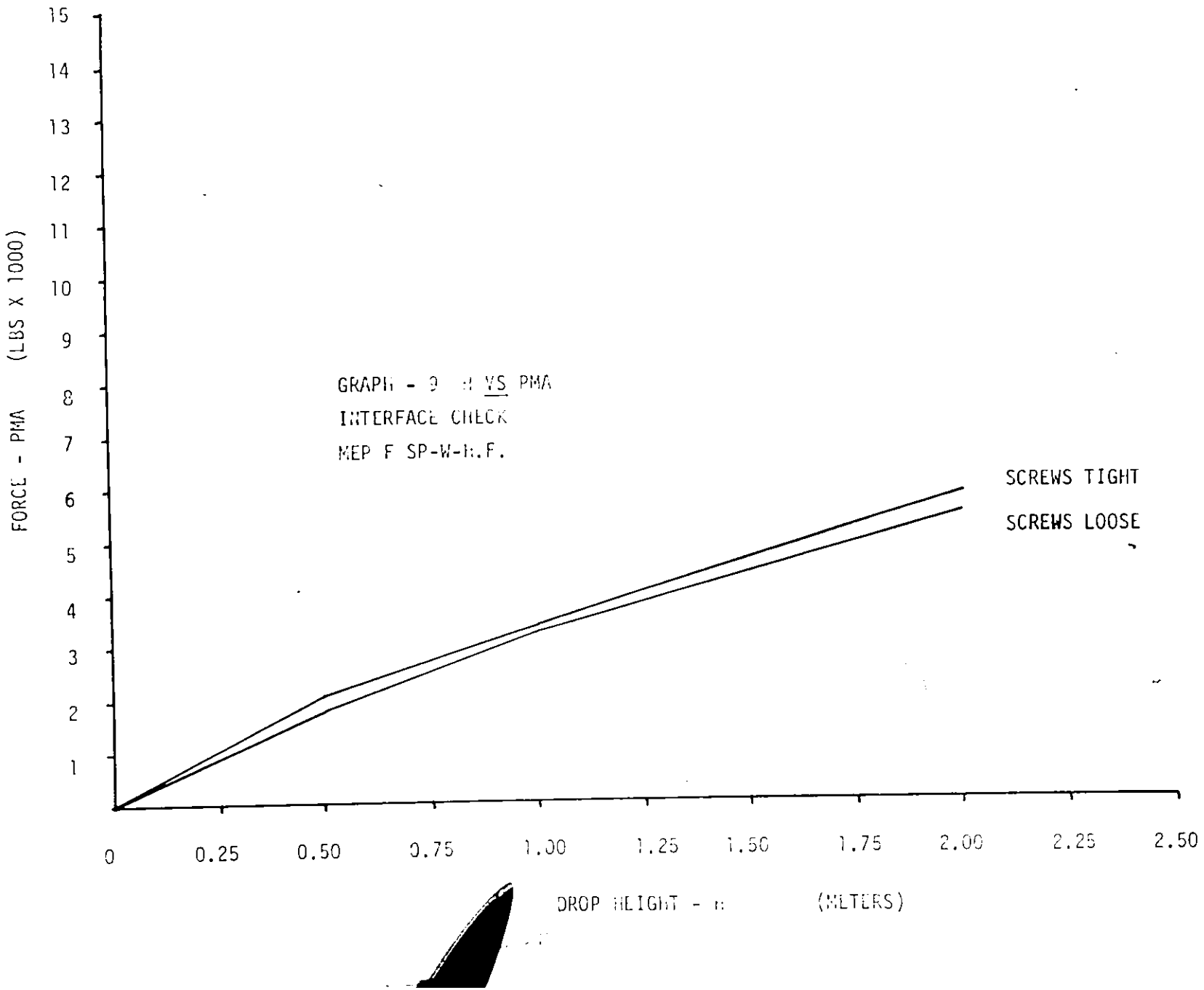
15
14
13
12
11
10
9
8
7
6
5
4
3
2
1
FORCE - PMA (LBS X 1000)
GRAPH - 9 H VS PMA
INTERFACE CHECK
MEP F SP-W-H.F.
SCREWS TIGHT
SCREWS LOOSE
0
0.25
0.50
0.75
1.00
1.25
1.50
1.75
2.00
2.25
2.50
DROP HEIGHT - H (METERS)

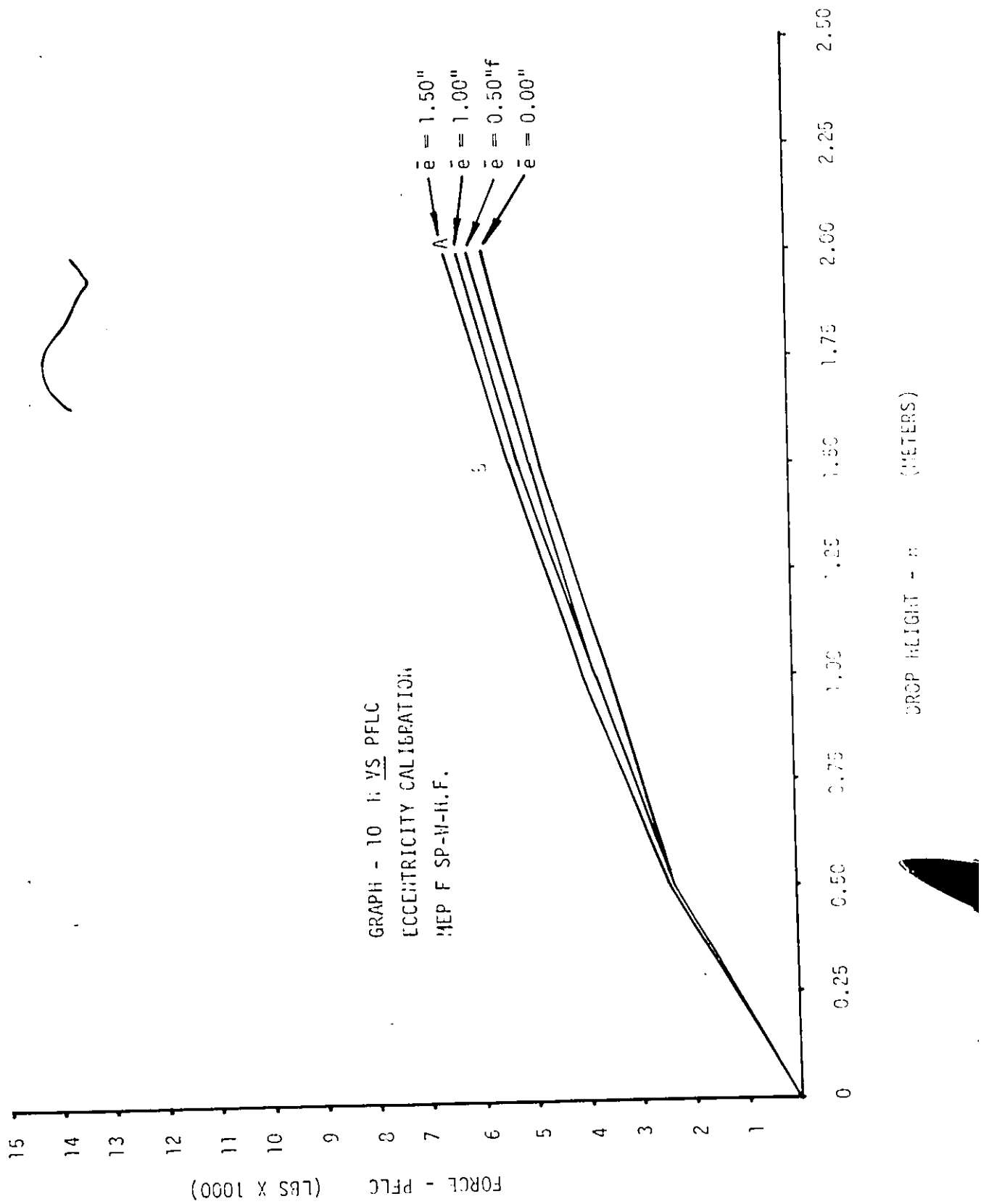
GRAPH - 10 h VS PFLC
ECCENTRICITY CALIBRATION
MEP F SP-W-H.F.
$\bar{e}$ = 1.50"
$\bar{e}$ = 1.00"
$\bar{e}$ = 0.50"f
$\bar{e}$ = 0.00"
A
FORCE - PFLC (LBS X 1000)
DROP HEIGHT - h (METERS)
0
0.25
0.50
0.75
1.00
1.25
1.50
1.75
2.00
2.25
2.50
1
2
3
4
5
6
7
8
9
10
11
12
13
14
15

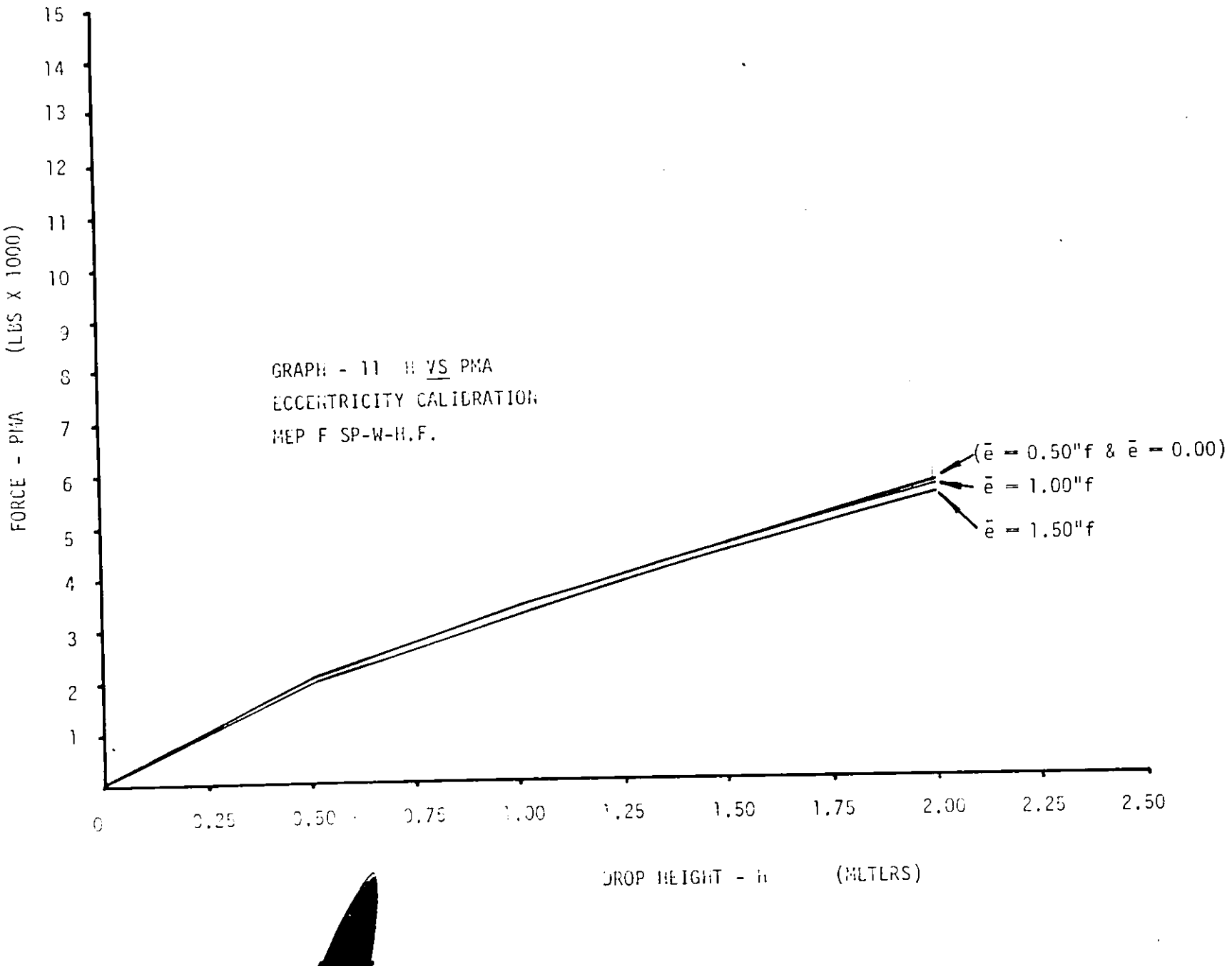
15
14
13
12
11
10
9
8
7
6
5
4
3
2
1
FORCE - PMA (LBS X 1000)
GRAPH - 11 H VS PMA
ECCENTRICITY CALIBRATION
MEP F SP-W-H.F.
(ē = 0.50"f & ē = 0.00)
ē = 1.00"f
ē = 1.50"f
0
0.25
0.50
0.75
1.00
1.25
1.50
1.75
2.00
2.25
2.50
DROP HEIGHT - h (METERS)

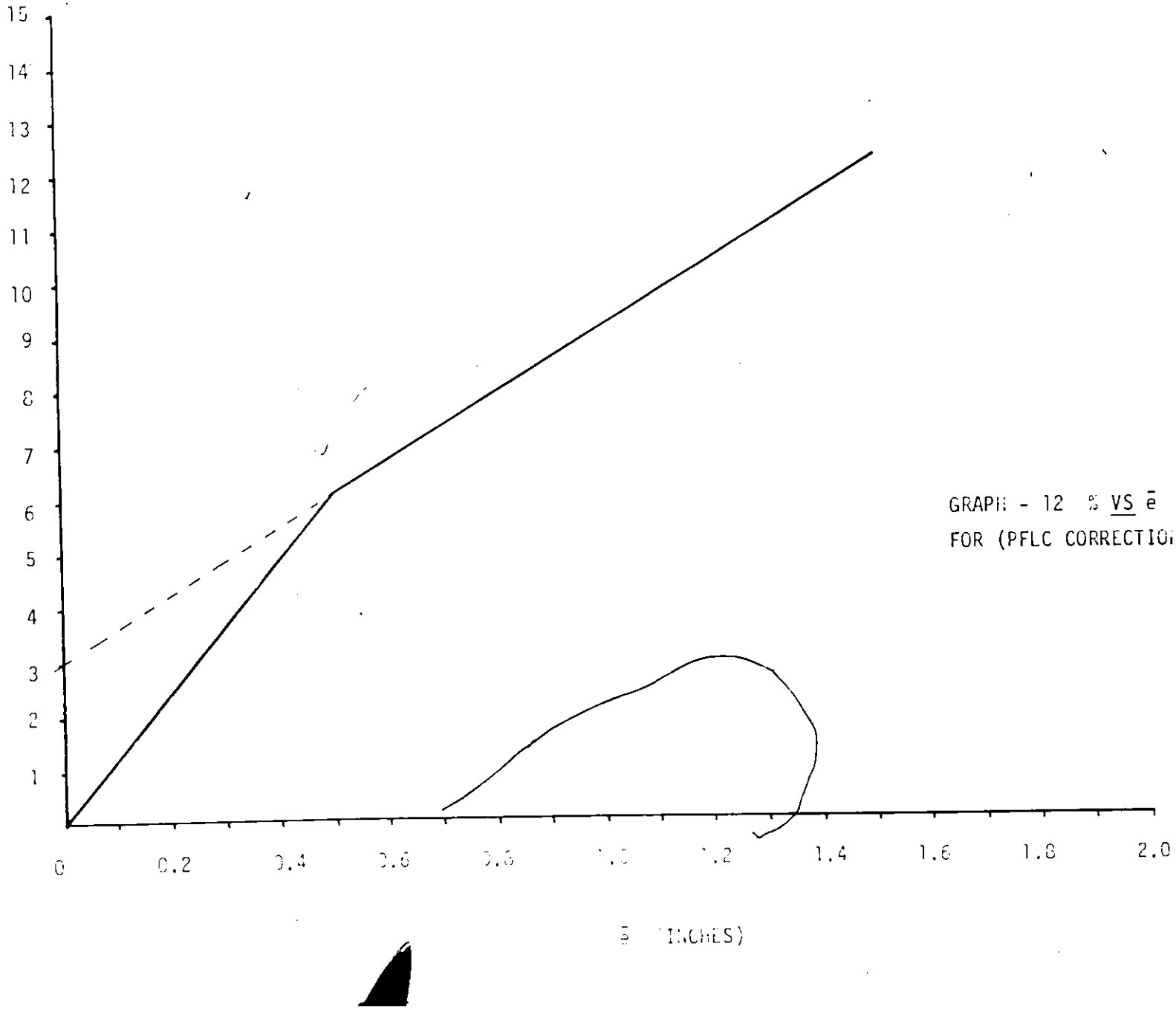

GRAPH - 12 % VS ē
FOR (PFLC CORRECTION)

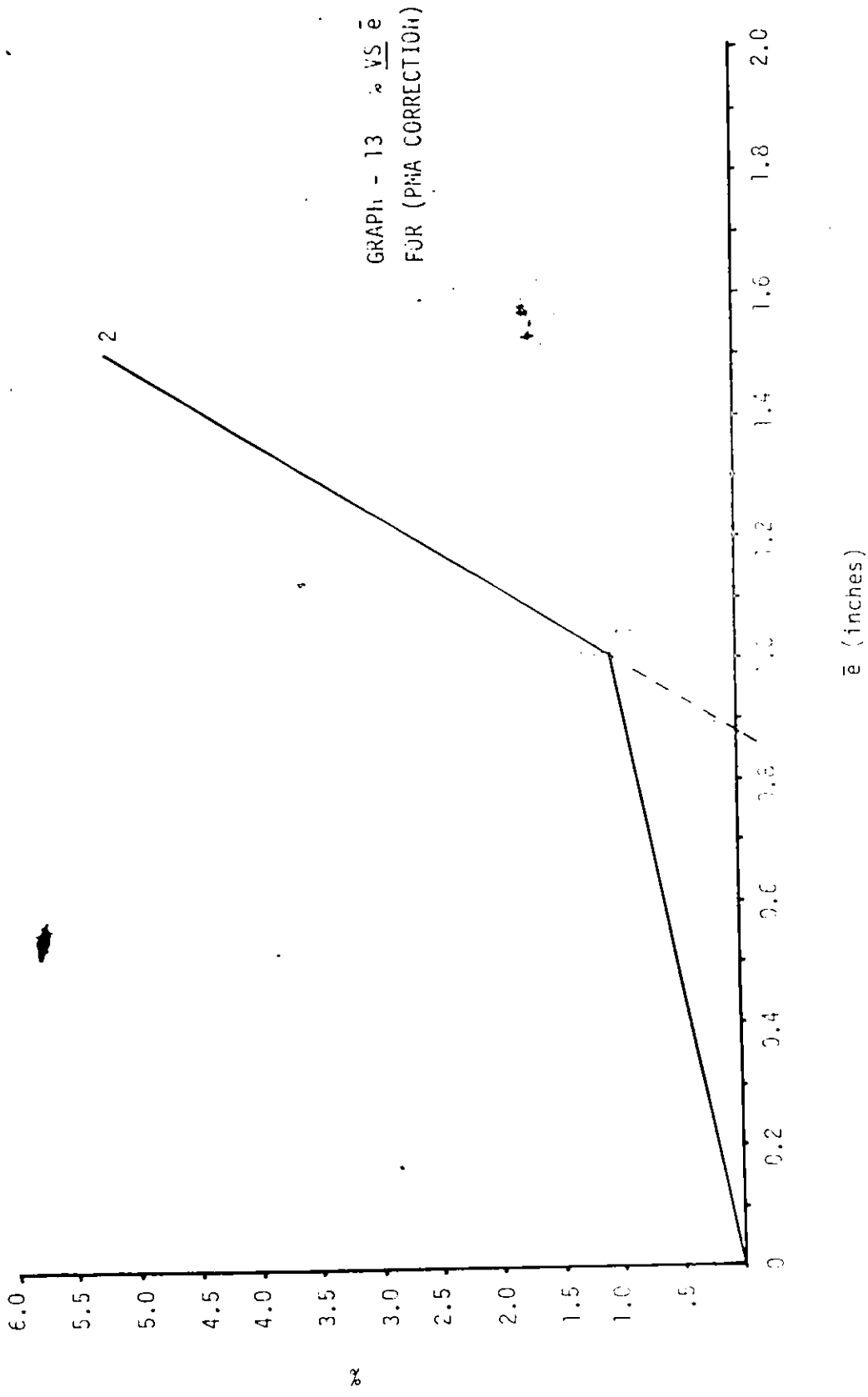
GRAPH - 13 ≈ VS ē
FOR (PHA CORRECTION)
2
6.0
5.5
5.0
4.5
4.0
3.5
3.0
2.5
2.0
1.5
1.0
.5
%
0
0.2
0.4
1.4
1.6
1.8
2.0
ē (inches)

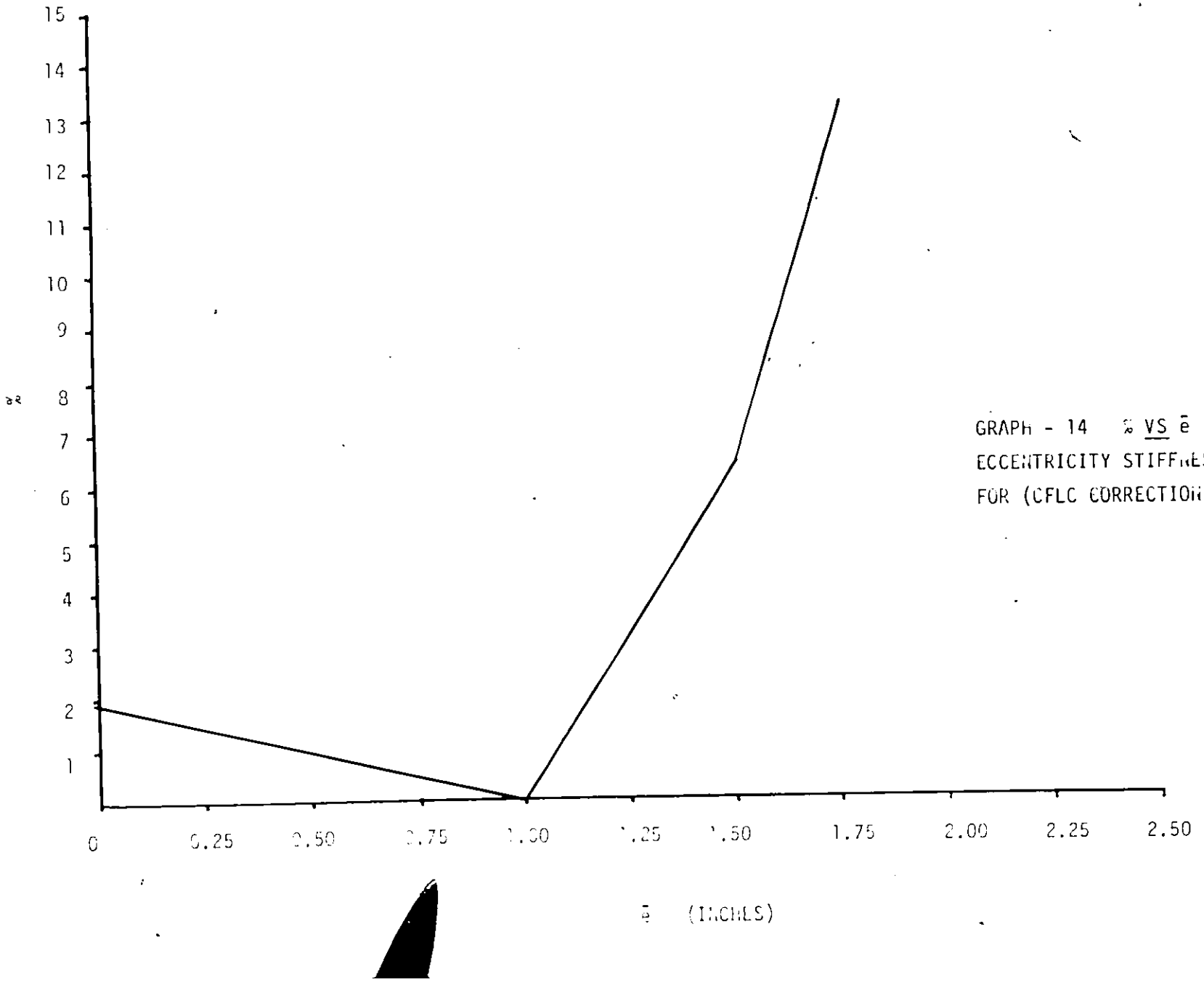

GRAPH - 14 ϕ VS $\bar{e}$
ECCENTRICITY STIFFNESS
FOR (CFLC CORRECTION)

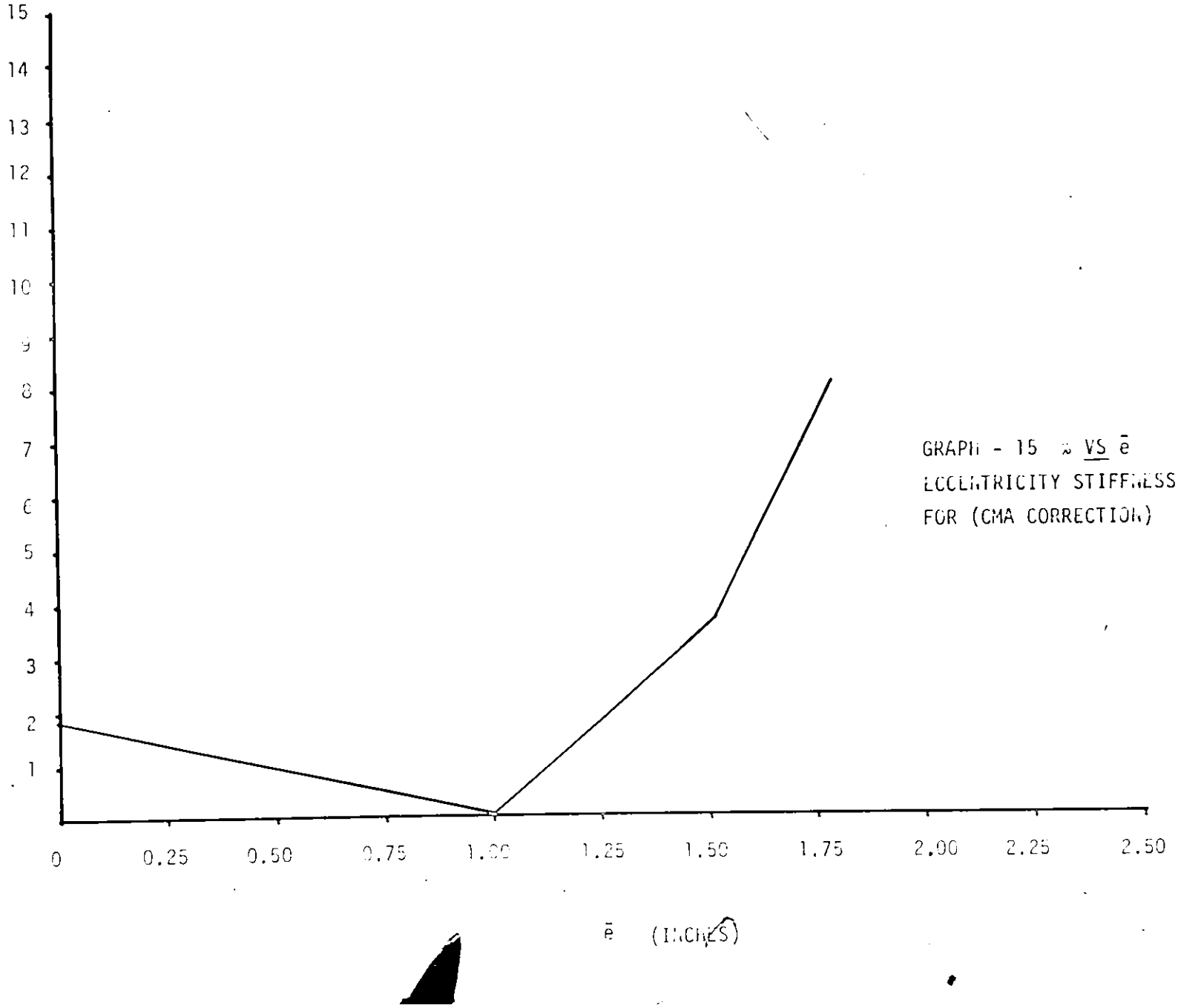

GRAPH - 15 % VS ē
ECCENTRICITY STIFFNESS
FOR (CMA CORRECTION)

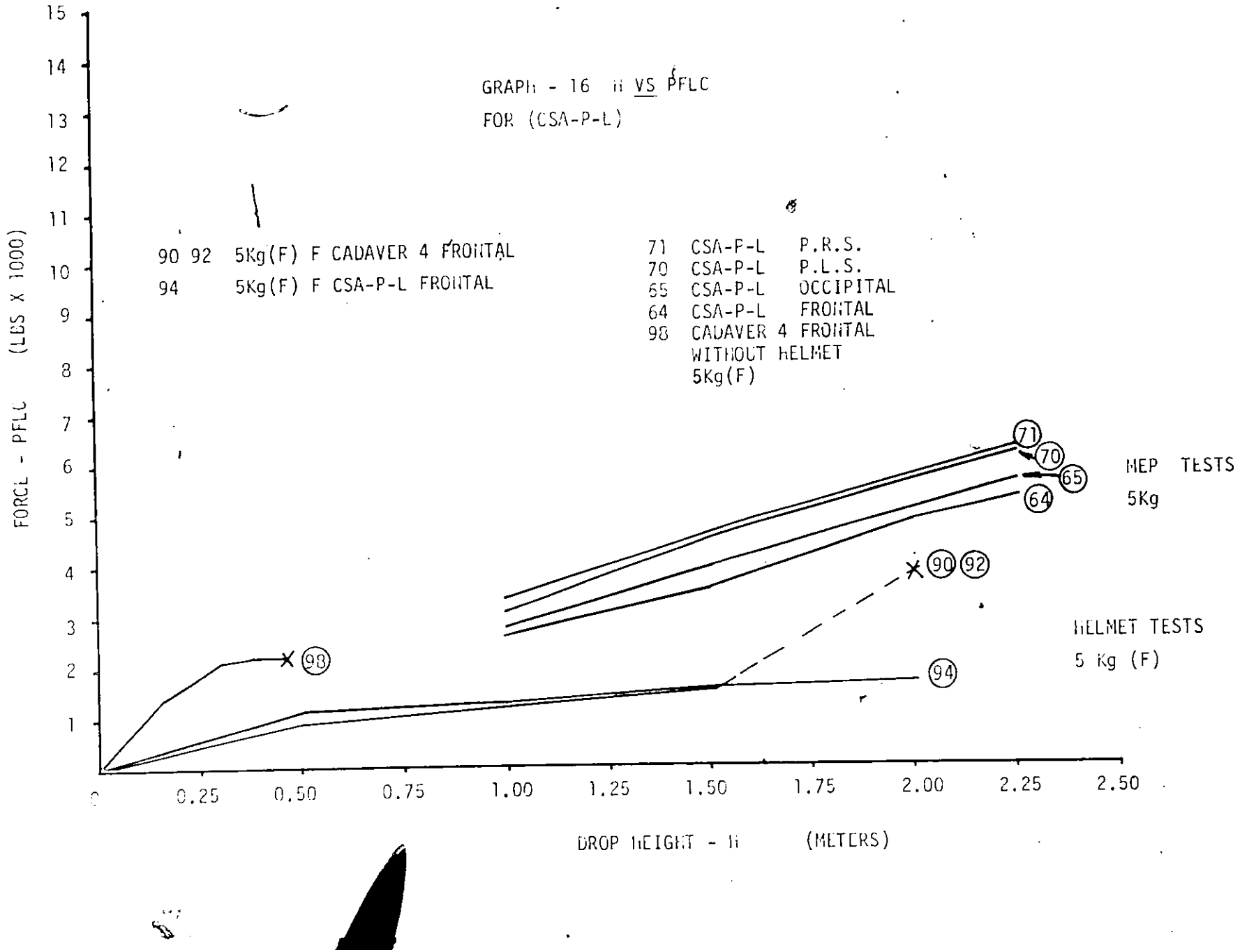
GRAPH - 16 H VS PFLC
FOR (CSA-P-L)
90 92 5Kg(F) F CADAVER 4 FRONTAL
94 5Kg(F) F CSA-P-L FRONTAL
71 CSA-P-L P.R.S.
70 CSA-P-L P.L.S.
65 CSA-P-L OCCIPITAL
64 CSA-P-L FRONTAL
98 CADAVER 4 FRONTAL WITHOUT HELMET 5Kg(F)
MEP TESTS 5Kg
HELMET TESTS 5 Kg (F)
FORCE - PFLC (LBS X 1000)
DROP HEIGHT - H (METERS)
15
14
13
12
11
10
9
8
7
6
5
4
3
2
1
0.25
0.50
0.75
1.00
1.25
1.50
1.75
2.00
2.25
2.50

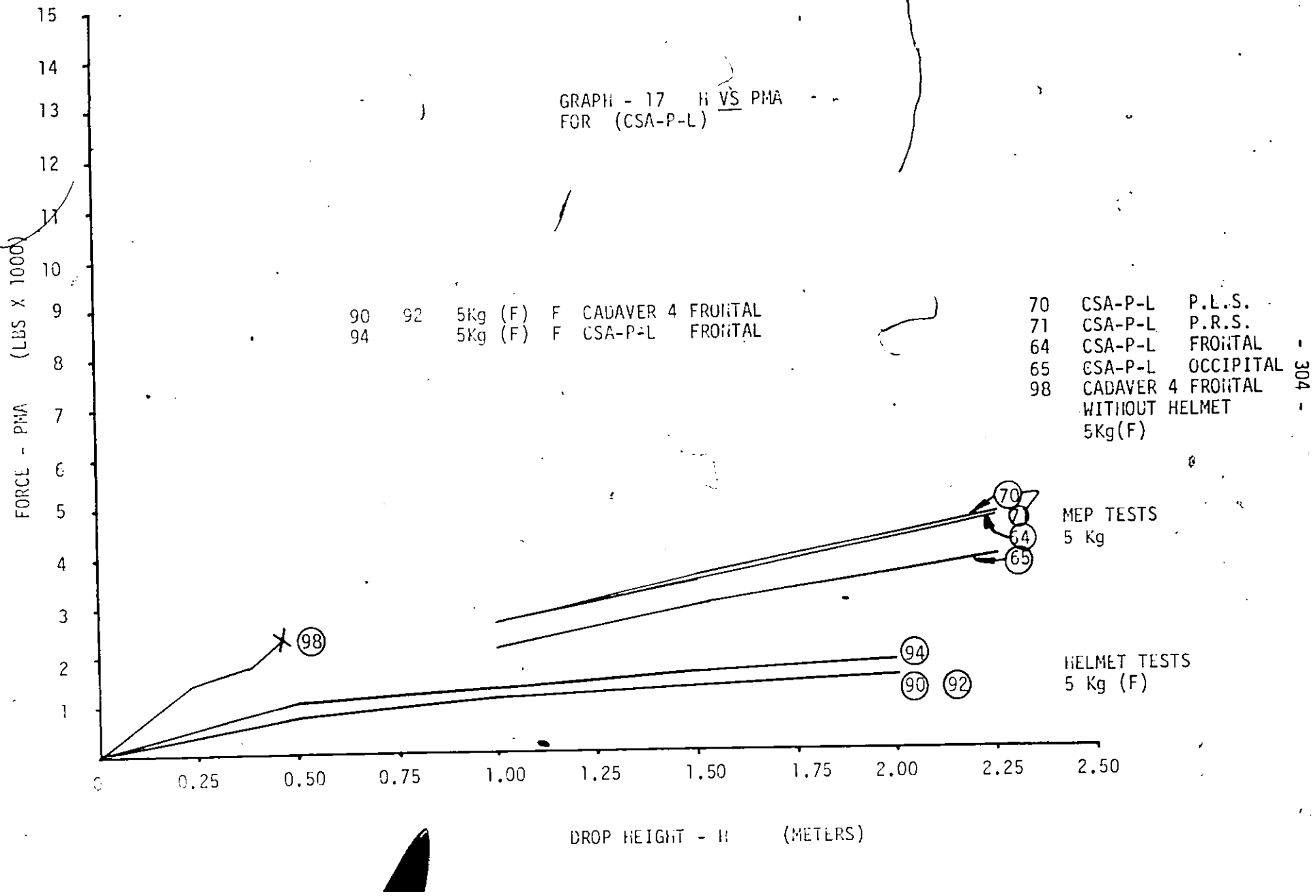
GRAPH - 17 H VS PMA
FOR (CSA-P-L)
90 92 5Kg (F) F CADAVER 4 FRONTAL
94 5Kg (F) F CSA-P-L FRONTAL
70 CSA-P-L P.L.S.
71 CSA-P-L P.R.S.
64 CSA-P-L FRONTAL
65 CSA-P-L OCCIPITAL
98 CADAVER 4 FRONTAL WITHOUT HELMET 5Kg(F)
MEP TESTS
5 Kg
HELMET TESTS
5 Kg (F)
FORCE - PMA (LBS X 1000)
DROP HEIGHT - H (METERS)
15
14
13
12
11
10
9
8
7
6
5
4
3
2
1
0
0.25
0.50
0.75
1.00
1.25
1.50
1.75
2.00
2.25
2.50

GRAPH - 18 H VS PFLC

FOR (SIERRA)

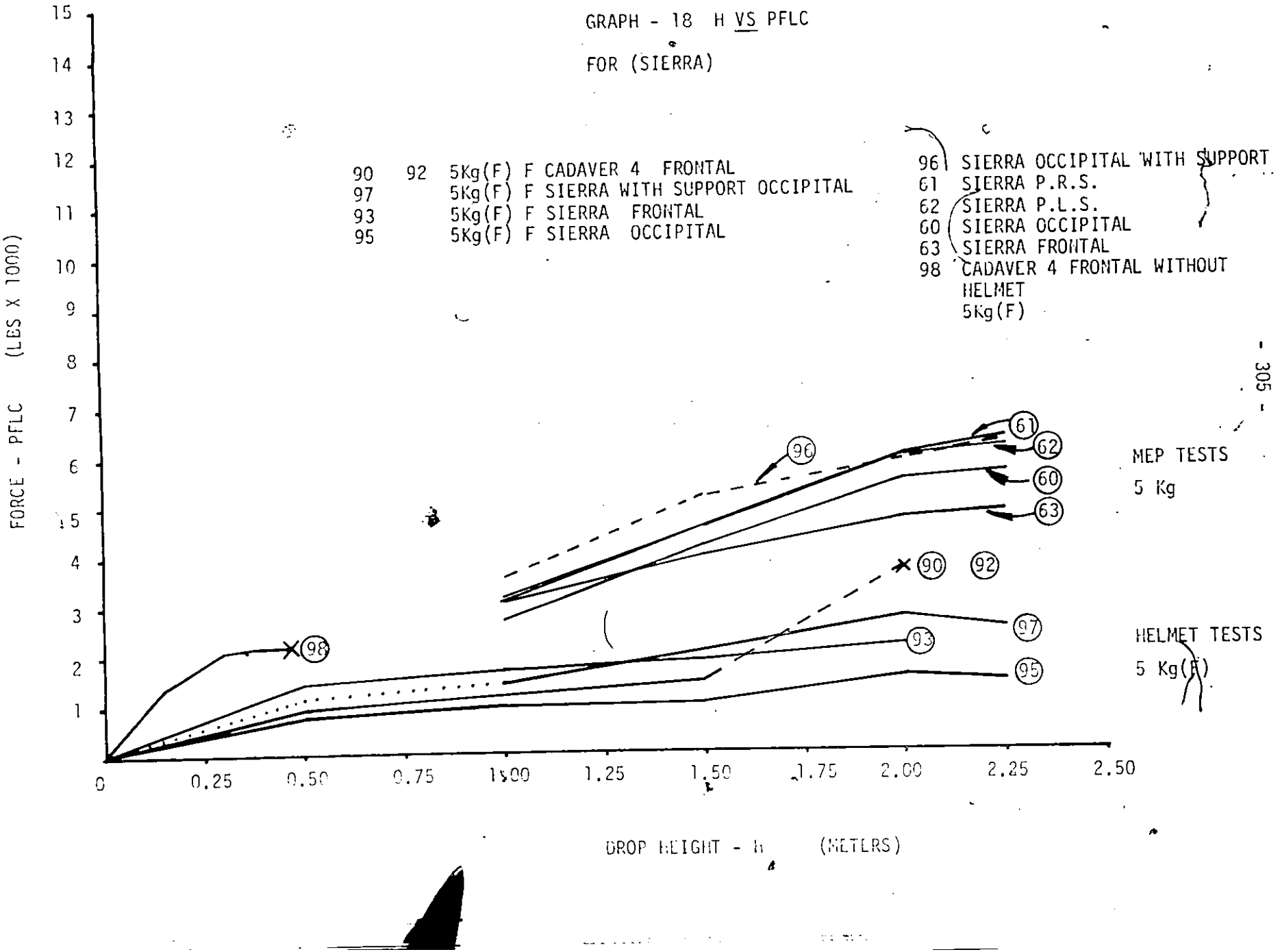

GRAPH - 19 H VS PMA

FOR (SIERRA)

90 92 5Kg(F) F CADAVER 4 FRONTAL
97 5Kg(F) F SIERRA WITH SUPPORT OCCIPITAL
93 5Kg(F) F SIERRA FRONTAL
95 5Kg(F) F SIERRA OCCIPITAL

96 SIERRA OCCIPITAL WITH SUPPORT
62 SIERRA P.L.S.
61 SIERRA P.R.S.
63 SIERRA FRONTAL
60 SIERRA OCCIPITAL
98 CADAVER 4 FRONTAL WITHOUT HELMET
5Kg(F)

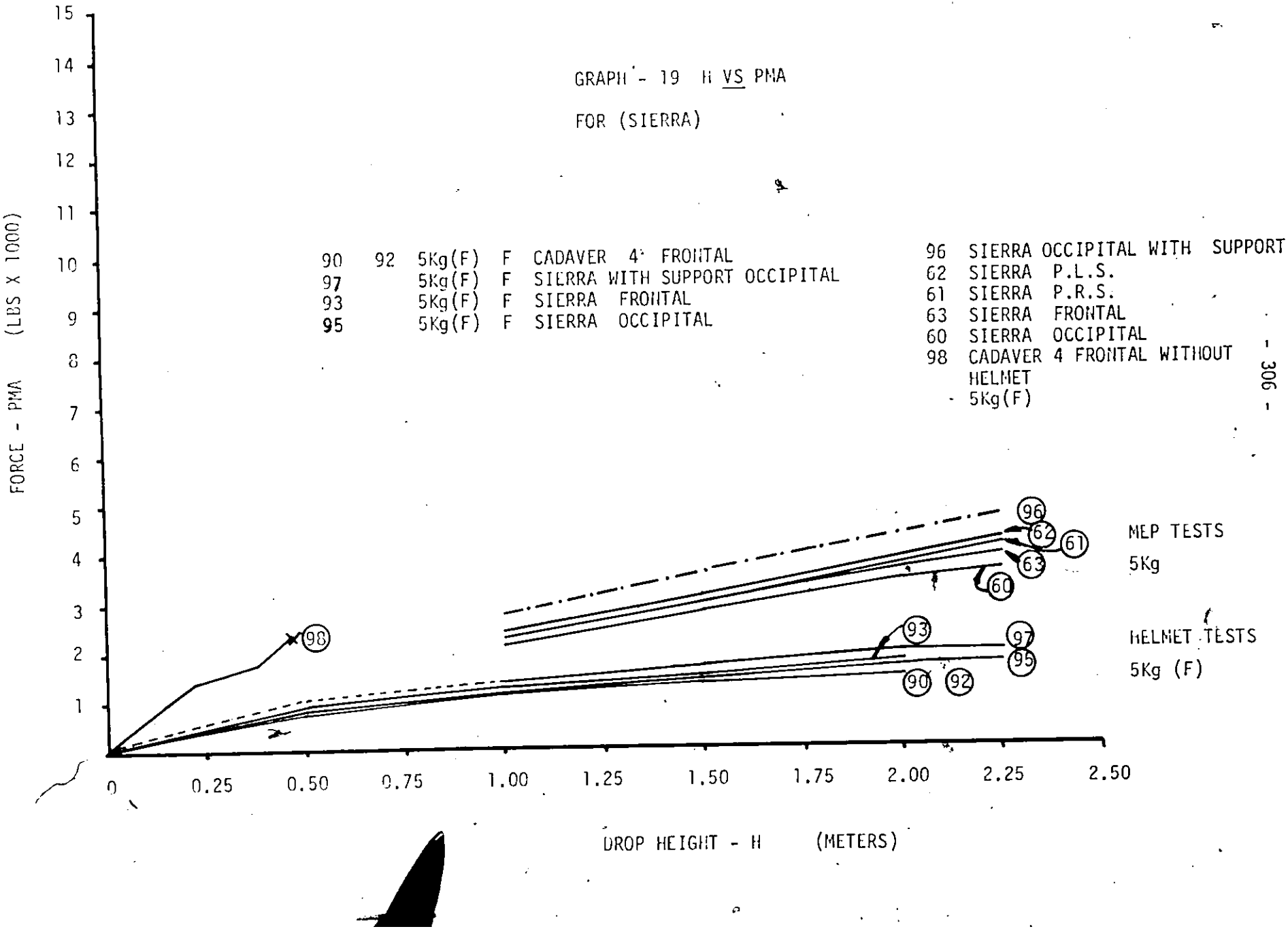

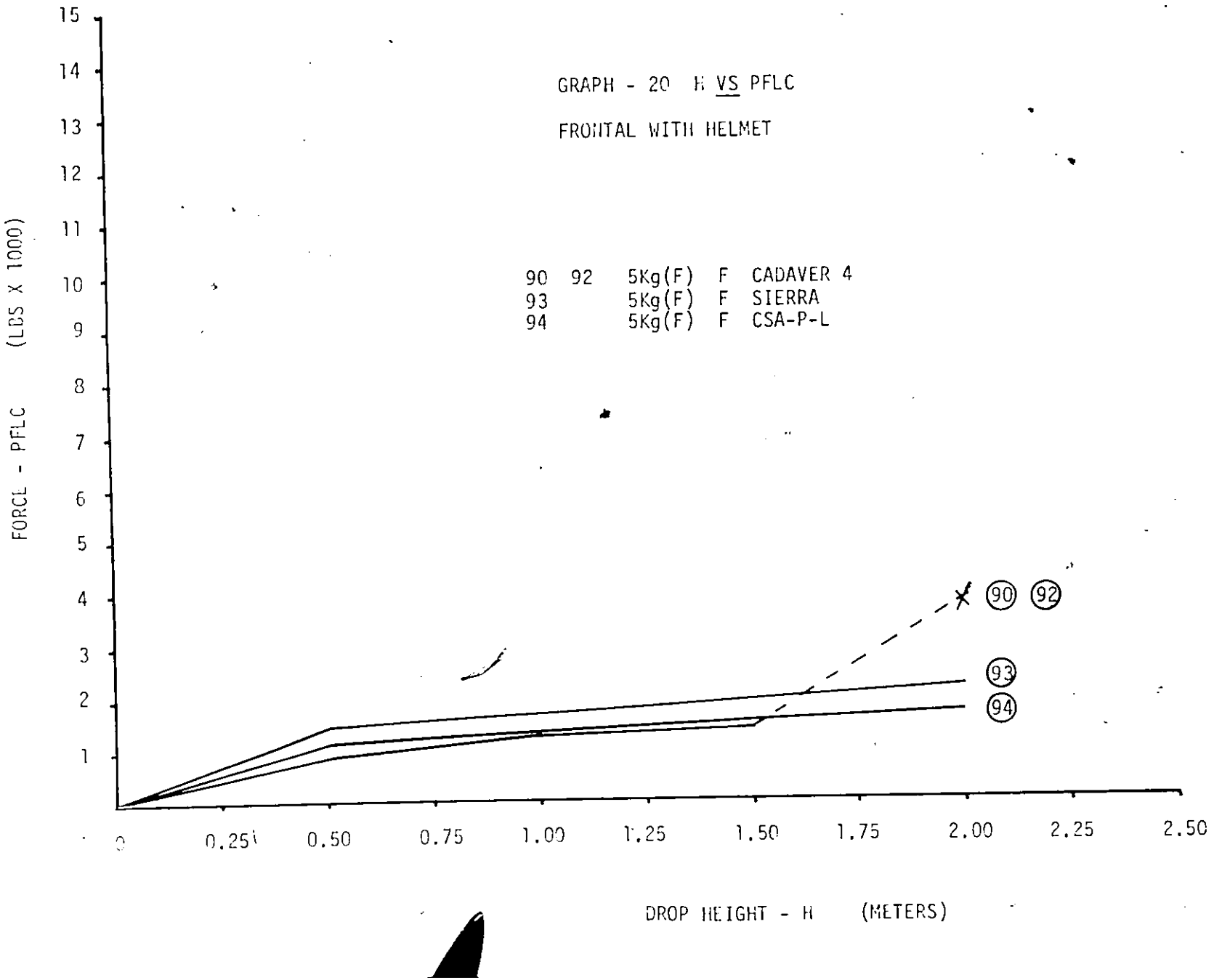
GRAPH - 20 H VS PFLC
FRONTAL WITH HELMET
90 92 5Kg(F) F CADAVER 4
93 5Kg(F) F SIERRA
94 5Kg(F) F CSA-P-L
FORCL - PFLC (LBS X 1000)
15
14
13
12
11
10
9
8
7
6
5
4
3
2
1
0
0.25
0.50
0.75
1.00
1.25
1.50
1.75
2.00
2.25
2.50
90
92
93
94
DROP HEIGHT - H (METERS)

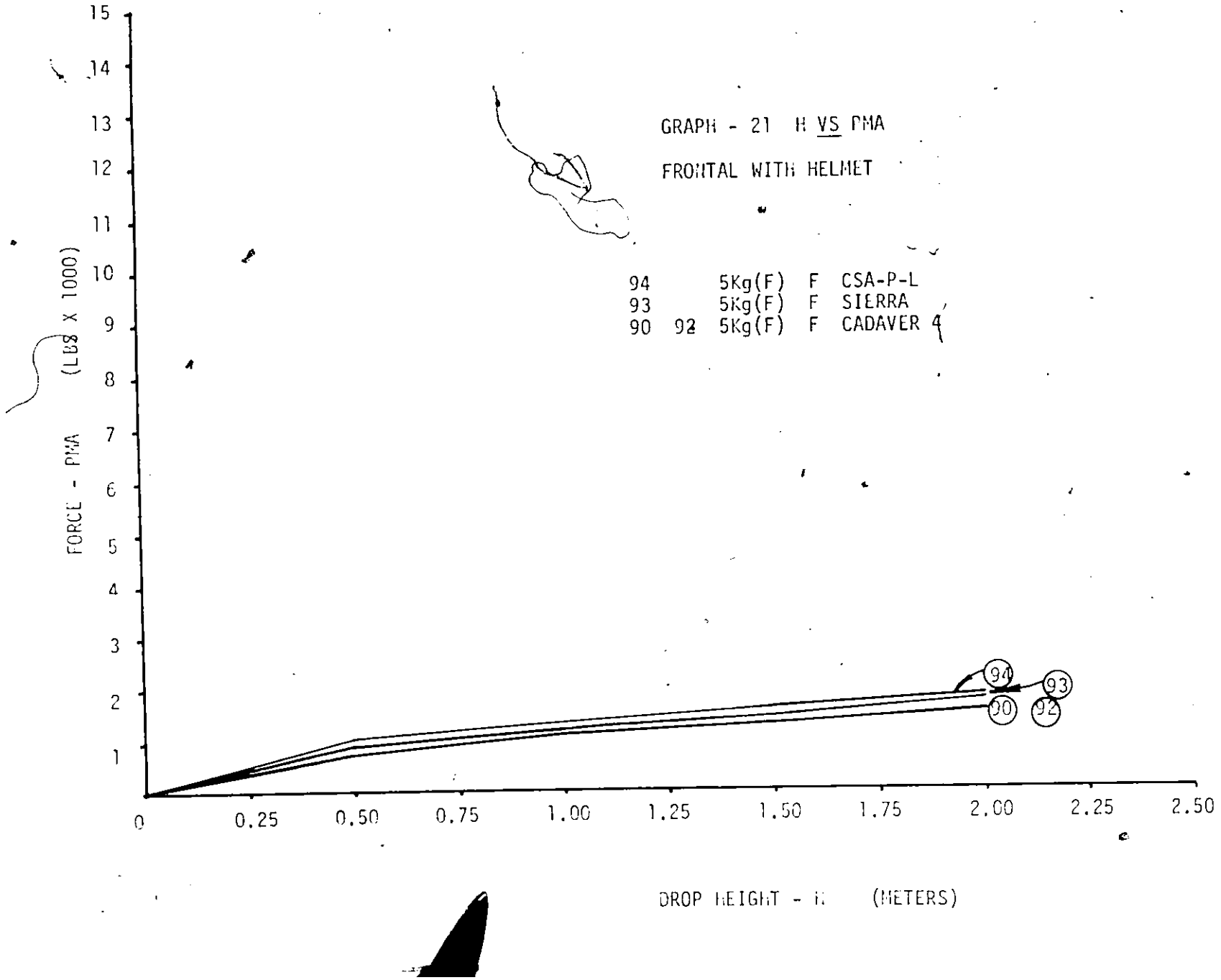
GRAPH - 21 H VS PMA
FRONTAL WITH HELMET
94 5Kg(F) F CSA-P-L
93 5Kg(F) F SIERRA
90 92 5Kg(F) F CADAVER 4
FORCE - PMA (LBS X 1000)
15
14
13
12
11
10
9
8
7
6
5
4
3
2
1
0
0.25
0.50
0.75
1.00
1.25
1.50
1.75
2.00
2.25
2.50
94
93
90
92
DROP HEIGHT - H (METERS)

GRAPH - 22 H VS PFLC

CALIBRATION OF SIERRA M.F.
OCCIPITAL (MSP) STOCK EXTENSION = .325"
96 AND 97 WITH SUPPORT
60 AND 95 WITHOUT SUPPORT

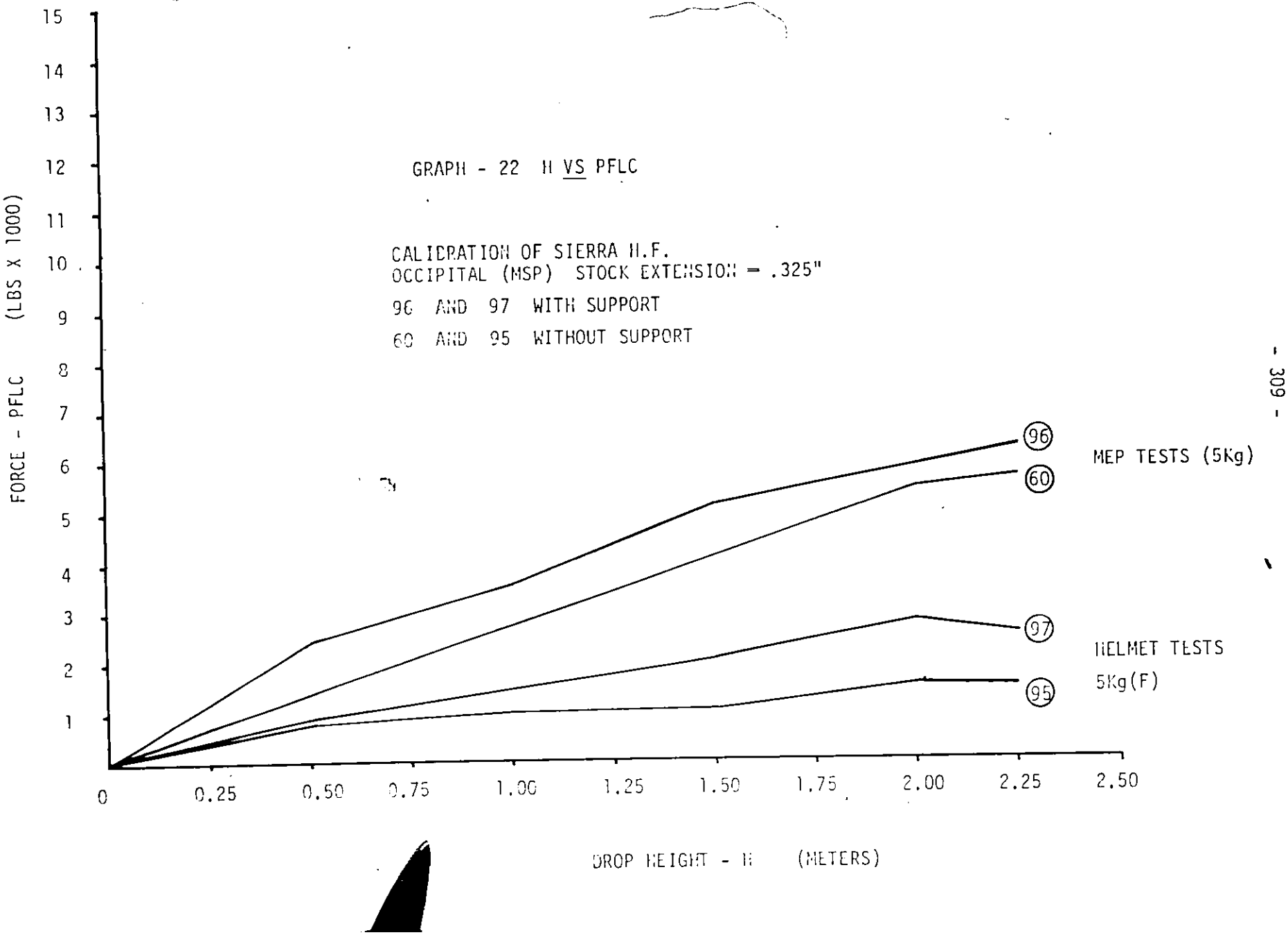

GRAPH - 23 H VS PMA

CALIBRATION OF SIERRA H.F.
OCCIPITAL (MSP) STOCK EXTENSION = .325"

96 AND 97 WITH SUPPORT

60 AND 95 WITHOUT SUPPORT

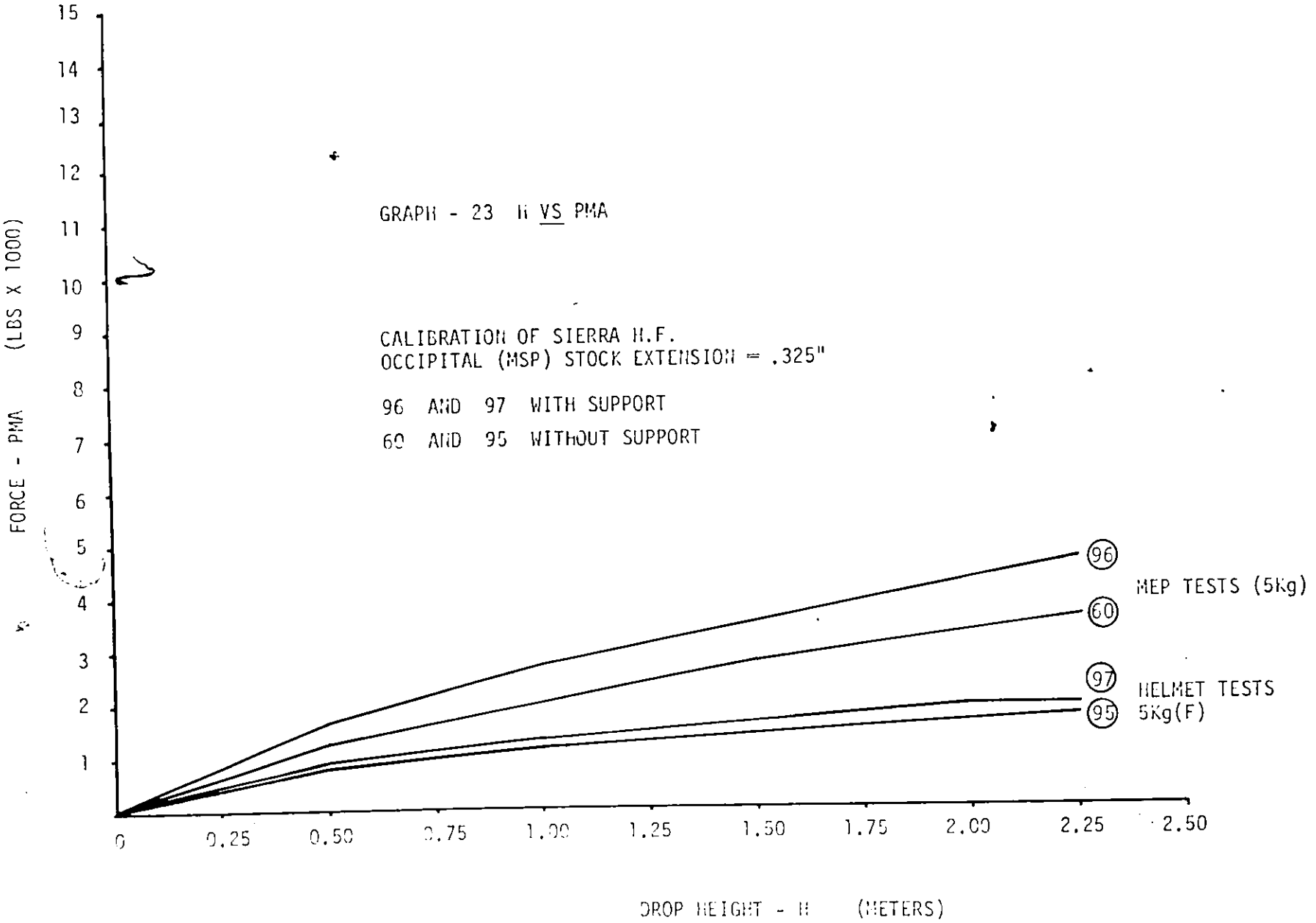

GRAPH - 24 t VS $\ddot{x}$

TEST # 48 TRACE # 185

H = 2.50 METERS

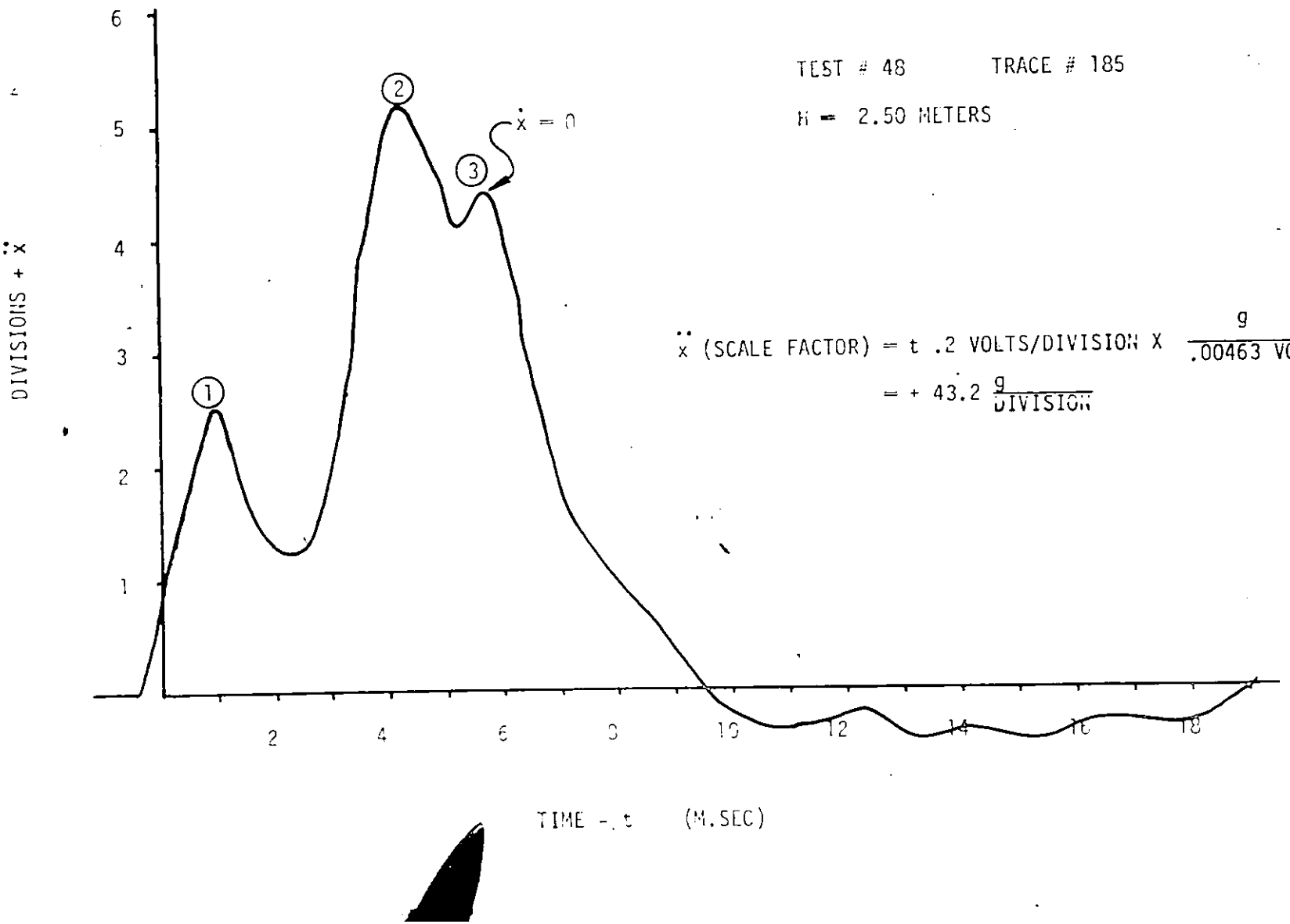

$\ddot{x}$ (SCALE FACTOR) = t .2 VOLTS/DIVISION X $\frac{g}{.00463 \text{ VOLTS}}$

$= + 43.2 \frac{g}{\text{DIVISION}}$

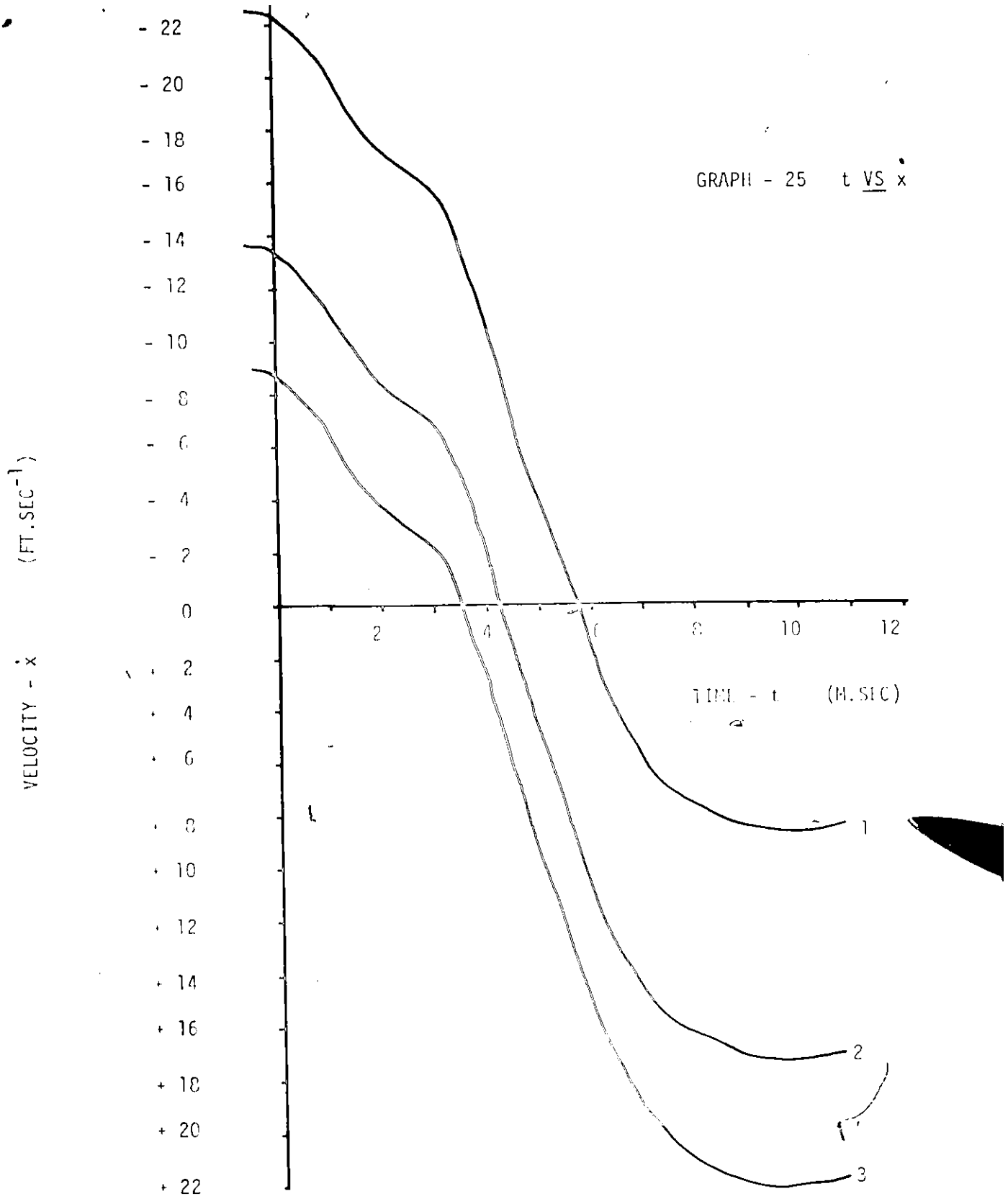
GRAPH - 25 t VS ẋ
VELOCITY - ẋ (FT.SEC⁻¹)
- 22
- 20
- 18
- 16
- 14
- 12
- 10
- 8
- 6
- 4
- 2
0
+ 2
+ 4
+ 6
+ 8
+ 10
+ 12
+ 14
+ 16
+ 18
+ 20
+ 22
2
4
6
8
10
12
TIME - t (M.SEC)
1
2
3

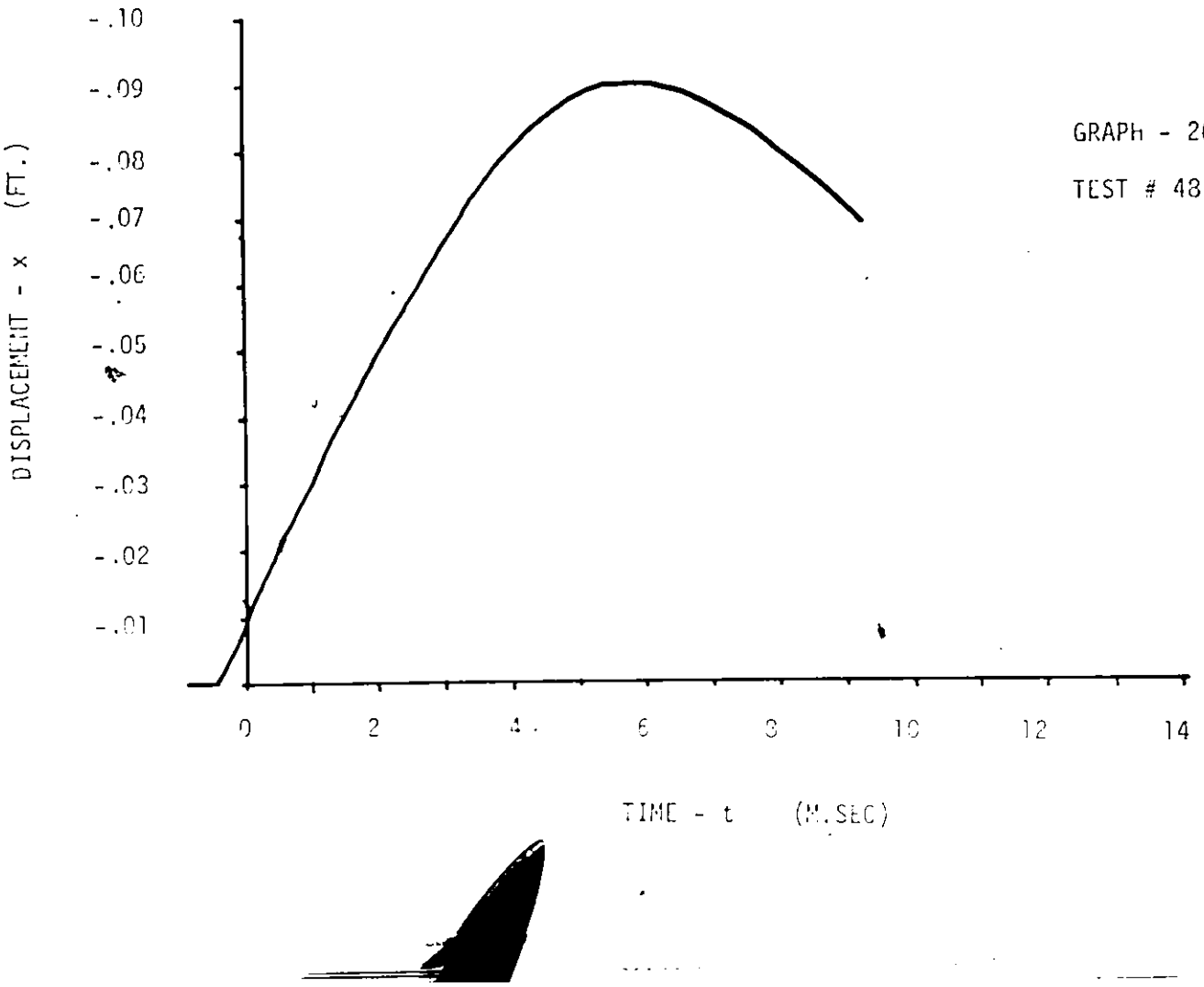

GRAPh - 26 t VS x

TEST # 48 TRACE # 185

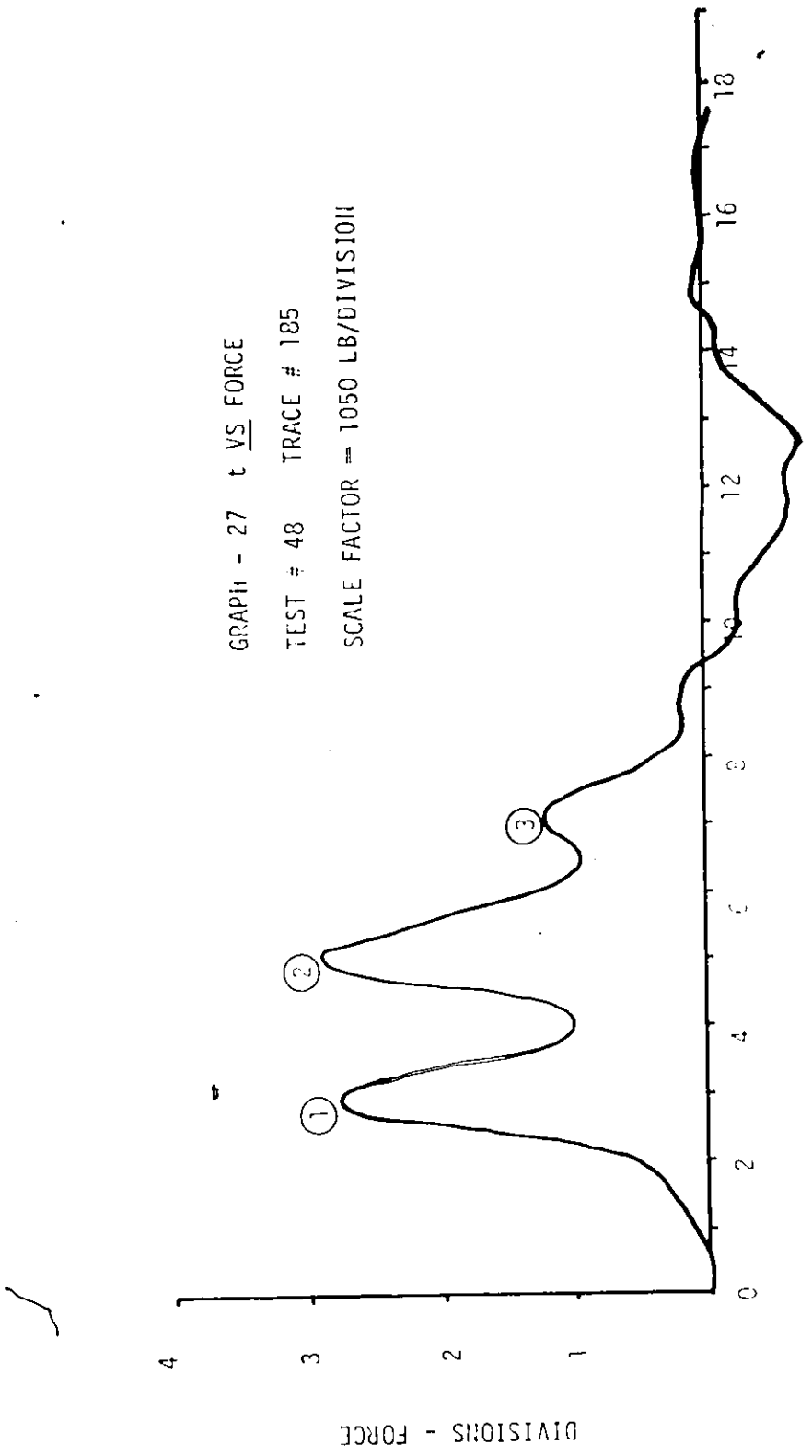
GRAPH - 27 t VS FORCE
TEST # 48 TRACE # 185
SCALE FACTOR = 1050 LB/DIVISION
DIVISIONS - FORCE
TIME - t (M.SEC)
0
2
4
8
12
14
16
18
1
2
3
4
①
②
③

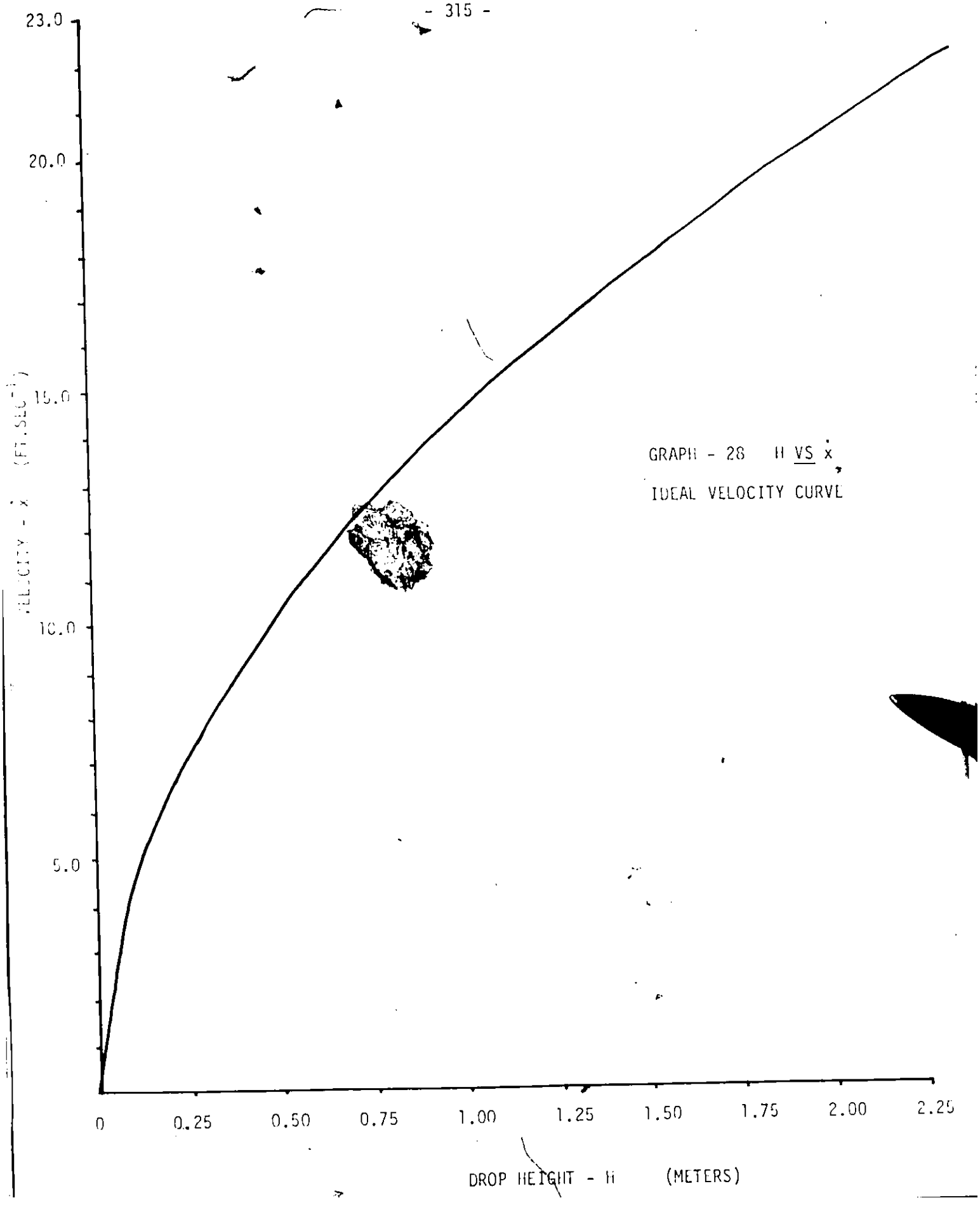

GRAPH - 28 H VS $\dot{x}$

IDEAL VELOCITY CURVE

GRAPH - 29 H VS t

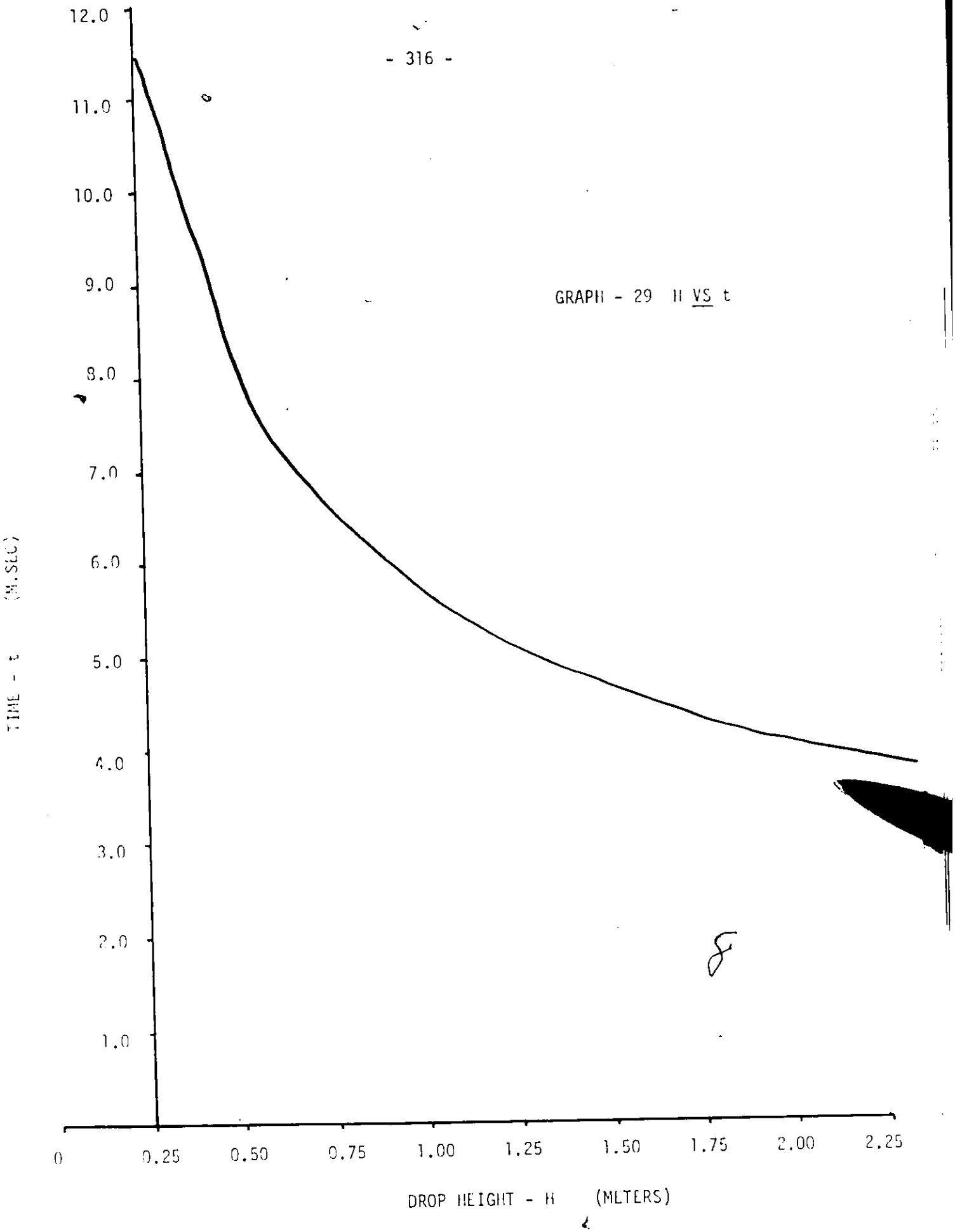

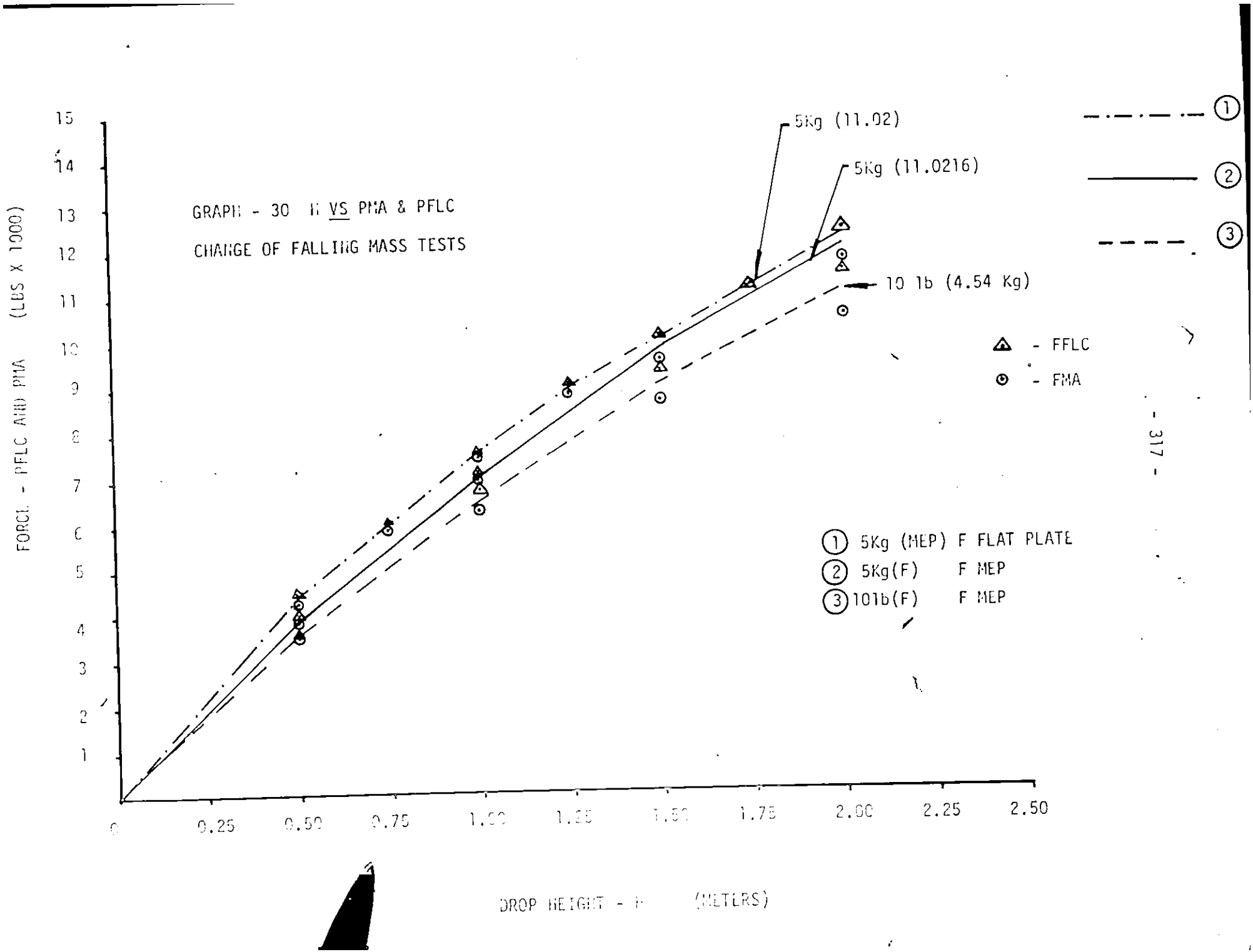
GRAPH - 30 H VS PMA & PFLC
CHANGE OF FALLING MASS TESTS
FORCE - PFLC AND PMA (LBS X 1000)
DROP HEIGHT - H (METERS)
5Kg (11.02)
5Kg (11.0216)
10 lb (4.54 Kg)
- FFLC
- FMA
① 5Kg (MEP) F FLAT PLATE
② 5Kg(F) F MEP
③ 10lb(F) F MEP
15
14
13
12
11
10
9
8
7
6
5
4
3
2
1
0
0.25
0.50
0.75
1.00
1.25
1.50
1.75
2.00
2.25
2.50

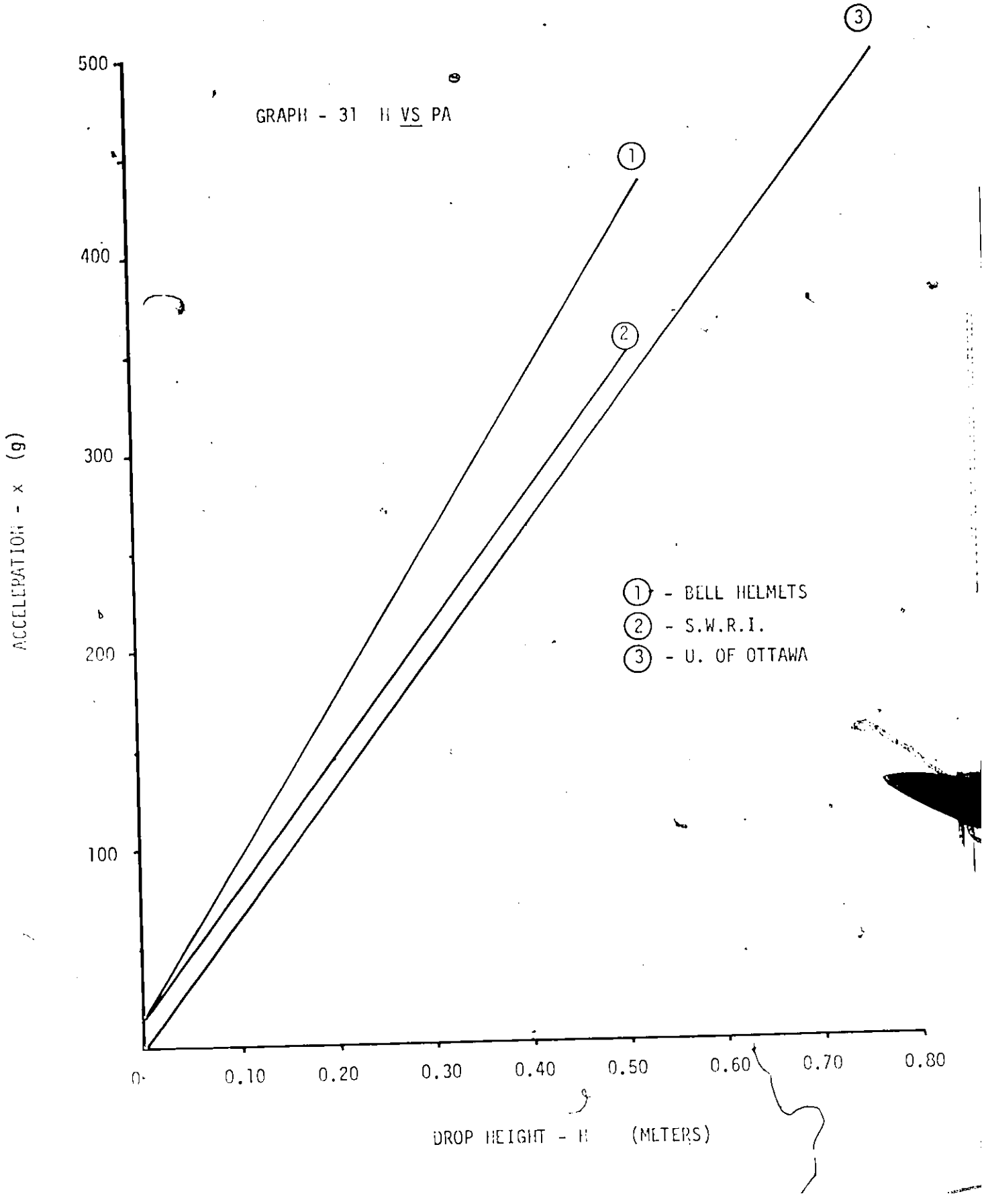
GRAPH - 31 H VS PA
ACCELERATION - x (g)
500
400
300
200
100
0
0.10
0.20
0.30
0.40
0.50
0.60
0.70
0.80
DROP HEIGHT - H (METERS)
1
2
3
1 - BELL HELMETS
2 - S.W.R.I.
3 - U. OF OTTAWA

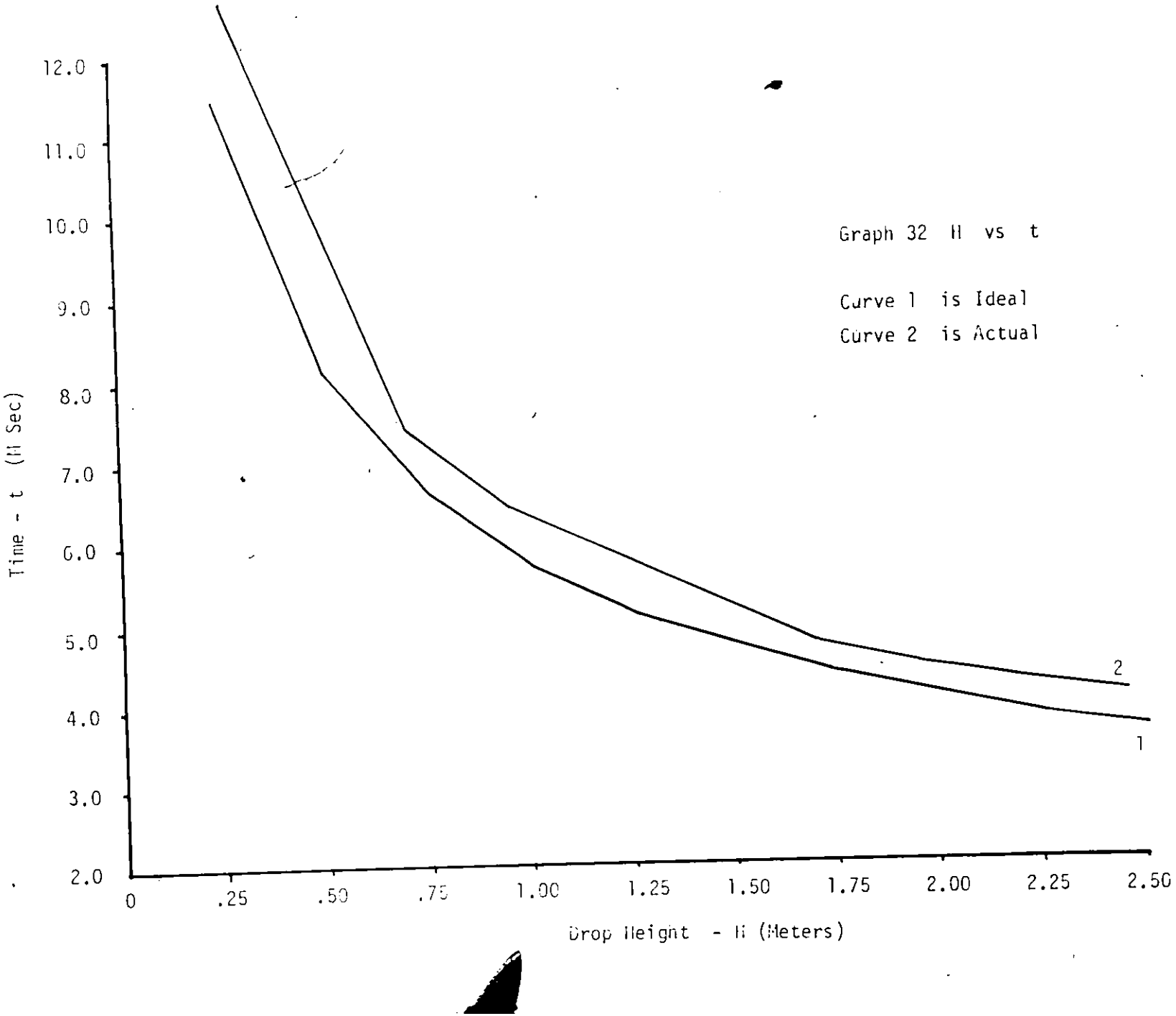

Graph 32 H vs t

Curve 1 is Ideal

Curve 2 is Actual

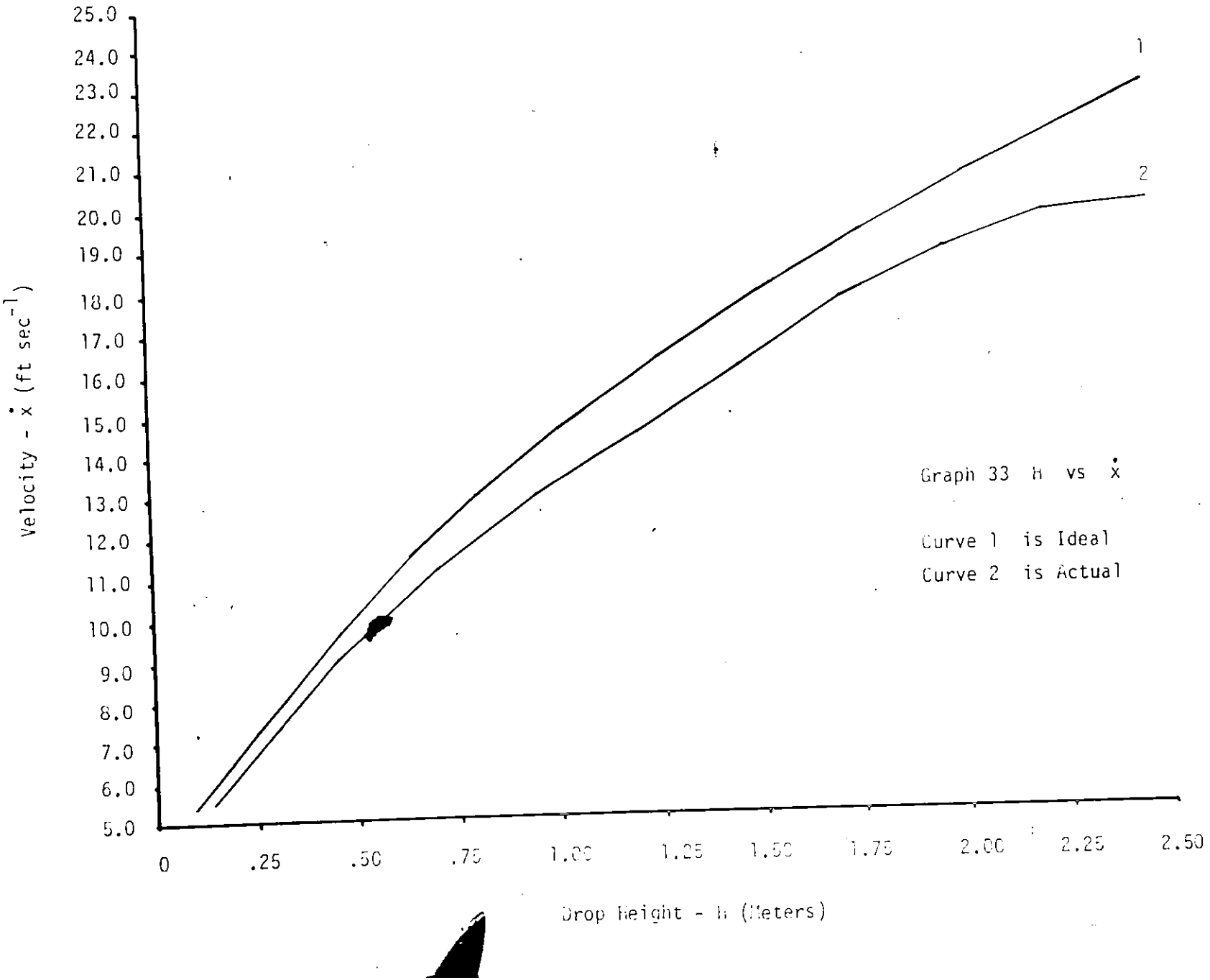

Graph 33 h vs $\dot{x}$

Curve 1 is Ideal

Curve 2 is Actual

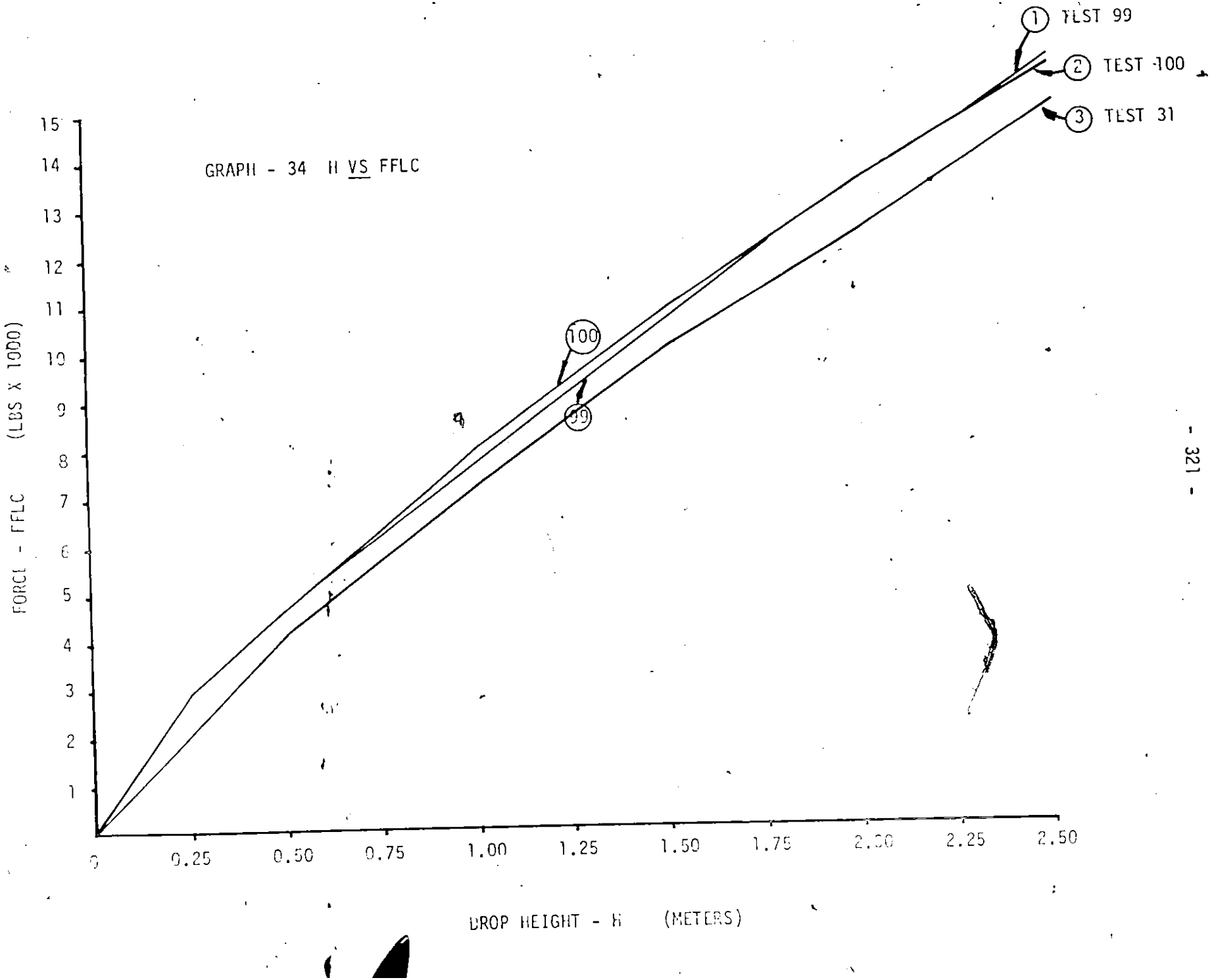
GRAPH - 34 H VS FFLC
1 TEST 99
2 TEST 100
3 TEST 31
100
99
FORCE - FFLC (LBS X 1000)
15
14
13
12
11
10
9
8
7
6
5
4
3
2
1
0
0.25
0.50
0.75
1.00
1.25
1.50
1.75
2.00
2.25
2.50
DROP HEIGHT - H (METERS)

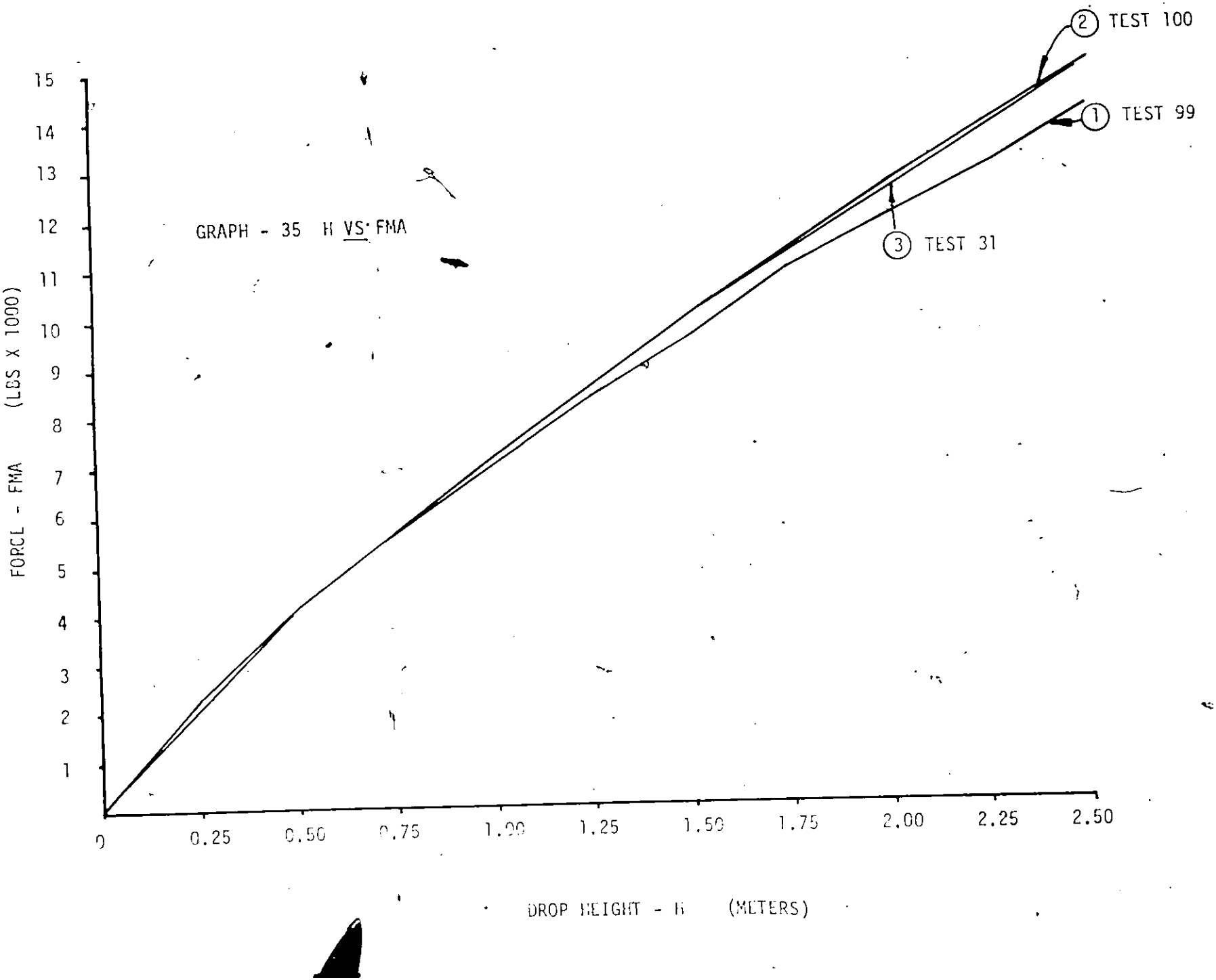
GRAPH - 35 H VS FMA
FORCE - FMA (LBS X 1000)
15
14
13
12
11
10
9
8
7
6
5
4
3
2
1
0
0.25
0.50
0.75
1.00
1.25
1.50
1.75
2.00
2.25
2.50
DROP HEIGHT - H (METERS)
2 TEST 100
1 TEST 99
3 TEST 31

VI-5 TIME TRACES OF TESTS

TOP TRACE IS LOADCELL

BOTTOM TRACE IS ACCELLROMETER

t_d = 1 m.sec/div (UNLESS SPECIFIED) BY * AFTER TRACE #

H = Meters

POLAROID TRACE NO.	TEST NO.	DROP HEIGHT (H)	IMPACT DESCRIPTION		
102	24	2.00	MEP	F	F.P.
103		1.50			
104		1.00			
105		0.50			
106		2.00			
108		1.50			
109	26	2.00	MEP	F	H.S. WITH SLOTTED PLATE
110		1.50			
111		1.00			
112		0.50			
113	27	2.25	MEP	F	H.S. WITH SLOTTED PLATE AND LEAD DISC
114		1.50			
115		1.00			
116		0.50			
118	29	2.25	MEP	F	CAST AL. (TH1H)
119		2.00			
120		1.50			
121		1.00			
122		0.50			
123	30	2.00	5Kg(F)	F	CAST AL. (TH1H)
124	33	2.00	MEP	F	HEMISPHERICAL ANVIL
125	34	2.25	MEP	F	CSA-W-L-C
126		2.00			
127		1.50			
128		1.00			
129		0.50			

POLAROID TRACE NO.	TEST NO.	DROP HEIGHT	IMPACT DESCRIPTION
130	35	2.00	MEP F CSA-W-L-B
131		1.50	
132		1.00	
133		0.50	
134	36	2.00	MEP F CSA-W-S-C
135		1.50	
136		1.00	
137		0.50	
138	37	2.00	MLP F CSA-W-S-B
139		1.50	
140		1.00	
141		0.50	
142-R	38-1	2.00	MLP F CSA-P-L
143-R	38-1	1.50	
142	38	2.00	MLP F CSA-P-L
143		1.50	
144		1.00	
145		0.50	
146	39	2.00	MLP F CSA-P-L
147		1.50	
148		1.00	
149		0.50	
150	40	2.00	MLP F CSA-P-S
151		1.50	
152		1.52	
153		1.53	
154	41	1.66	MLP F SP-W-H.F.
155	42	2.00	MLP F SP-W-H.F.
156		1.50	
157		1.00	
158		0.50	
159	43	2.00	MLP F CAST AL. (THICK)
160		1.50	
161		1.00	
162		0.50	

POLAROID TRACE NO.	TEST NO.	DROP HEIGHT	IMPACT DESCRIPTION
163	44	2.00	MLP F SILRRA
164		1.50	
165		1.00	
166		0.50	
167	45	2.00	MLP F Z90.1
168		1.50	
169		1.00	
170		0.50	
171	46*	0.50	5Kg(F) F Z90.1
172		1.00	*(2 m.sec/div)
173		1.50	
174		2.00	
175		2.50	
176	47*	0.50	5Kg(F) F CAST AL. (THIN)
177		1.00	*(2 m.sec/div)
178		1.50	
179		2.00	
180		2.50	
181	48*	0.50	5Kg(F) F SILRRA
182		1.00	*(2 m.sec/div)
183		1.50	
184		2.00	
185		2.50	
186	49*	0.50	5Kg(F) F CSA-P-L
187		1.00	*(2 m.sec/div)
188		1.50	
189		2.00	
190		2.50	
191	50*	0.50	5Kg(F) F CSA-W-L-B
192-A		1.00	*(2 m.sec/div)
192-B		1.00	
192-C		1.00	
192-D		1.00	
193		1.50	
194-A		2.00	
194-B		2.00	
196		2.50	
195-B		2.50	

POLAROID TRACE NO.	TEST NO.	DROP HEIGHT	IMPACT DESCRIPTION
196-1	51	2.00	MLP F HEMISPHERICAL ANVIL CHECK
197	52	2.00	MLP F FLAT PLATE CHECK
198	53*	2.00	5Kg(F) F Z90.1 *(2 m.sec/div)
199	54*	2.00	5Kg(F) F Z90.1 *(2 m.sec/div)
201	55*	1.00	5Kg(F) F CADAVER 1 WITH HELMET *(2 m.sec/div)
202		1.50	
203		2.00	
204		2.50	
205	56	0.50	5Kg(MLP) F CADAVER 1 WITH HELMET
206		1.50	
207	57	2.00	MLP F FLAT PLATE CHECK
207-1	58	0.50	5Kg(F) F CADAVER 2 WITH HELMET *(2 m.sec/div)
208		1.00	
209		1.50	
210		2.00	
211*		2.50	
212	59*	0.15	5Kg(F) F CADAVER 2 WITHOUT HELMET *(2 m.sec/div)
213		0.30	
214	60	2.25	MLP F SIERRA OCCIPITAL
215		2.00	
216		1.75	
217		1.50	
218		1.00	
219		0.50	
220	61	2.25	MLP F SIERRA PARIETAL R.S.
221		2.00	
222		1.50	
		1.00	
223		0.50	

POLAROID TRACE NO.	TEST NO.	DROP HEIGHT	IMPACT DESCRIPTION
224	62	2.25 2.00 1.50	MLP F SILRRA PARIETAL L.S.
225		1.00 0.50	
226	63	2.25 2.00 1.50 1.25 1.00 0.50	MLP F SILRRA FRONTAL
227	64	2.25 2.00 1.50 1.00 0.50	MLP F CSA-P-L FRONTAL
228	65	2.25 2.00 1.50 1.00 0.50	MLP F CSA-P-L OCCIPITAL
229 230	66	2.25 2.25 2.25	MLP F CSA-P-L PARIETAL R.S.
231	67-1	1.50	MLP F EBAR PLATE ($\bar{e}$ = 0.00)
232	67-2	1.50	MLP F EBAR PLATE ($\bar{e}$ = 0.50)
233	67-3	1.50	MLP F EBAR PLATE ($\bar{e}$ = 1.00)
234	67-4	1.50	MLP F EBAR PLATE ($\bar{e}$ = 1.50)
235	66	2.25	MLP F CSA-P-L PARIETAL R.S.
69-1	69	1.52	101b(F) F SP-W-H.F. , MINING HELMETS
69-2*-1		1.52	*-1 (2 m.sec/div)
69-3*-2		1.52	*-2 (5 m.sec/div)
69-4*-3		1.22	*-3 (5 m.sec/div)
69-5*-4		1.22	*-4 (5 m.sec/div)

POLAROID TRACE NO.	TEST NO.	DROP HEIGHT	IMPACT DESCRIPTION
69-6*-5		1.22	*-5 (5 m.sec/div)
69-7*-6		1.22	*-6 (5 m.sec/div)
69-8*-7		1.22	*-7 (5 m.sec/div)
69-9*-8		1.22	10lb(F) F SP-W-H.F.(*-8) (5 m.sec/div)
69-10*-9		1.22	10lb(F) F SP-W-H.F.(*-9) (5 m.sec/div)
69-11*-10		1.22	10lb(F) F SP-w-H.F.(*-10) (5 m.sec/div)
236	70	2.25 2.00 1.50 1.00 0.50	MLP F CSA-P-L PARIETAL L.S.
237	71	2.25 2.00 1.50 1.00 0.50	MEP F CSA-P-L PARIETAL R.S.
238*	72	0.50	5Kg(F) F CSA-P-L PARIETAL L.S.
239		1.00	*(2 m.sec/div)
240		1.50	
241		2.00	
242*	73	0.50	5Kg(F) F CADAVER 3 FRONTAL WITH HELMET *(2 m.sec/div)
246	75	0.25	5Kg(*) F MEP (* - SHELL HEAD FORM)
247		0.19	
248		0.38	
249		0.38	
250		0.51	
251		0.51	
252		0.25	
253		0.19	
254		0.13	
255		0.64	
256		0.64	
257		0.64	

POLAROID TRACE NO.	TEST NO.	DROP HEIGHT	IMPACT DESCRIPTION
258	76	0.50 1.00	5Kg(F) F MLP (SHELL)
259		1.50	
260		2.00	
259-1	77	1.00	10lb(F) F MLP (SHELL)
260-1		1.50	
261		2.00	
262	78	0.50 1.00	MLP F LBAR PLATE , ($\bar{e}$ = 0.00)
263		1.50	
264		2.00	
265	79	0.50 1.00 1.50	MLP F LBAR PLATE , ($\bar{e}$ = 0.00)
266		2.00	
267	80	0.50 1.00 1.50	MLP F LBAR PLATE , ($\bar{e}$ = 0.50)
268		2.00	
269	81	0.50 1.00 1.50	MLP F LBAR PLATE , ($\bar{e}$ = 1.00)
270		2.00	
271	82	0.50 1.00 1.50 2.00	MLP F LBAR PLATE, ($\bar{e}$ = 1.50)
272	83	0.50 1.00 1.50 2.00	MLP F LBAR PLATE , ($\bar{e}$ = 1.75)
273	85	0.50 1.00	MLP F SP-W-H.F. , ($\bar{e}$ = 0.00)
274		1.50 2.00	

POLAROID TRACE NO.	TEST NO.	DROP HEIGHT	IMPACT DESCRIPTION
275	86	0.50	MLP F SP-W-H.F. , ($\bar{e}$ = 0.00)
276		1.00	
277		1.50	
278		2.00	
279	87	0.50	MLP F SP-W-H.F. , ($\bar{e}$ = 0.50)
		1.00	
280		1.50	
		2.00	
281	88	0.50	MLP F SP-W-H.F. , ($\bar{e}$ = 1.00)
		1.00	
282		1.50	
		2.00	
283	89	0.50	MLP F SP-W-H.F. , ($\bar{e}$ = 1.50).
		1.00	
284		1.50	
		2.00	
285(a)	90	0.50	5Kg(F) F CADAVER 4 FRONTAL WITH HELMET
285(b)		0.50	
286*-1		1.00	*-1 (2 m.sec/div)
287*-2		1.50	*-2 (2 m.sec/div)
288	91*	0.50	5Kg(F) F SILRRA FRONTAL
289		1.00	*(2 m.sec/div)
290		1.50	
291		2.00	
292	92*	1.50	5Kg(F) F CADAVER 4 WITH HELMET AND REINFORCED NECK 1
293		2.00	*(2 m.sec/div)
294	93*	0.50	5Kg(F) F- SIERRA FRONTAL
295		1.00	*(2 m.sec/div)
296		1.50	
297		2.00	
298	94*	0.50	5Kg(F) F CSA-P-L FRONTAL
299		1.00	*(2 m.sec/div)
300		1.50	
301		2.00	

POLAROID TRACE NO.	TEST NO.	DROP HEIGHT	IMPACT DESCRIPTION
302	95*	0.50	5Kg(F) F SIERRA OCCIPITAL
303		1.00	*(2 m.sec/div)
304		1.50	
305		2.00	
306		2.25	
307	96*	0.50	MEP F SIERRA OCCIPITAL WITH SUPPORT
308		1.00	*(2 m.sec/div)
309		1.50	
310		2.00	
311		2.25	
312	97*	2.00	5Kg(F) F SIERRA OCCIPITAL WITH SUPPORT AND HELMET
313		1.50	
314		1.00	*(2 m.sec/div)
312-1	98*	0.15	5Kg(F) F CADAVER 4 WITHOUT HELMET BUT WITH REINFORCED NECK 2
313-1		0.23	
314-1		0.30	*(2 m.sec/div)
315		0.38	
316		0.46	
317	99	0.50	5Kg(F) F MEP
318		1.00	
319		1.50	
320		2.00	
321		2.25	
322	100	0.50	5Kg(MEP) F FLAT PLATE
323		1.00	
324		1.50	
325		2.00	
326		2.50	

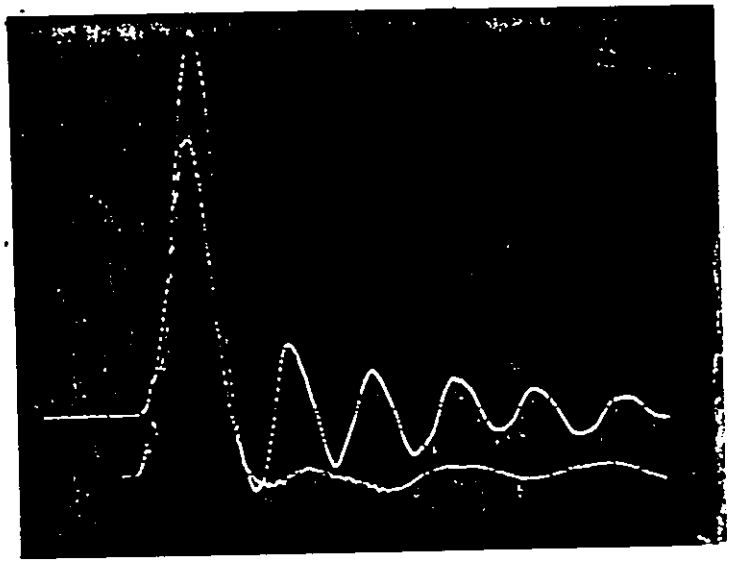

102

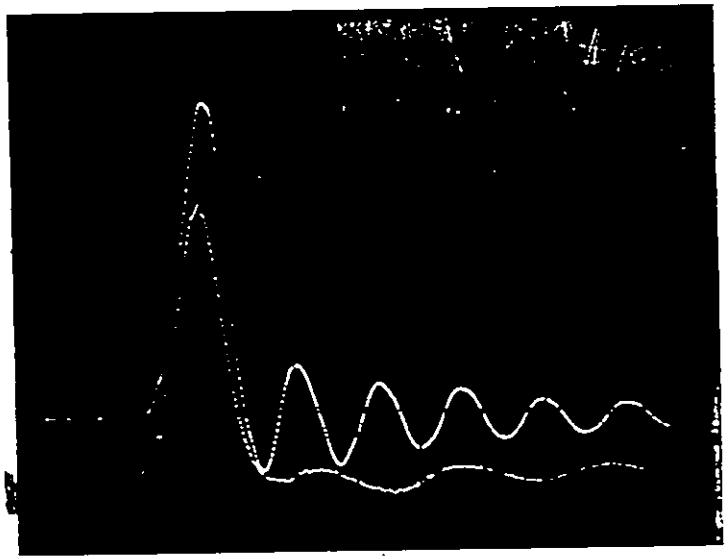

103

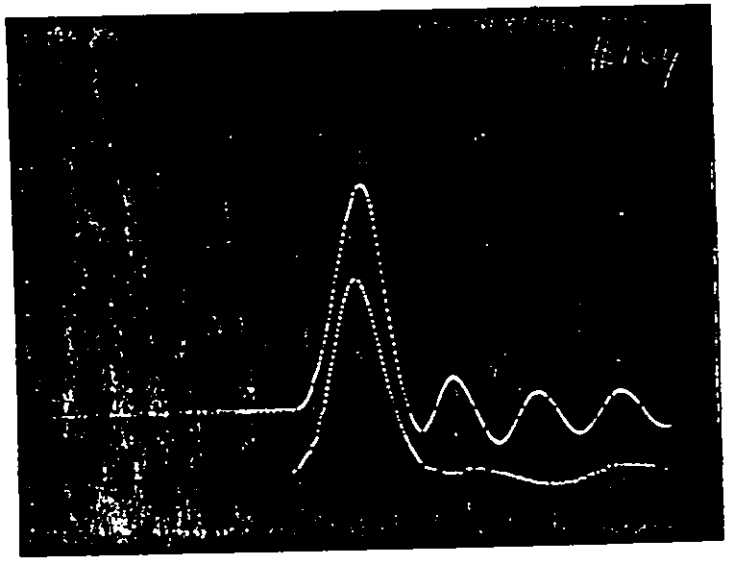

104

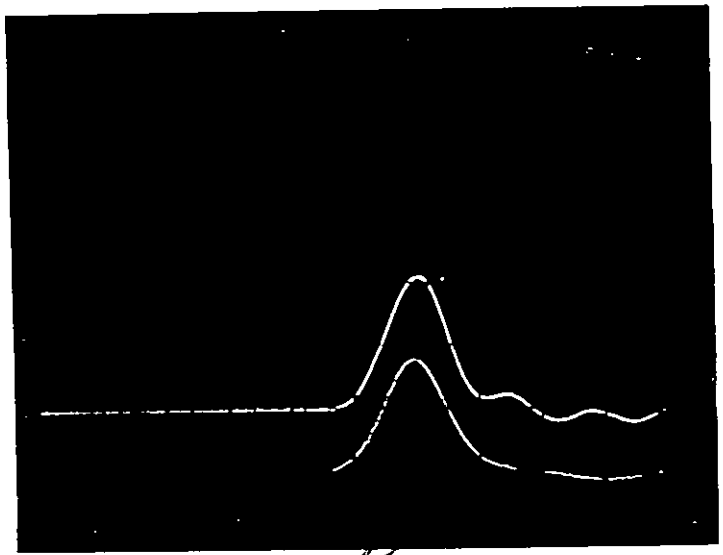

105

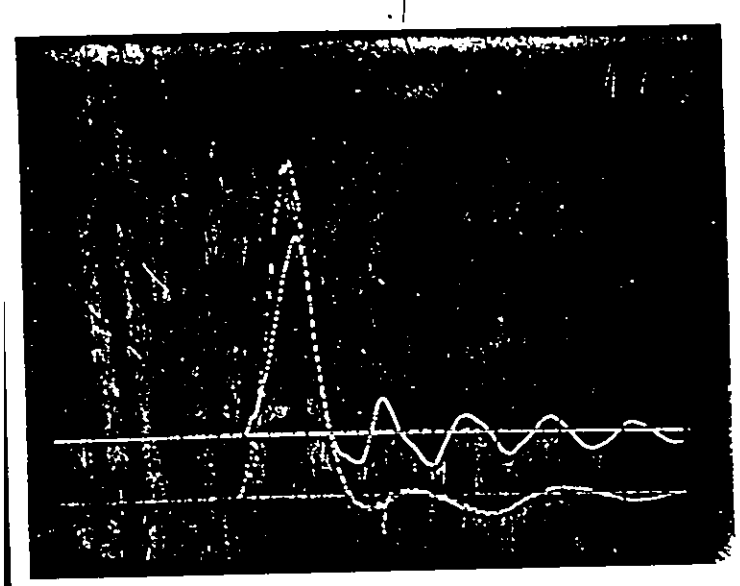

106

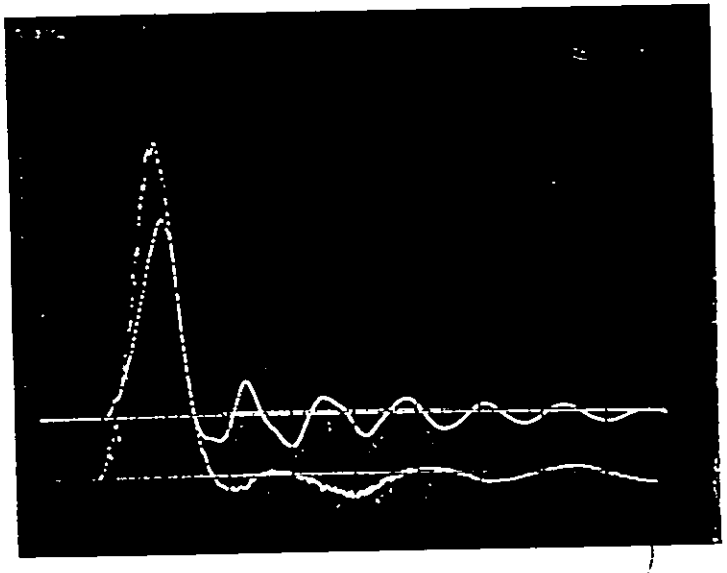

108

109

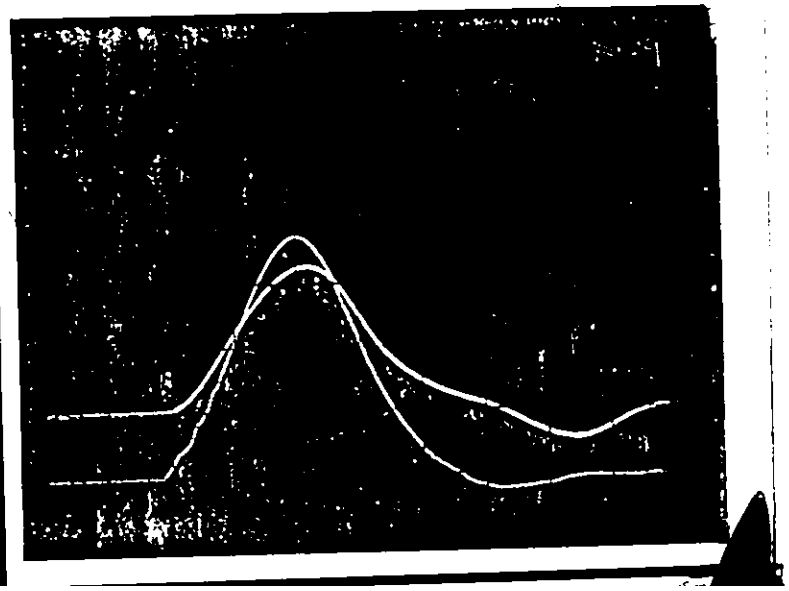

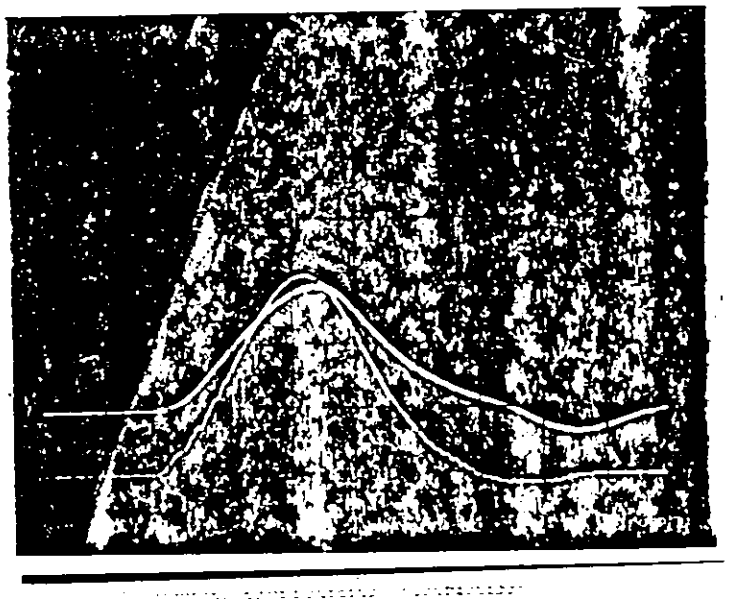

110

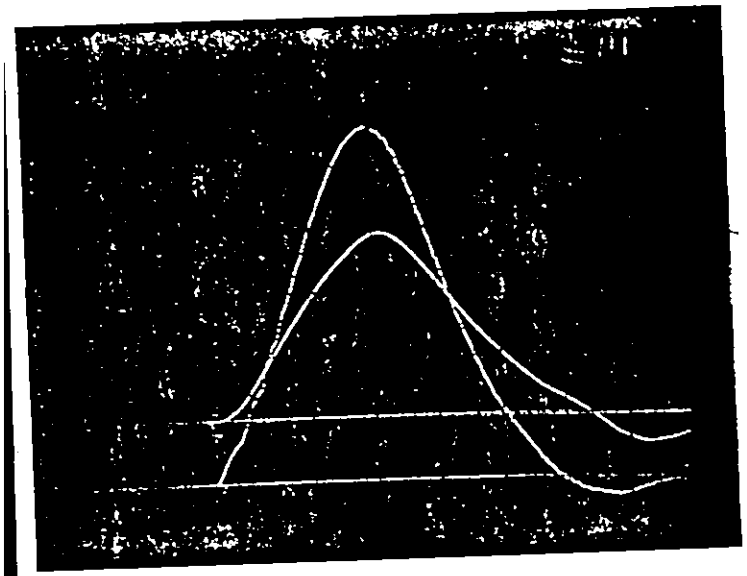

111

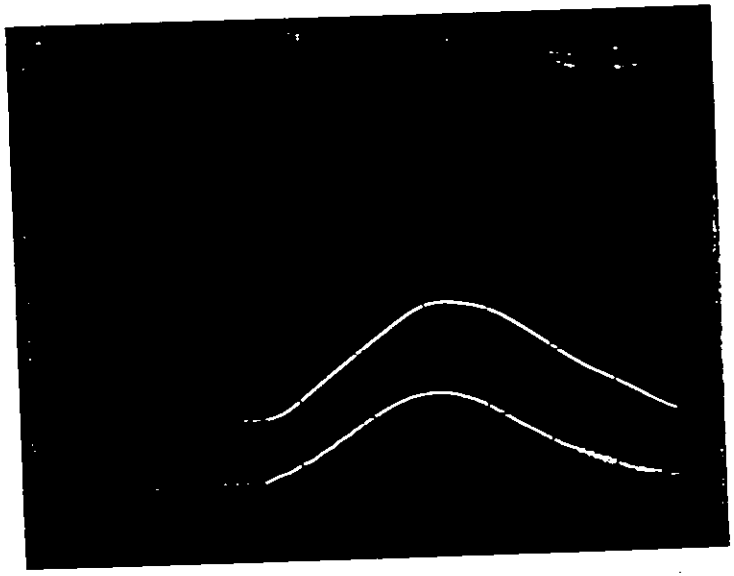

112

113

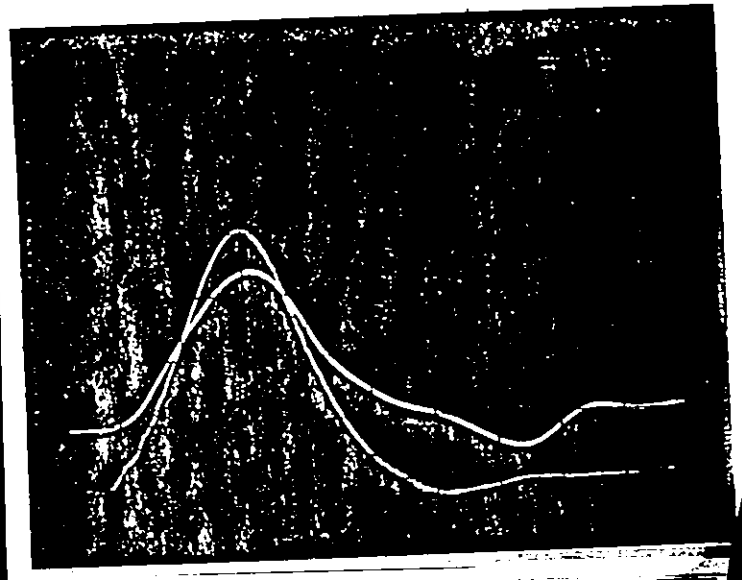

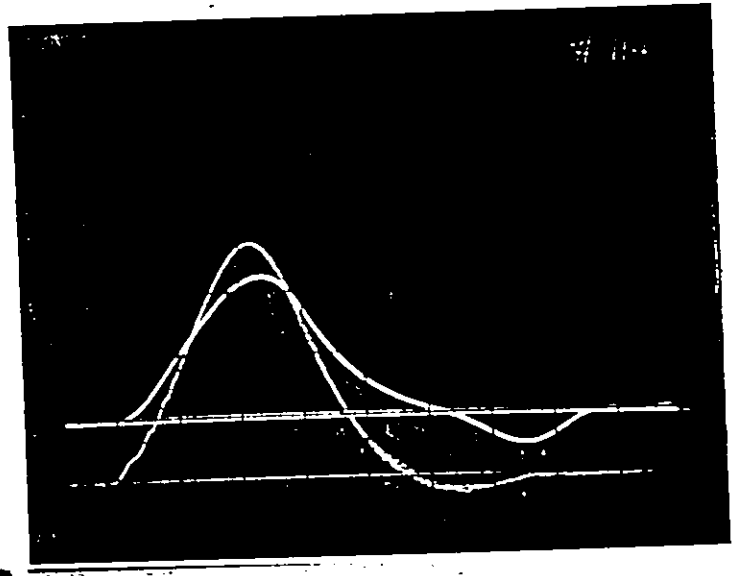

114

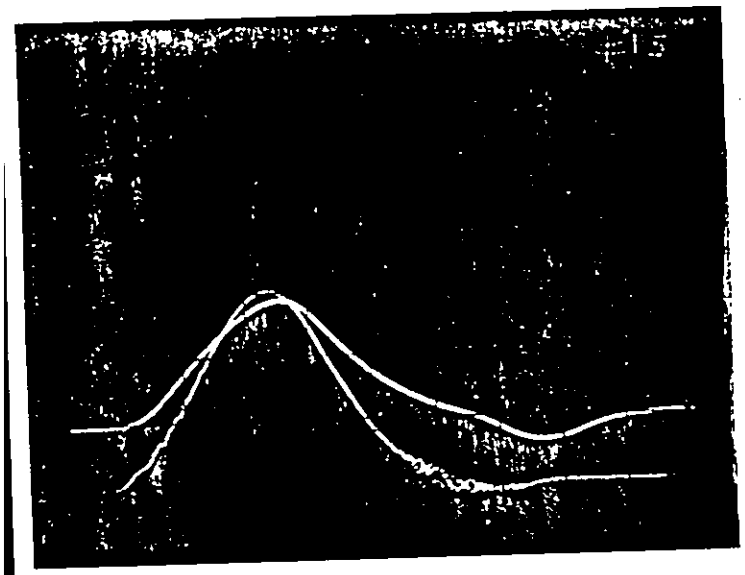

115

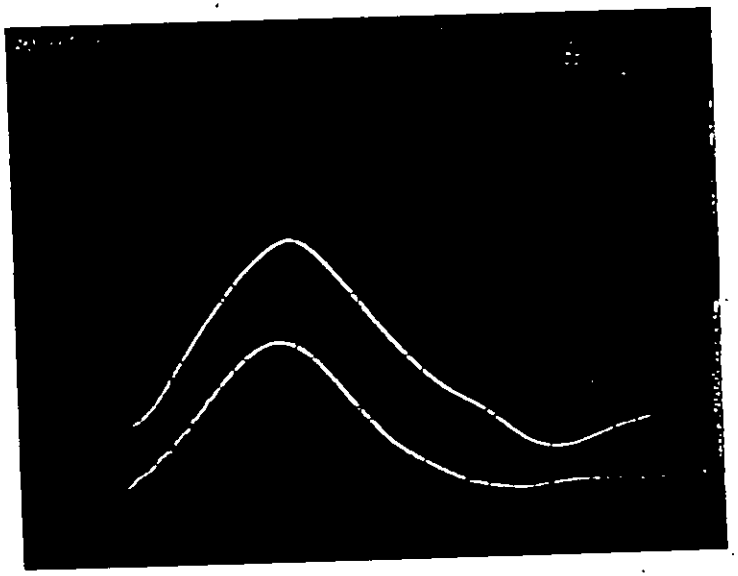

116

118

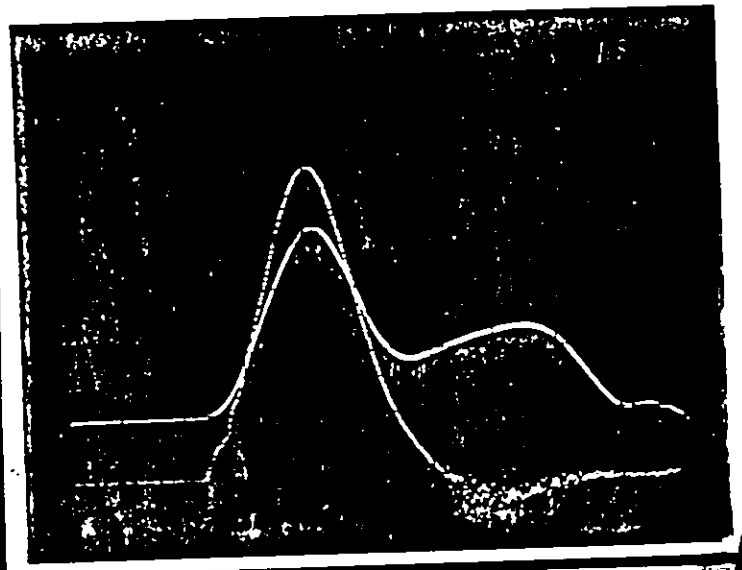

119

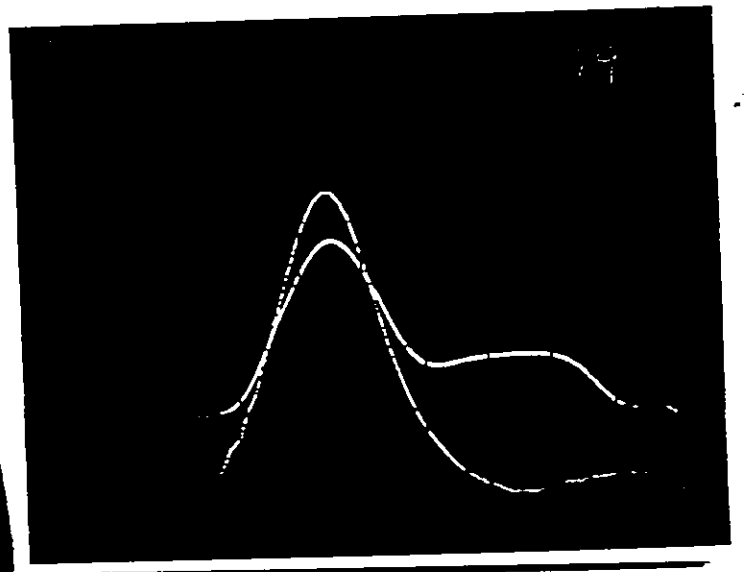

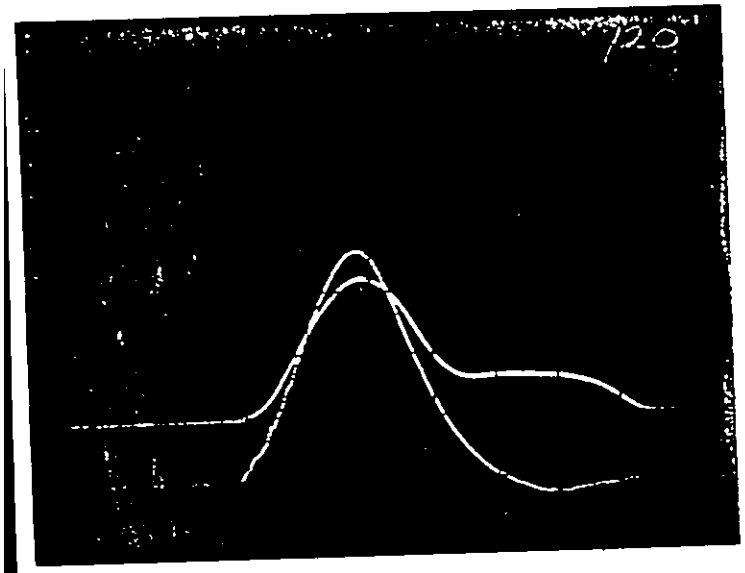

120

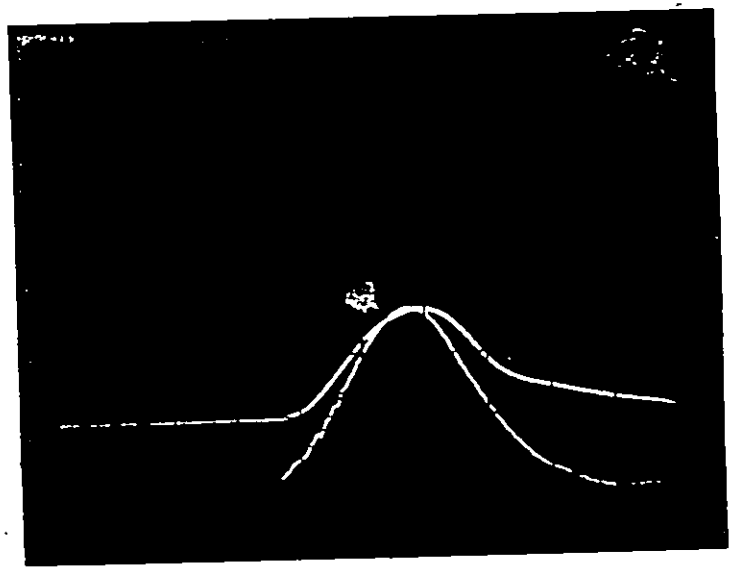

121

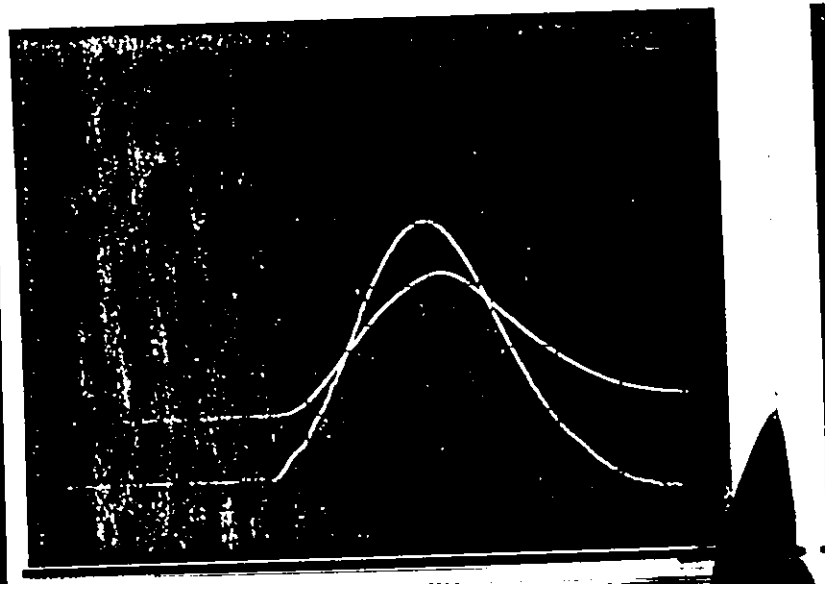

122

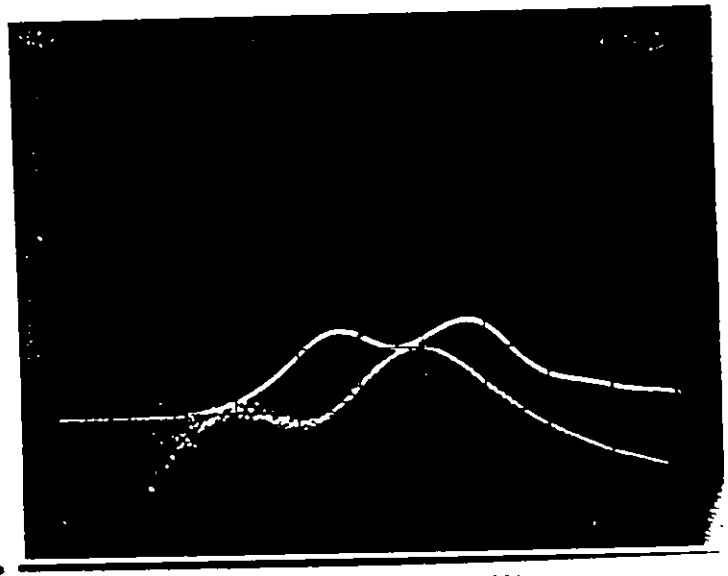

123

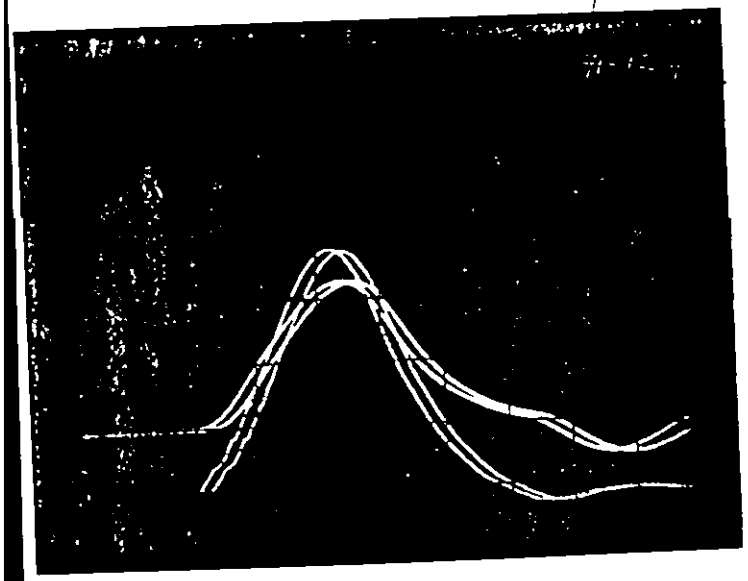

124

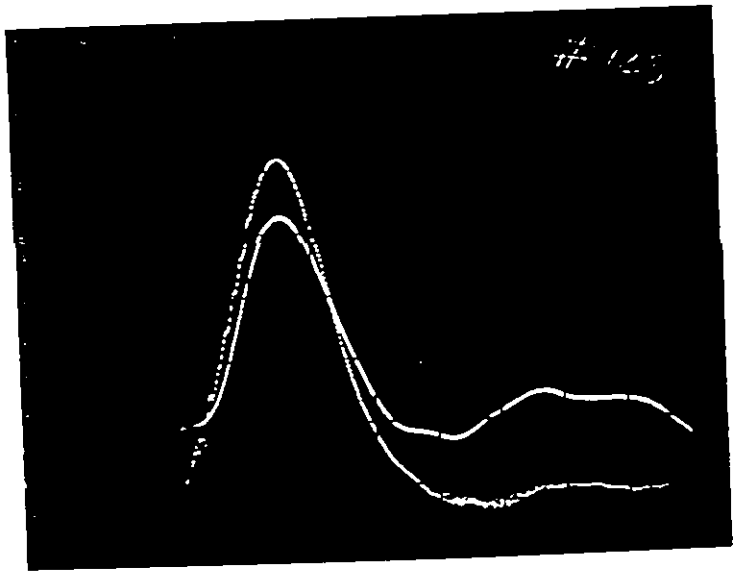

125

126

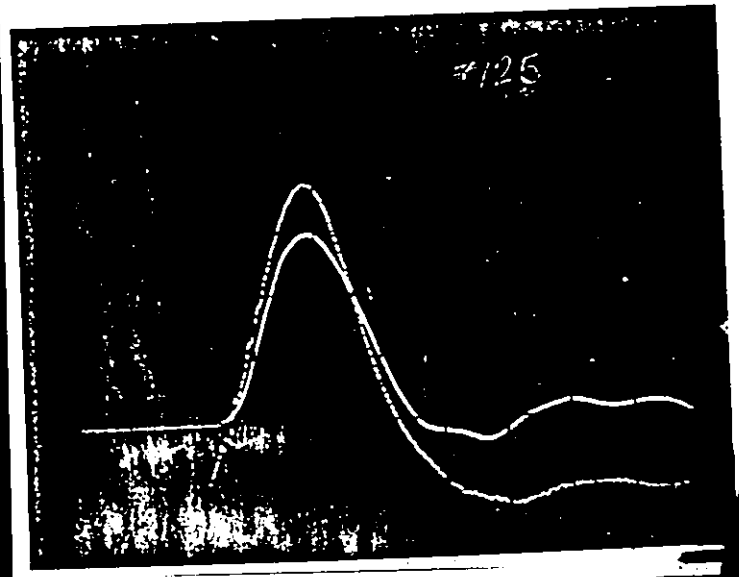

127

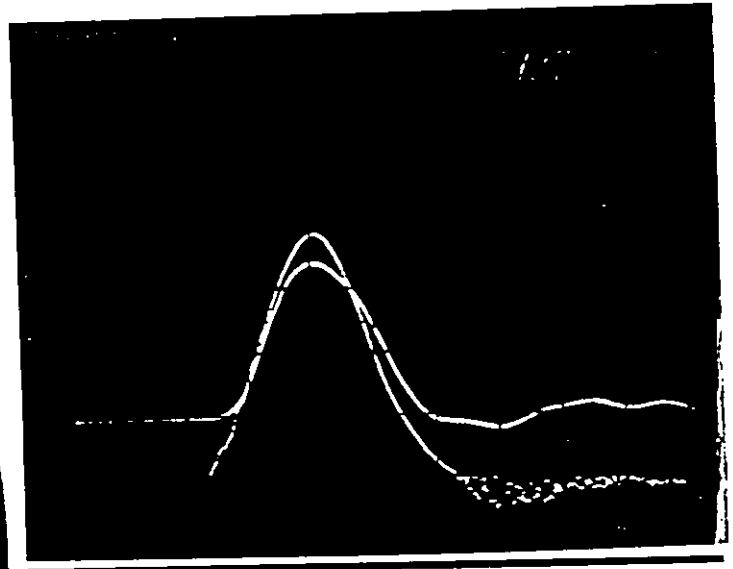

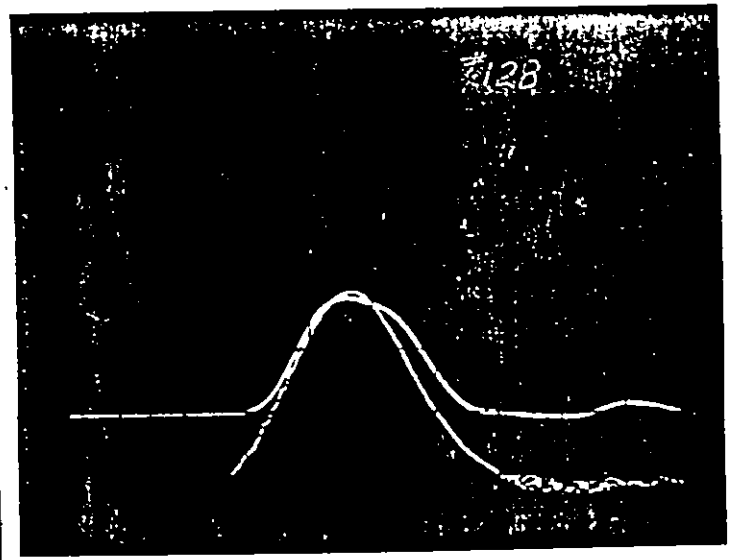

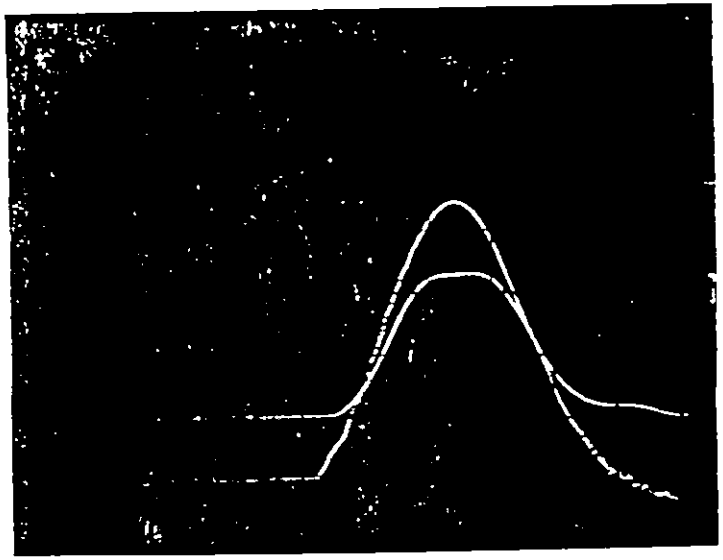

128 129

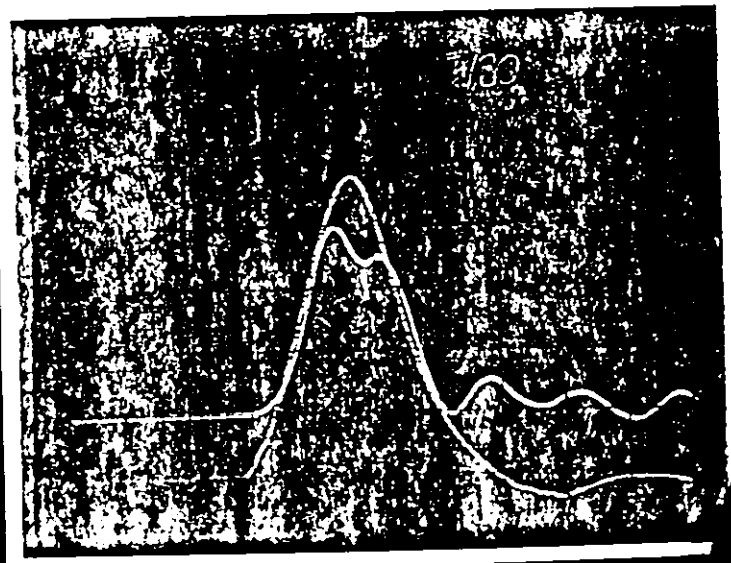

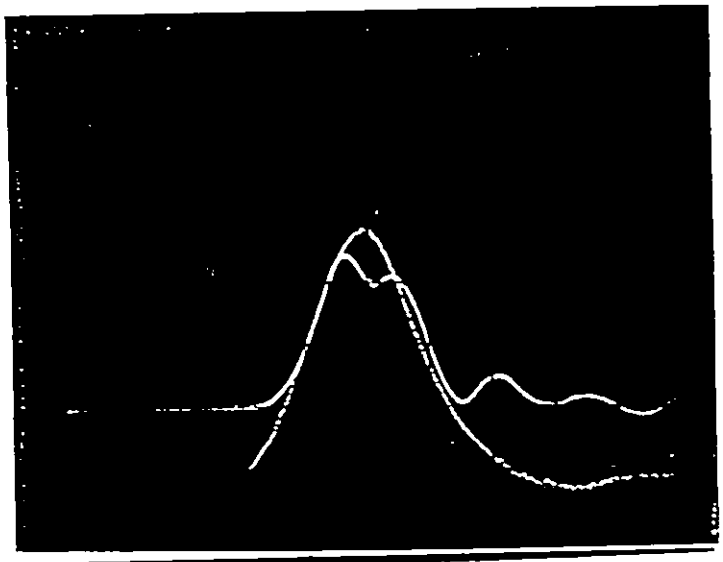

130 131

132 133

134 135

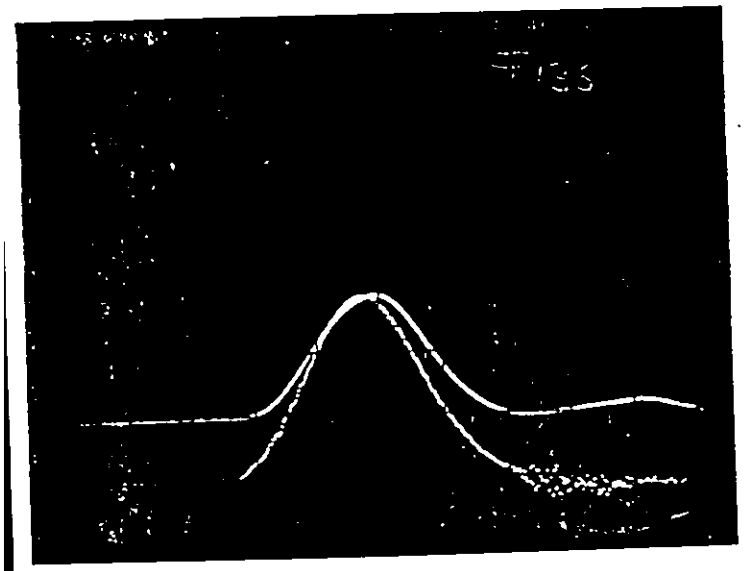

136

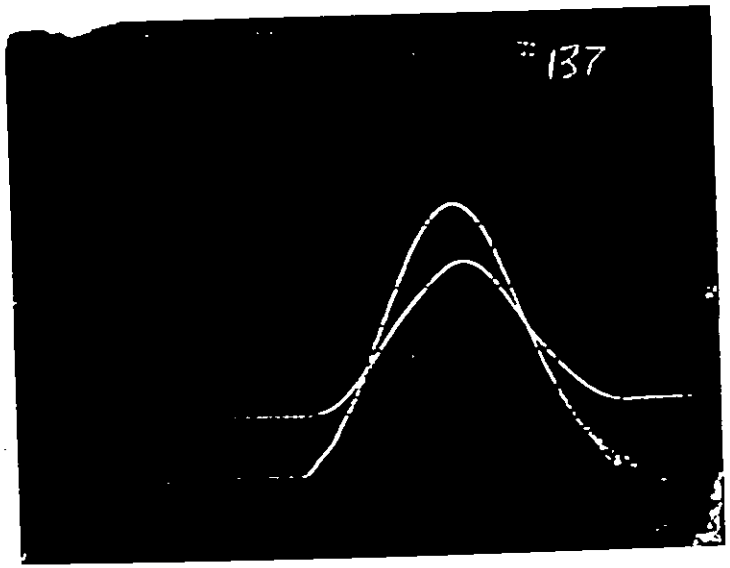

137

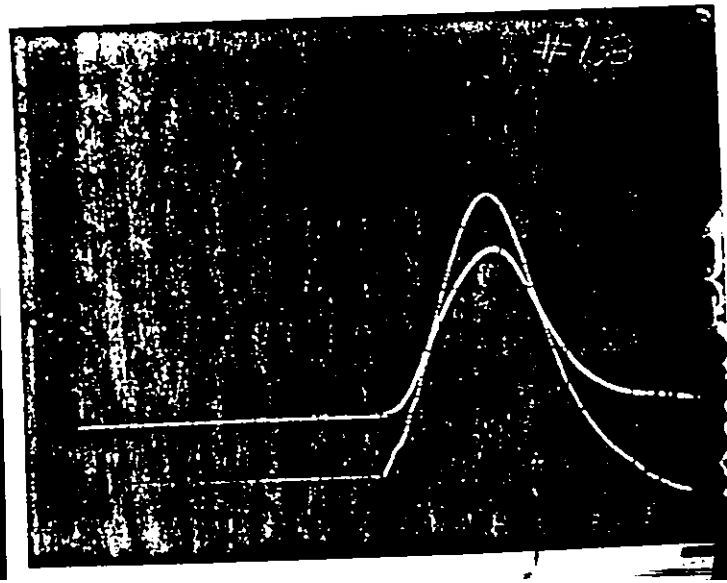

138

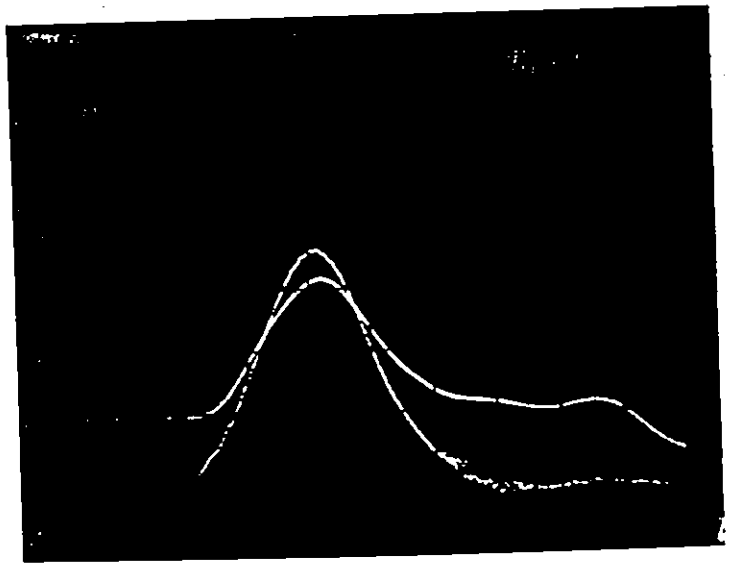

139

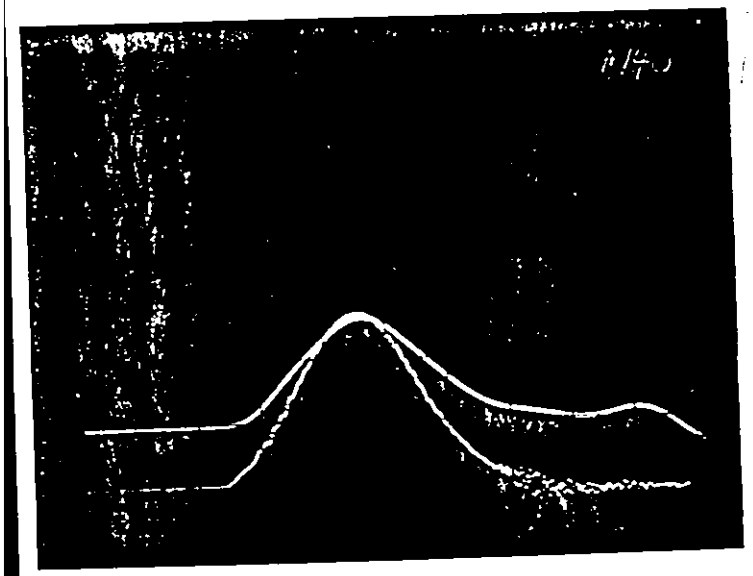

140

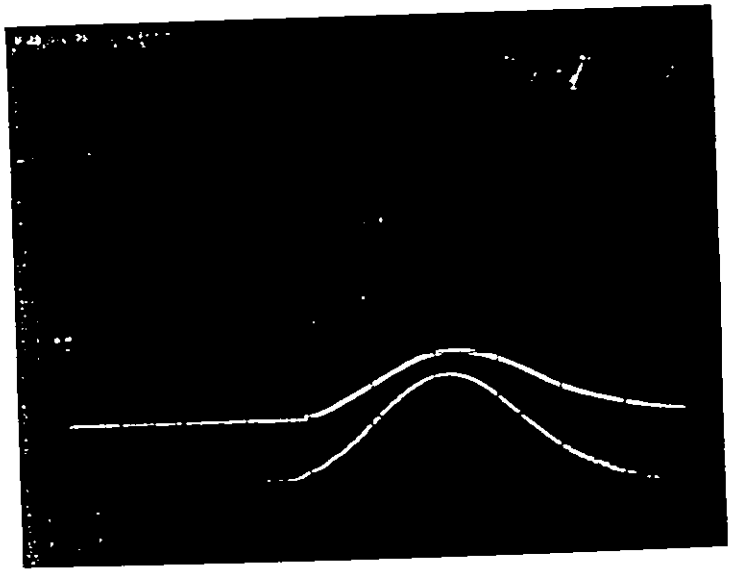

141

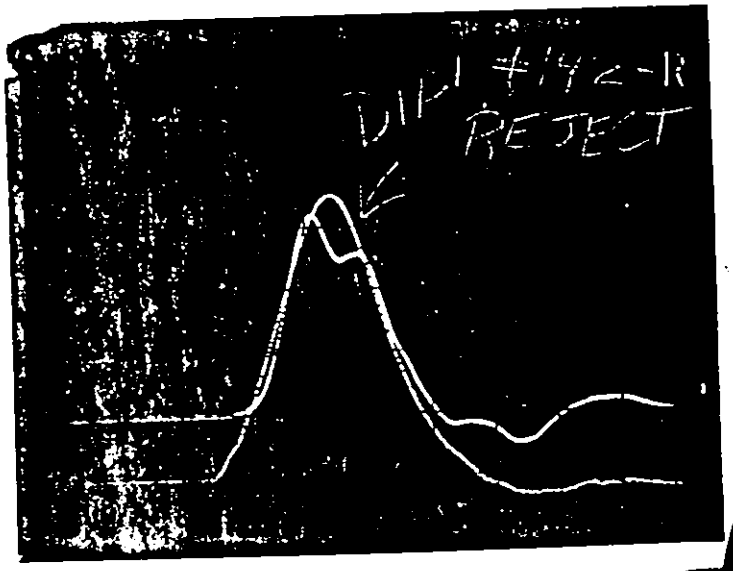

142R

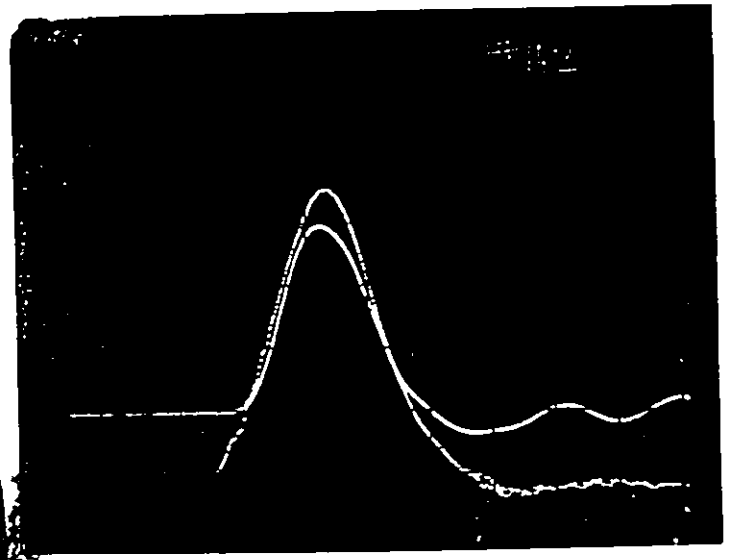

142

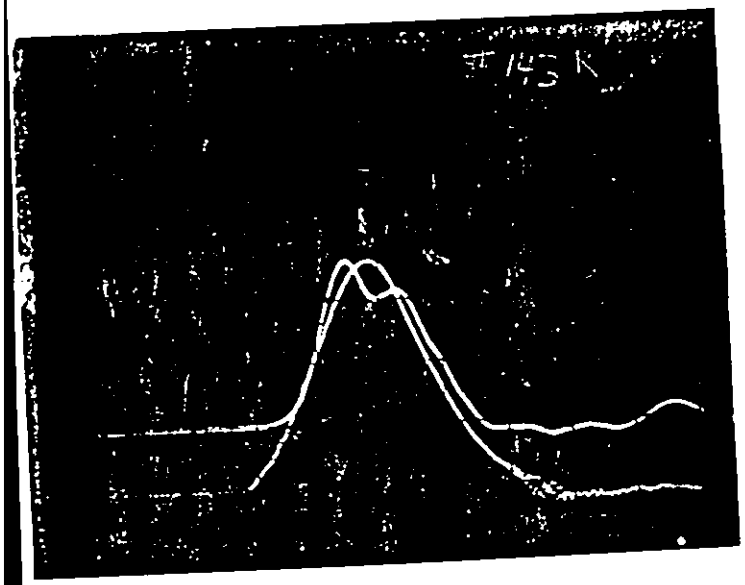

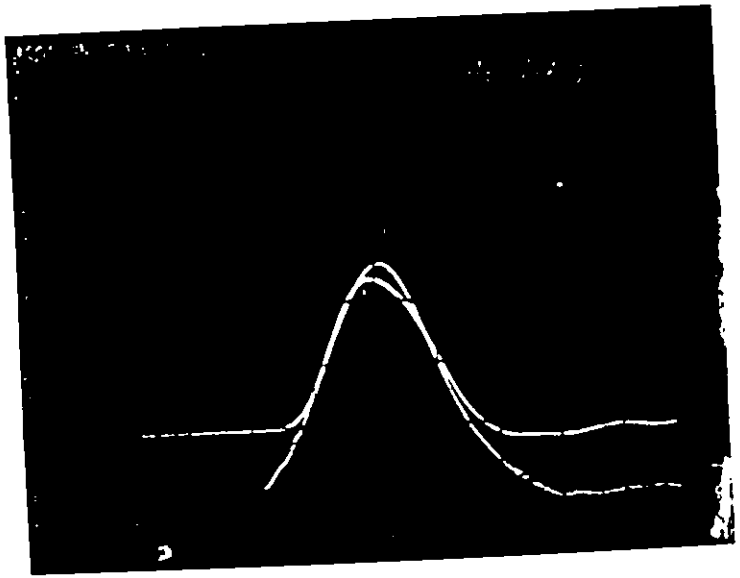

143R 143

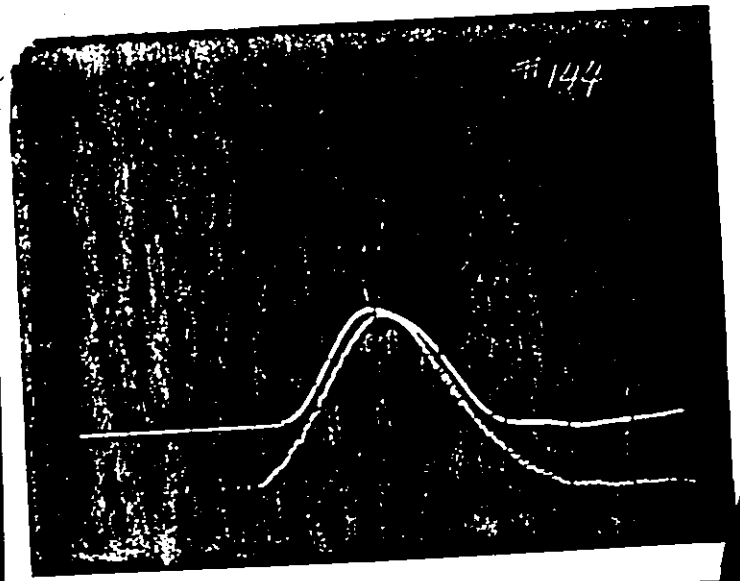

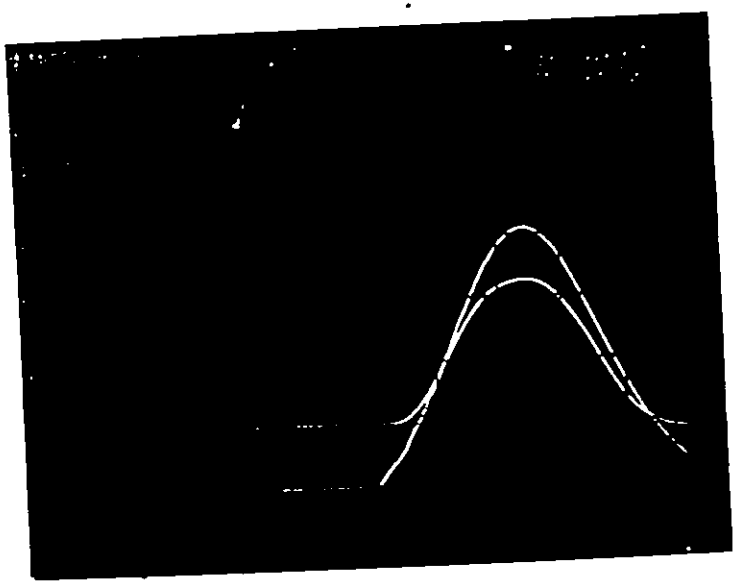

144 145

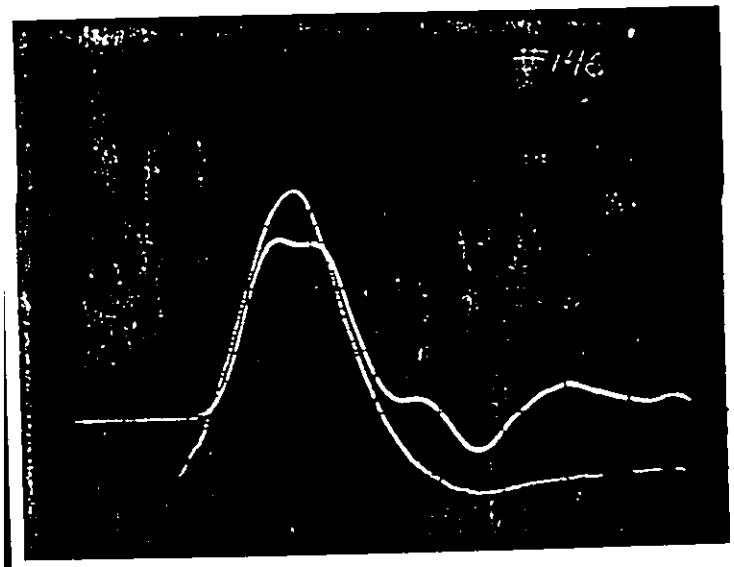

146

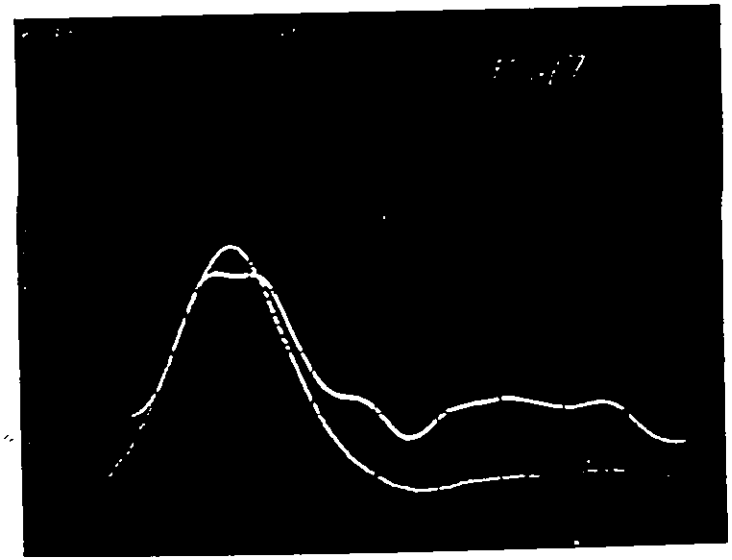

147

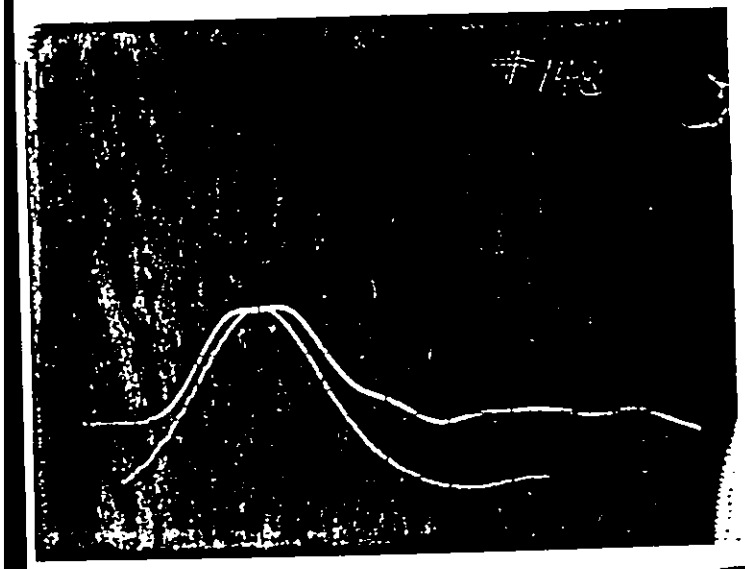

148

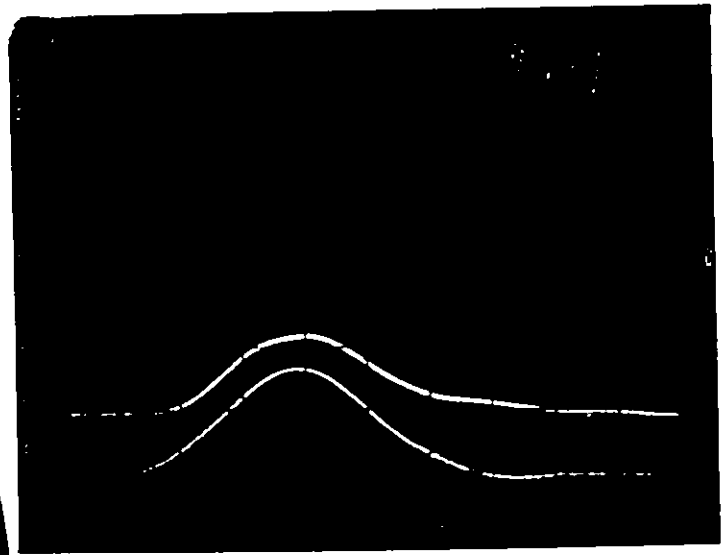

149

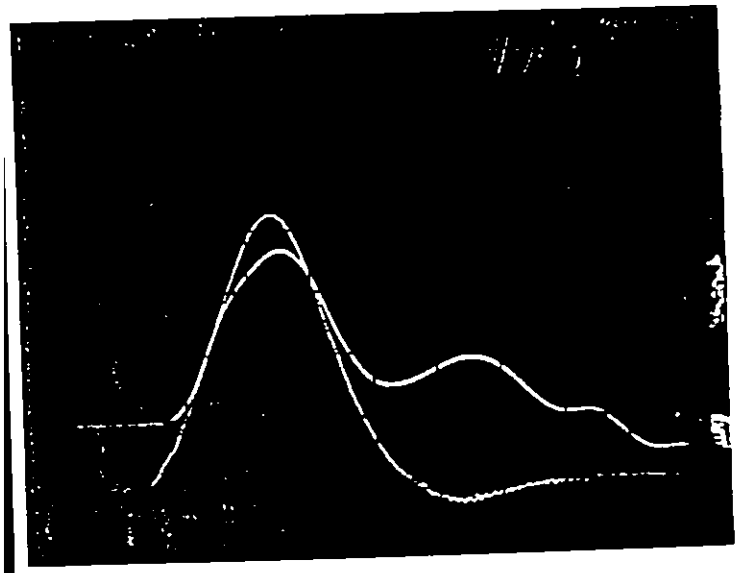

150

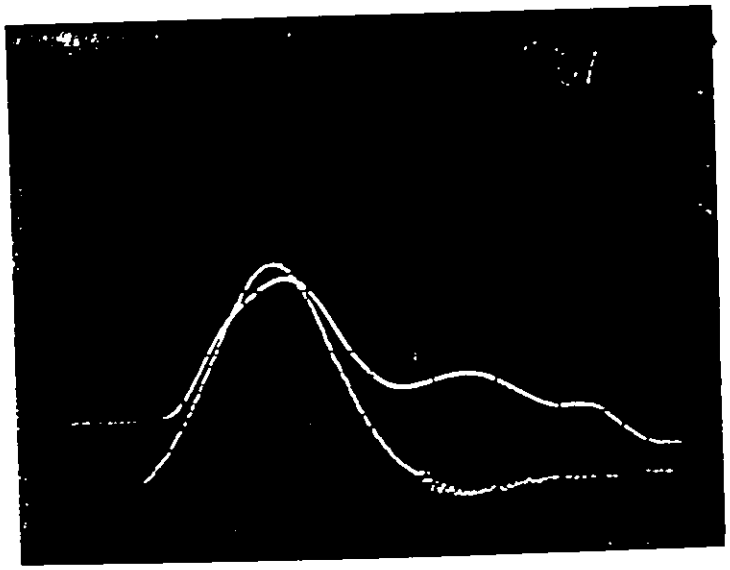

151

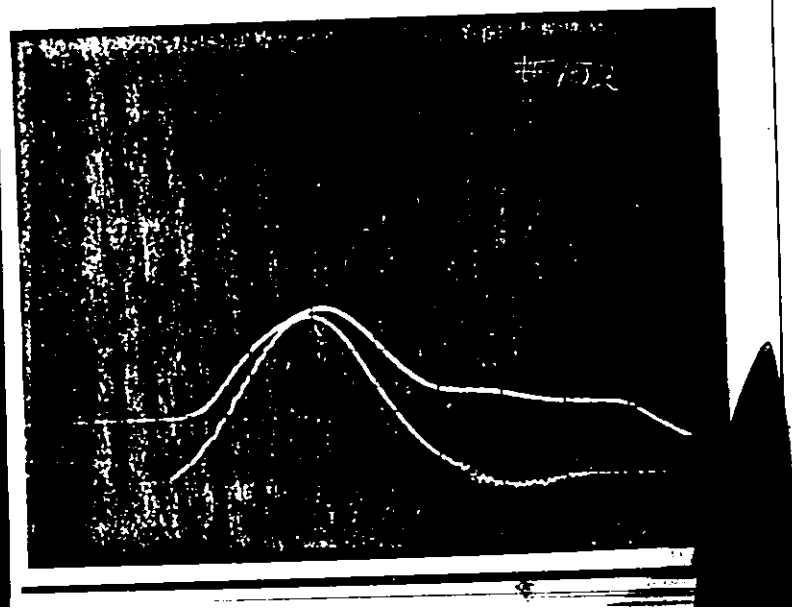

152

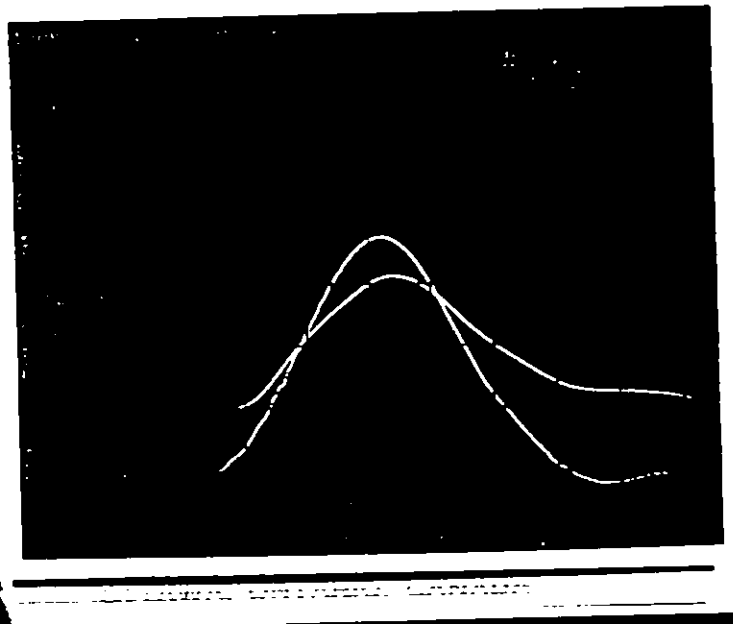

153

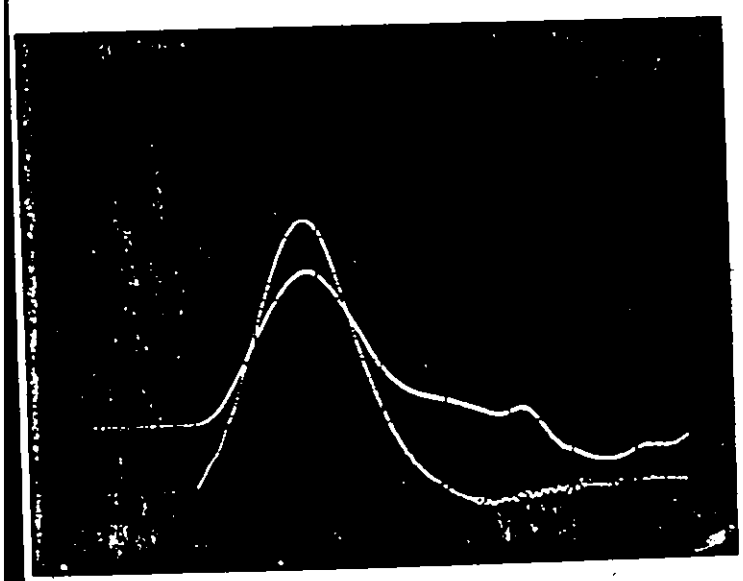

154

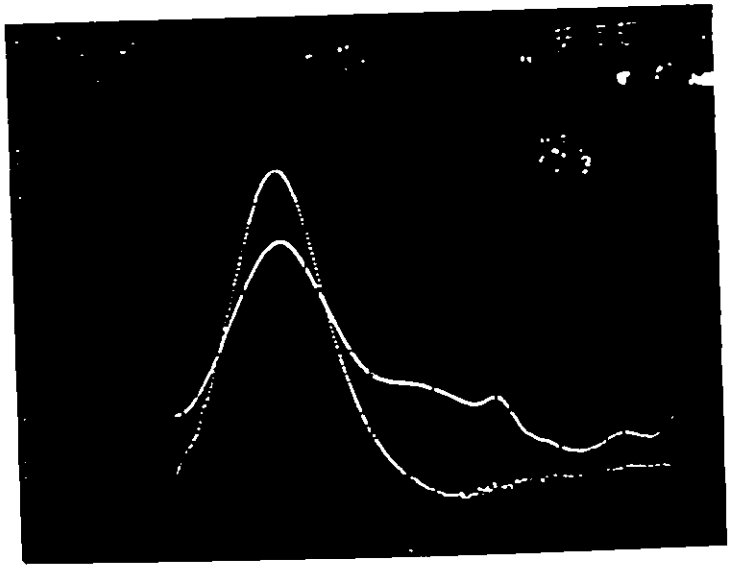

155

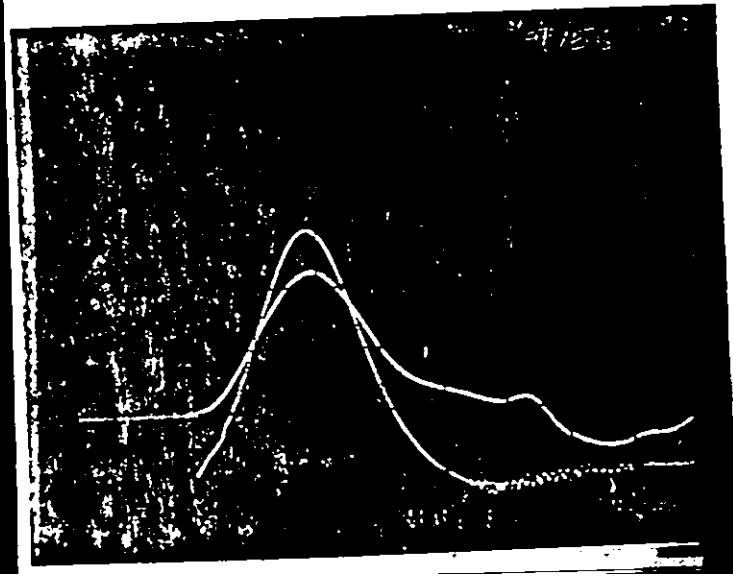

156

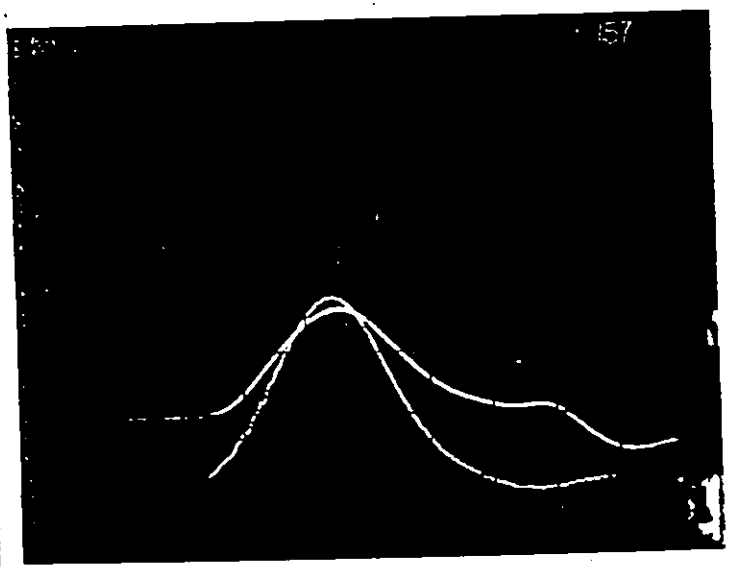

157

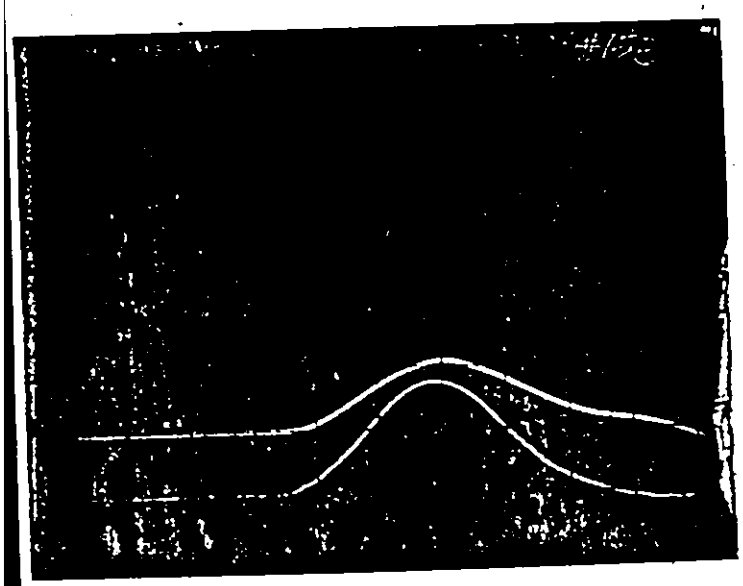

158

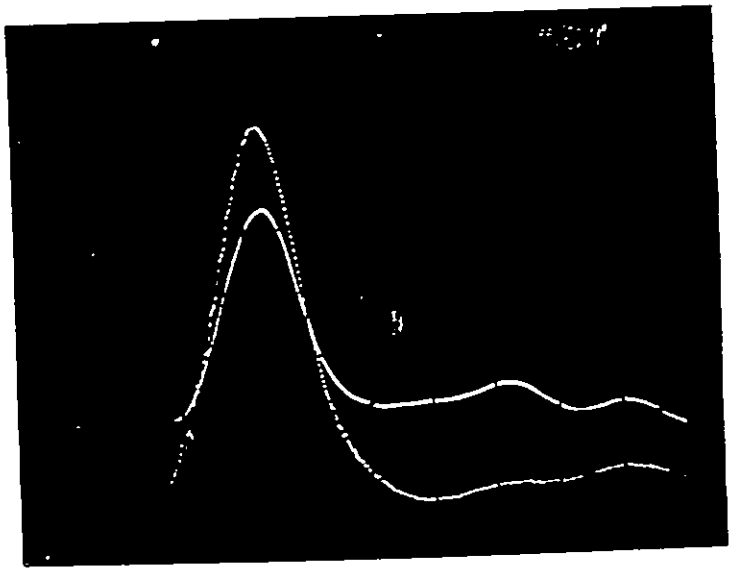

159

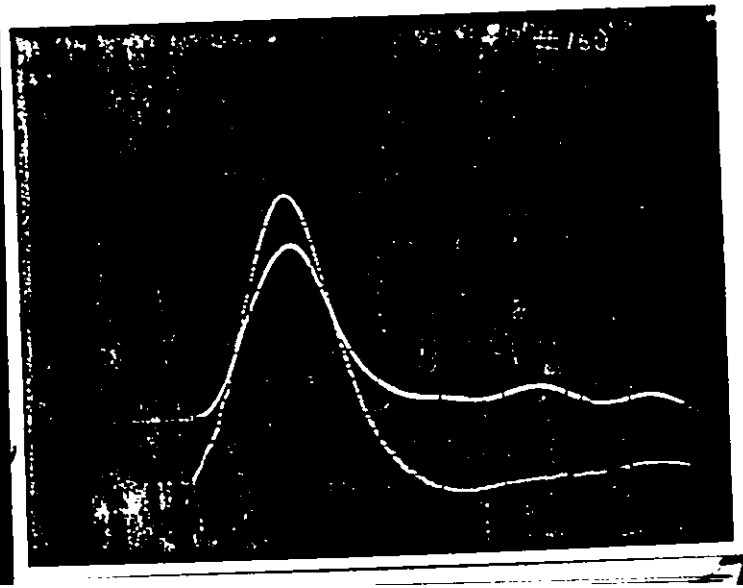

160

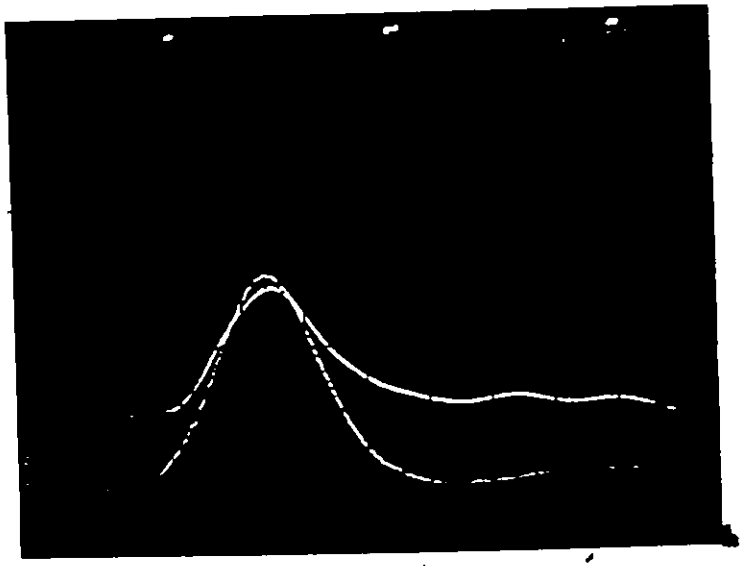

161

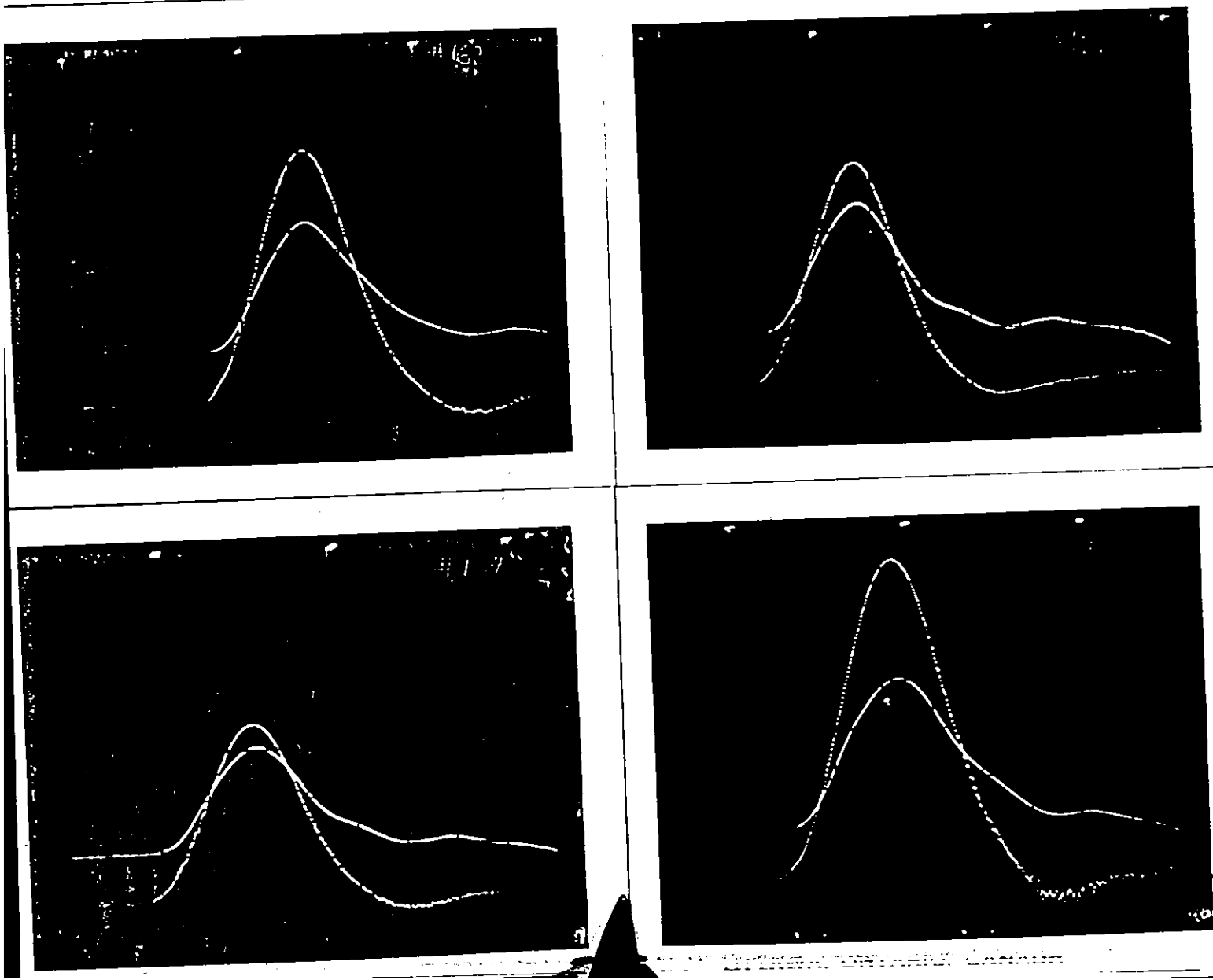

162 163

164 165

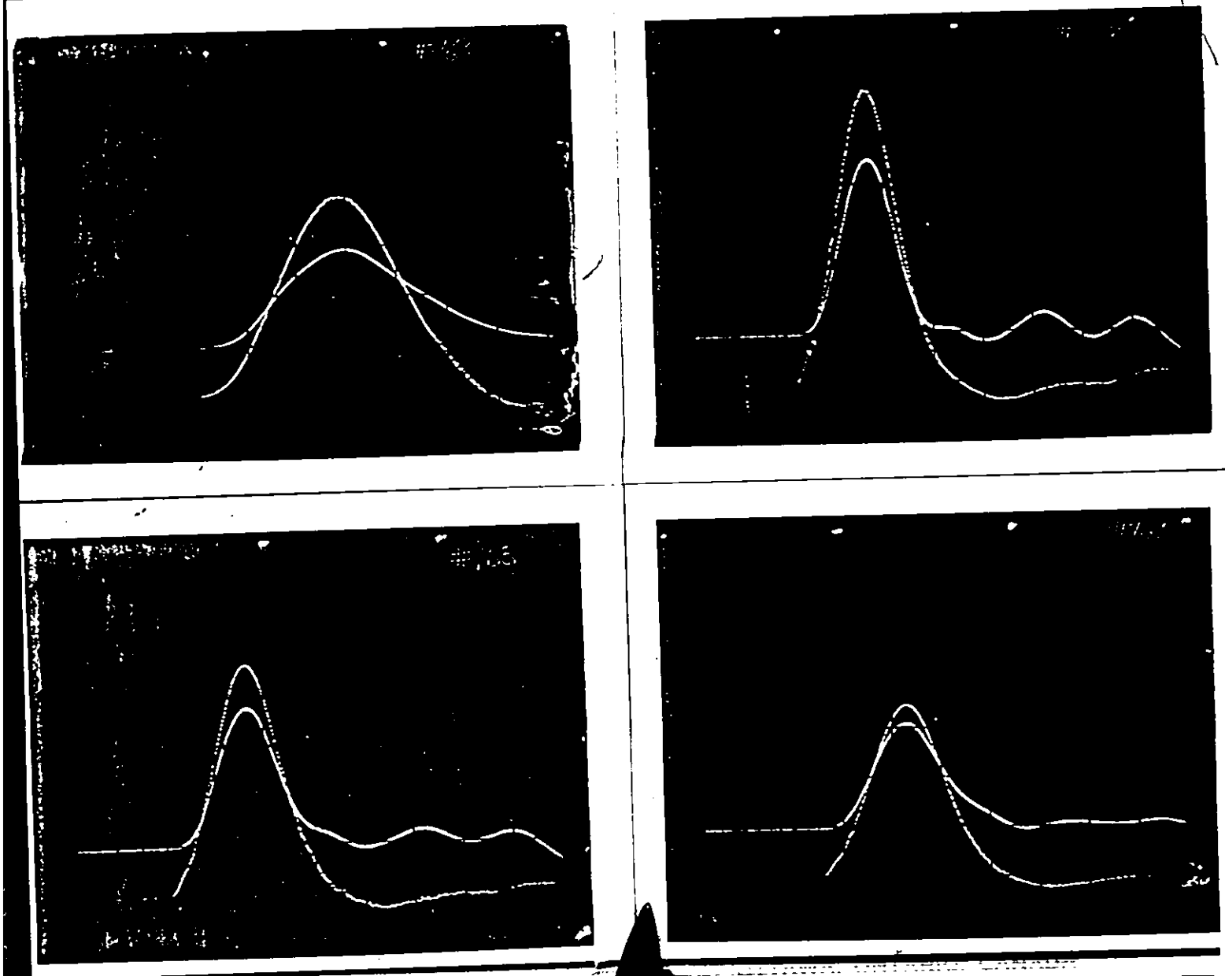

166 167

168 169

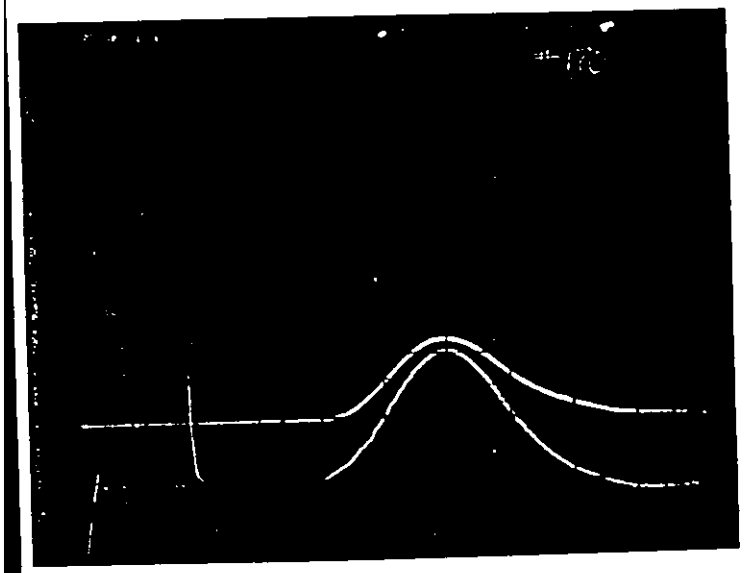

170 171

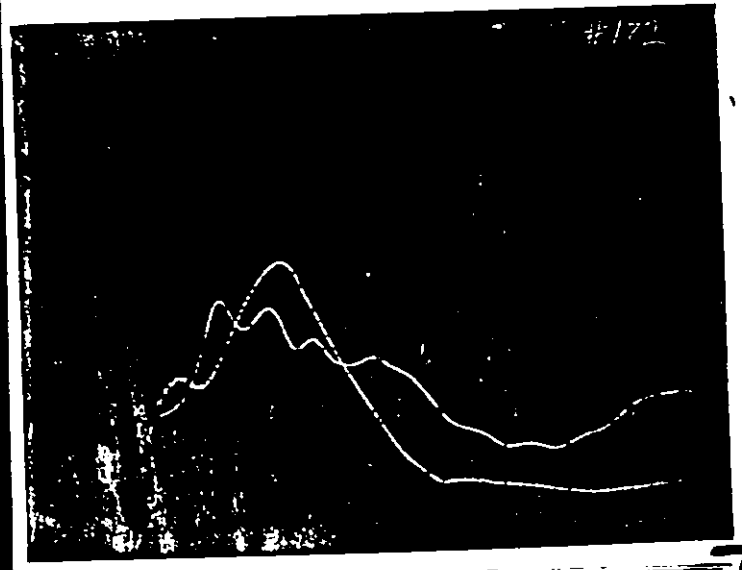

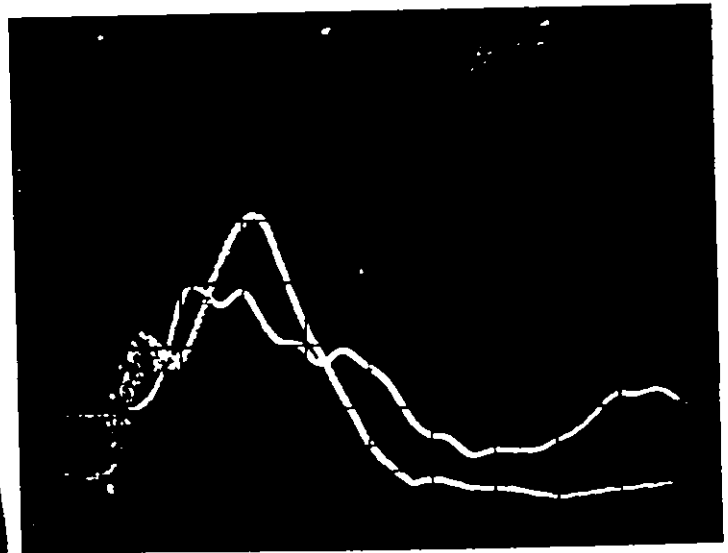

172 173

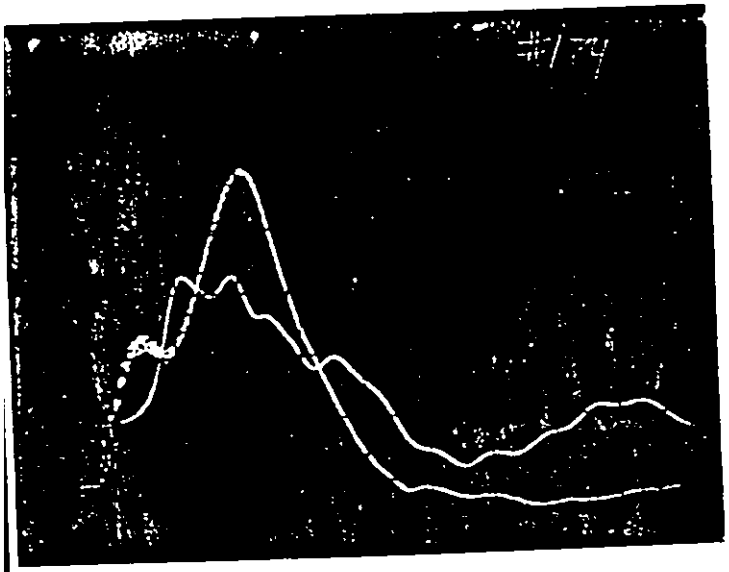

174

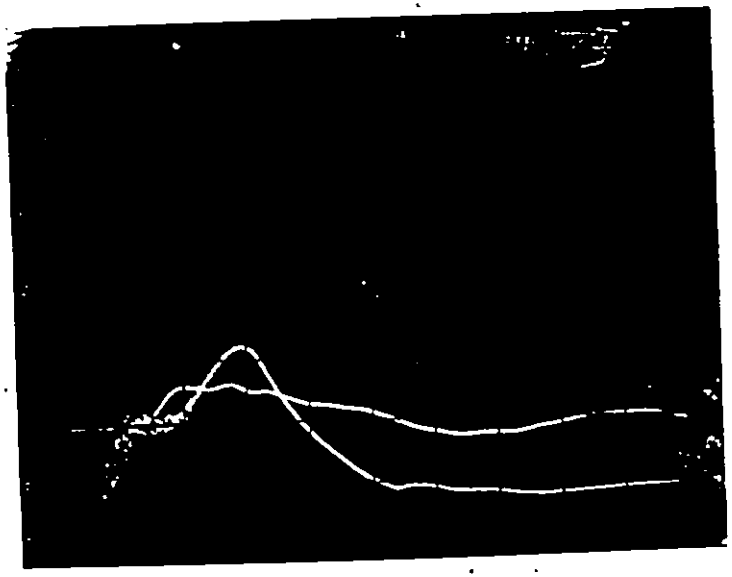

175

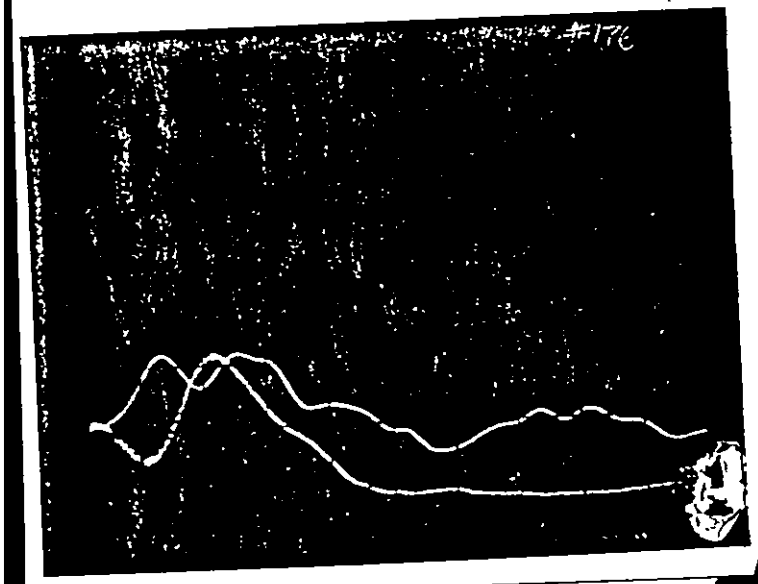

176

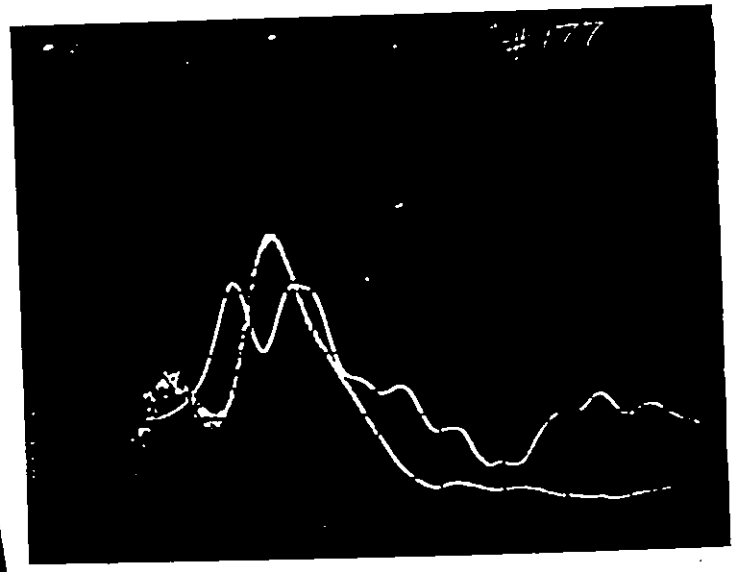

177

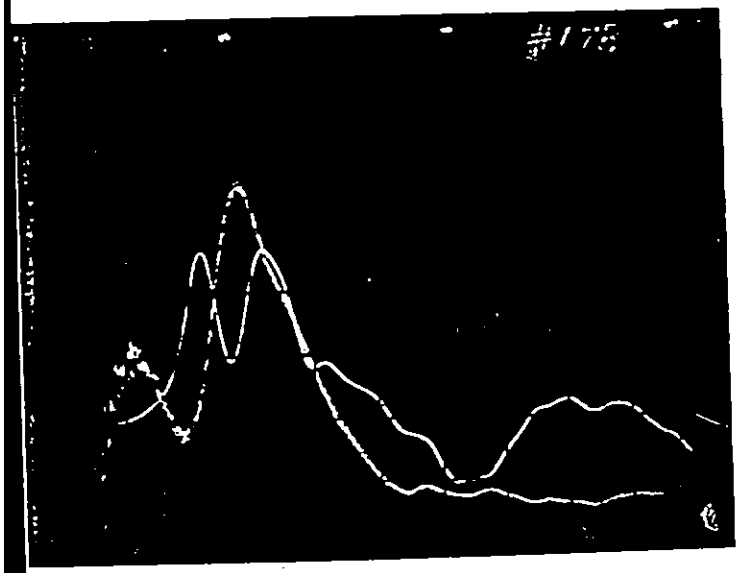

178

179

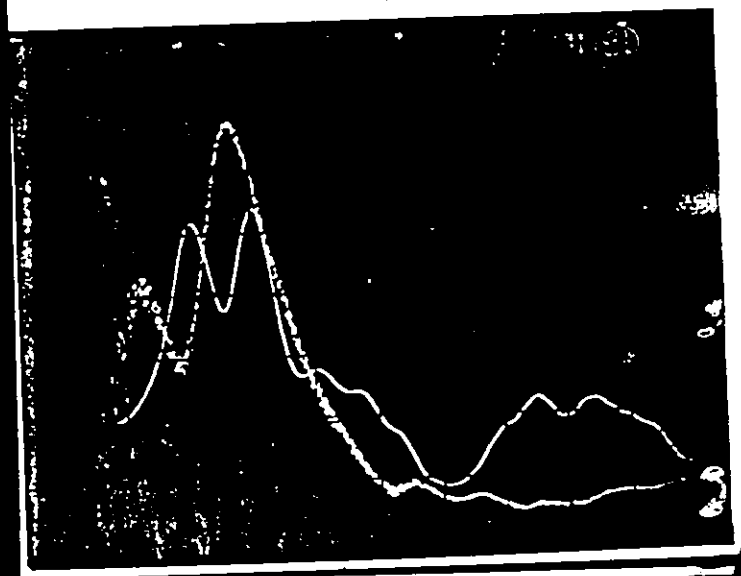

180

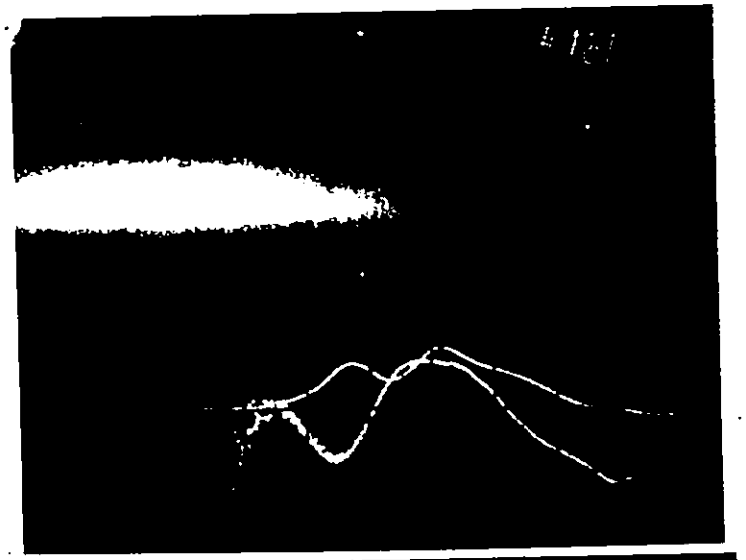

181

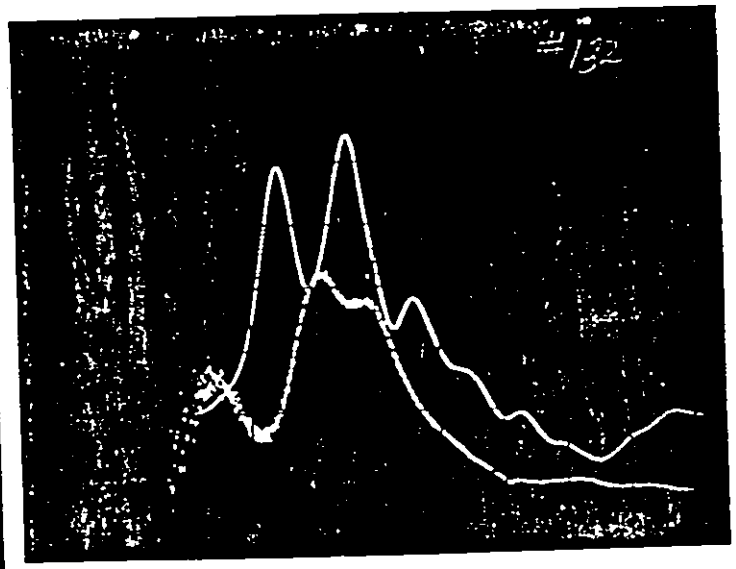

182

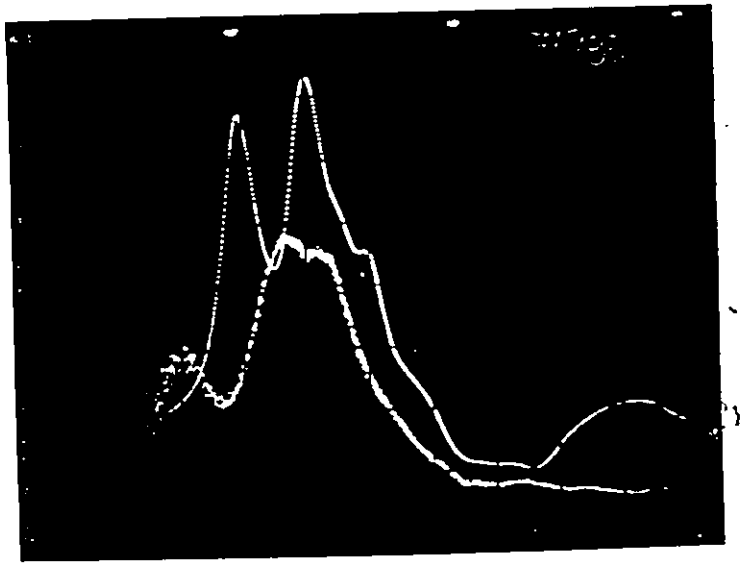

183

184

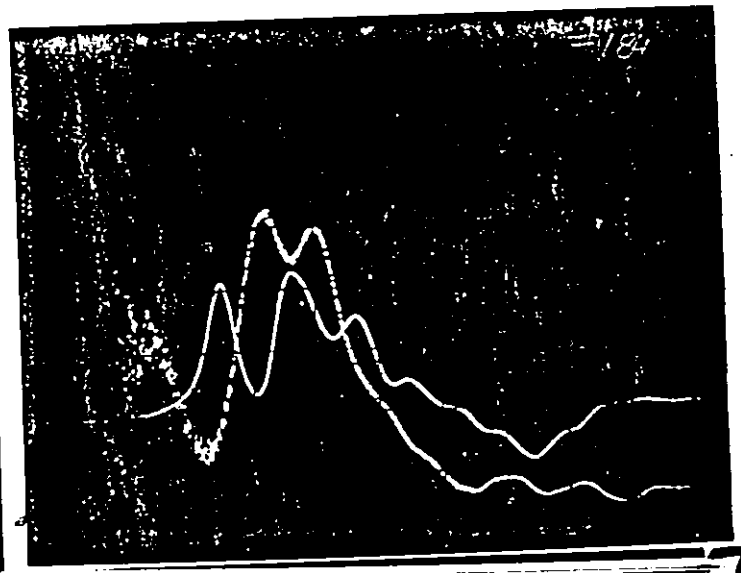

185

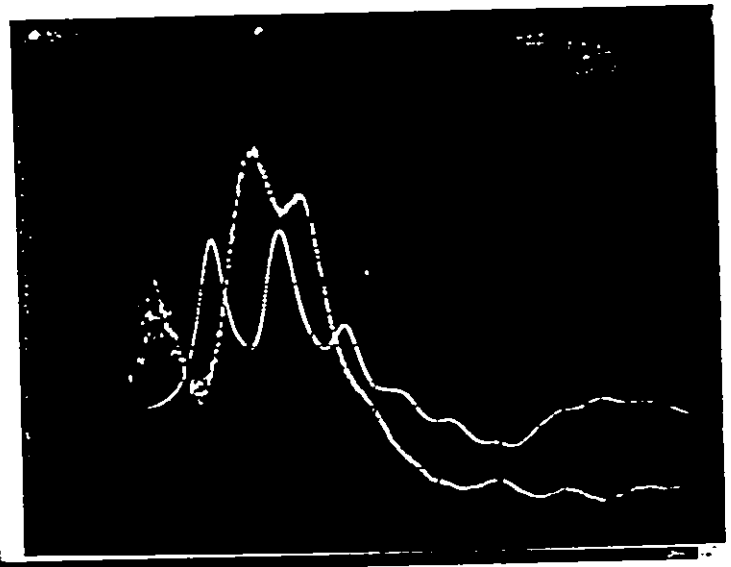

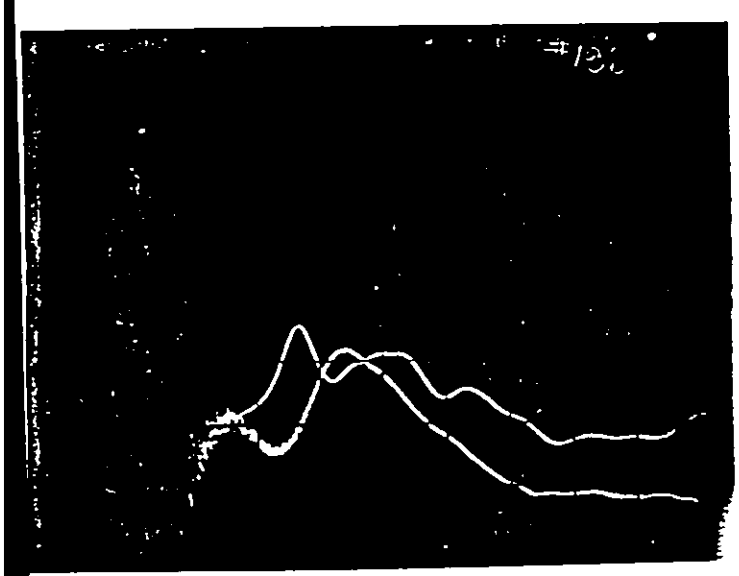

186

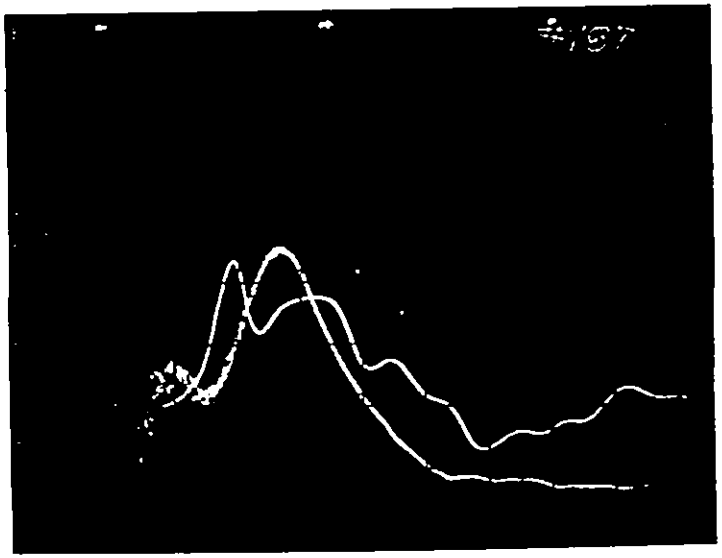

187

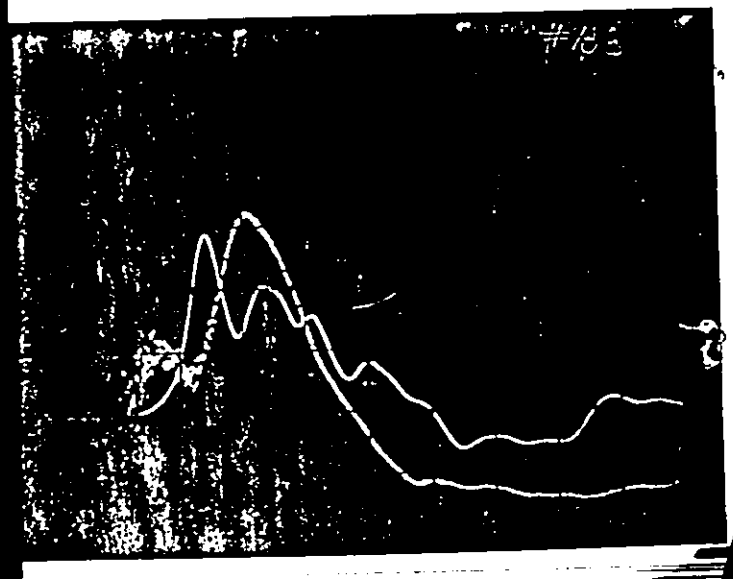

188

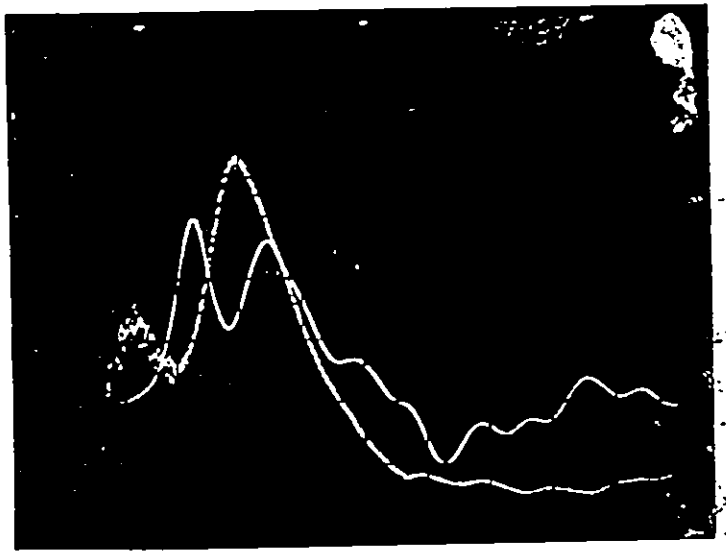

189

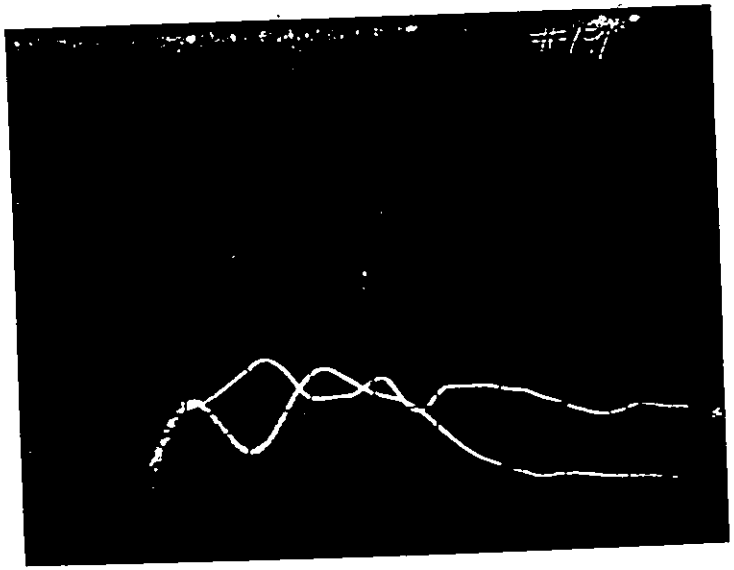

191

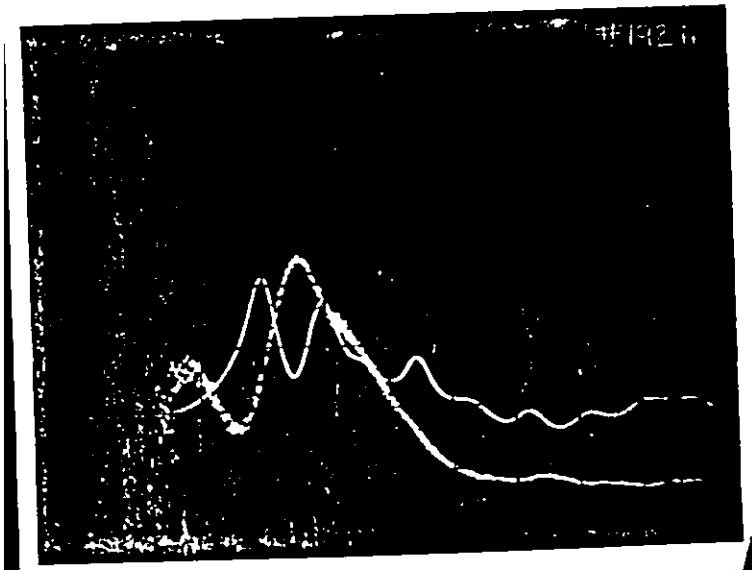

192A

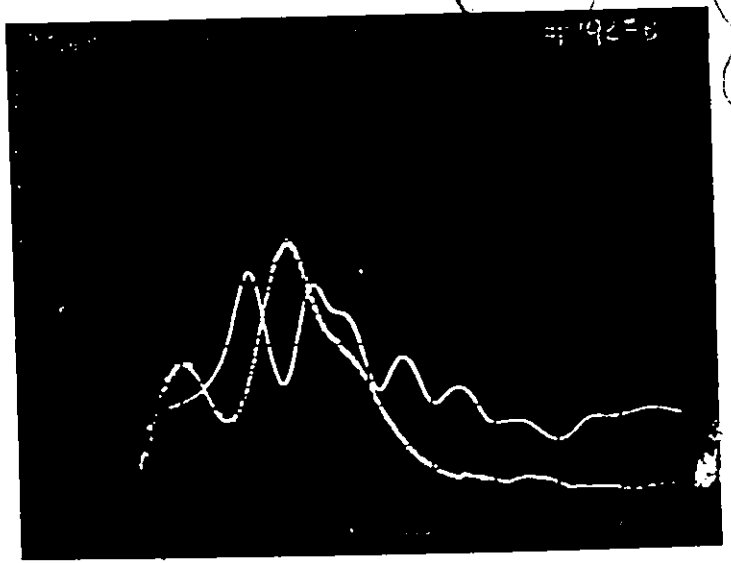

192B

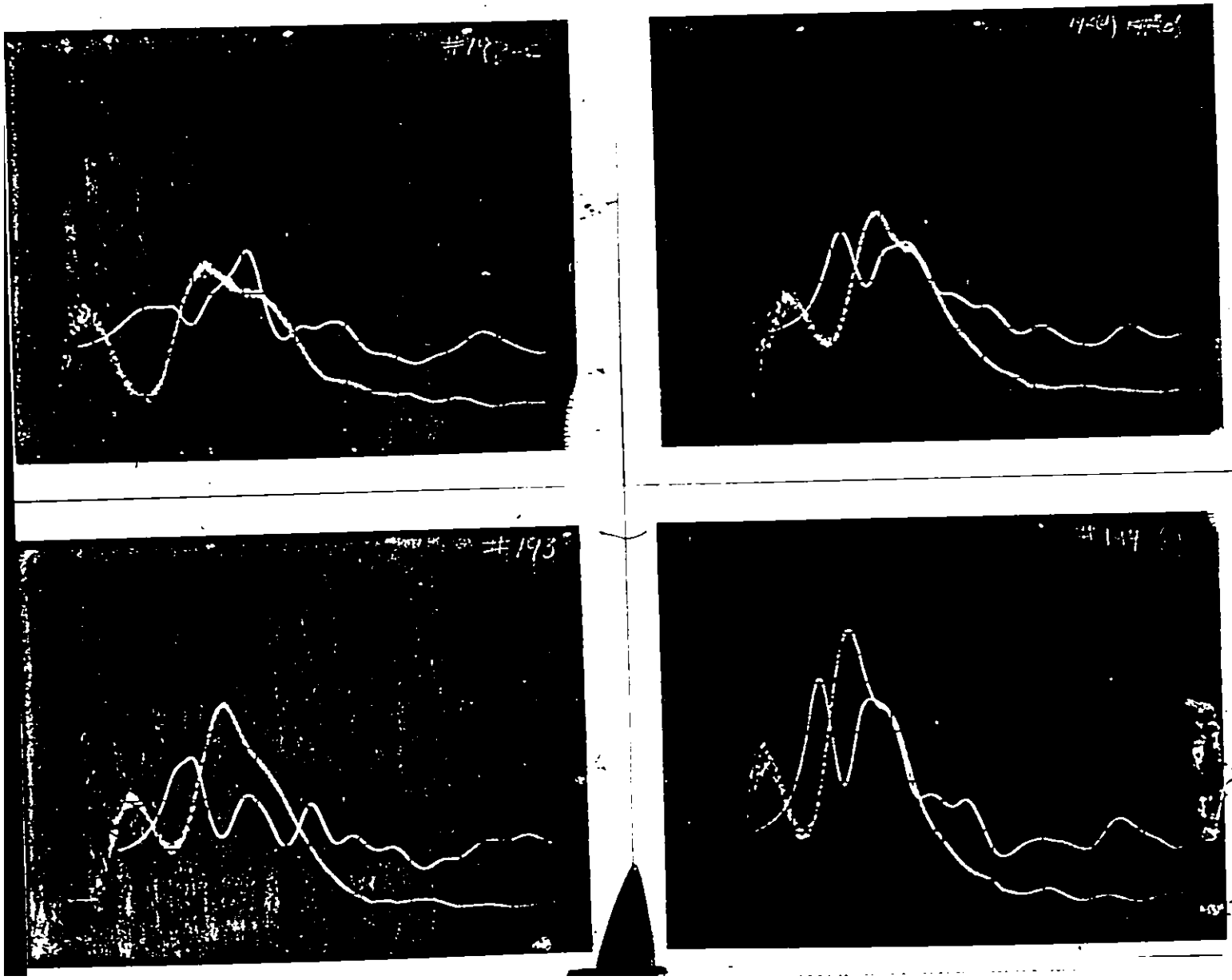

192C 192D

193 194A

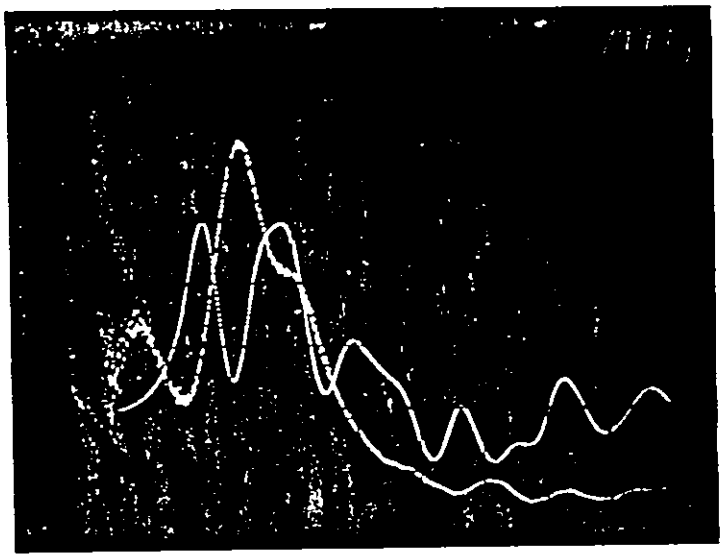

194B

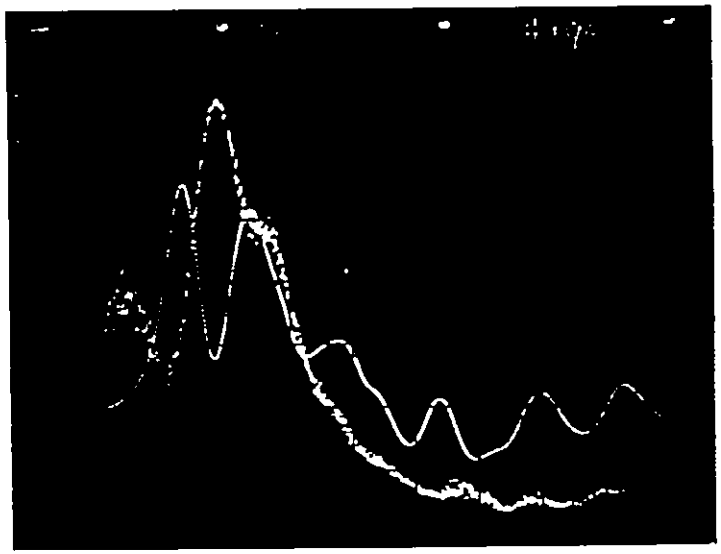

196

195B

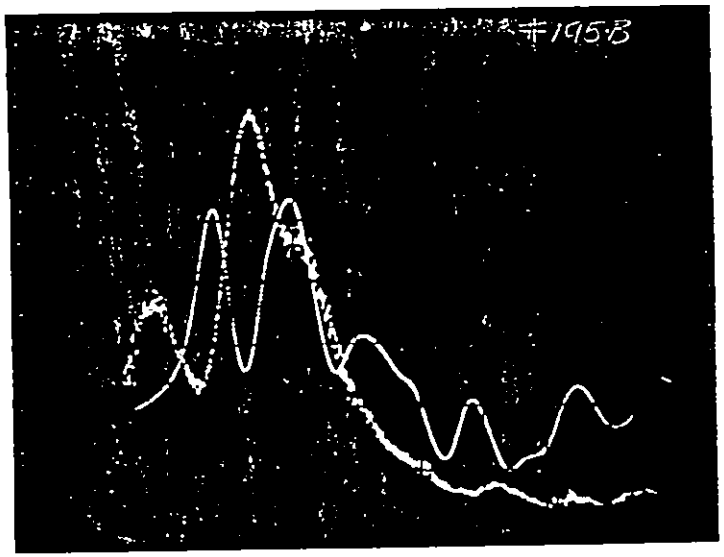

196-1

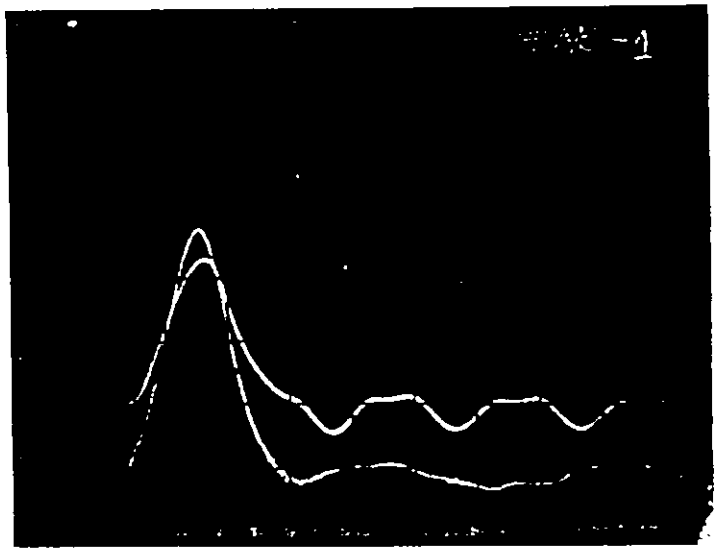

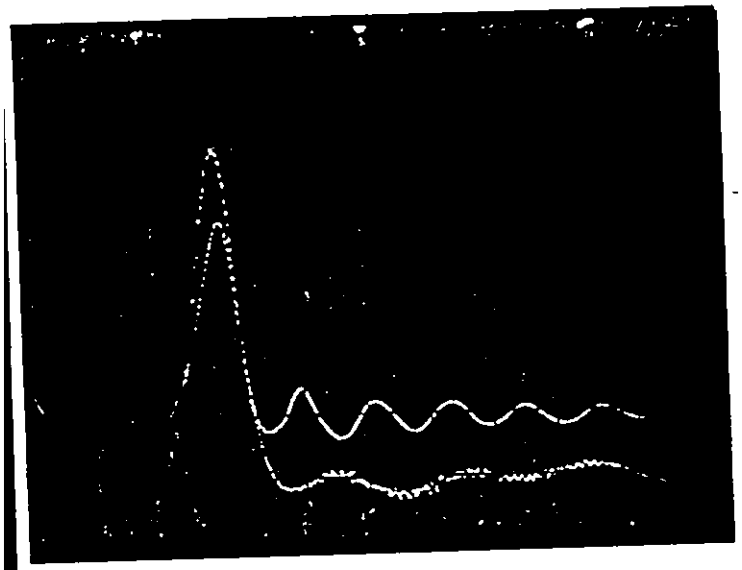

197

198

199

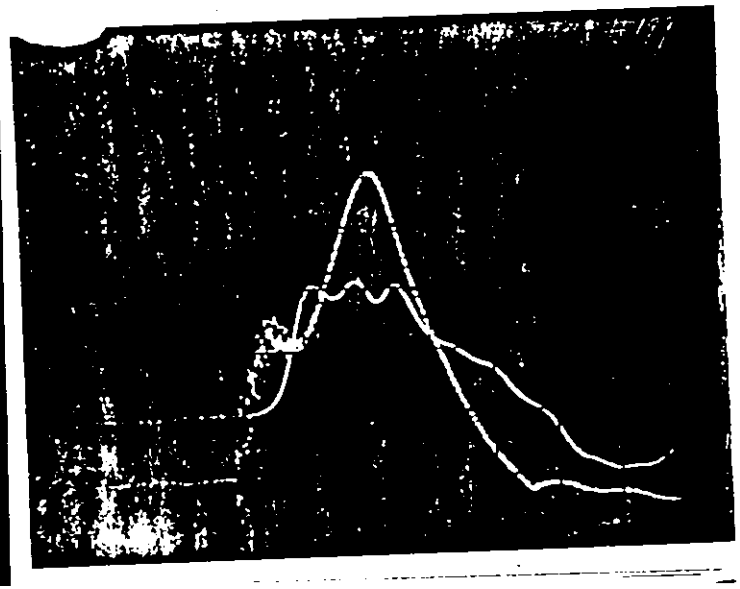

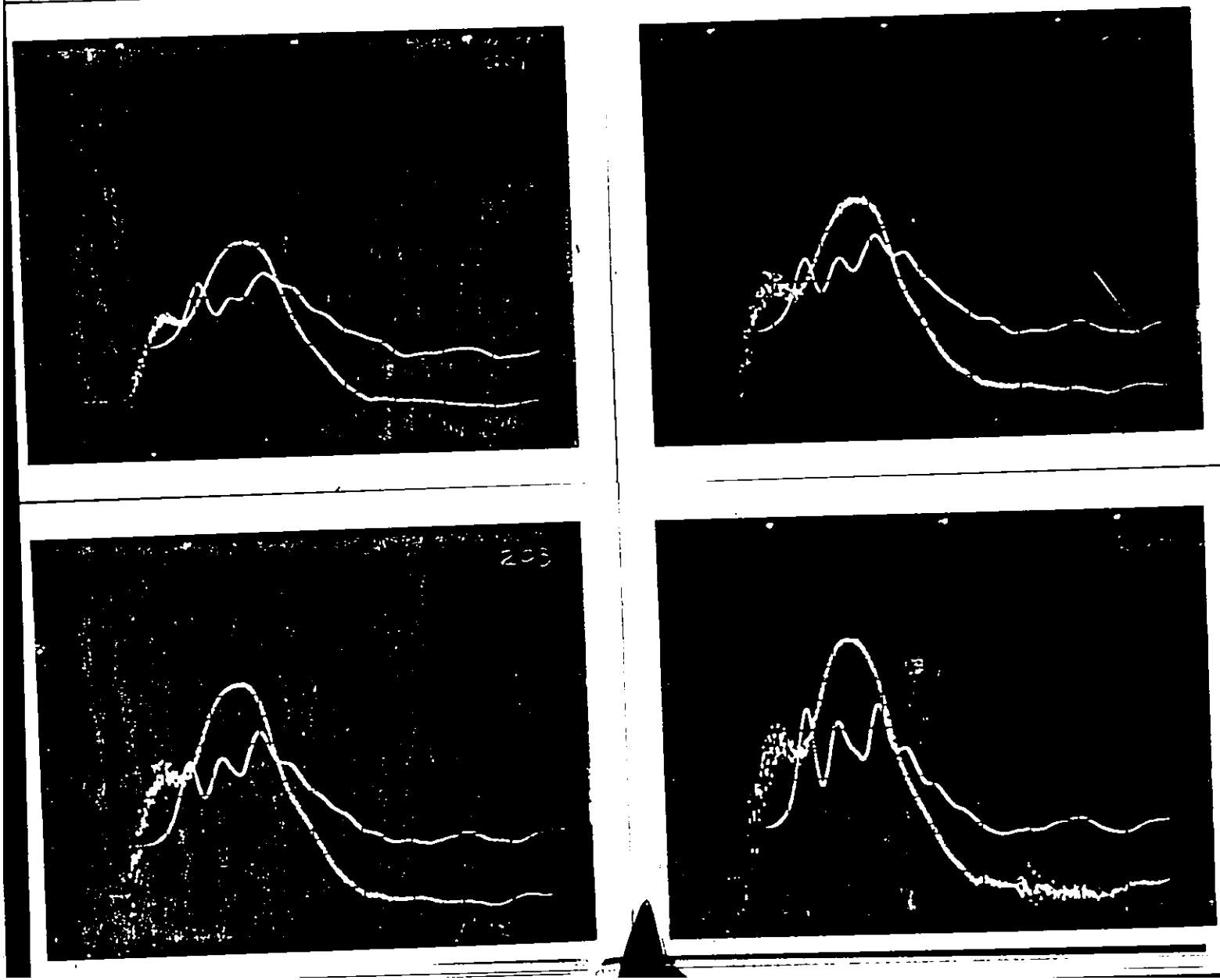

201 202

203 204

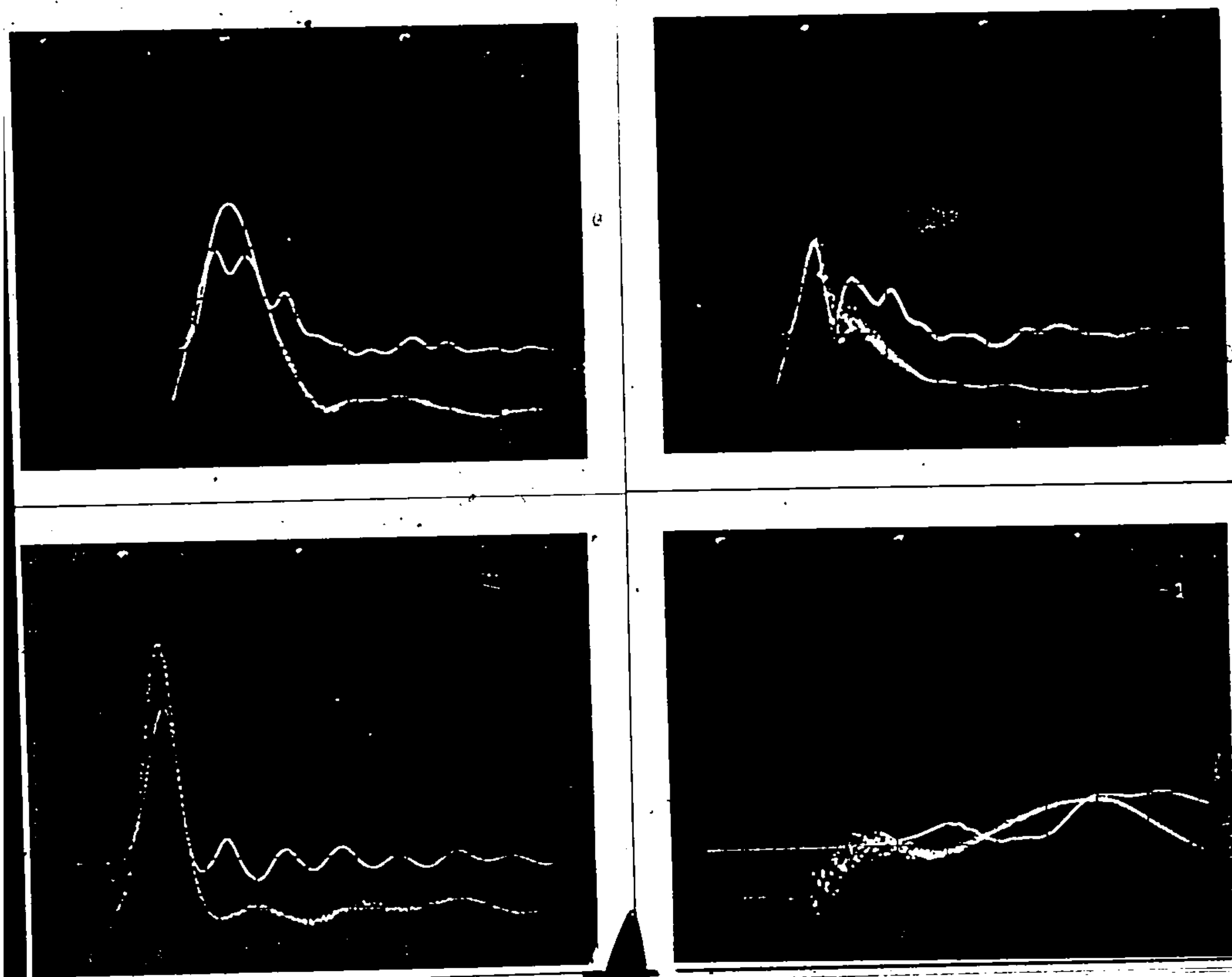

205 206

207 207-1

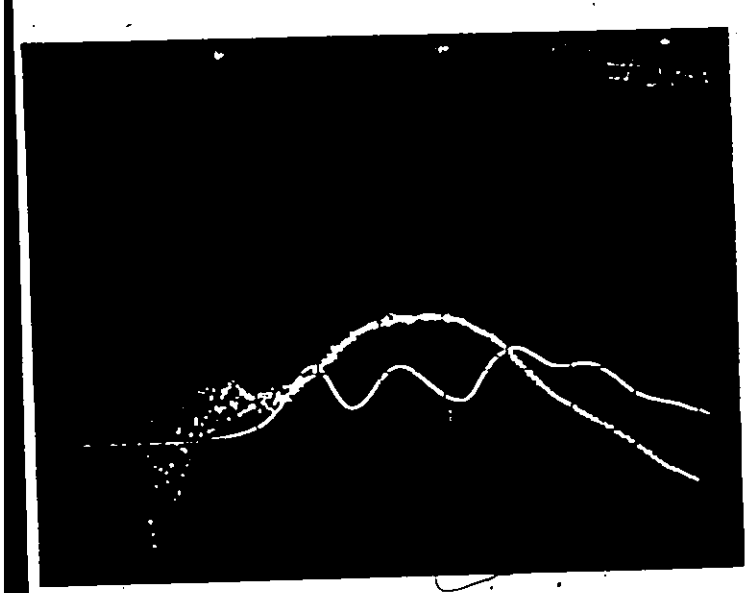

208

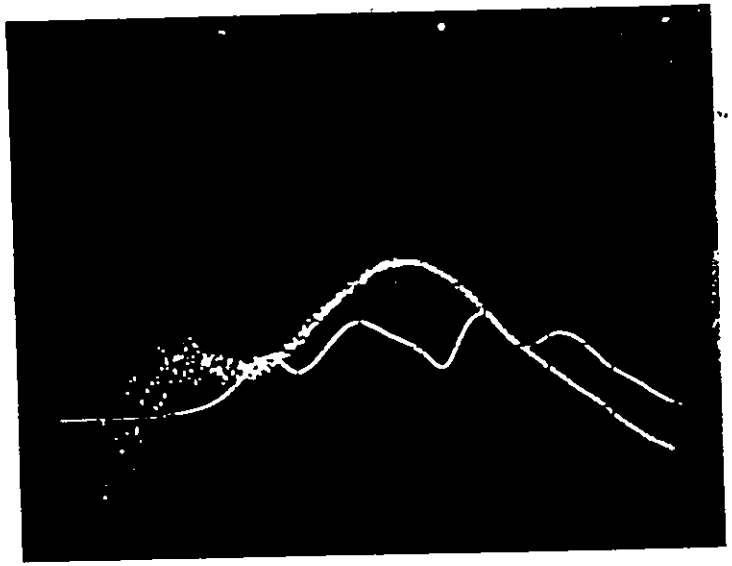

209

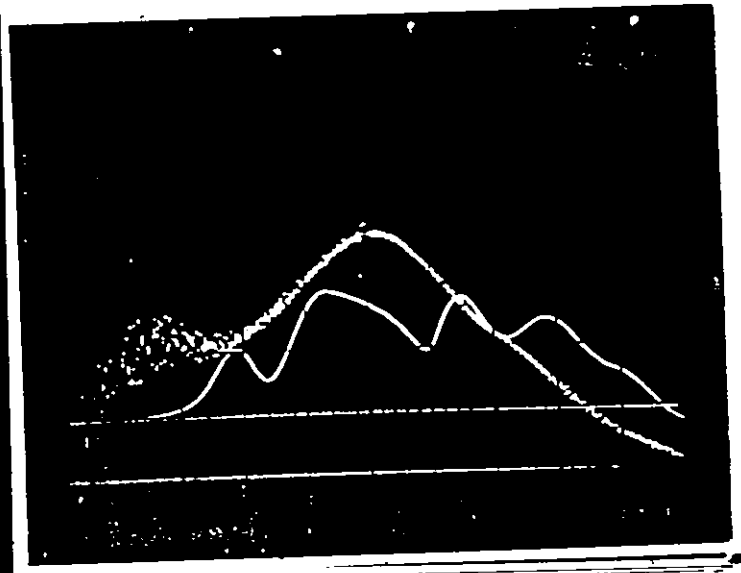

210

211

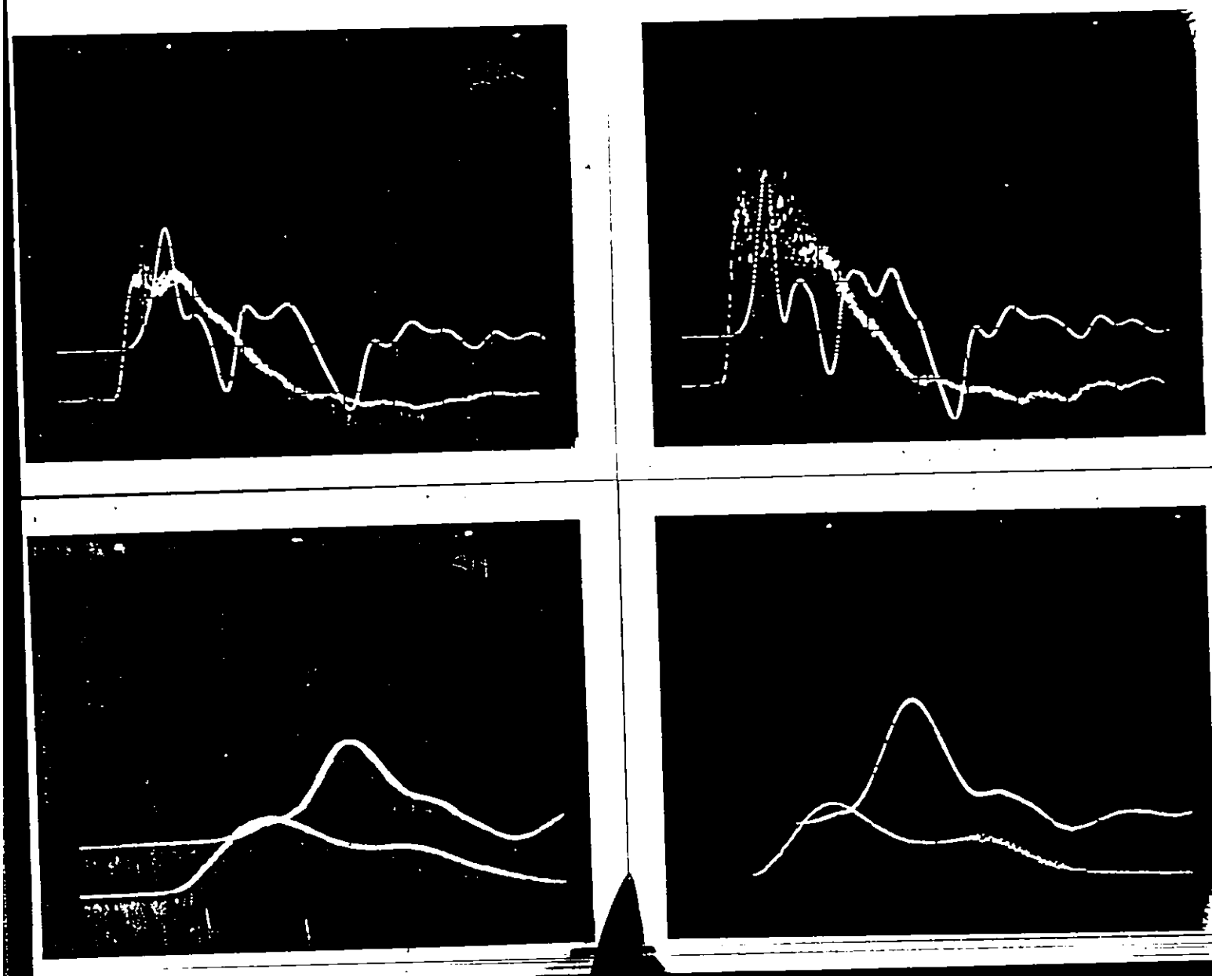

212 213

214 215

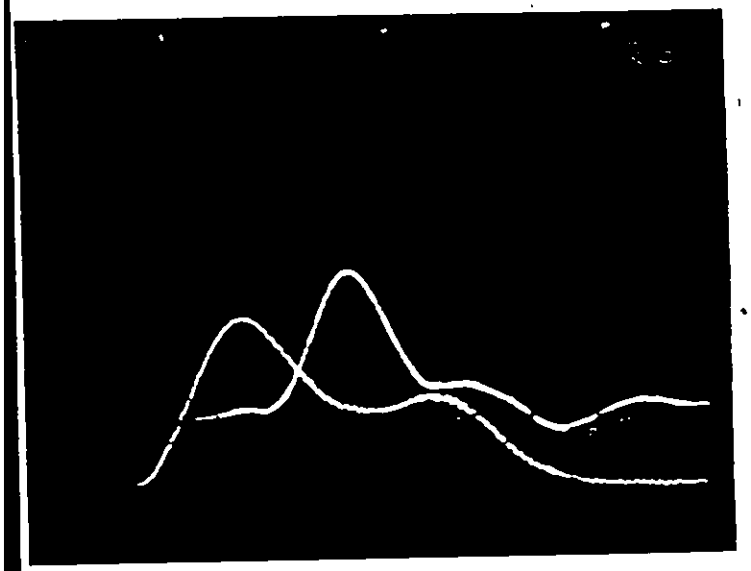

216

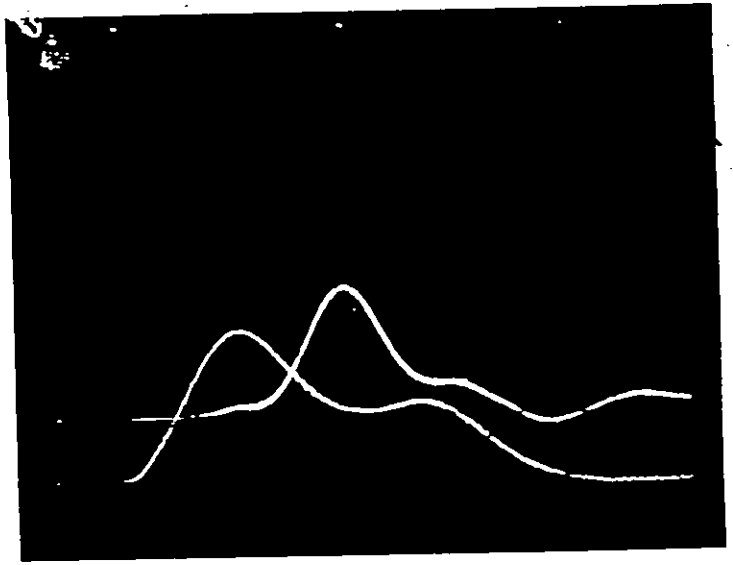

217

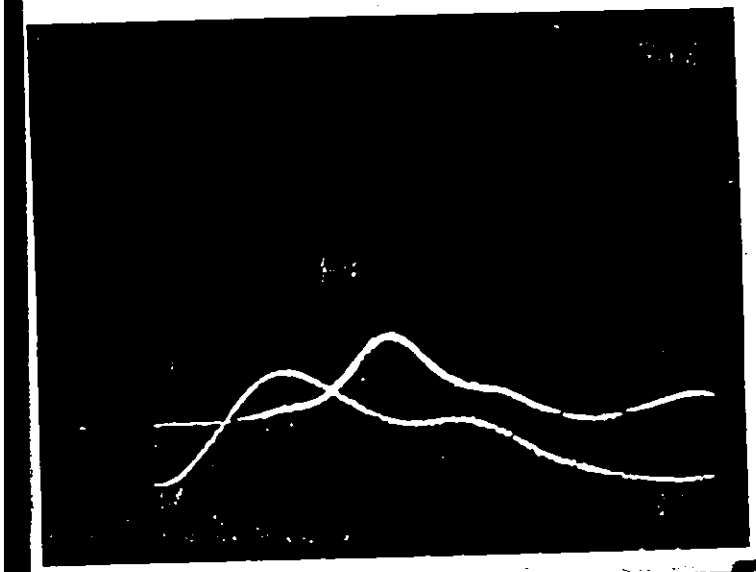

218

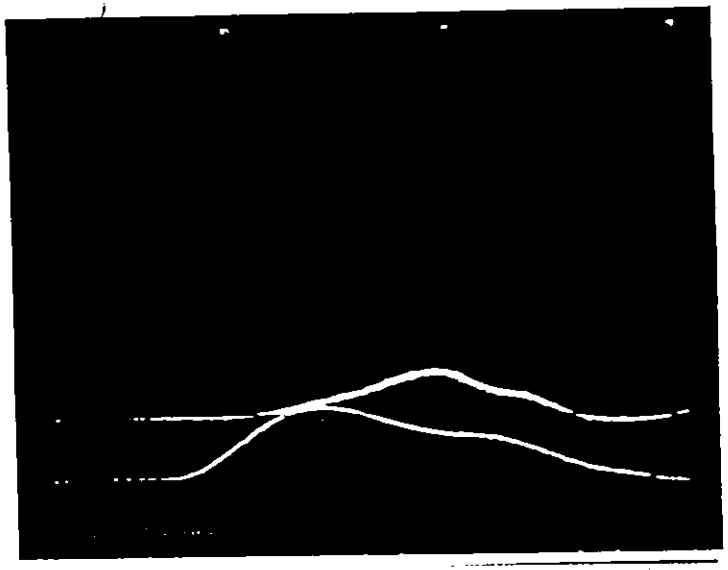

219

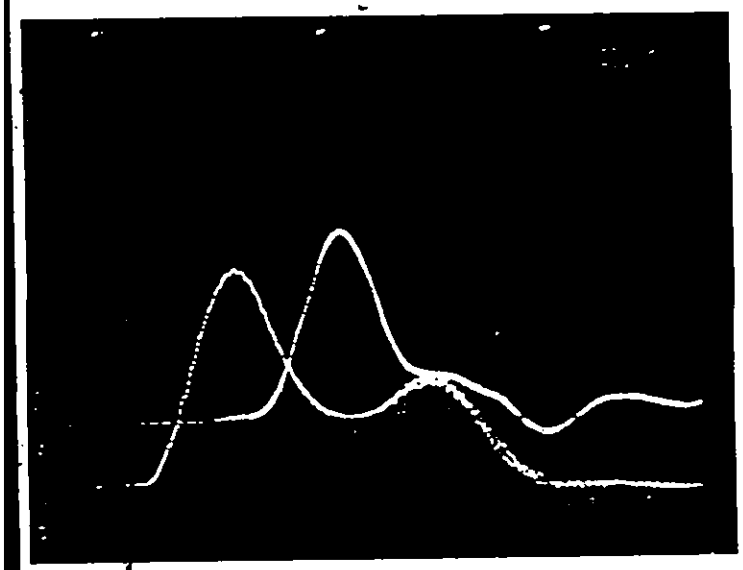

220

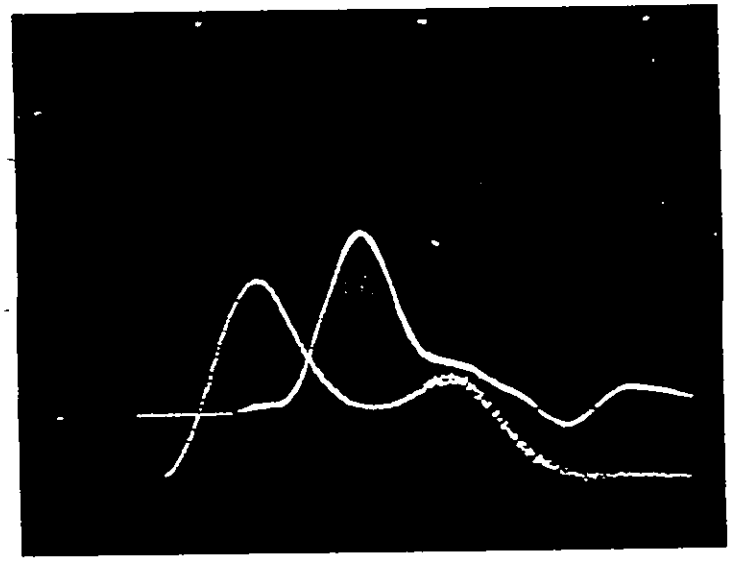

221

222

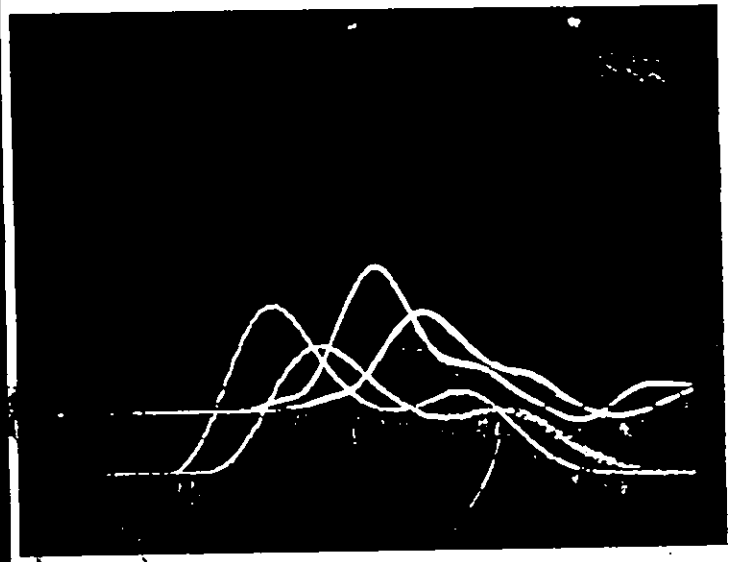

223

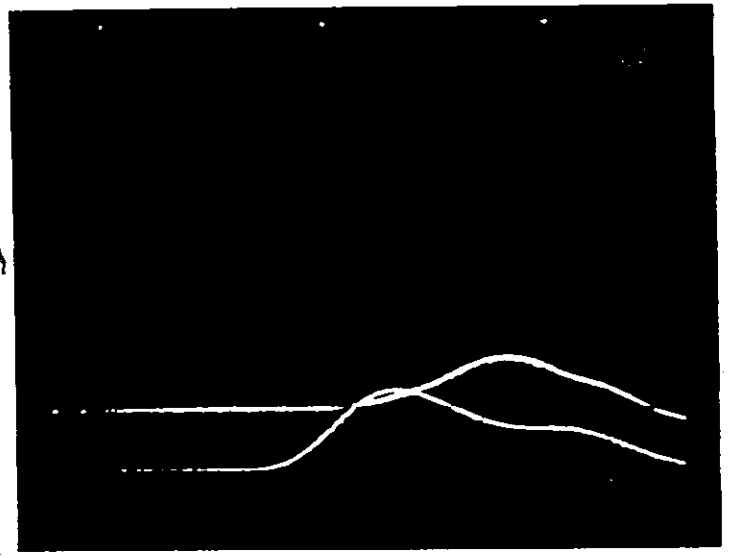

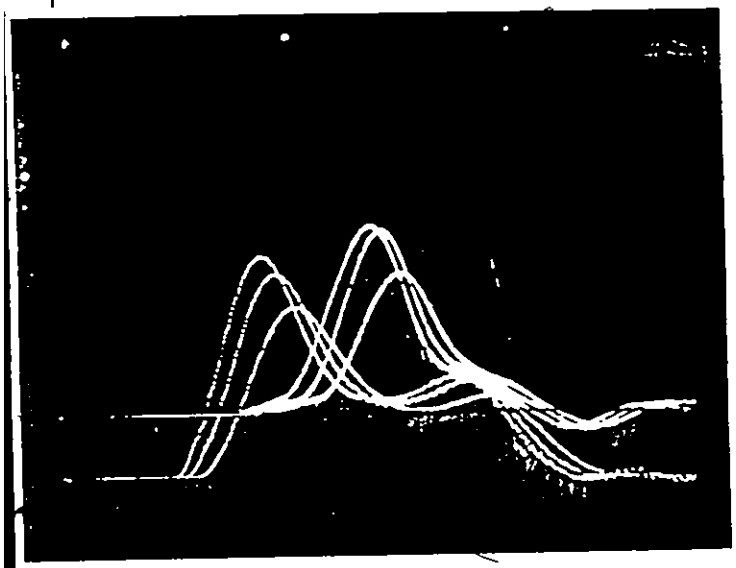

224

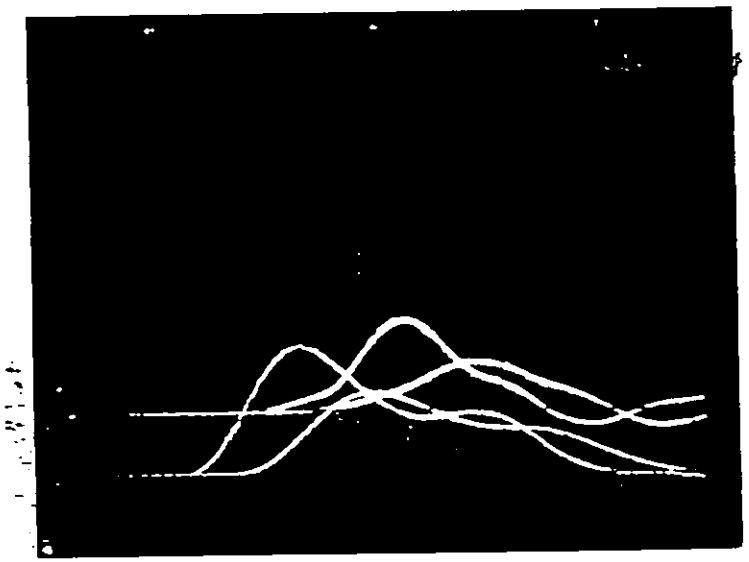

225

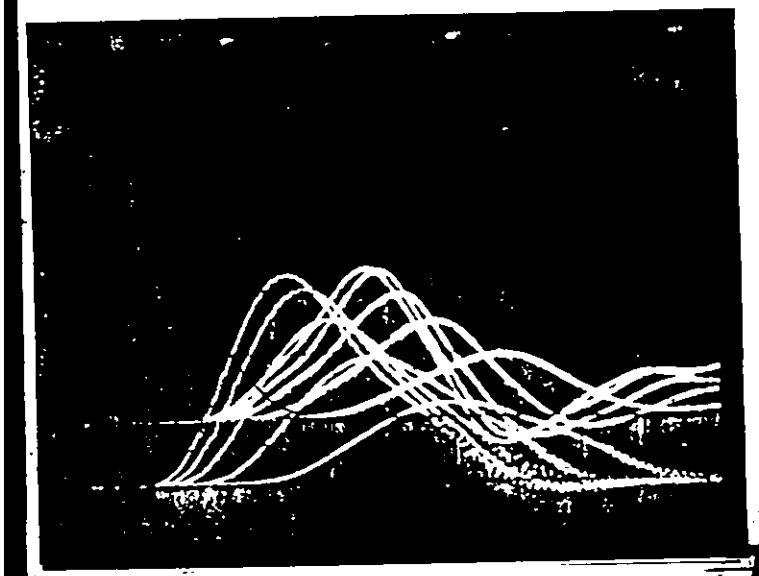

226

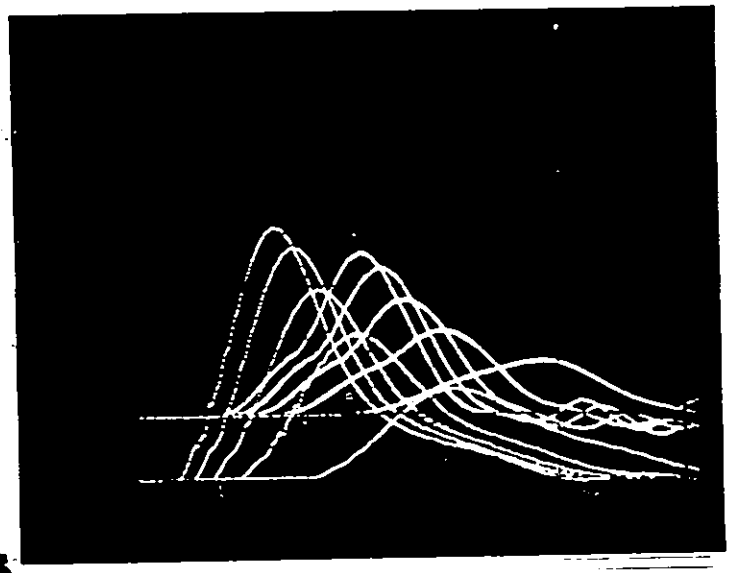

227

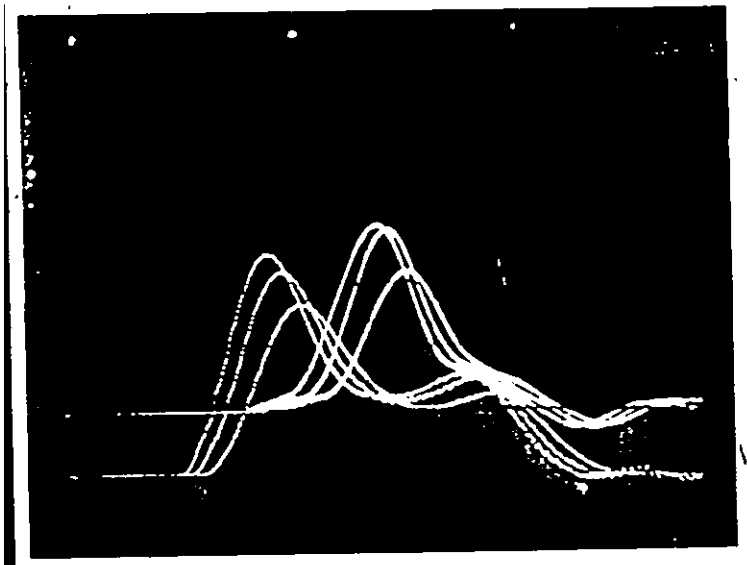

224

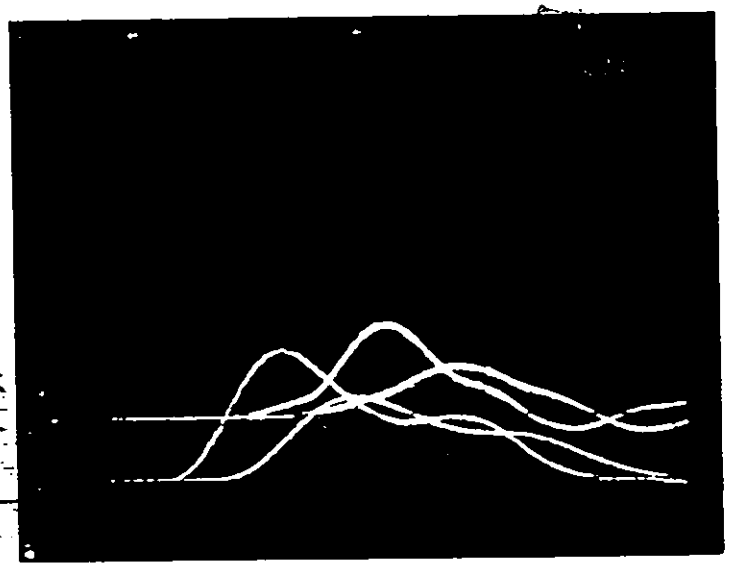

225

226

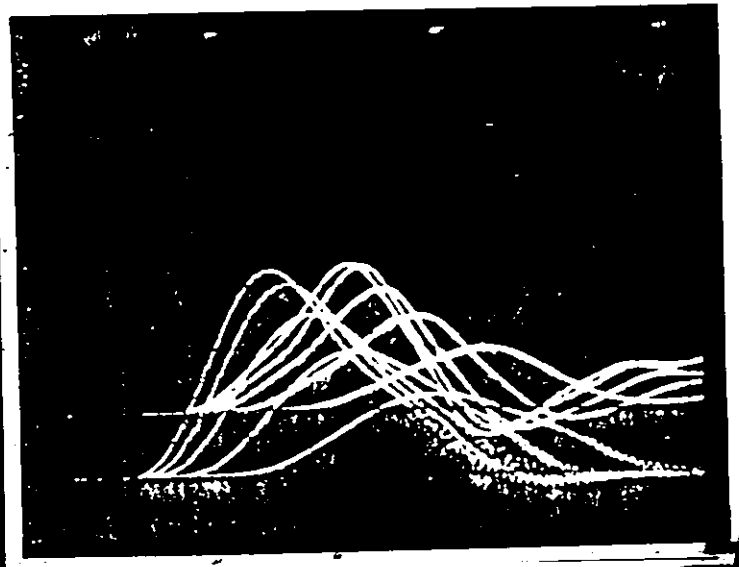

227

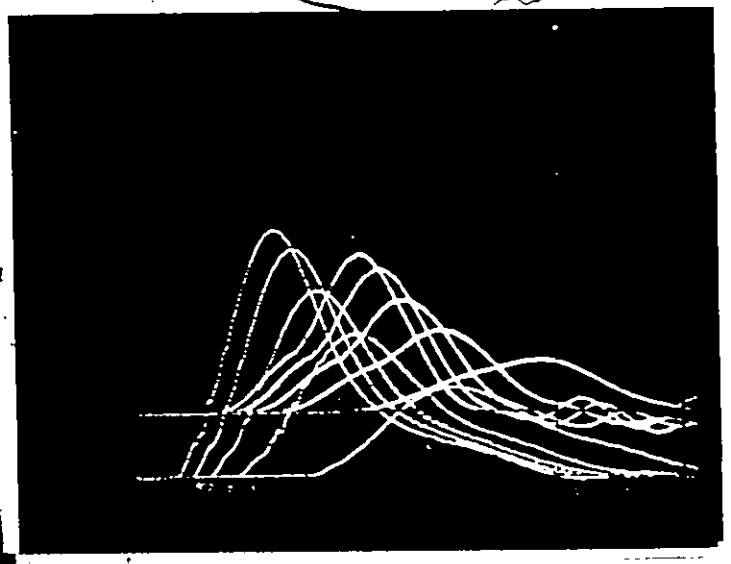

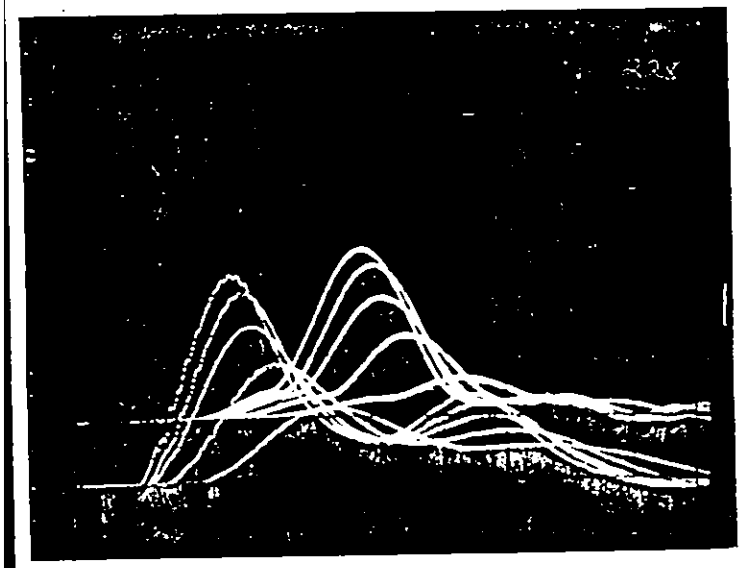

228

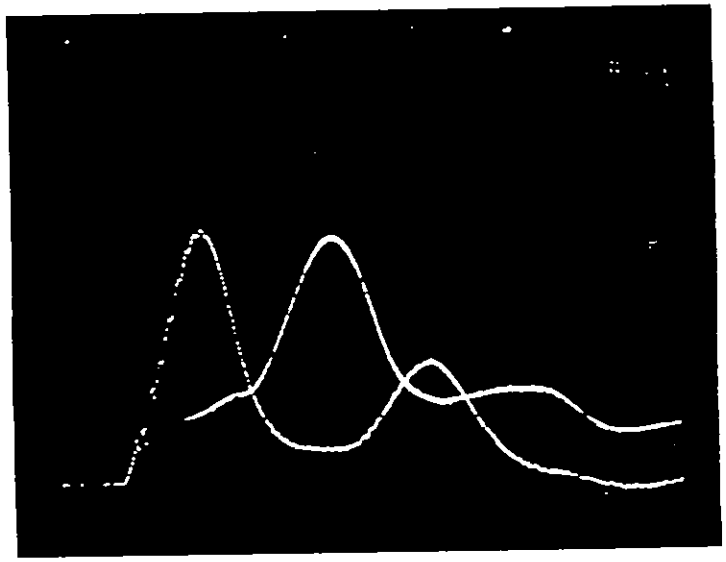

229

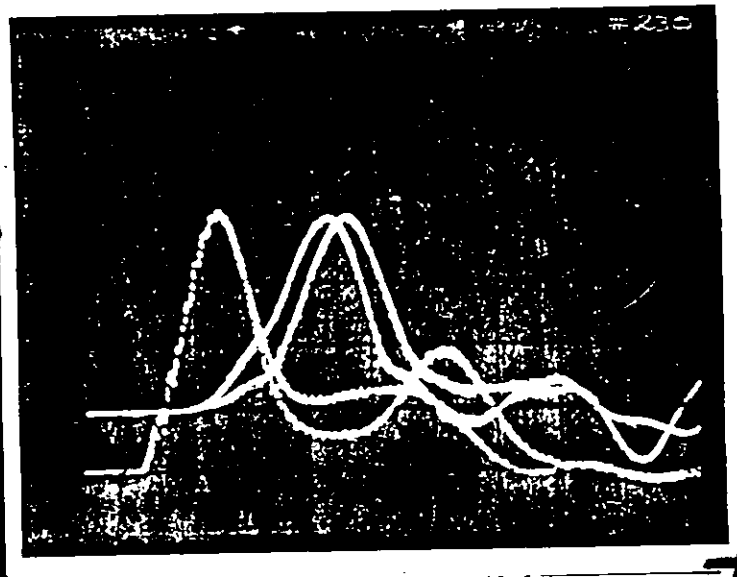

230

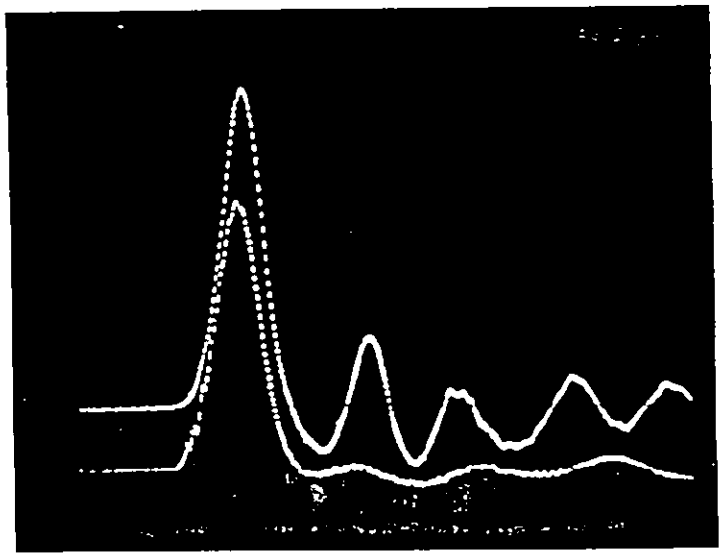

231

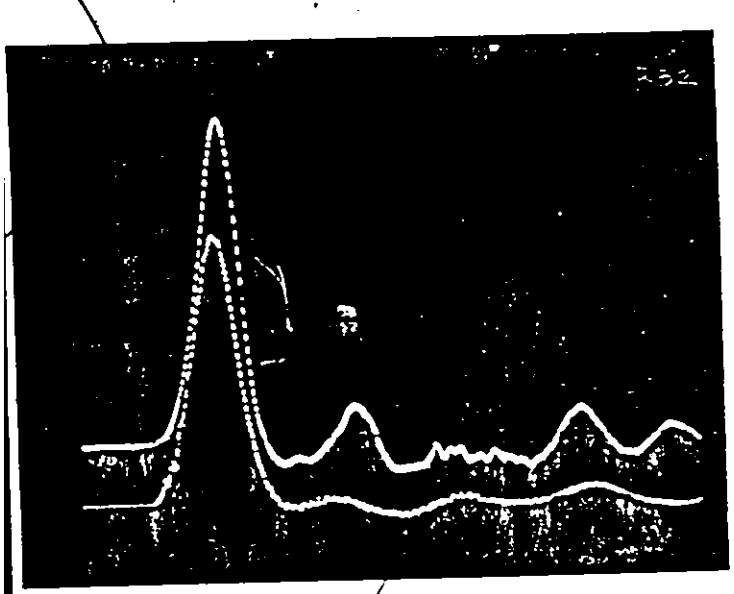

232

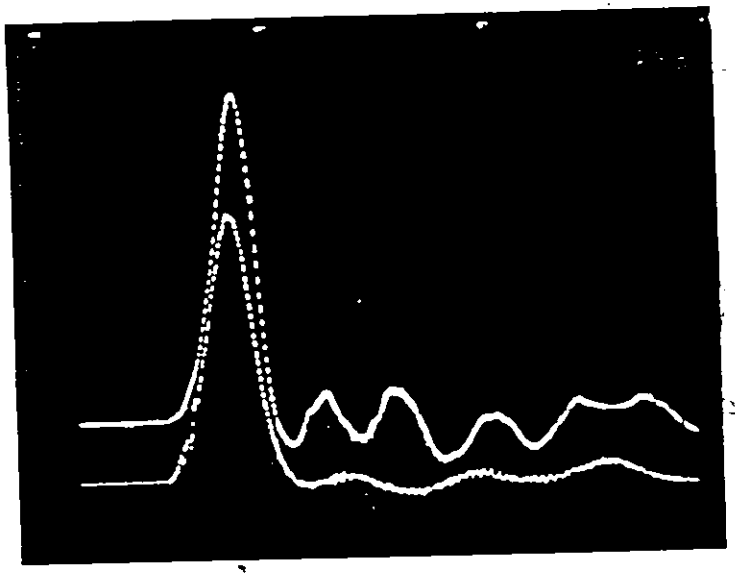

233

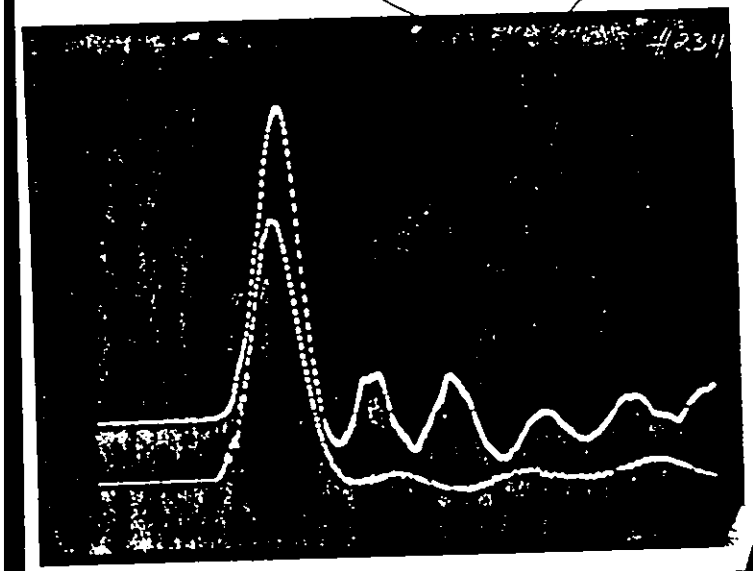

234

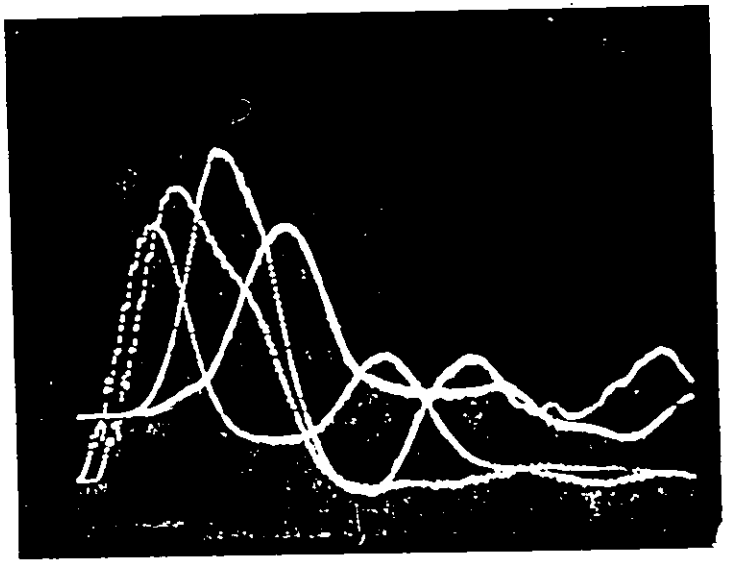

235

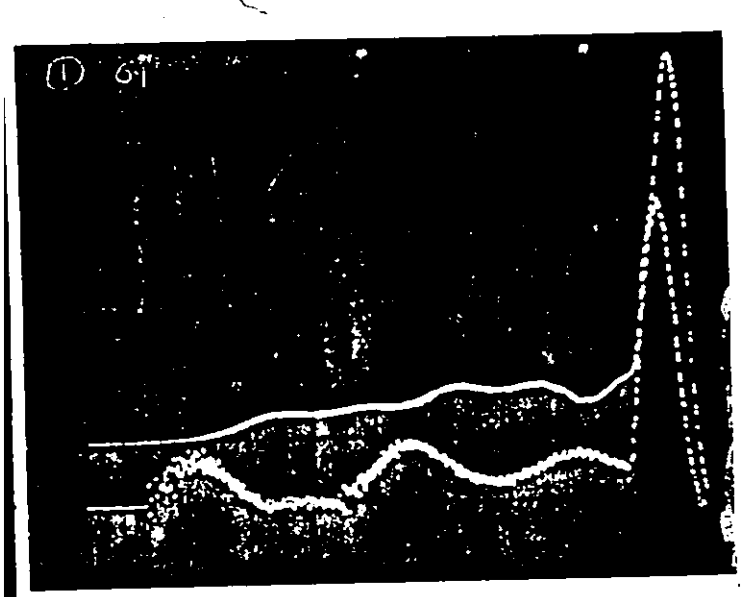

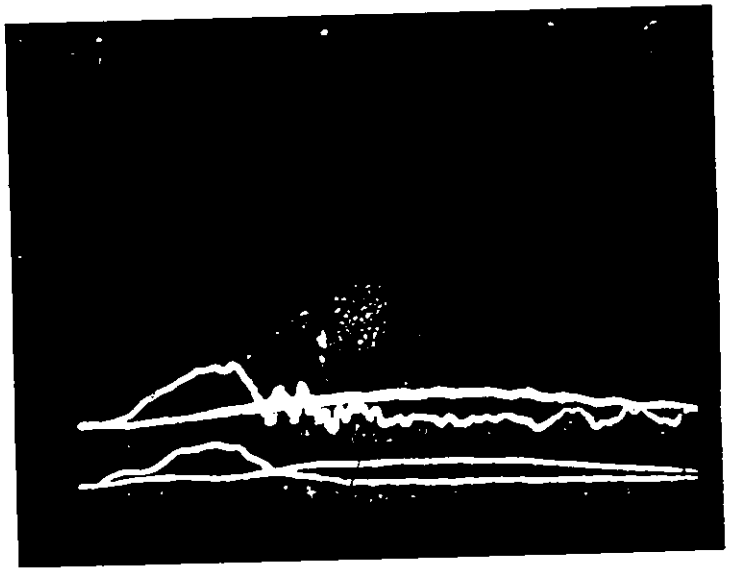

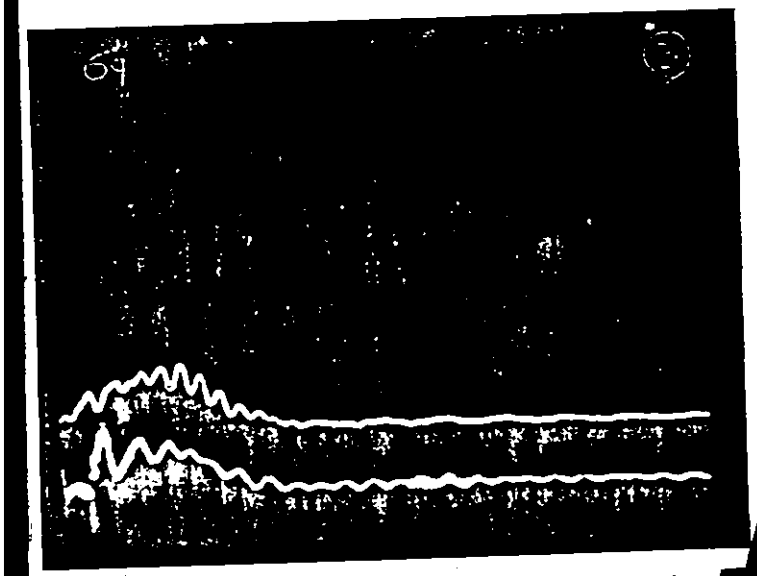

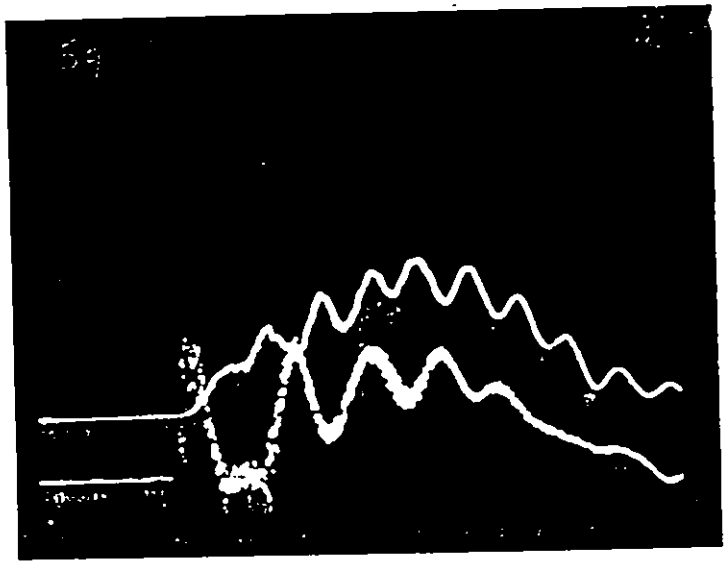

1 2

3 4

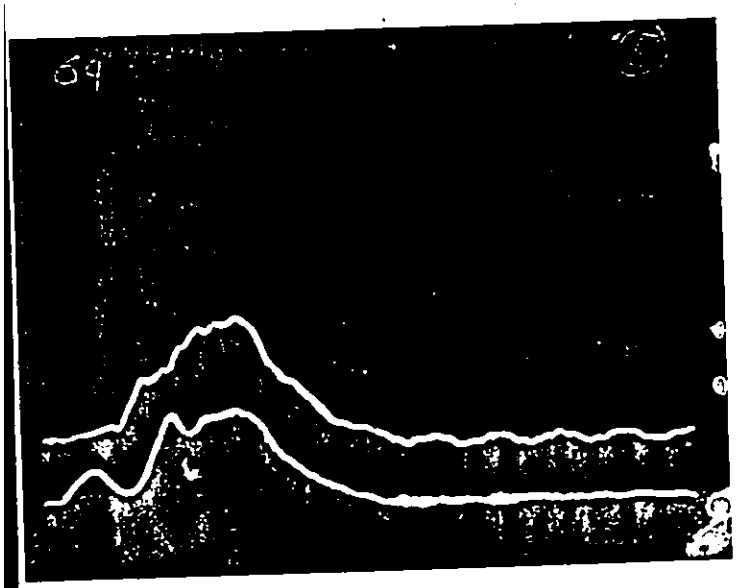

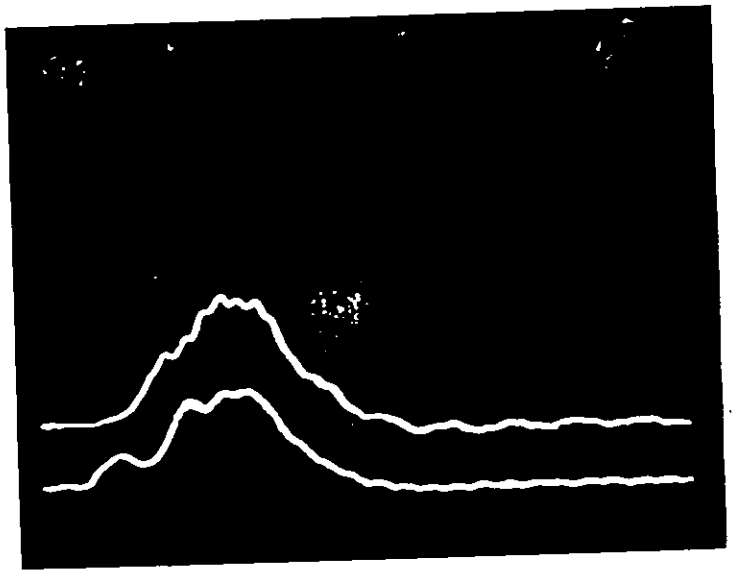

5 6

7 8

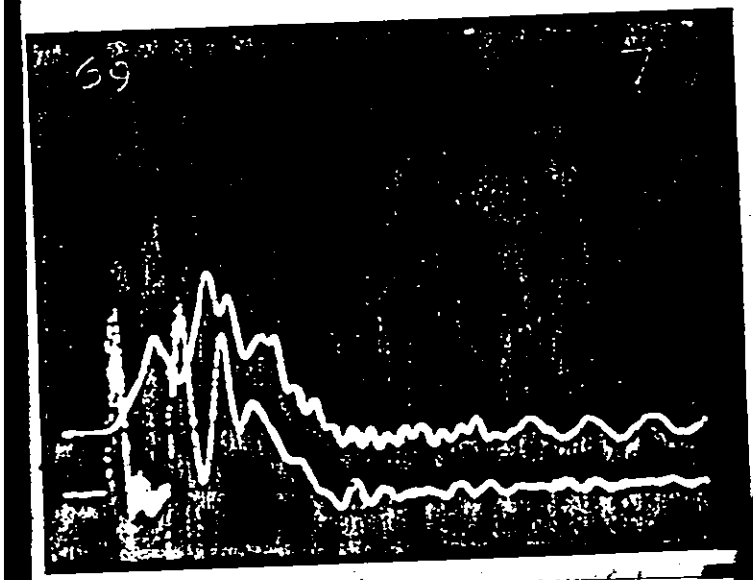

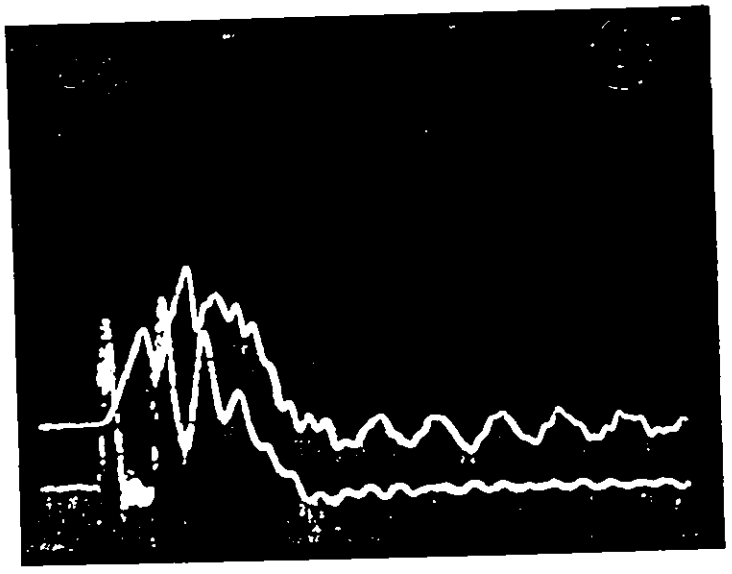

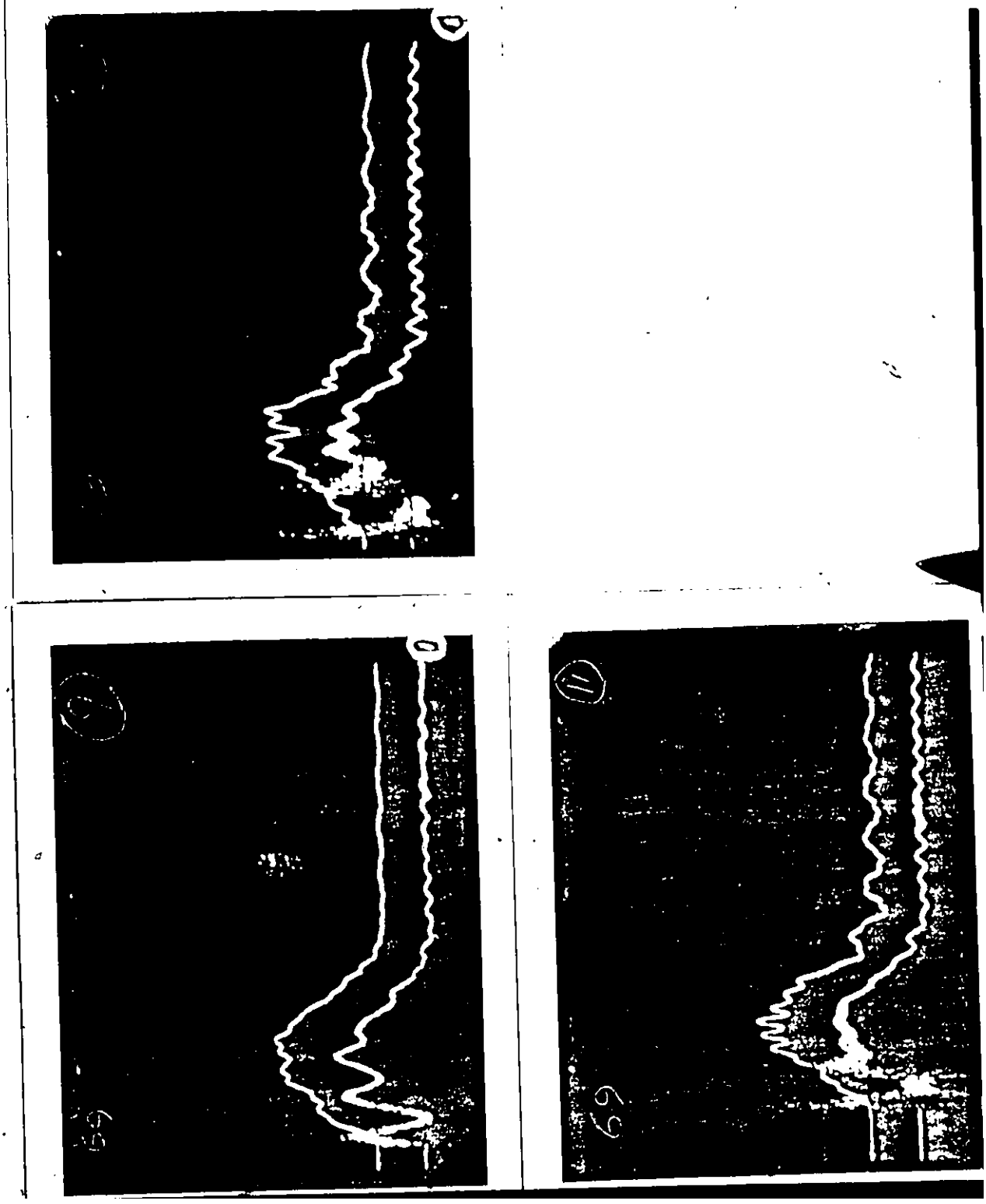

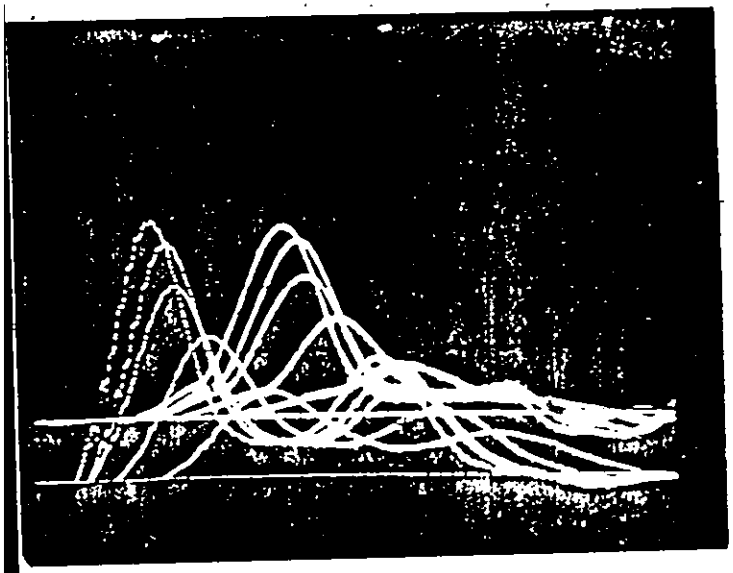

236

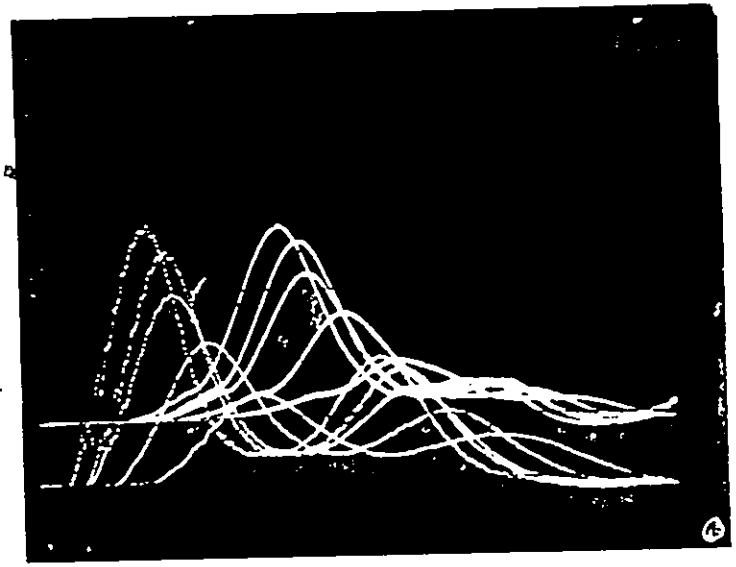

237

238

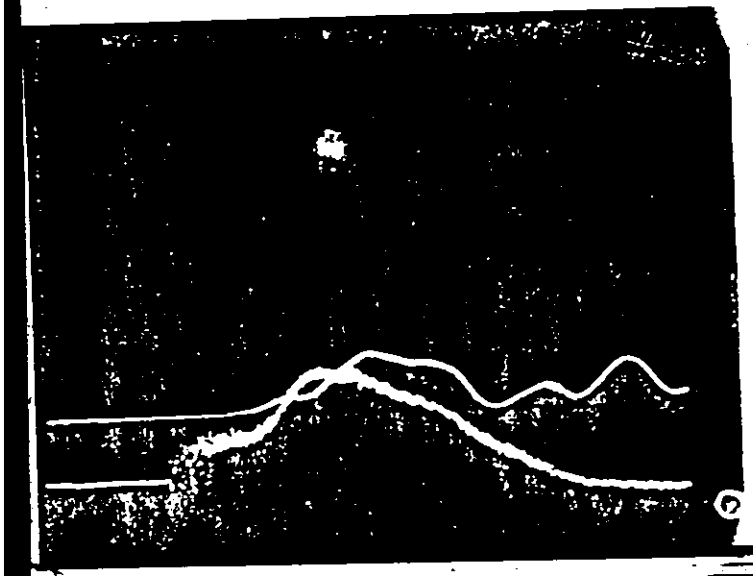

239

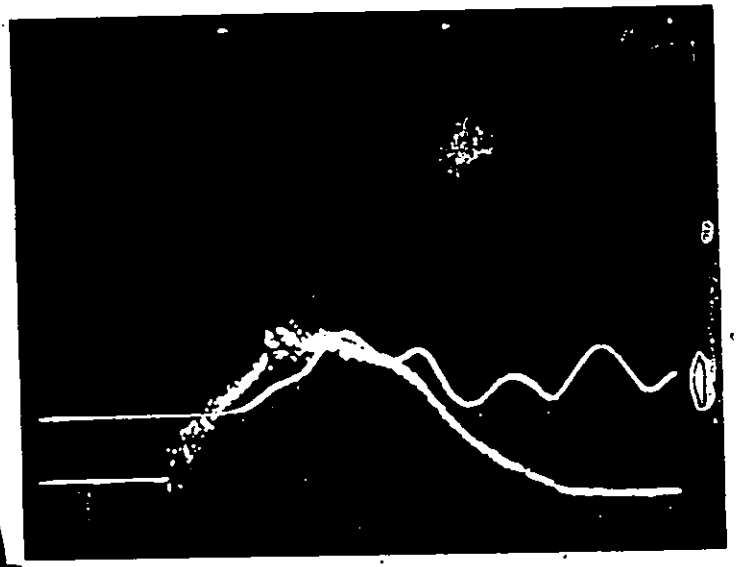

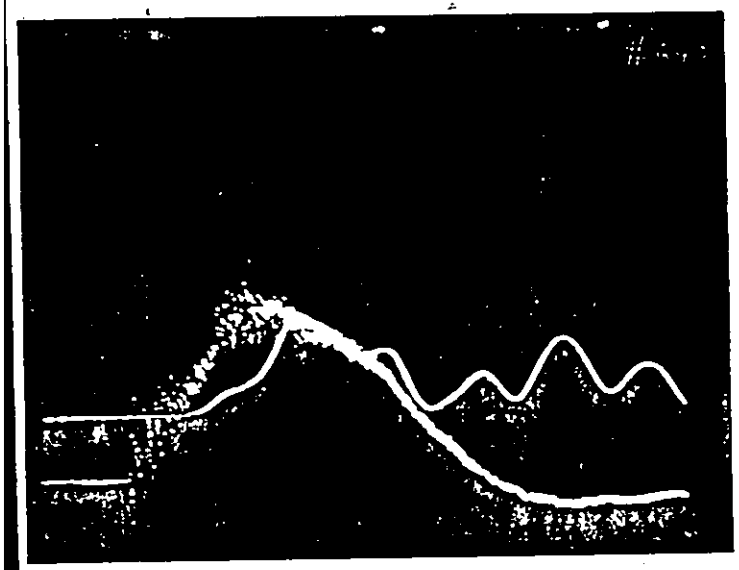

240

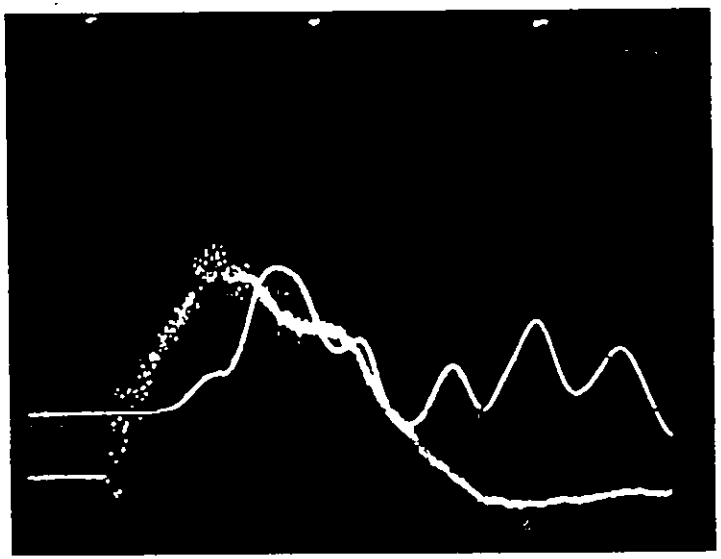

241

242

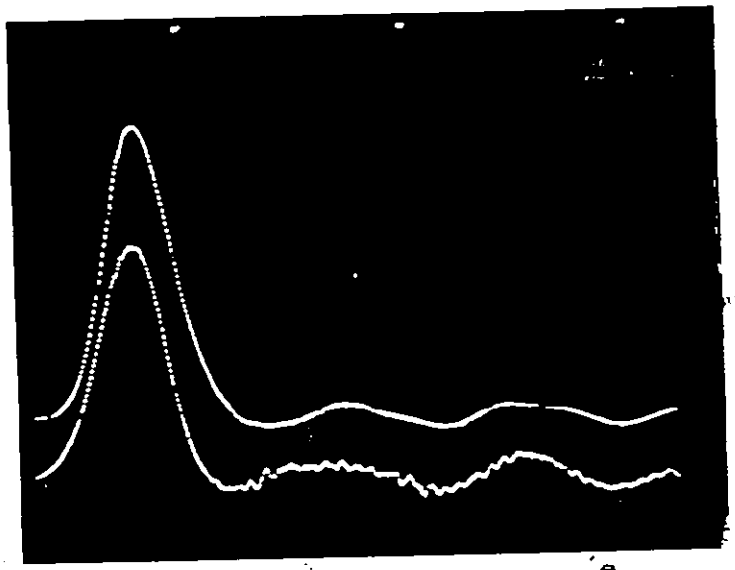

245

246

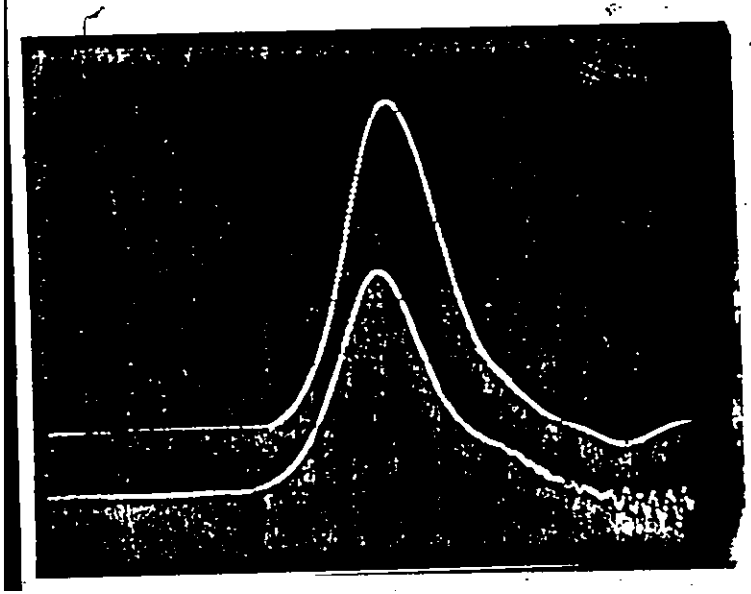

247

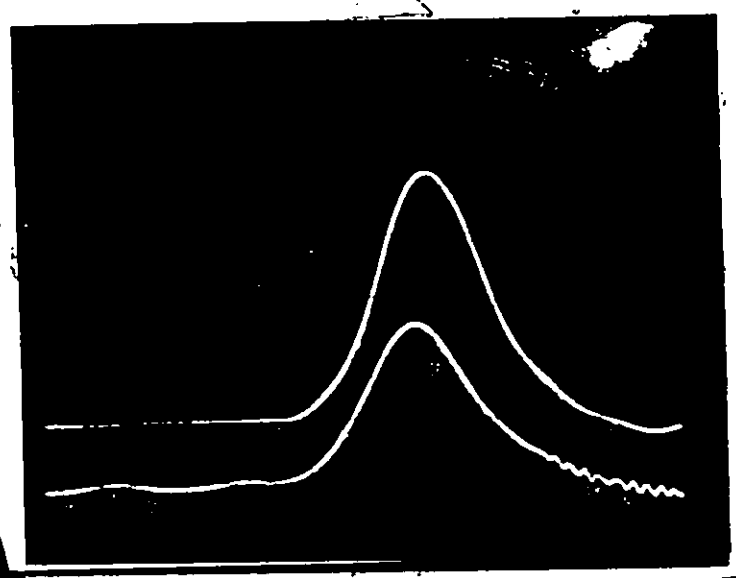

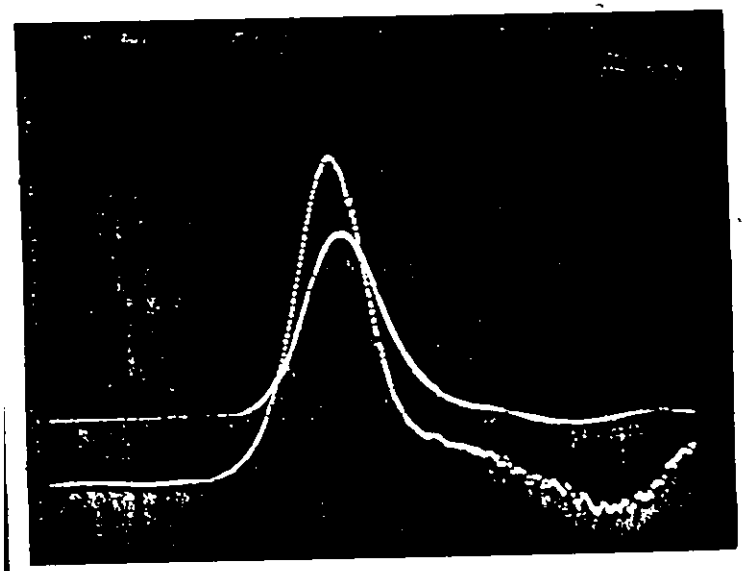

248

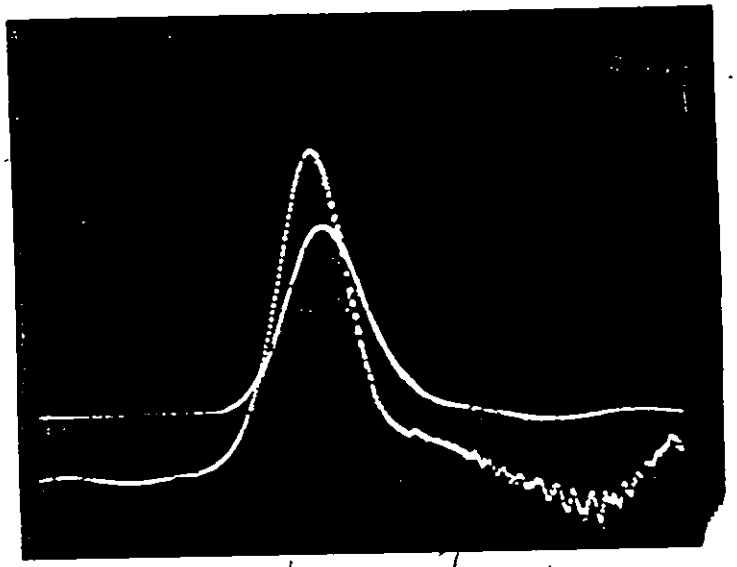

249

250

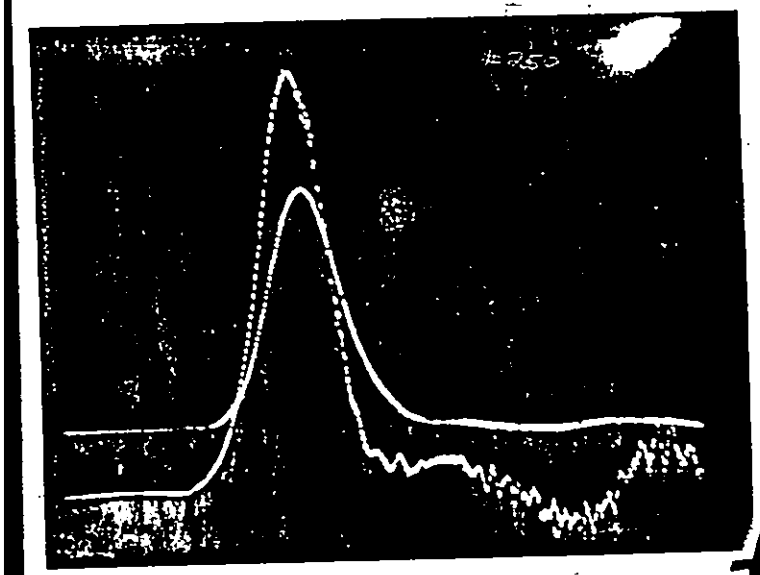

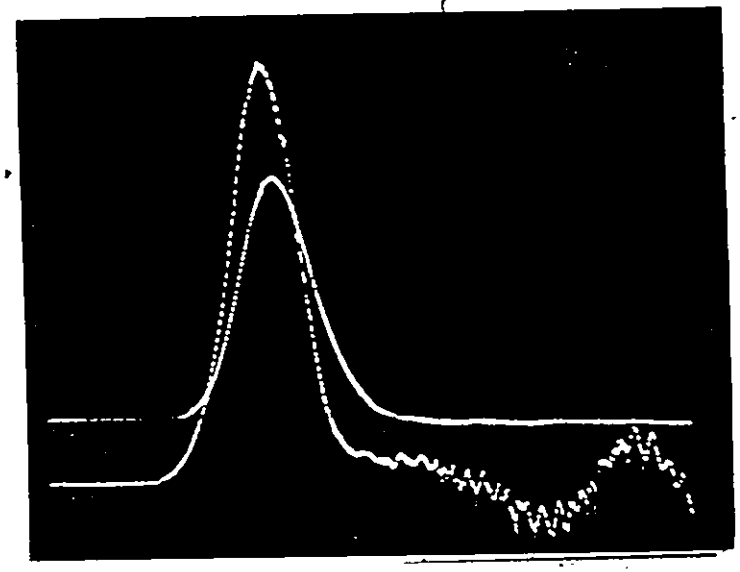

251

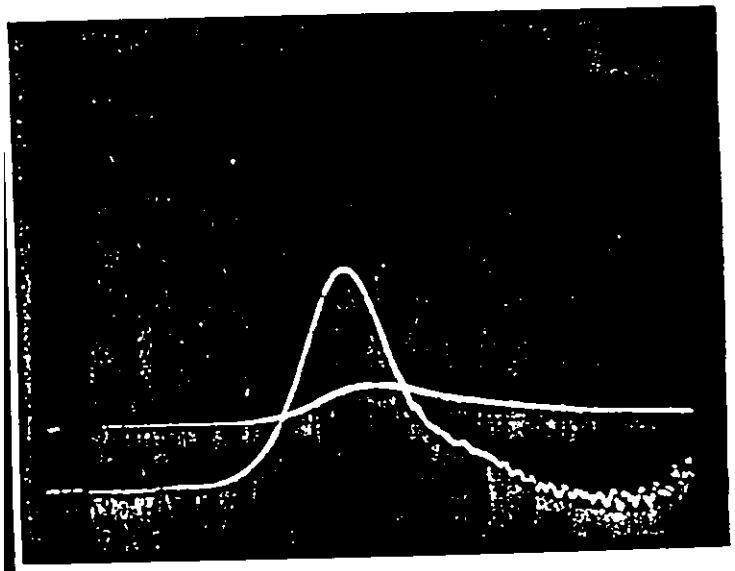

252

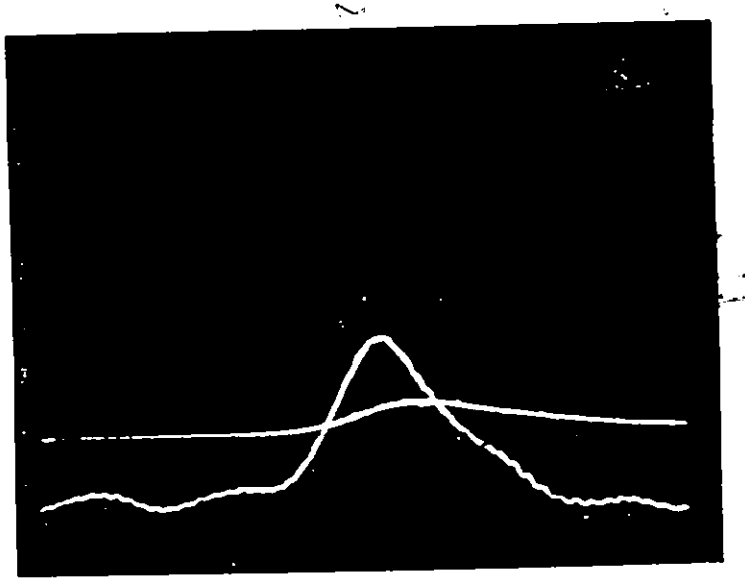

253

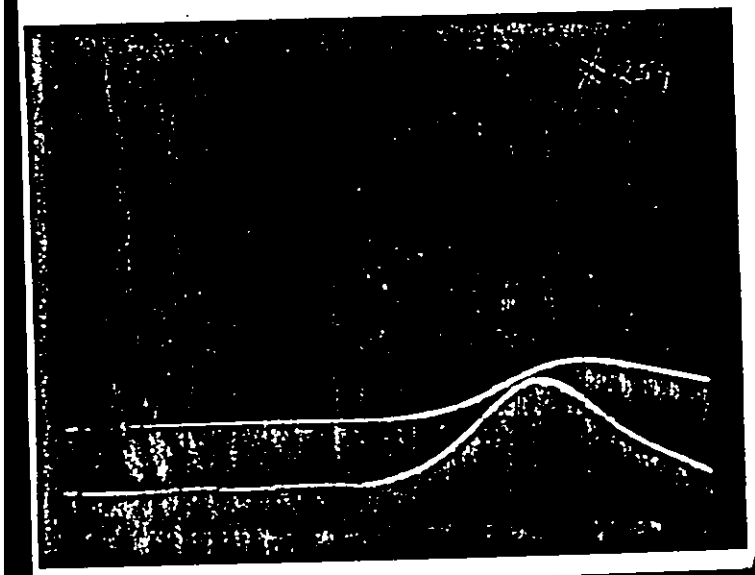

254

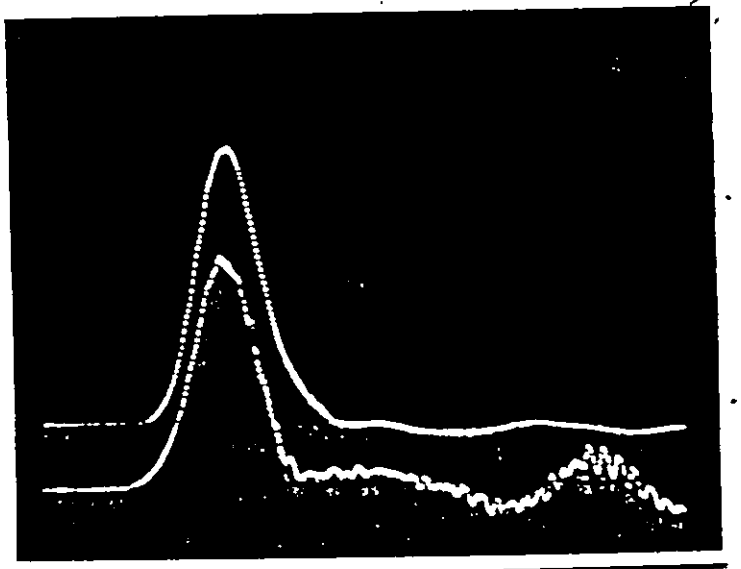

255

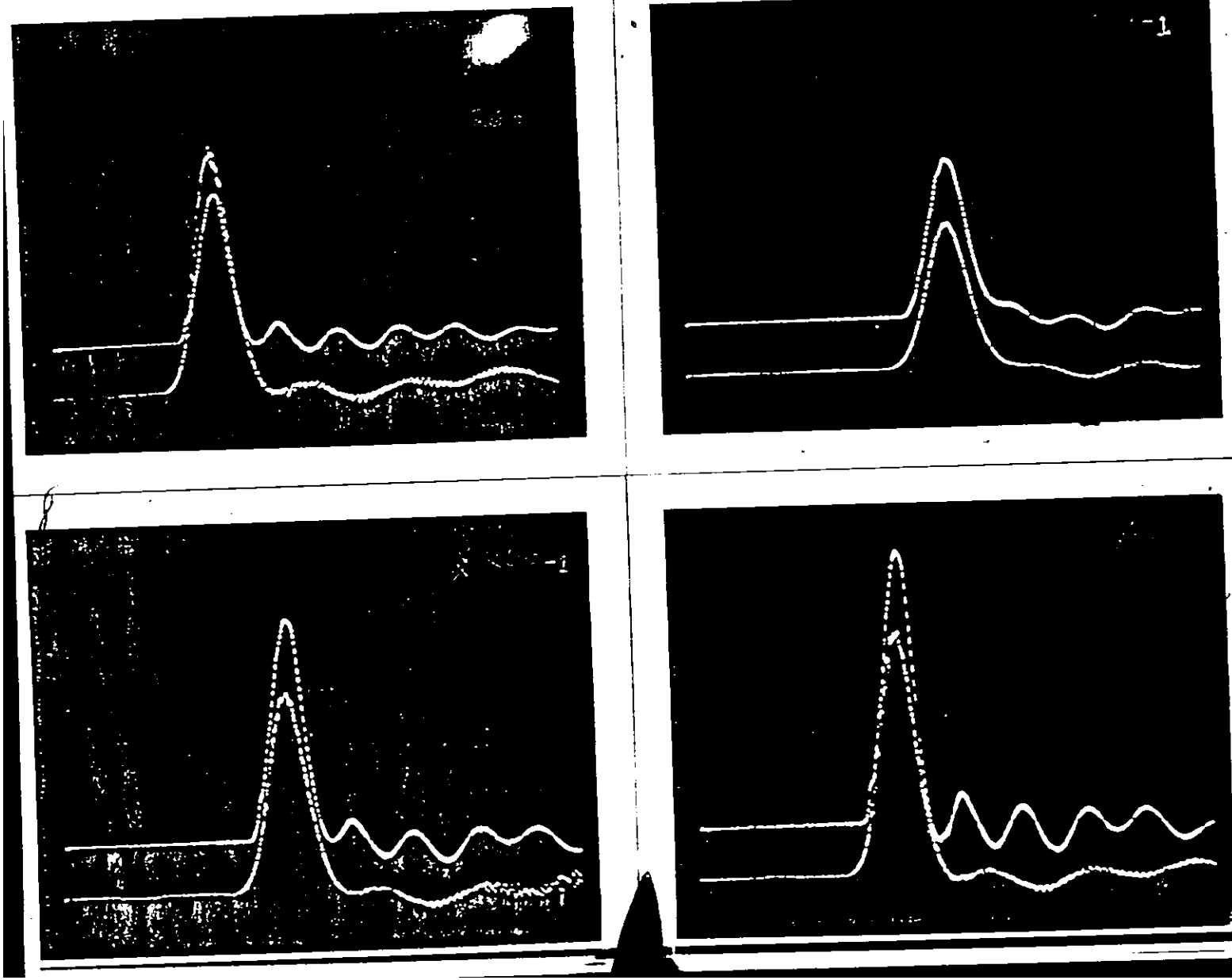

260 259-1

260-1 261

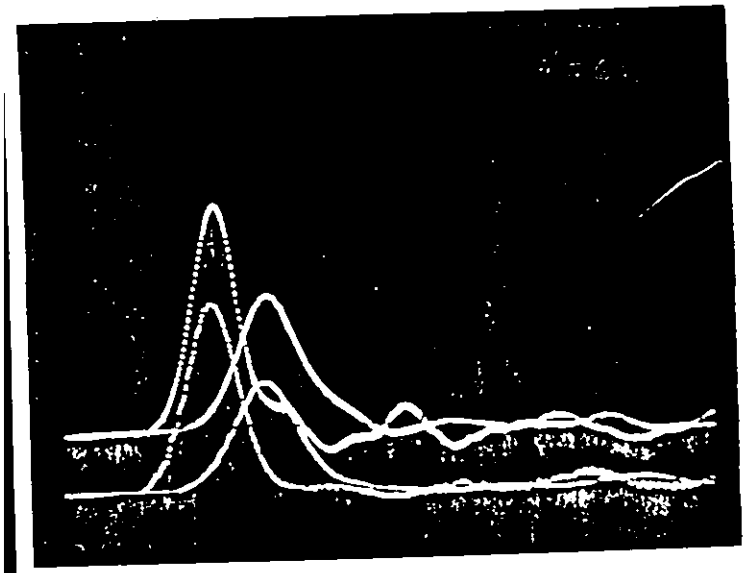

262

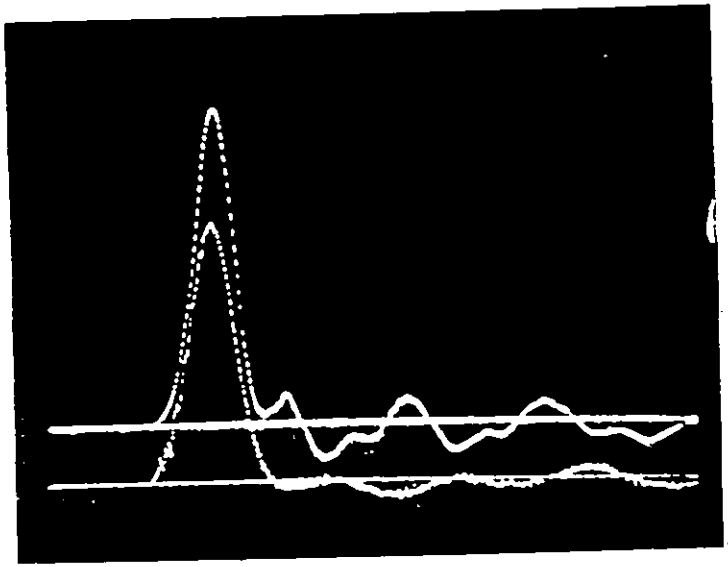

263

264

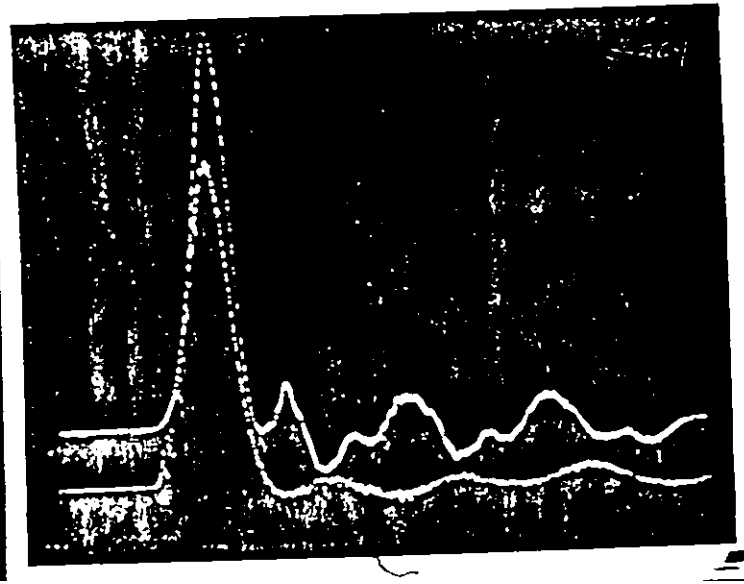

265

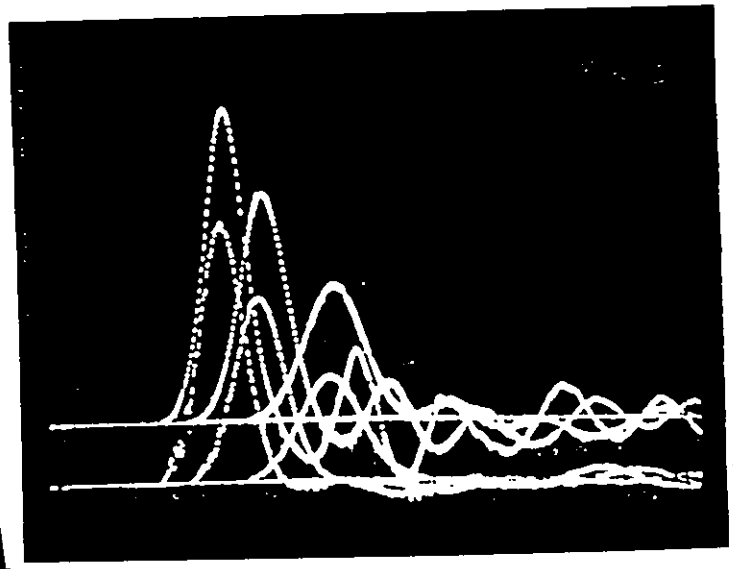

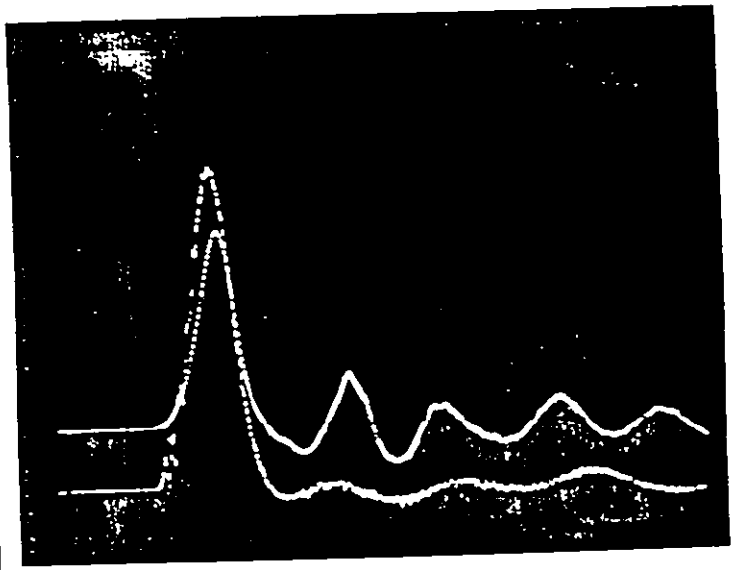

266

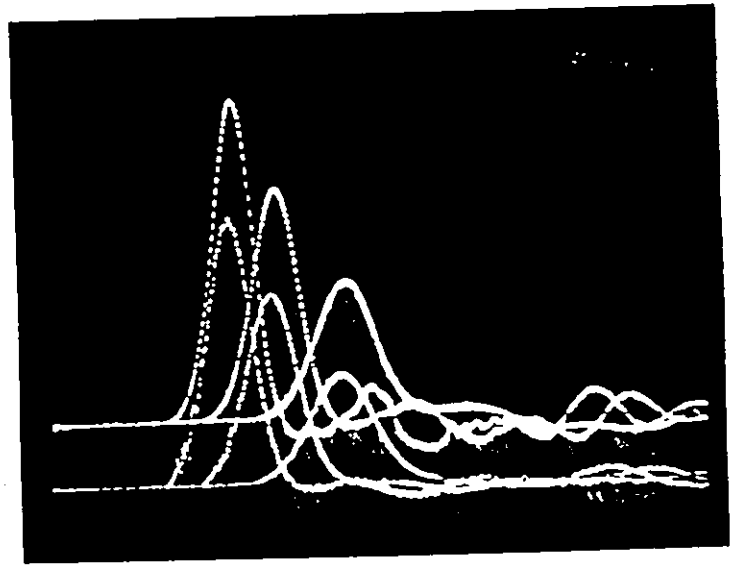

267.

268

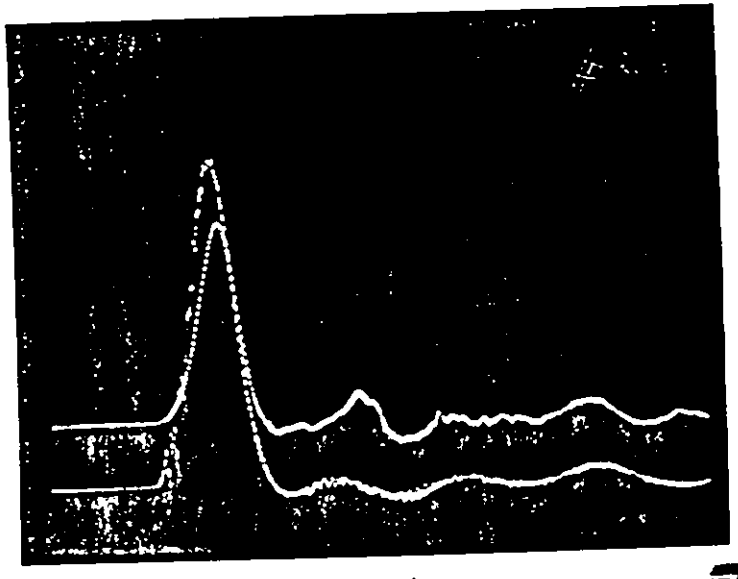

269

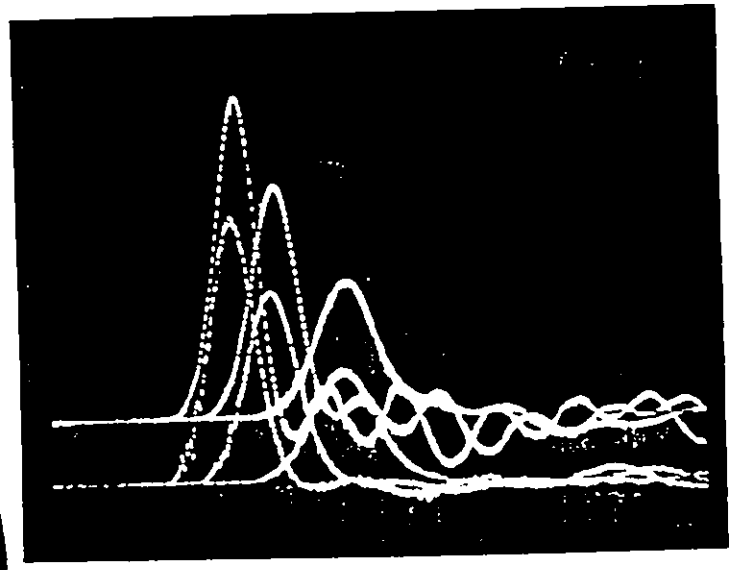

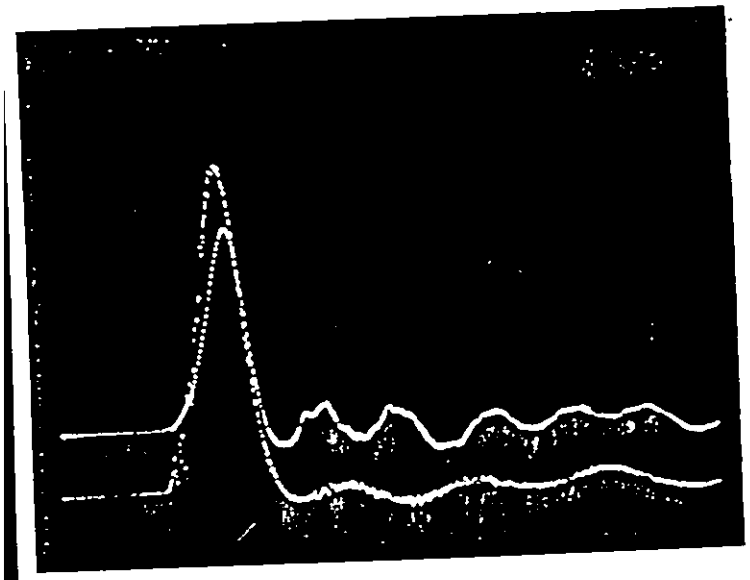

270

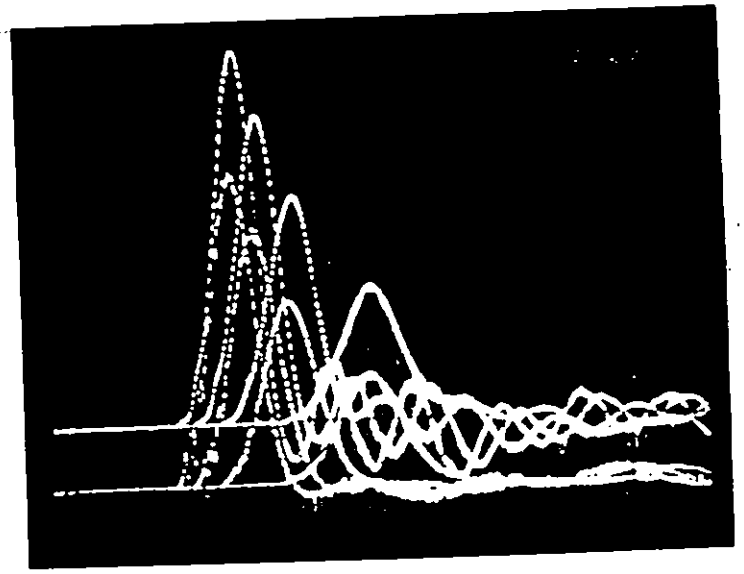

271

272

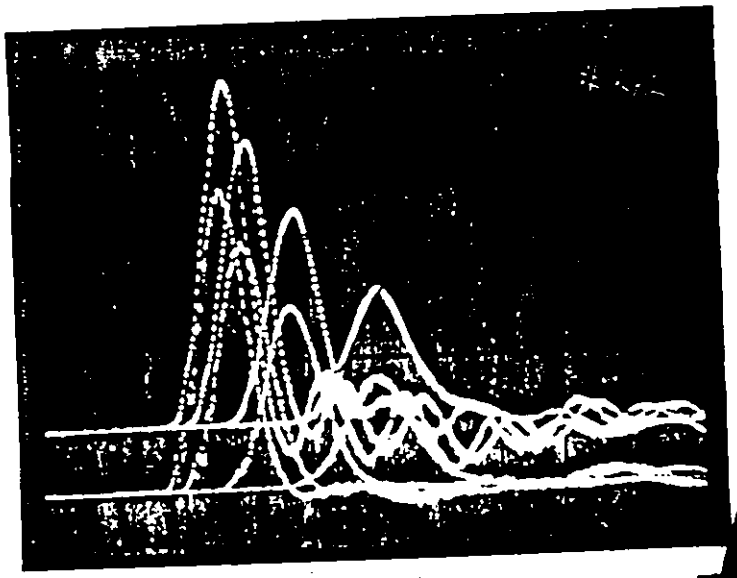

273

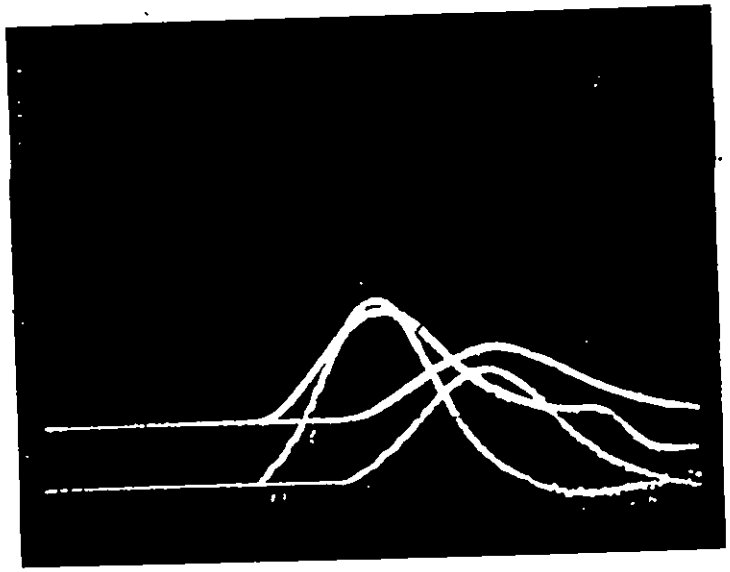

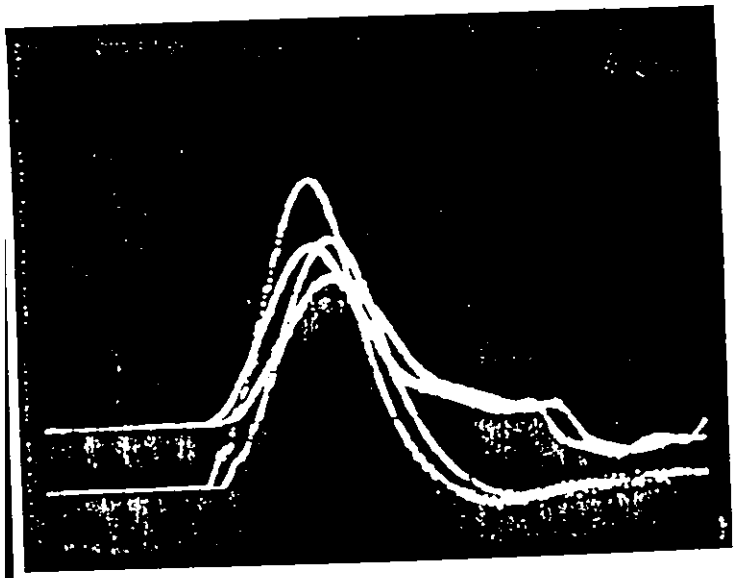

274

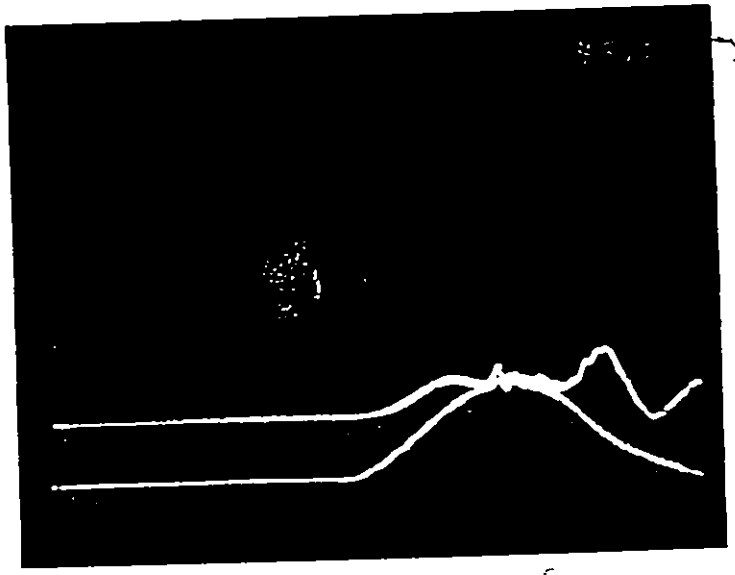

275

276

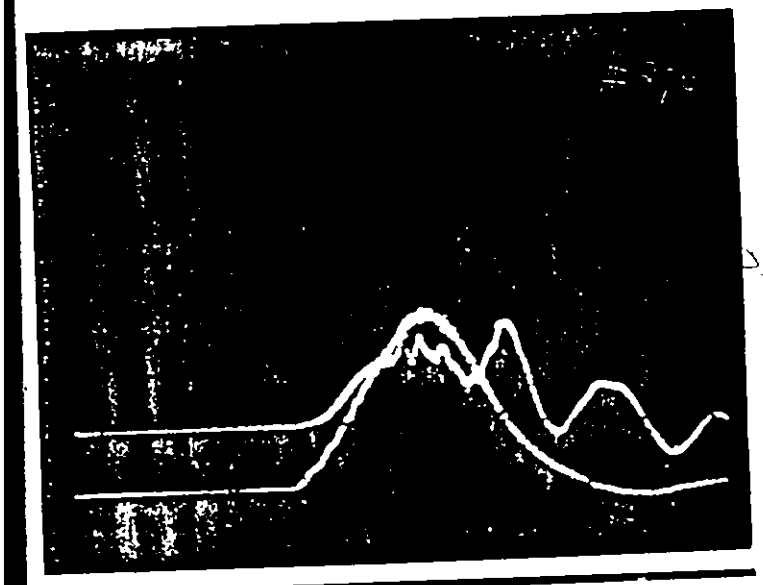

277

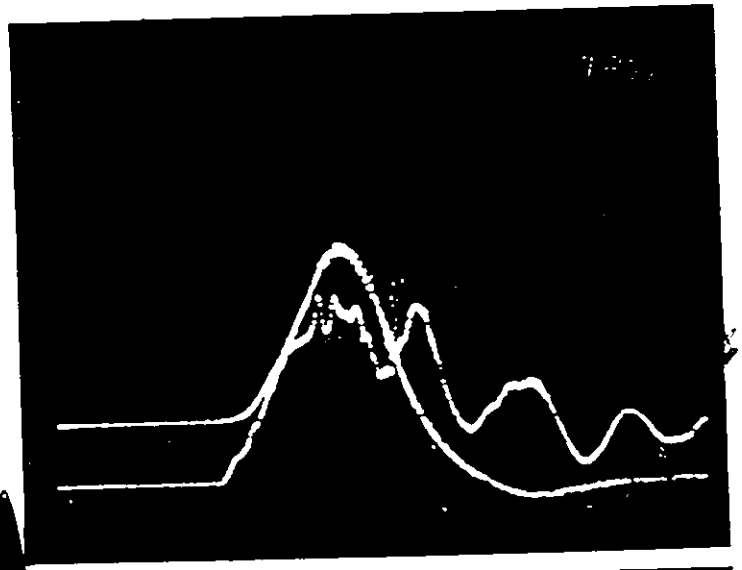

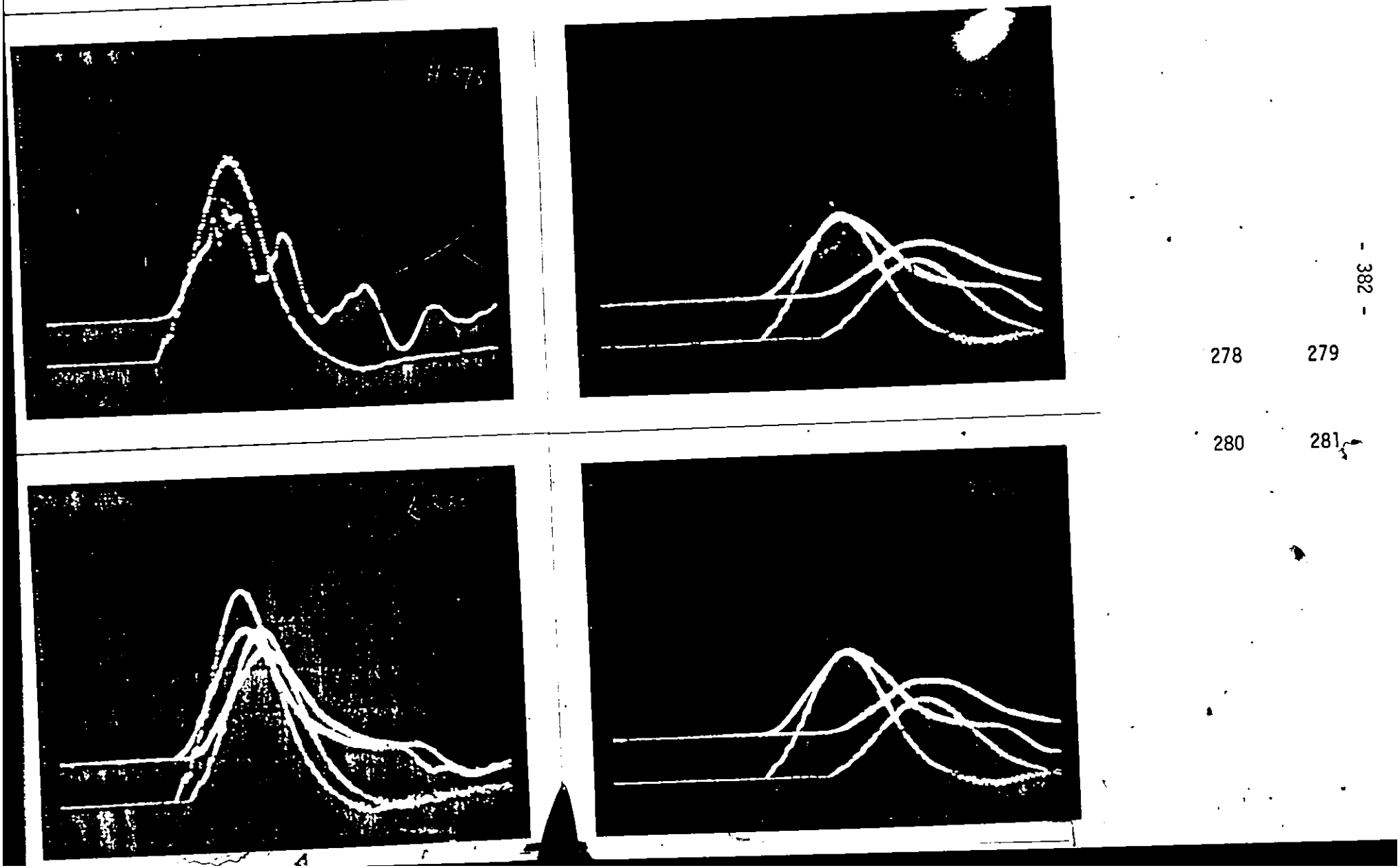

278 279

280 281

285B 286

287 288

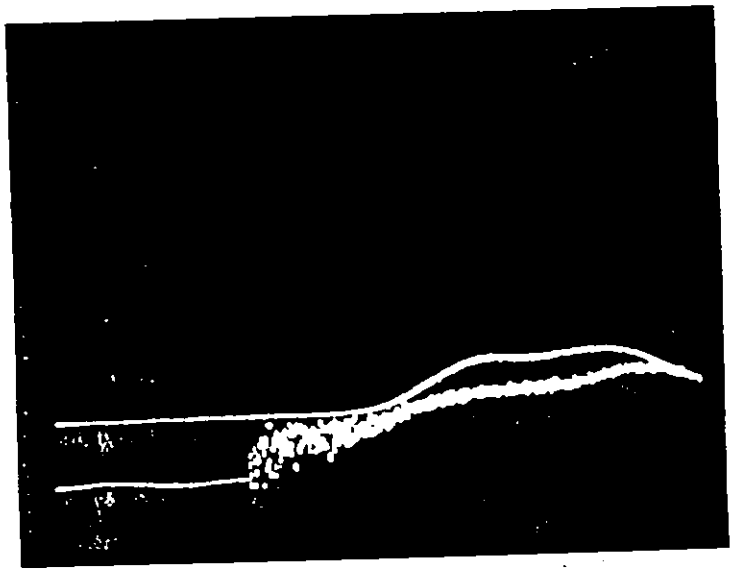

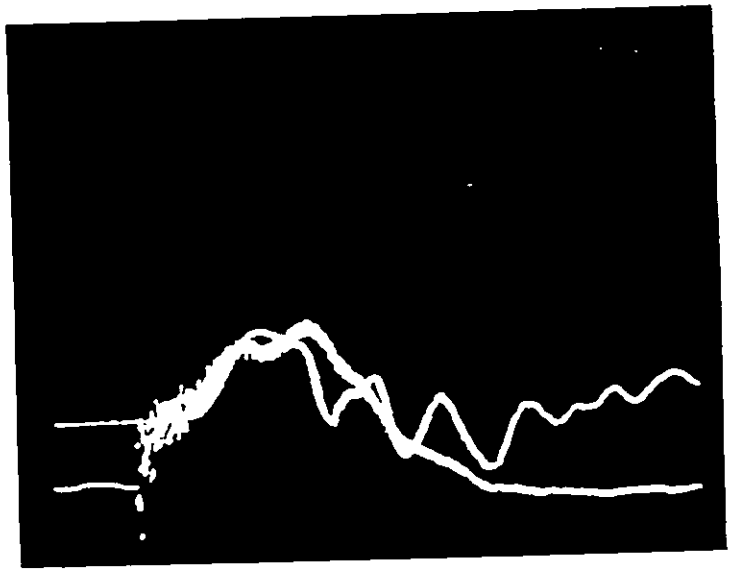

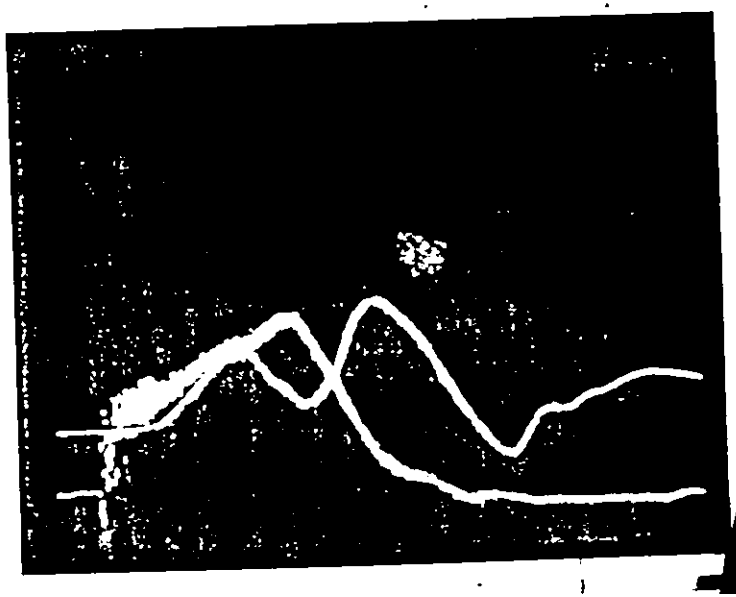

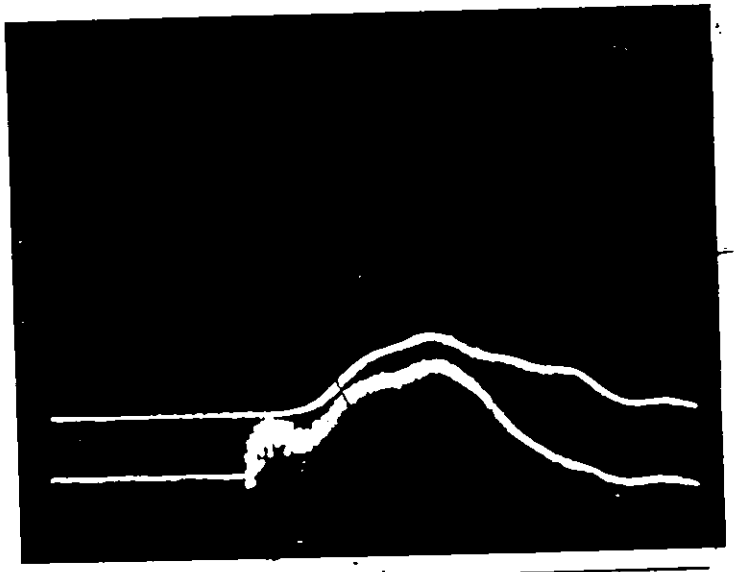

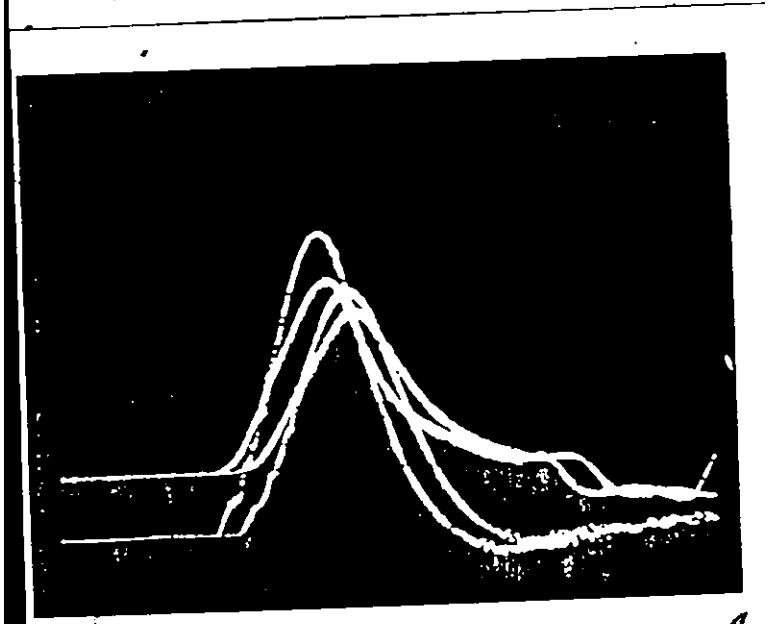

282

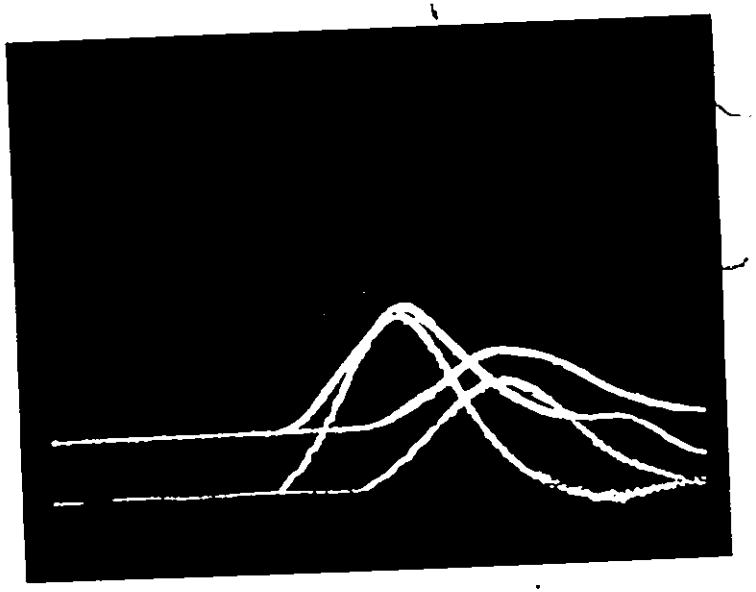

283

284

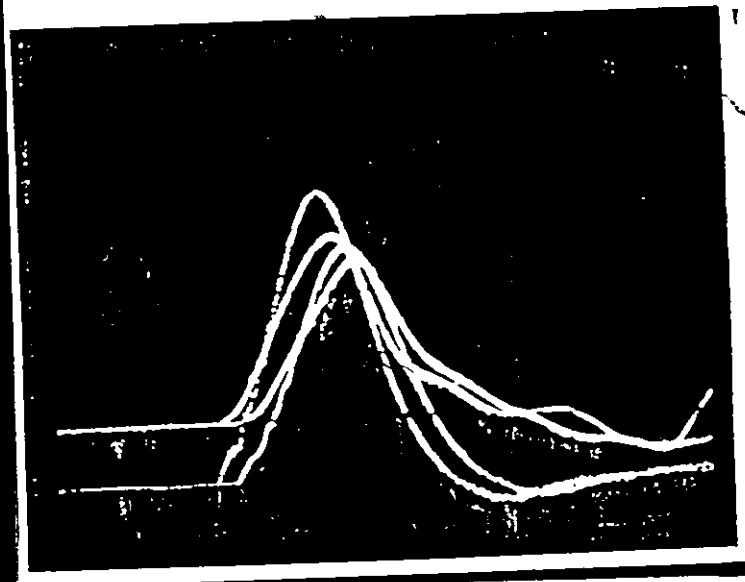

285A

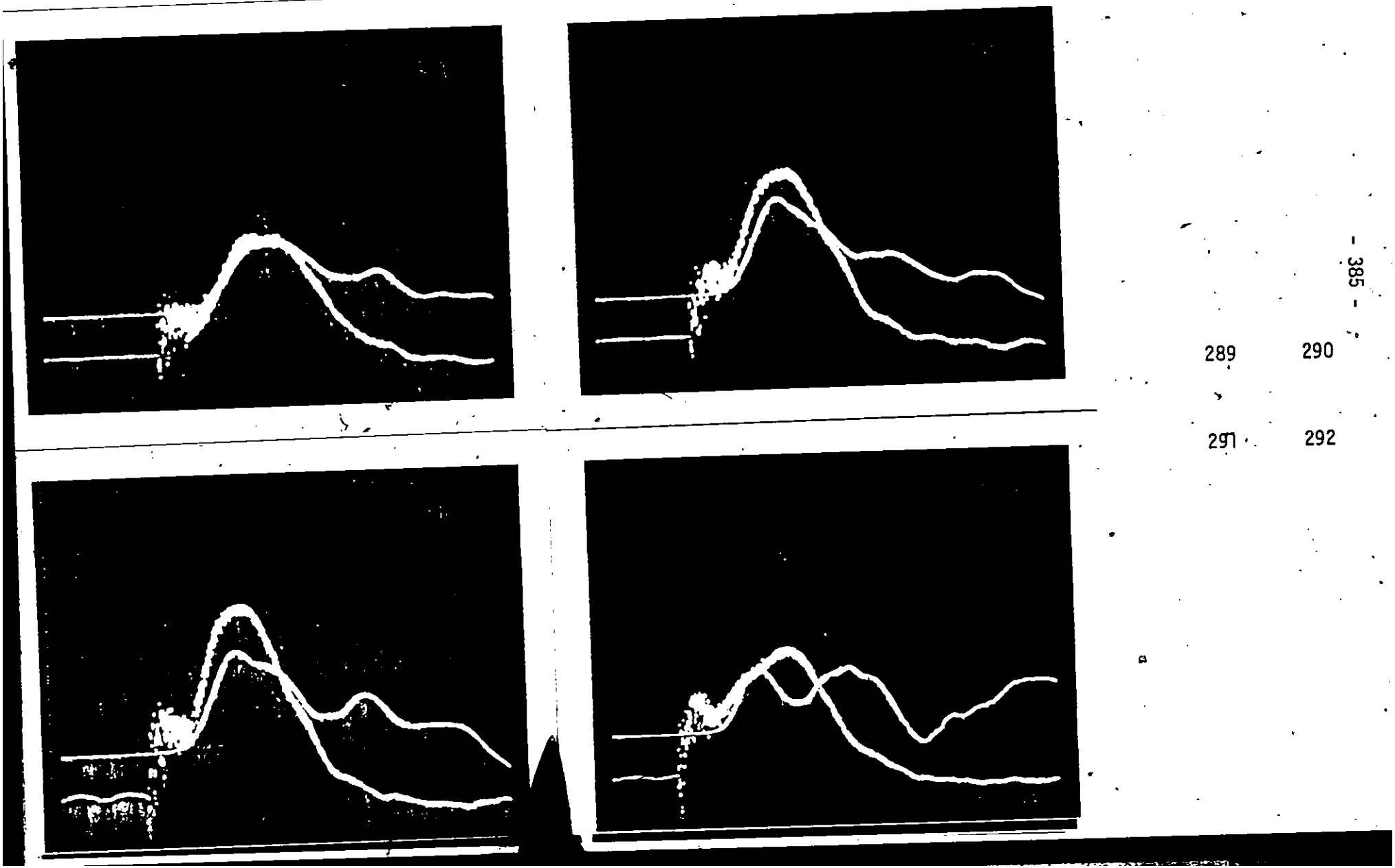
289
290
291
292

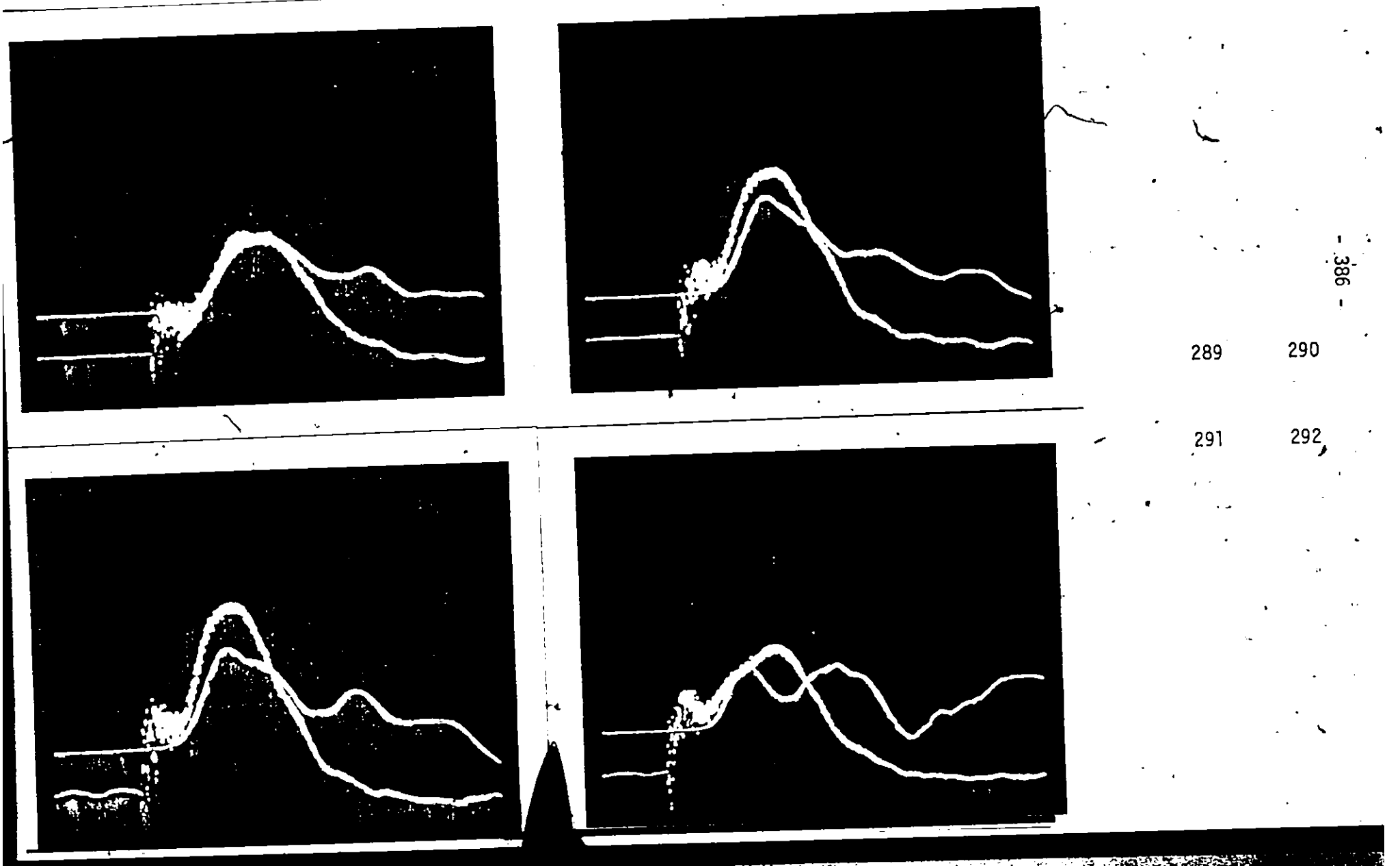

289 290

291 292

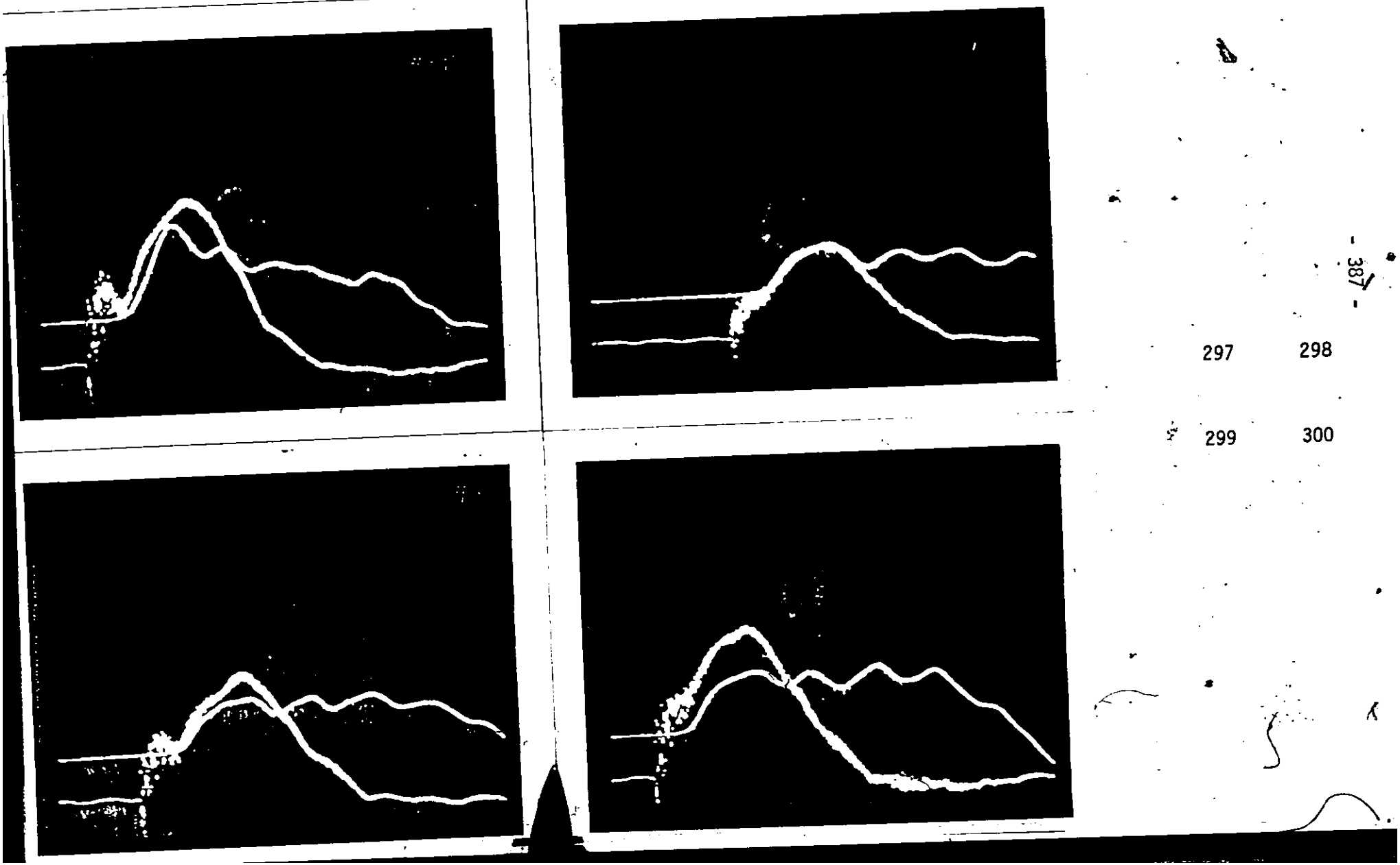

297 298

299 300

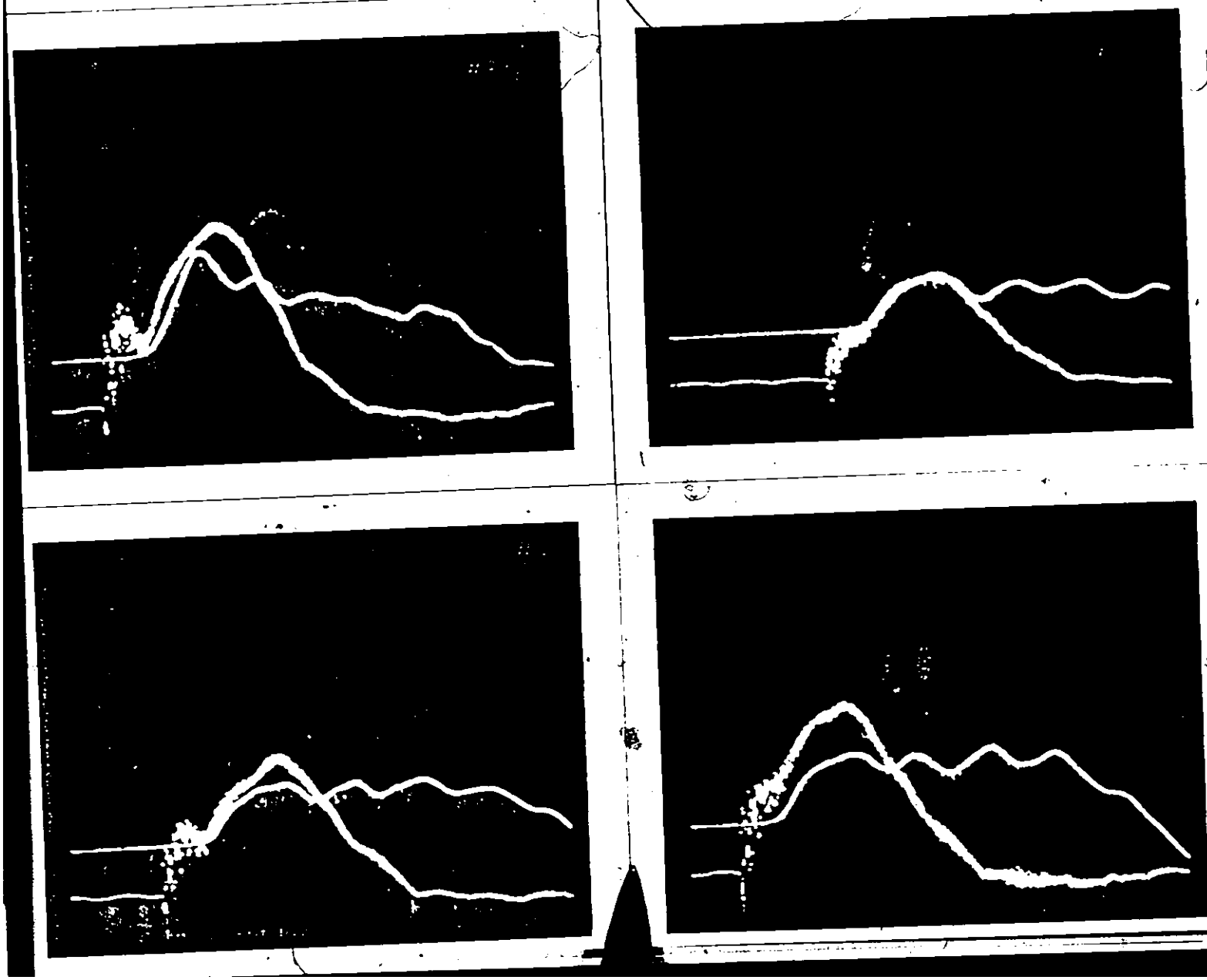
297
298
299
300

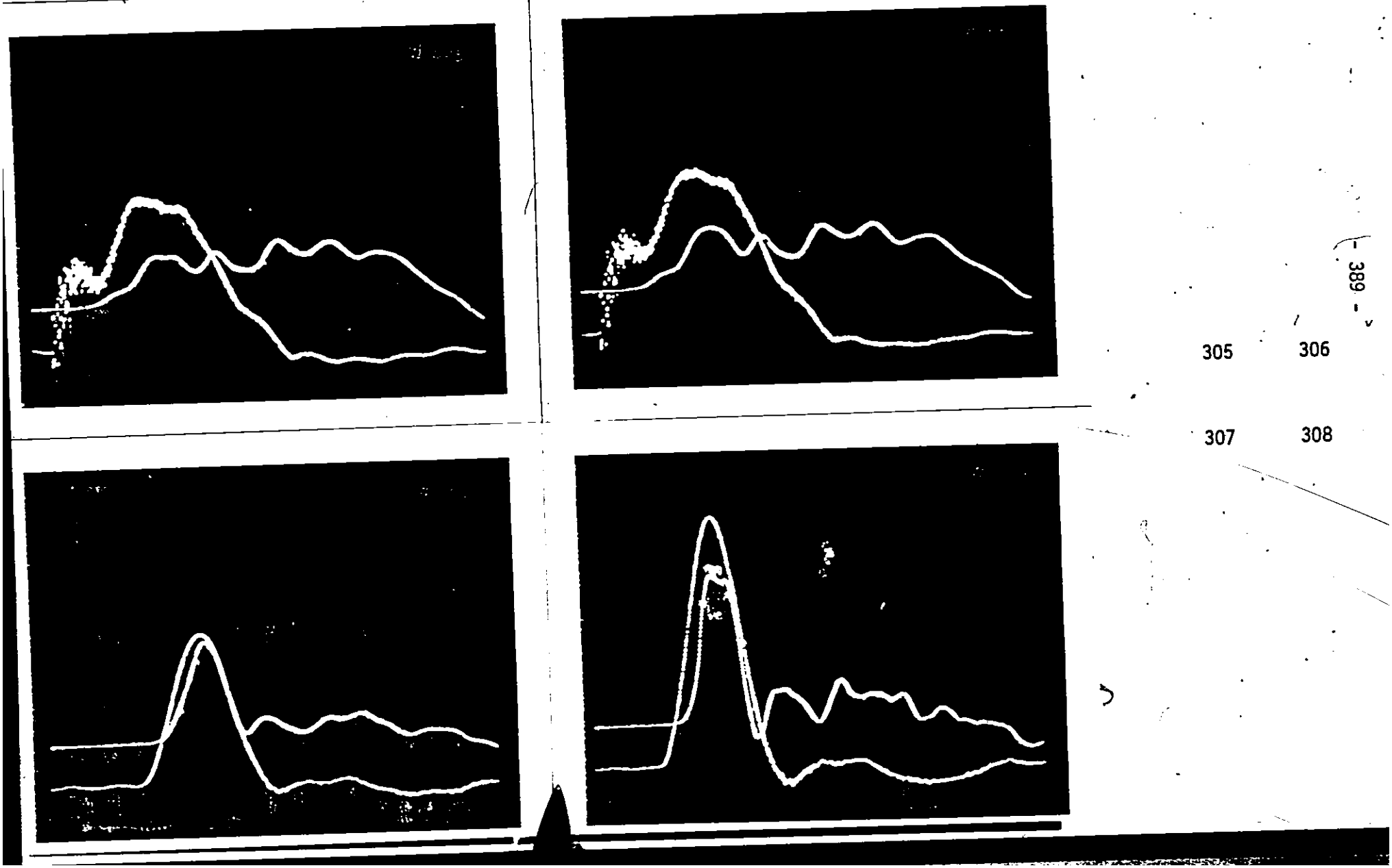

305 306

307 308

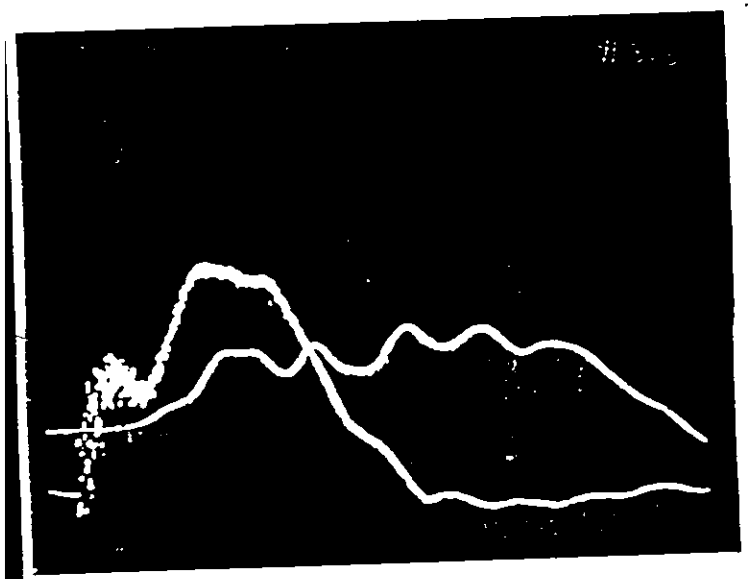

305

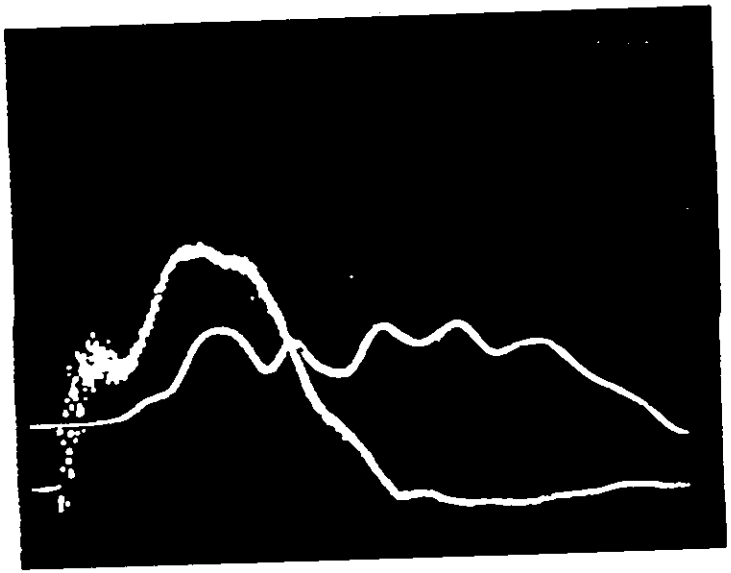

306

307

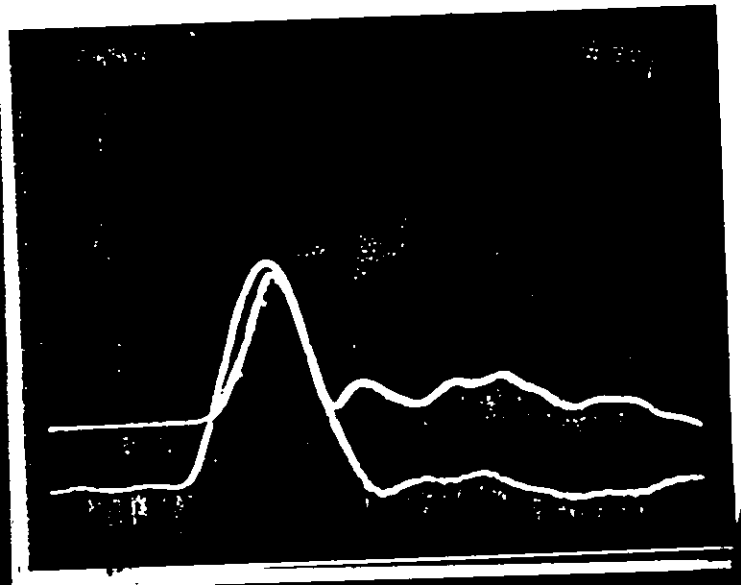

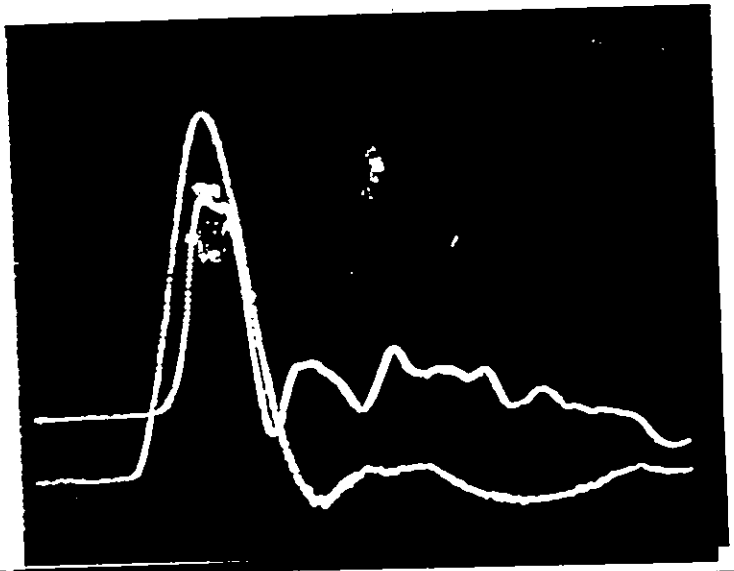

308

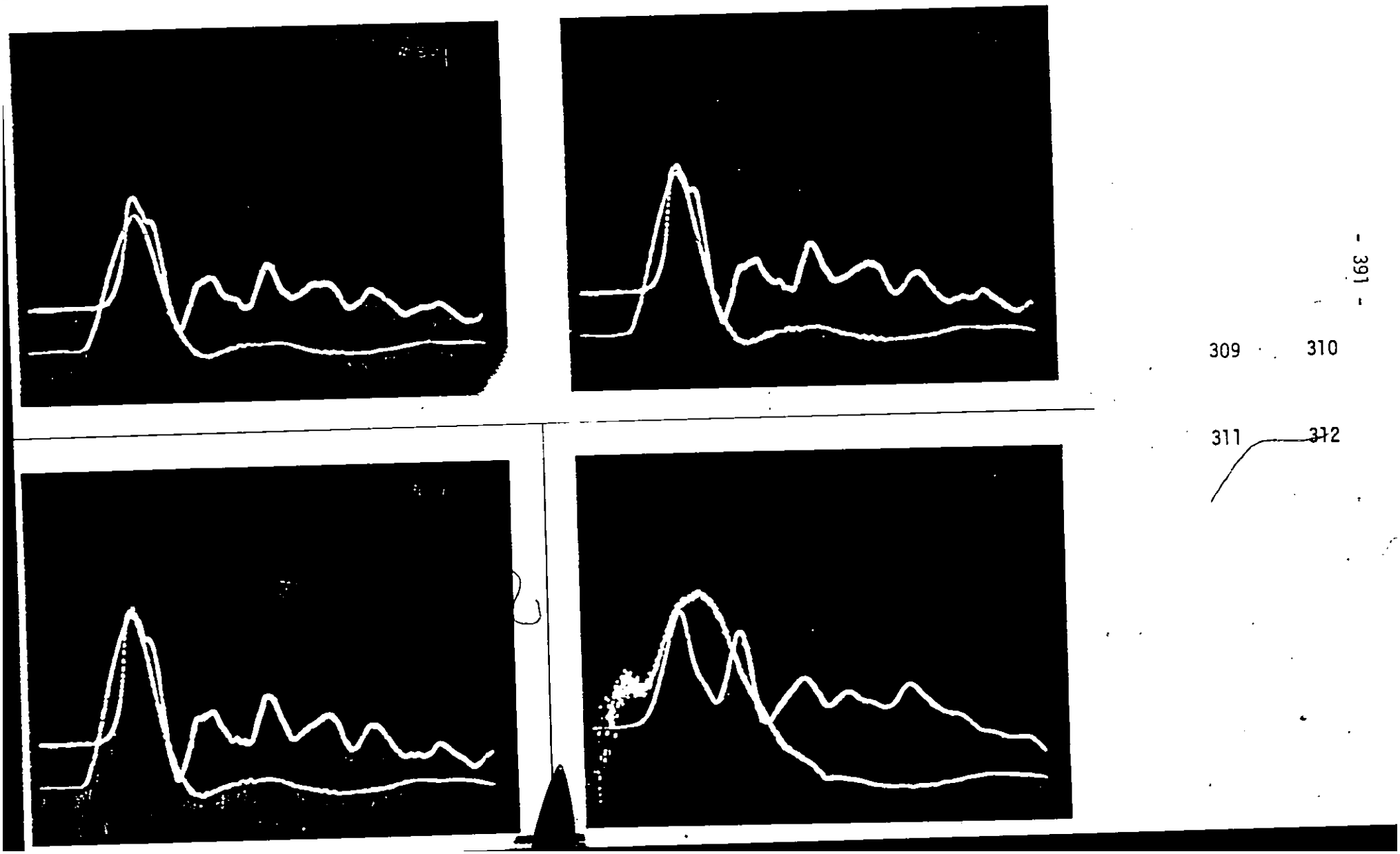

309 310

311 312

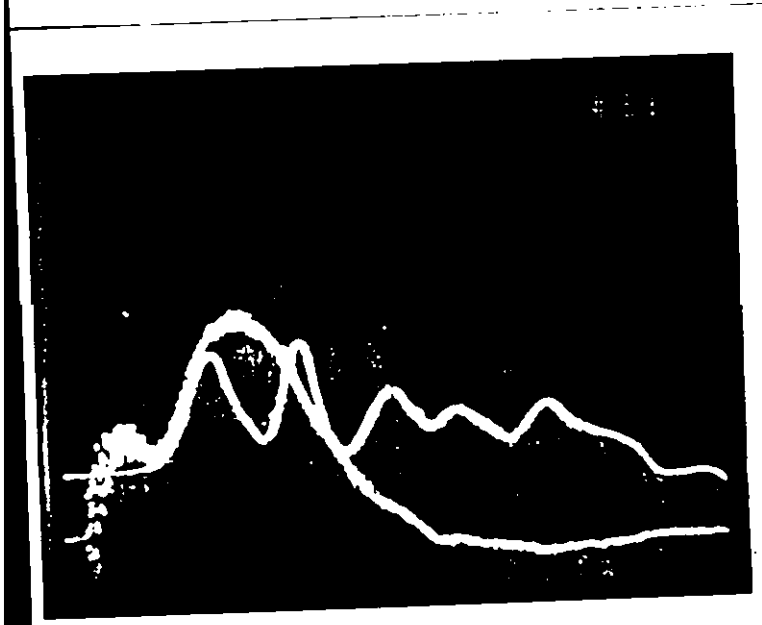

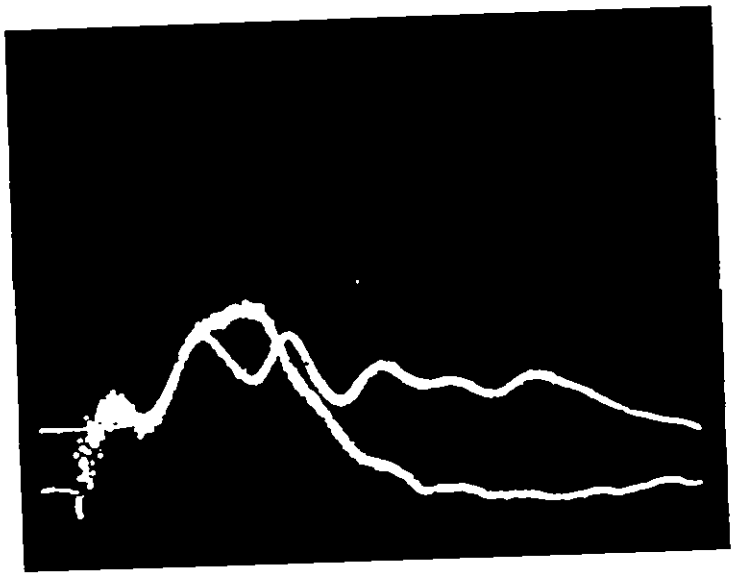

313 314

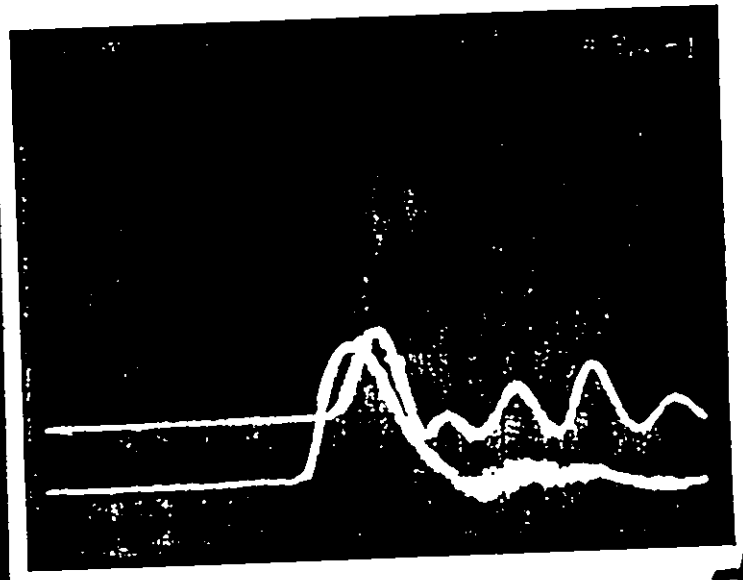

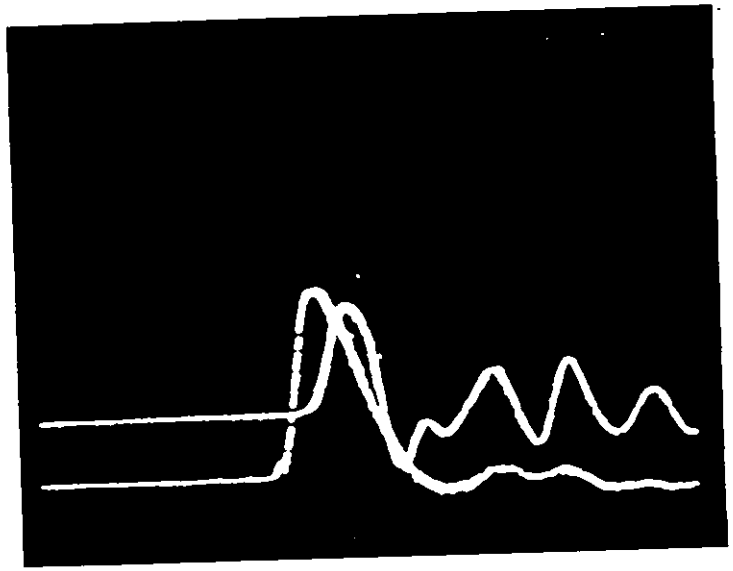

312-1 313-1

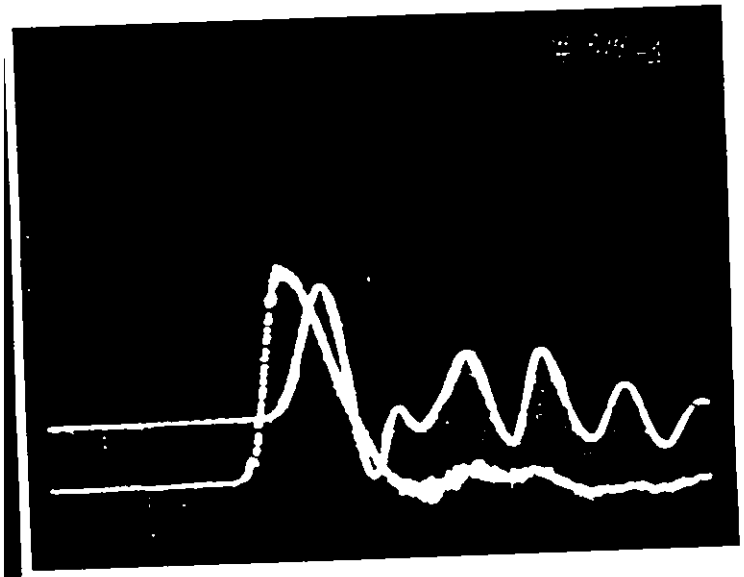

314-1

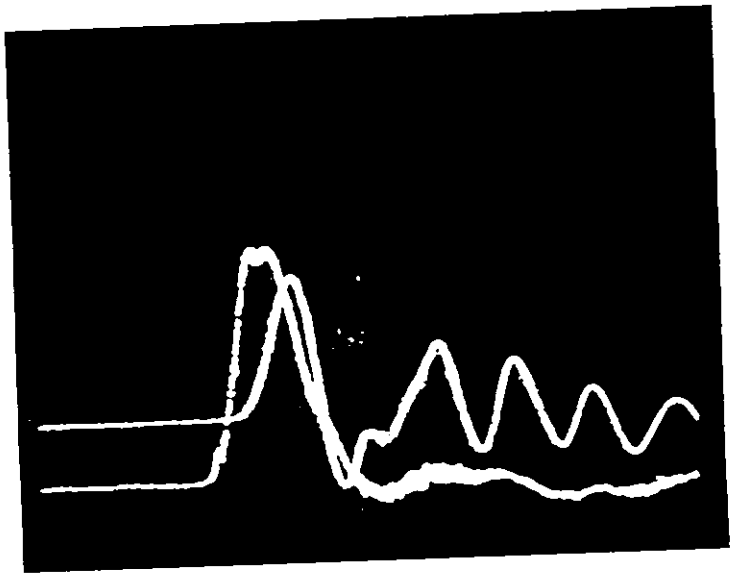

315

316

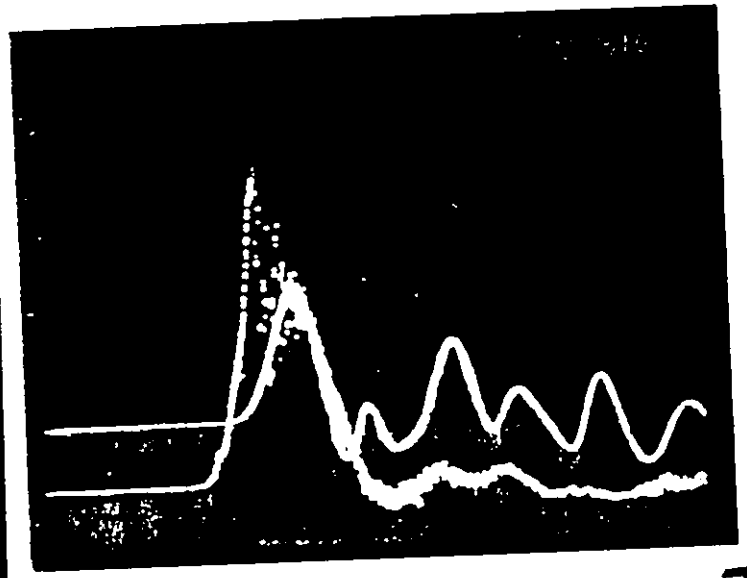

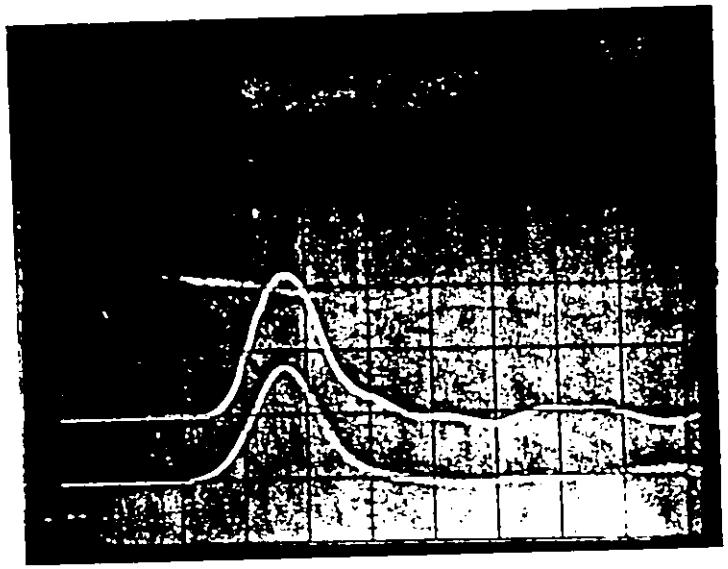

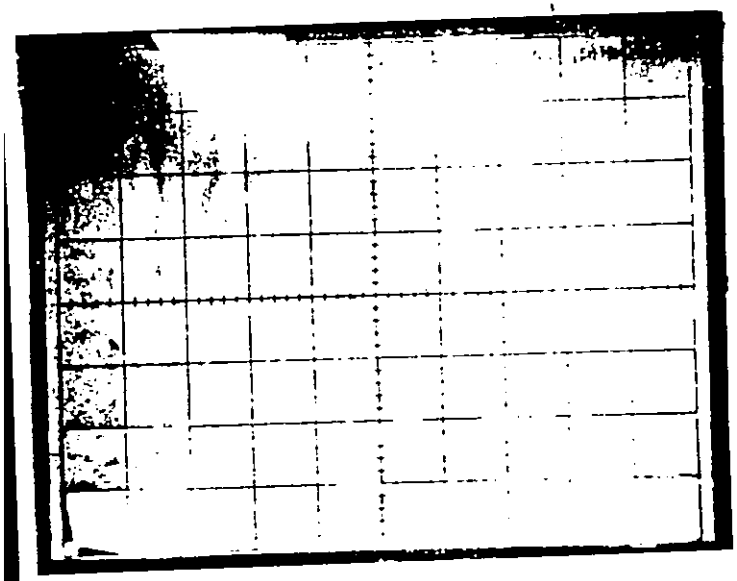

318

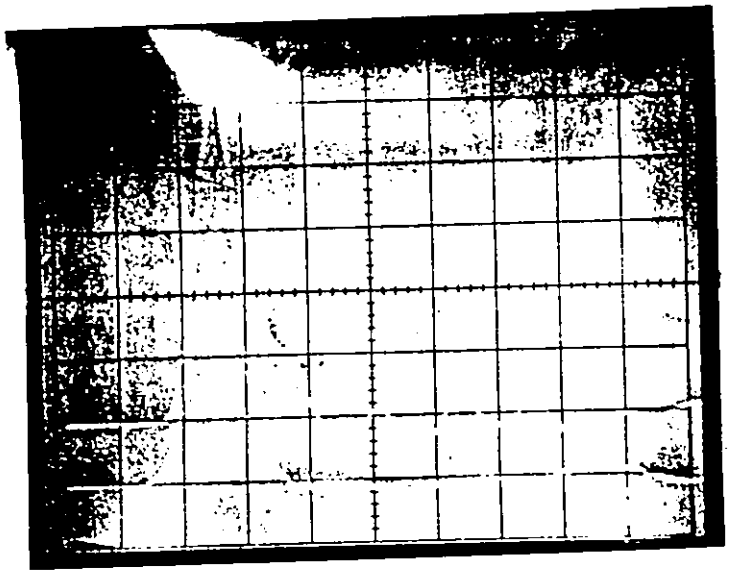

319

320

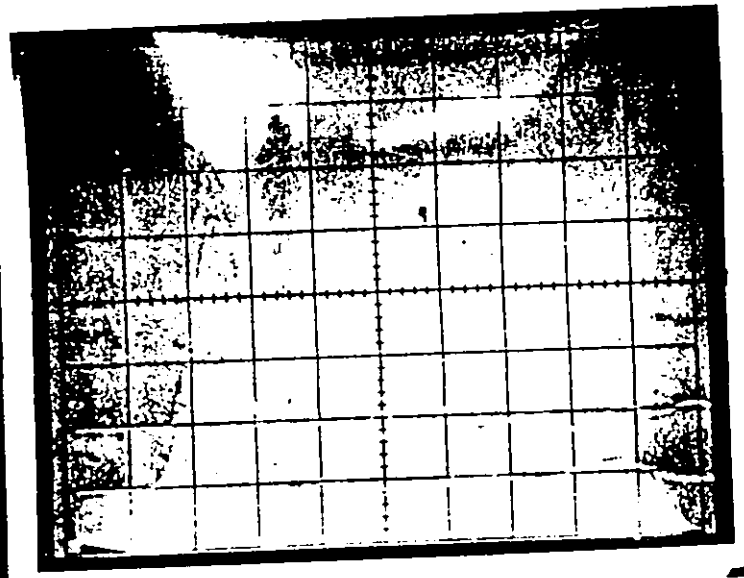

321

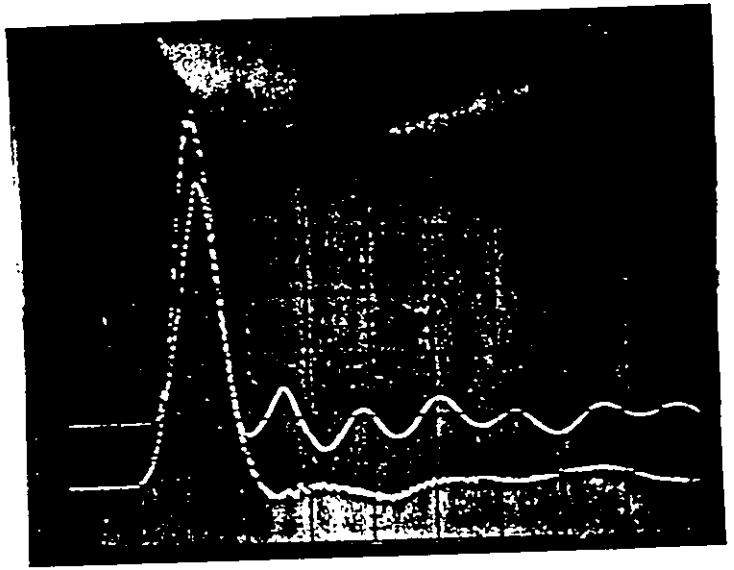

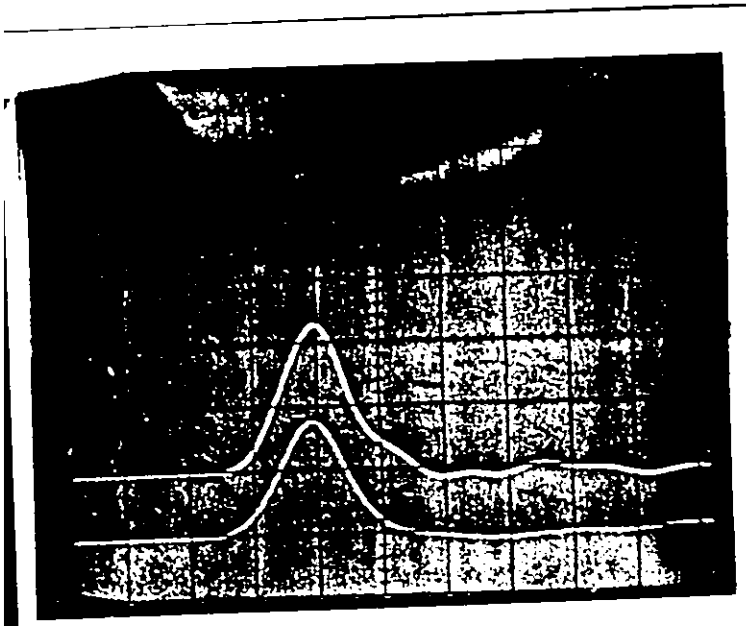

322

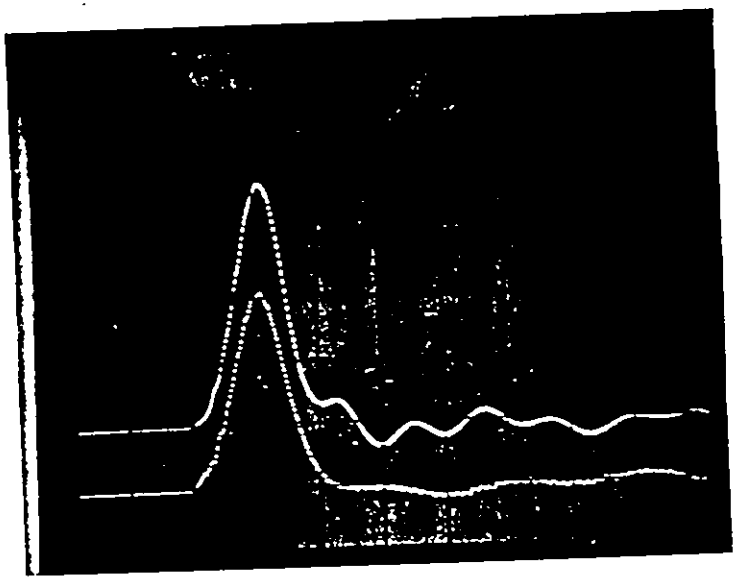

323

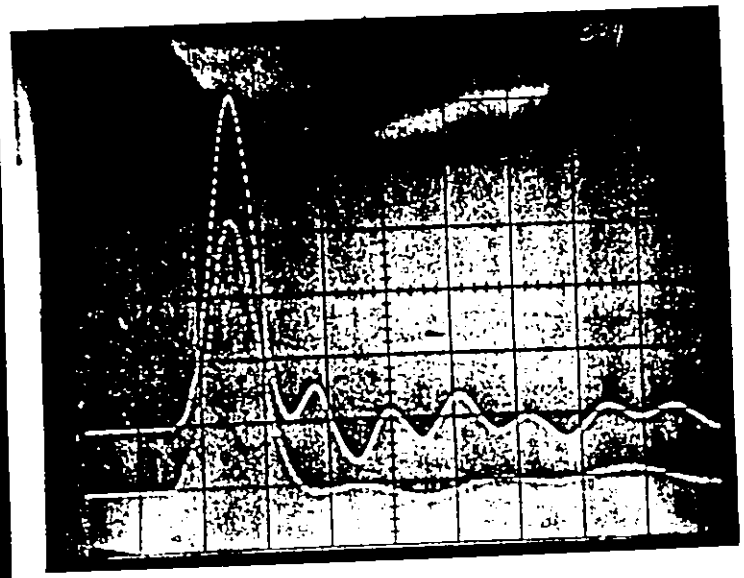

324

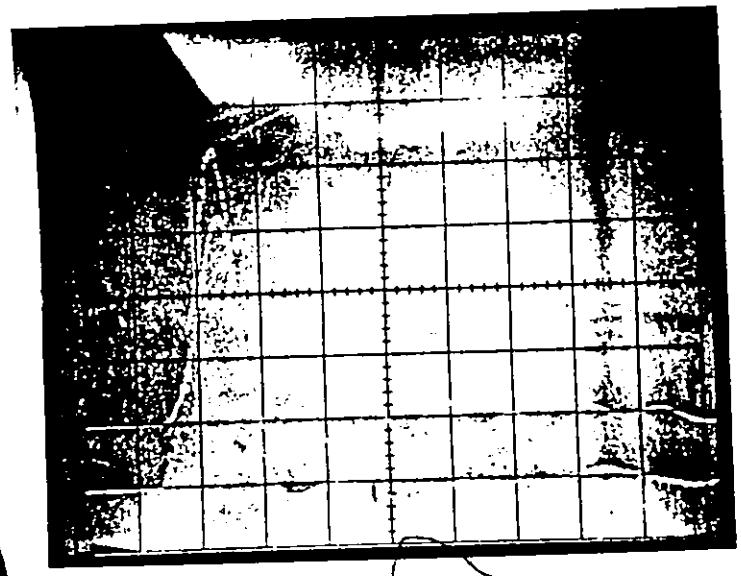

325

326

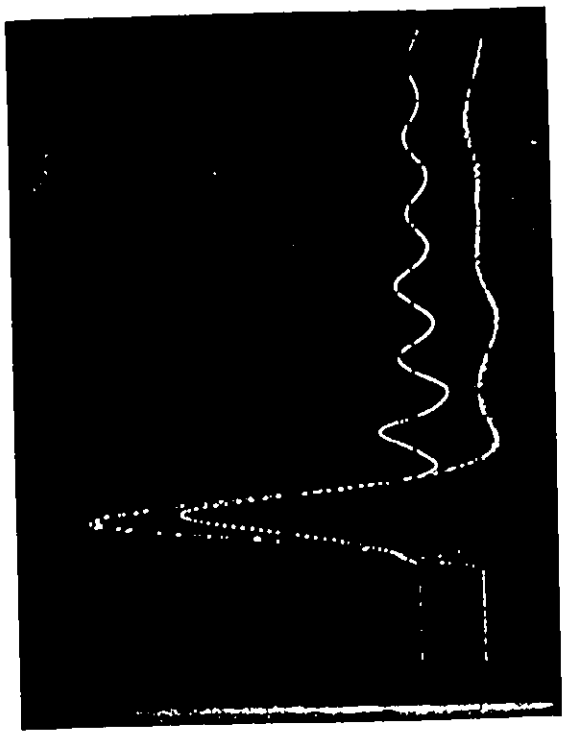

VI-6 CADAVER INFORMATION TABLE

CADAVER HEAD INFORMATION TABLE

CADAVER HEAD #	SEX	AGE	HEAD SIZE(IN.)	RACE	SCALP CONDITION	ELAPSED TIME BETWEEN DEATH AND TESTING	CAUSE OF DEATH
I	M	Approx. 70	21 3/4"	C.W.	DRY, WITH SCALP REMOVED AT CROWN	6 MONTHS (EMBALMED)	NOT KNOWN
II	M	Approx. 70	22"	C.W.	MOIST, WITH NO HAIR	2 MONTHS (EMBALMED)	NOT KNOWN
IV	F	72	23"	C.W.	MOIST, WITH HAIR SHAVED OFF	1 MONTH (EMBALMED)	NOT KNOWN

C.W. - CAUCASIAN WHITE

M - MALE

F - FEMALE